Identification of novel physiological processes regulated by Neprilysin activity in *Drosophila melanogaster*

Dissertation

zur Erlangung des akademischen Grades

Doktor der Naturwissenschaften

(Dr. rer. nat.)

vorgelegt am

Fachbereich Biologie/Chemie

der Universität Osnabrück

M.Sc. Benjamin Christoph Hallier

Osnabrück, März 2017

Table of contents

Summary

Drosophila insulin like peptides (DILPs) and their human homolog insulin act as messengers to control many physiological processes in the body. Fields in which insulin signaling is crucial are e.g. growth, stress responses and aging. Consequently, many diseases are caused by disturbed insulin signaling, of which diabetes is the most prominent. During the last decades the functions of insulins and their signaling pathways have been studied in detail; what remains less well understood is how the production of insulin and insulin like peptides is regulated.

The family of Neprilysins (Neps) belongs to the M13-zinc ion binding metallopeptidases. Neprilysins cleave peptides that regulate a wide range of cellular processes and are therefore linked to a variety of diseases like cancer, analgesia, hypertension or Alzheimer's disease. In the fruit fly _Drosophila melanogaster_, five Neprilysins are expressed; but their _in vivo_ substrates have not yet been identified. One of the _Drosophila_ Neprilysins, Nep4, is expressed in the CNS, in muscle tissue, in cardiac tissue and in male reproductive organs. Nep4 is expressed in two isoforms, Nep4A and Nep4B. Isoform A is composed of a short intracellular domain, a transmembrane domain and a large extracellular domain containing the catalytically active center, whereas soluble Nep4B only consists of the extracellular domain.

This thesis reveals that overexpression of catalytically active Nep4A in muscle tissue leads to animals with impaired insulin expression, decreased size and weight, affected feeding behavior and reduced locomotion speed. Further phenotypes are an impaired energy metabolism and larval lethality. Knockdown of the whole enzyme or knockout of its catalytic activity also interferes with feeding and locomotion speed and, in addition, causes pupal lethality.

As an explanation for the phenotypes, Nep4 mediated hydrolysis of different short neuropeptide F (sNPF) species, which were identified as novel substrates of the peptidase, is proposed. sNPF is known to regulate insulin signaling and knockdown of sNPF phenocopies the Nep4 overexpression phenotypes, which suggests that Nep4 mediated hydrolysis of sNPF regulates insulin expression in the fly.

Based on these results additional regulatory peptides were identified as novel Nep4 substrates. Among them are peptides that do not only regulate insulin signaling, but also feeding behavior (Hallier et al., 2016). These findings represent good evidence that muscle bound Nep4 is key to regulate homeostasis of distinct hemolymph circulating peptide hormones. Nep4 localizing to the surface of the central nervous system is likely

necessary to ensure effective ligand clearance and thus proper regulation of corresponding peptide receptors.

1 Introduction

1.1 Neprilysins

Neutral endopeptidases or neprilysins (NEPs) are highly conserved ectoenzymes that belong to the family of M13-zinc binding metallopeptidases (reviewed by Turner et al., 2001). Initially, they were discovered in the brush-border membranes of rabbit kidneys, where their capability to hydrolyze the insulin B chain was shown (Kerr and Kenny, 1974). Neprilysins are also known as enkephalinases, common acute lymphoblastic leukemia antigen (CALLA) or Cluster of differentiation 10 (CD10) (Brown et al., 1975; Hershl and Morihara, 1986) and are classified as type 2 integral membrane proteins. These glycoproteins are composed of a short N-terminal intracellular domain, a hydrophobic transmembrane region and a large C-terminal extracellular region harboring two highly conserved sequence motifs (HExxH; ExxA/GD) that are essential for catalytic activity (Matthews, 1988; Oefner et al., 2000). Due to their transmembrane domain, most neprilysins are plasma membrane bound with their catalytic site facing the extracellular space. However, in addition to membrane bound neprilysins also soluble forms are known, which are Neprilysin-like 1 and Secreted endopeptidase (SEP) in vertebrates, and Nep2 and Nep4B in *Drosophila melanogaster* (Meyer et al., 2009; Sitnik et al., 2014; Turner et al., 2001). The main function of neprilysins is the degradation of signaling peptides within the cardiovascular-, nervous-, and immune-system (Barnes et al., 1995; Bayes-Genis et al., 2016; Turner et al., 2001). However, up to now knowledge on neprilysin substrates or *in vivo* functionality is based almost completely on the analysis of a single family member, namely human Neprilysin (NEP).
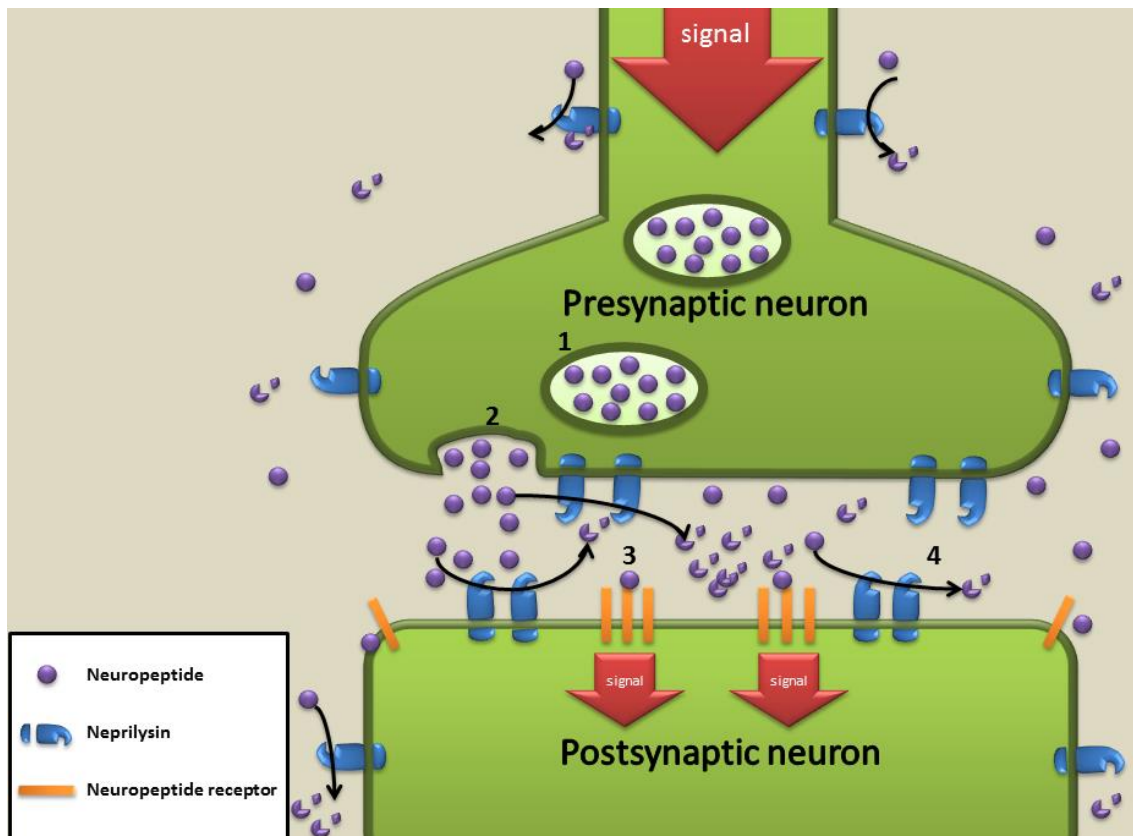
Figure 1| Schematic representation of neprilysins regulating synaptic signal transduction. A signal arriving at the presynapse results in the release of neuropeptides (2), stored in synaptic vesicles (1), into the synaptic cleft. This release signals to postsynaptic neurons via binding of distinct neuropeptides to their respective receptor (3). The signal intensity and duration is controlled via cleavage of the neuropeptides mediated by peptidases like Neprilysin (4).

Thus, this protein represents by far the best characterized member of the neprilysin family. Known substrates of human NEP are e.g. endothelins, angiotensins I and II, enkephalins, bradykinin, atrial natriuretic peptide, substance P, and the amyloid-beta peptide (Bayes-Genis et al., 2016; Turner et al., 2001). Based on this function in maintaining homeostasis of physiologically highly relevant peptides, NEPs are considered putative targets for the treatment of various diseases, such as hypertension (Khalid et al., 2016; Molinaro et al., 2002), analgesia (De Felipe et al., 1998; Whitworth, 2003) cancer (Turner et al., 2001), or Alzheimer's disease (Belyaev et al., 2009; Chen et al., 2016b; Saido et al., 2000). However, beside these substrates of human Neprilysin, very little is known about the physiological relevance or *in vivo* substrates of the remaining neprilysins.

1.1.1 Neprilysins belong to the family of M13 zinc-metallopeptidases and exhibit a conserved mechanism of catalysis

In addition to neprilysins, six other proteins belong to the family of M13 zinc-metallopeptidases. These include the endothelin-converting enzymes ECE-1 and ECE-2, PHEX (phosphate regulating gene with homologies to endopeptidases on the X chromosome), DINE (damage induced neutral endopeptidase), Secreted endopeptidase (SEP/NL-1), KELL, and MMEL-2 (membrane metallo-endopeptidase) (Bonvouloir et al., 2001; Turner et al., 2001). While these family members were initially identified in vertebrates, sequence alignments with human NEP identified many Nep/ECE-like proteins also in numerous invertebrate species, such as insects (Turner et al., 2001). Five of these homologs (Neprilysins 1 – 5) were shown to be expressed in *Drosophila melanogaster.* (Meyer et al., 2011; Sitnik et al., 2014)

All 5 *Drosophila* neprilysins, as well as every other family member, share the same mechanism of catalysis, which is based on two catalytically relevant motifs within the extracellular domain of the peptidases. In the first motif (**HE**xx**H**) the histidine residues H-583 and H-587 (position within human NEP) are required to co-ordinate the zinc atom. Co-ordination is further supported by a glutamate (E-646) located within the second catalytically relevant motif (**E**xx(A/G)**D**) (Gomis-Rüth, 2003; Roques et al., 1993). Consequently, neprilysins are classified as gluzincins, which belong to the tribe of zincins originating from the subclass of mononuclear metallopeptidases (Cerdà-Costa and Xavier Gomis-Rüth, 2013). The extracellular domain of neprilysins is composed of two α-helical subdomains. The 326 amino acids spanning N-terminal part of the extracellular D1 subdomain contains the zinc binding motifs, while the 286 amino acids of the D2 subdomain are critical to the formation of the substrate binding pocket (aa positions refer to human NEP). For steric reasons, access to this pocket is limited to peptide substrates with a size of ca. 3kDa or less (Bayes-Genis et al., 2016; Oefner et al., 2000, 2004). As a result of the polarization of a water molecule by Glu-584 within the **HE**xxH motif, two protons of the water are transferred to a nitrogen atom of the substrate, which hydrolyzes the peptide bond N-terminal to bulky and aromatic hydrophobic amino acids, with a strong preference for Phe or Leu at P1´ (Bayes-Genis et al., 2016; Hershl and Morihara, 1986; Matthews, 1988; Tiraboschi et al., 1999). In addition to the sequence motifs described above, members of the neprilysin family share

an NAYY/F motif, which is important to proper substrate binding. Furthermore, a conserved CxxW motif at the C-terminus appears to be critical to the correct formation of the respective tertiary structures (Bland et al., 2008; Sitnik et al., 2014) (**Figure 2**).
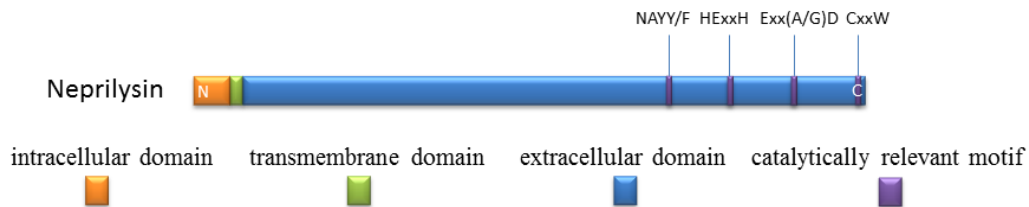
Figure 2| Schematic representation of human Neprilysin structure. The intracellular domain is depicted in orange, the transmembrane domain in green, and the extracellular domain in blue. The latter domain contains the sequence motifs that are critical to enzymatic activity.

Insect Neprilysins cluster in four different clades of conserved genes that delineate with the five *D. melanogaster* neprilysins showing the greatest similarity to human NEP (**Figure 3**). Every *Drosophila* Nep has a *D. pseudoobscura*, *An. gambiae*, and *Ap. mellifera* homolog. This fact indicates that the respective genes evolved before the divergence of the Hymenoptera and Diptera (Bland et al., 2008). However, only *Drosophila* Nep1 and Nep4 share the same cluster, indicating a close phylogenetic relation and thus putatively similar substrate specificities. It seems possible that these two neprilysins were formed from a gene duplication before or after divergence of the Nematoda and Insecta. By contrast, *Drosophila* Nep3 clusters together with the ECE-like subgroup of enzymes in the same clade (**Figure 3**| III). Of note, this enzyme is the only insect neprilysin that clusters with vertebrate homologs in the given analysis (Bland et al., 2008). With respect to the soluble *Drosophila* Nep2 (**Figure 3**| IX) it is interesting that the mammalian group of soluble peptidases (MmuSEP and HsaMMELII) appears to have evolved recently (**Figure 3**| IV), after the split from the urochordates, which explains why the mammalian and the *Drosophila* enzymes are largely unrelated (Bland et al., 2008). A rather limited homology to vertebrate neprilysins is also observed for *Drosophila* Nep5 (**Figure 3**| VIII).

Figure 3| Consensus tree of M-13 metallopeptidases. The tree depicts the phylogenetic relationship within the family of M13 metallopeptidases. Except for Nep1 and Nep4 the *Drosophila melanogaster* neprilysins (black arrows) allocate to individual clades (III, VI, VII, IX). Dme *Drosophila melanogaster*, Aga *Anopheles gambiae*, Dps *Drosophila pseudoobscura*, Lmi *Locusta migratoria*, Bmo *Bombyx mori*, Ame *Apis mellifera*, Hsa *Homo sapiens*, Rno *Rattus norvegicus*, Mmu *Mus musculus*, Fru *Fugu rubripes*, Pfl *Perca flavescens*, Xla *Xenopus laevus*, Ocu *Oryctolagus cuniculus*, Bta *Bos taurus*, Cpo *Cavia porcelllus*, Cin *Ciona intestinalis*, Cel *Caenorhabditis elegans*, Cbr *Caenorhabditis briggsae* (modified after Bland et al., 2008)

1.1.2 Neprilysin function and substrates in vertebrates

Zinc binding metallopeptidases like neprilysins are evolutionarily conserved and can be found in basal organisms like Archaea and Bacteria, in invertebrates like mollusks, insects, nematodes and annelids, as well as in the already mentioned vertebrates (Bland et al., 2008; Turner et al., 2001).

According to current data, the main function of neprilysins appears to be controlling homeostasis of regulatory peptides in diverse tissues. Based on this functionality, NEP

activity is critical to the proper physiology of signaling processes in the central nervous system, the cardio-renal system, the respiratory system, the energy metabolism, inflammation events, and the immune system (Bayes-Genis et al., 2016; Turner et al., 2001). The respective activities of individual neprilysins depend on their tissue- and cell-specific localization within the animal and their substrate specificity. Most of the known substrates of neprilysins are neuropeptides and peptide hormones, which activate signaling cascades by binding to their respective receptors (Turner et al., 2001). Due to their transmembrane domains Neprilysins are generally anchored to the plasma membrane with their catalytic site facing the extracellular space. Noticeably, most of the physiological functions were identified solely on the basis of vertebrate NEP, while the biological relevance of the remaining members of the neprilysin family is still largely unknown. Within the central nervous system (CNS), vertebrate NEP is expressed in a broad manner and localizes to the plasma membrane of nerve cells (Matsas et al., 1984). Identified CNS-specific substrates include enkephalins, endorphins, neuropeptide Y, and the famous amyloid-beta peptide (Bayes-Genis et al., 2016). In addition to the CNS, the peptidase is also present in a number of other tissues, like the renal brushborder, heart, peripheral vasculature, adrenal gland, lungs, gastrointestinal secretory epithelial brush borders, thyroid, placental syncytiotrophoblasts and the male genital tract, where it affects, based on its substrate specificity, distinct physiological processes. A summary of the tissue-specific substrates currently known for vertebrate NEP as well as of associated physiological processes is depicted in **Table 1** (Bayes-Genis et al., 2016).

Nervous System:

Amyloid-beta (1-40), (1-42); enkephalins (met and leu); alpha-endorphin, gamma-endorphin; alpha-neoendorphin; beta-neoendorphin; nociceptin; corticotrophin-releasing factor; luteinizing hormone-releasing hormone; oxytocin; arginine vasopressin; neurotensin; neuropeptide Y; neurokinin A

Cardio-renal system:

atrial natriuretic peptide (ANP), B-type natriuretic peptide (BNP), C-type natriuretic peptide (CNP); angiotensins 1, 2, 3, 1-9; endothelin-1, -2, and -3; adrenomedullin; bradykinin

Gastrointestinal system:

Gastrin-releasing peptide; gastric inhibitory peptide; vasoactive intestinal peptide; cholecystokinin

Respiratory system:

Substance P, other tachykinins

Metabolic processes:

Glucagon; glucagon-like peptide; beta-lipotropin; insulin B-chain; secretin; CGRP; somatostatin

Inflammation:

Chemotactic peptide; interleukin 1-beta

Table 1| Confirmed and putative substrates of human Neprilysin (Bayes-Genis et al., 2016).

Among the substrates of the neprilysin are numerous well-characterized peptides that are known to regulate essential physiological processes. These include the **atrial natriuretic peptide** (ANP) which controls blood pressure via regulation of the sodium water balance and thus the blood volume (Kenny and Stephenson, 1988). Since a reduced blood volume alleviates the effects of heart insufficiency, neprilysin inhibition and thus accumulation of natriuretic peptides is considered a potent therapeutic strategy against chronic heart failure. Interestingly, recent clinical trials have demonstrated a significant efficacy of neprilysin inhibitors in the treatment of corresponding indications (McMurray et al., 2014). **Enkephalin** is an opioid that represses pain by binding to its respective receptor. Thus, NEP mediated cleavage regulates the extent of pain

perception (Roques et al., 1993). **Bradykinin** is another important substrate, which plays a role in nociception and hyperalgesia, as well as in vasodilation and maintenance of the blood-brain barrier (Fischer et al., 2002; Wang et al., 2007). **Endothelin** is a potent vasoconstrictor synthesized by endothelial cells. In addition, the peptide is known to play a role in the development of diseases like hypertension or atherosclerosis (Khalid et al., 2016). The tachykinin family member **substance P** is a critical mediator of inflammations associated with infectious and neurodegenerative diseases of the CNS. Furthermore, the peptide is involved in the regulation of the cardiovascular system, the immune response, and nociception. Thus, cleavage of this multifaceted substrate already renders NEP as a multisystem regulator (De Felipe et al., 1998; Martinez and Philipp, 2016; Mashaghi et al., 2016; Matsas et al., 1983; Mistrova et al., 2015). **Bombesin** and **Enkephalin** are mitogenic peptides. It has been shown that inhibition of NEP, and thus decreased degradation of Bombesin and Enkephalin, may be causative to the development of small carcinoma (Shipp et al., 1991; Turner et al., 2001). **Glucagon like peptide-1** (GLP-1) is cleaved by human Neprilysin at six positions within the C-terminal region (Hupe-Sodmann et al., 1995). In line with these *in vitro* data, it was shown that mice with a neprilysin deficiency exhibit elevated levels of GLP-1. This increase is accompanied by an enhanced beta-cell function and improved insulin sensitivity (Willard et al., 2016). Another and probably the most prominent substrate of NEP is the **β-amyloid-peptide** (Aβ). Subsequent to the proteolytic generation from an amyloid precursor protein, Aβ aggregates and accumulates in Alzheimer plaques within the brain of vertebrates. These plaques are considered to be one of the main causes of Alzheimer's disease (Iwata et al., 2005). Due to its ability to degrade the ß-amyloid-peptide, NEP represents a promising candidate for a therapeutic against the disease (Chen et al., 2016b).

1.1.3 Neprilysins in *Drosophila melanogaster*

In *Drosophila* 25 NEP/ECE-like proteins could be identified based on sequence similarity studies. However, up to now expression of only five of these genes was confirmed. These genes are Neprilysin 1, Neprilysin 2, Neprilysin 3, Neprilysin 4 and Neprilysin 5 (Nep 1-5) (**Figure 4**| A, B) (Meyer et al., 2011; Sitnik et al., 2014).
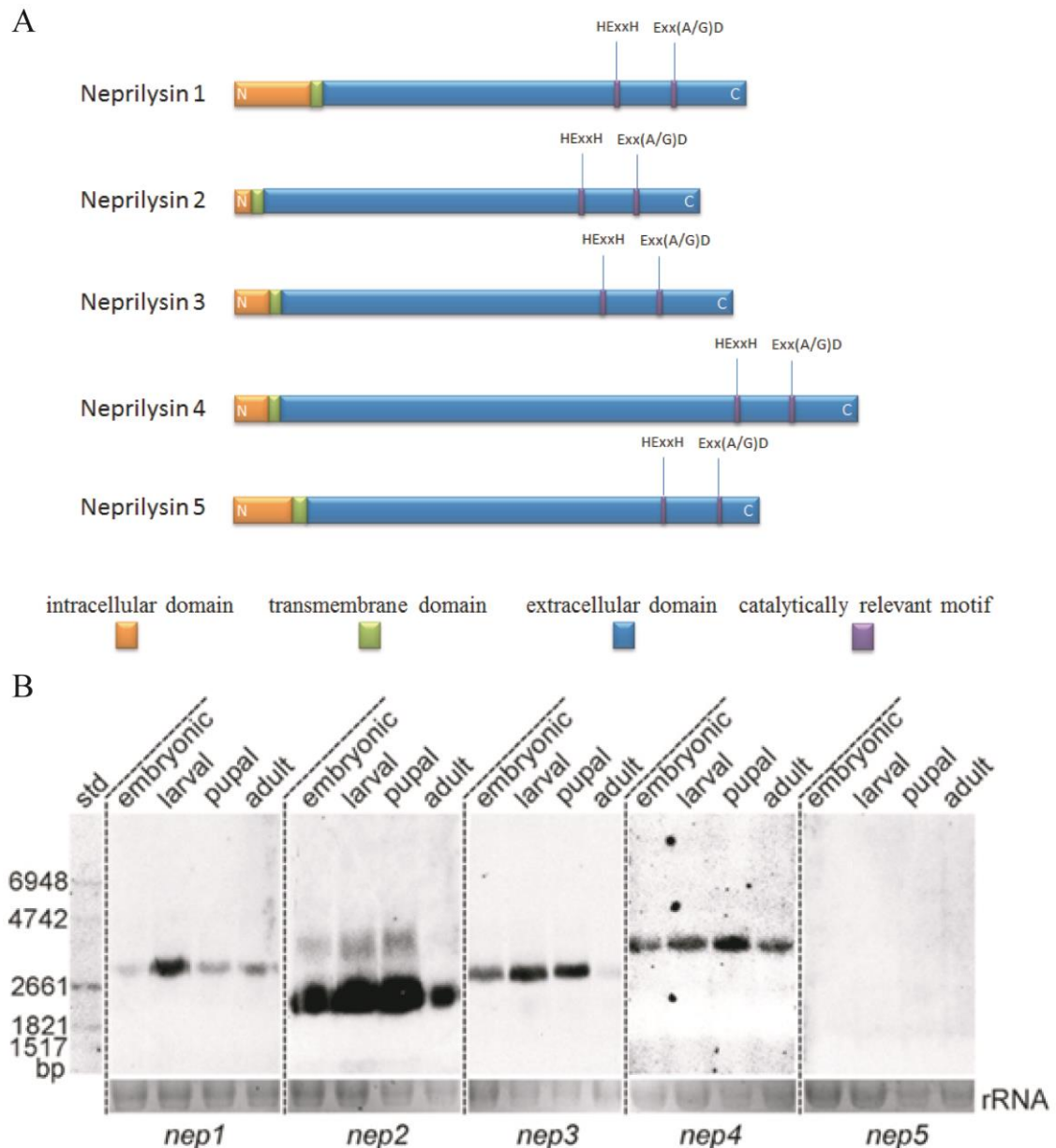
Figure 4| Structure and expression of Neprilysin 1-5 in *Drosophila melanogaster*. A: Neprilysin 1-5 consist of an N-terminal intracellular domain (orange), a transmembrane domain (green), and a large extracellular domain (blue) containing the motifs relevant to catalytic activity (purple). **B:** Northern Blot (Meyer et al., 2011) depicting the transcript levels of Neprilysin 1-5 in every developmental stage of *Drosophila melanogaster*.

All of these enzymes exhibit the characteristic features of neprilysins, such as a short N-terminal intracellular domain, followed by a single transmembrane domain and a large extracellular part, with the latter holding the catalytically relevant motifs (**Figure 4|** A).

Drosophila neprilysins are expressed in distinct spatio-temporal patterns. The *neprilysin 1* gene is located on the X-Chromosome and expresses two isoforms, Nep1A and Nep1B (http://flybase.org/reports/FBgn0029843.html). Gene expression is detected

during every developmental stage (**Figure 4**| B). During embryogenesis *nep1* is expressed within the peripheral nervous system, within the antenno-maxillary complex, in cells of the pharynx, and in midgut cells. During larval development expression was detected in mushroom bodies, neurons of the pars intercerebralis and neurons of the ventral ganglia. In adult flies the expression can additionally be detected in cells of the midgut and of the male reproductive organs were *nep1* is expressed at the end of the testicular tube near and within the seminal vesicle. Finally, strong expression could also be detected within female reproductive organs (Sitnik et al., 2014).

Similar to Nep1, Nep2 is also expressed in every developmental stage of *Drosophila* (**Figure 4**| B). The gene is located on chromosome 3R (http://flybase.org/reports /FBgn0027570.html). During embryogenesis expression was detected in foregut and hindgut cells, in the tracheal system, and in epidermal cells. During larval stages the expression pattern shows additional expression in the brain as well as in six neurons of the ventral ganglion. In adult flies *nep2* is expressed in the male gonads. Nep2 is one of the rare soluble, secreted members of the neprilysin family. Its expression in male testes was located to somatic cyst cells and tail cyst cells surrounding spermatid bundles and waste bags. The *nep2* transcript could furthermore be detected in stellate cells of the Malpighian tubule main segment and in bar-shaped cells in the Malpighian tubule initial segment. Additionally, the protein was found in the same stellate and bar shaped cells intercalating with the principal cells of the renal tubules (Bland et al., 2007; Sitnik et al., 2014; Thomas et al., 2005).

neprilysin 3 is located on the X-chromosome (http://flybase.org/reports/ FBgn0031081.html). In contrast to many other neprilysins, expression is already starting in stage 14 of embryonic development. From that time point on, *nep3* is expressed throughout the whole *Drosophila* development, however, it is only weakly expressed during adult stage (**Figure 4**| B). During embryogenesis substantial expression is apparent in the CNS. In addition to some ventral ganglia, during larval development *nep3* is expressed mainly in the two hemispheres of the larval brain. The only additional sites of *nep3* expression appear to be a few cells of the midgut (Meyer et al., 2011; Sitnik et al., 2014).

The gene coding for *neprilysin 4* is located on chromosome 3R. *nep4* is translated into two isoforms, Nep4A and Nep4B (http://flybase.org/reports/FBgn0038818.html). In contrast to isoform A, Nep4B exhibits no intracellular and transmembrane domains, thus only Nep4A represents a typical membrane bound member of the neprilysin

family, whereas Nep4B is a soluble and secreted protein (Meyer et al., 2009). The two Isoforms of Nep4 are expressed during the whole development of *D. melanogaster*, including adulthood (**Figure 4**| B). However, the ratio of isoform-specific expression varies throughout development. Nep4B is expressed stronger during embryogenesis and larval stages, whereas afterwards expression of Nep4A increases and expression of Nep4B decreases. In pupae, expression levels are largely equal. In adult flies expression of Nep4A is stronger than that of isoform B (Meyer et al., 2009). Expression of Neprilysin 4 starts in embryonic stage 13 and persists until stage 17. It is mainly detectable in even skipped positive pericardial cells, glial cells of the CNS, dorsal myoblasts, and gonads. During larval development Nep4 is expressed in the CNS, the ventral nerve cord, and in body wall muscles. In adult flies *nep4* expression is evident in cells of the CNS, of body wall muscles, and of male gonads (Meyer et al., 2009, 2011; Panz et al., 2012).

The *neprilysin 5* gene is also located on the right arm of the 3rd chromosome (http://flybase.org/reports/FBgn0039478.html). Expression of *nep5* it restricted to 4 small groups of cells in the anterior part of the animal during stage 17 of embryogenesis. This spatially and temporally small window of expression explains why up to now *nep5* RNA could not be detected by Norther blot (**Figure 4**| B). While no expression was reported in larval stages, in adult flies Nep5 was detected in membranes of the seminal vesicles where mature spermatids are stored after transport from the testicular tubes. Nevertheless, the peptidase appears to be non-essential for fertility (Sitnik et al., 2014).

1.1.4 Neprilysin function in *Drosophila melanogaster*

In *Drosophila melanogaster*, two of the five neprilysins known to be expressed have been reported to be catalytically active: Neprilysin 2 and Neprilysin 4 (Bland et al., 2007; Meyer et al., 2009; Thomas et al., 2005). For Nep4 it has been demonstrated that the N-terminal intracellular domain, which is not catalytically active, causes a muscle degeneration phenotype when overexpressed. Furthermore, corresponding animals exhibit larval lethality. As causative to these phenotypes, a carbohydrate kinase has been proposed, which interacts with the intracellular domain of Nep4 and somehow affects proper energy metabolism (Panz et al., 2012). In addition, altered *nep2* expression induced an abnormal locomotion behavior of adult flies (Bland et al., 2009).

With respect to Neprilysins 1-4 it was reported that knockdown of each of these Neprilysins results in impaired formation of middle- and long-term memory (Turrel et al., 2016). Another peptide cleaved by Neprilysins is the neurotransmitter pigment dispersing factor (PDF), which controls rhythmic circadian locomotion behavior (Isaac et al., 2007). Finally, *Drosophila* Neprilysins play an important role in male fertility (Sitnik et al., 2014).

Despite these data on the functional roles of Neprilysins in *Drosophila*, still very little is known about physiologically relevant *in vivo* substrates. Consequently, generating comprehensive, enzyme specific lists of such substrates is critical in order to understand the physiological functionality of neprilysins in a complete manner.

2 Materials and Methods

The materials used and the experimental procedures performed in this thesis are listed in the following sections.

2.1 Materials

2.1.1 Fly strains

genotype	description	origin	reference
white[1118]	Spontaneous partial deletion of white	BDSC BL3605, Robert Levis	-
mef2-Gal4	Gal4 expression under control of the *mef2* enhancer	H. Nguyen, Erlangen, Germany	-
repo-Gal4	Gal4 expression under control of the *repo* enhancer	BL7415, BDSC	-
dilp2-Gal4	Gal4 expression under control of the *Drosophila insulin like peptide 2* enhancer	BL37156, BDSC	-
snpfr-Gal4	Gal4 expression under control of the *short neuropeptide F receptor* enhancer	BL46547, BDSC	-
UAS-mCherry	mCherry under control of UAS	BL38424, BDSC	-
UAS-2xeGFP	eGFP under the control of UAS	BL6874	-
UAS-Nep4A (#2)	*nep4A* under control of UAS	Zoology, University of Osnabrück	Panz et al., 2012
UAS-Nep4Ainact	*nep4* allele with exchange of amino acid E973 to Q causing loss of catalytic activity under control of UAS	Zoology, University of Osnabrück	(Panz et al., 2012)
nep4-nGFP	*nep4*-nGFP reporter line	Zoology, University of Osnabrück	Meyer et al., 2009
nep4 RNAi	*nep4* knockdown KK library, no off-	VDRC100189	Panz et al.,

	targets		2012
Nep4$^{\Delta281\text{-}1040}$/TM3	Truncated *nep4* allele, balanced over TM3-chromosome	Zoology, University of Osnabrück	Benjamin Hallier unpublished
Nep4$^{\Delta281\text{-}1040}$/TDLZ	Truncated *nep4* allele, balanced over TDLZ-chromosome	Zoology, University of Osnabrück	Benjamin Hallier unpublished
Nep4$^{\Delta281\text{-}1040}$/TM3, *Kr*>GFP	Truncated *nep4* allele, balanced over TM3, *Kr*>GFP-chromosome	Zoology, University of Osnabrück	Benjamin Hallier unpublished
BL36979	*nep4^{MI03765}* allele containing a MiMIC-element, balanced over TM3-chromosome	Bloomington *Drosophila* Stock Center	Venken et al., 2011
BL36979/ TDLZ	*nep4^{MI03765}* allele containing a MiMIC-element, balanced over TDLZ-chromosome	Bloomington *Drosophila* Stock Center	Venken et al., 2011 This thesis
BL36979/ TM3, *Kr*>GFP	*nep4^{MI03765}* allele containing a MiMIC-element, balanced over TM3, *Kr*>GFP-chromosome	Bloomington *Drosophila* Stock Center	Venken et al., 2011 This thesis

Table 2| Fly strains used in this thesis. BDSC = Bloomington *Drosophila* Stock Center; VDRC = Vienna *Drosophila* Resource Center,

2.1.2 Antibodies

2.1.2.1 Primary antibodies

antibody	host	dilution	donor	reference
Anti-Nep4	rabbit polyclonal	1:250 (ih)/1:2000 (wb)		Meyer et al., 2009
Anti-GFP	mouse, monoclonal	1:500 (ih)	Life Technologies	-
Anti-HA	mouse	1:200 (ih) / 1:1000 (wb)	Sigma-Aldrich	
Anti- reversed polarity	mouse	1:5 (ih)	Hybridoma Bank	
Anti-β3Tubulin	guinea pig	1:4000 (ih)	Zoology, University of Osnabrück	
Anti-Fas2 (fasciclin2)	mouse	1:50 (ih)	DSHB	
Anti-Odd skipped	rabbit	1:500 (ih)	Jim Skeath	Ward and Skeath, 2000
anti-ß-galactosidase	mouse	1:2000 (ih)	Promega	
anti-ß-galactosidase	rabbit	1:2000 (ih)	MP Biomedicals, Santa Ana, CA	

Table 3| First antibodies used in this thesis. ih= immunohistochemistry; wb= western blot; DSHB= Developmental Studies Hybridoma Bank, Iowa, U.S.A.

2.1.2.2 Secondary antibodies

antibody	host	dilution	donor	reference
Anti-mouse Cy2	goat	1:100 (ih)	Dianova GmbH, Hamburg	
Anti-mouse Cy3	goat	1:200 (ih)	Dianova GmbH, Hamburg	
Anti-rabbit Cy2	goat	1/100 (ih)	Dianova GmbH, Hamburg	
Anti-rabbit Cy3	goat	1:200 (ih)	Dianova GmbH, Hamburg	
Anti-rabbit alkaline phosphatase		1:10000 (wb)	Roche, Mannheim	
Anti-guinea pig Cy3	goat	1:200 (ih)	Jackson-Immuno Research	
Anti-digoxygenin alkaline phosphatase	sheep	1:10000 (nb)	Roche, Mannheim	

Table 4| secondary antibodies used in this thesis. ih= immunohistochemistry; wb= western blot; nb= northern blot

2.2 Methods

2.2.1 Fly handling

2.2.1.1 Stock keeping

Flies were kept on fly bottles filled to a quarter with standard cornmeal agar. Stocks were kept at room temperature according to standard protocols (Ashburner et al., 2005; William Sullivan et al., 2000).

2.2.2 The UAS/Gal4 system

The UAS/Gal4 system (Brand and Perrimon, 1993) was used to increase or reduce expression of specific proteins in defined tissues. Utilized UAS effector-, Gal4 driver- and RNAi-lines are depicted in section **Table 2**.

P): ♀ $\dfrac{\text{UAS Nep4A}}{\text{UAS Nep4A}}$; $\dfrac{+}{+}$ X   ♂ $\dfrac{+}{+}$; $\dfrac{\textit{mef2}\text{-Gal4}}{\textit{mef2}\text{-Gal4}}$

F_1): $\dfrac{\text{UAS Nep4A}}{+}$; $\dfrac{+}{\textit{mef2}\text{-Gal4}}$

100%
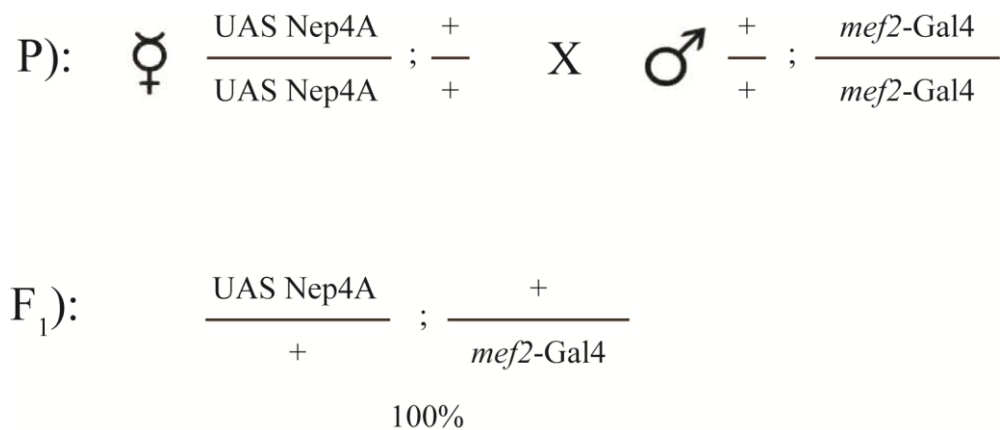
Figure 5| Example of a crossing scheme using the UAS-Gal4 system. Virgins of the effector line are crossed to males of the driver line (or vice versa) within the parental generation. In this case both parents are homozygous for their respective constructs, thus 100% of the F_1 generation ectopically expresses Nep4A in the musculature.

2.2.3 Size and weight measurements

5 individuals of staged (AEL 74-78 h) 3rd instar larvae where grouped in genotype specific cohorts. 6 different cohorts of each genotype where weighed to measure the mean weight of one respective larva. Prior to size measurements the larvae were put into 60°C water for 10s to achieve maximum relaxation of the larval bodies. The animals where photographed on scale paper using a Leica MZ16 FA stereomicroscope.

The body length of each larva was measured using Adobe Photoshop CS5 (Adobe systems, La Jolla, CA, U.S.A.) and the scale paper was used as a reference.

2.2.4 Fertility assay

Single pair crossings of mutant male flies and wildtype virgin female flies (and vice versa) were put on small fly vials. After 7 days of egg laying, the P-generation was removed from the vials and the hatching offspring (F_1 generation) of each respective crossing was counted.

2.2.5 Locomotion assay

Third instar larvae were placed on scale paper and movement was recorded. Straight runs of at least 10sec were measured and the crawling speed (distance/time) as well as the mean crawling speed for each respective genotype was calculated.

2.2.6 Feeding assay

Third instar lava were collected in cohorts of five and starved for 1h. Cohorts were then covered with red dyed yeast (o.3 mg Carmin; 4 mg dry Yeast; 10 ml H_2O) for 5-, 10-, 20- and 40min, cleaned and cooled on ice. Fed larvae were put on coverslips on top of white paper and photographed (Canon 1000D mounted on Zeiss Stemi2000-C) from the ventral side. The intensity of red dye within the larval intestine was measured using Fiji (http://fiji.sc/) and the highest intensity was set to 100%.

2.2.7 Image acquisition

Fluorescence images of antibody stainings were acquired using a Zeiss Pascal 5 confocal microscope (Zeiss, Jena, Germany). Images of complete larvae for size measurements were done using a Leica MZ16FA stereomicroscope by incident light. Images of larva fed with red dyed yeast and videos of larvae performing locomotion assays were taken using a Canon 1000D on a Zeiss Stemi2000-C. Images were further processed using ImageJ, Adobe Photoshop CS and Adobe Illustrator CS.

2.2.8 Generation of Nep4 Mutant via CRISPR/Cas9

Nep4$^{\Delta281-1040}$ was generated using the CRISPR/Cas9 system. Aiming to delete a huge part of *nep4*, including a MiMIC-element (BL36979), two CRISPR cutting sites were selected. Successful deletion would result in yellow flies, because of the loss of a *yellow*-gene located within the MiMIC-element. Oligonucleotides (Biolegio, Nijmegen, Netherlands) were designed and the respective amplificates were ligated into the pU6-BbsI-chiRNA vector. Primer sequences (6.1) contained the respective restriction site to allow for sticky end ligation. Sequenced vector constructs were sent to "The Best Gene" (Chino Hills. CA, U.S.A.) for injection into line BL36979 crossed to BL51323 (y[1] M{vas-Cas9}ZH2A w[1118]. Surviving flies were balanced over TM3. *yellow*$^-$ flies were selected for further analysis.

2.2.9 Molecular biology

2.2.9.1 Polymerase Chain Reaction (PCR)

PCRs were performed using standard protocols (Green and Sambrook, 2012). Utilized polymerases were Taq-polymerase (Biotherm, Genecraft) or ExTaq polymerase (proofreading activity, Takara, Clontech). Used primers are listed in Appendix 6.1.

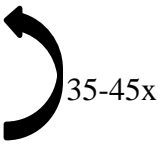| Reagent	Volume	Step	Temp.	Time	
DNA Template	1µl	Initial	94°C	2min	
10x reaction Buffer	5µl	denaturation			
dNTP (2,5mM each)	4µl	Denaturation	94°C	45sec	
Primer (10 pMol each)	1µl	Annealing	55-65°C	45sec	35-45x
Polymerase	0,5µl	Elongation	72°C	1min/kBp	
milliQ-H$_2$O	to 50µl	Final elongation	72°C	10min	
		Cooling	8°C	∞	

Table 5| Standard PCR. Components and protocol

2.2.9.2 Agarose gel-electrophoresis

To separate DNA samples according to their size agarose gel electrophoresis was used (Green and Sambrook, 2012). Separation was performed in 1% gels submerged in TAE

DNA-gel running buffer (40 mM Tris, 20 mM acetic acid, and 1 mM EDTA in milliQ-H_2O). 5µl DNA marker (HyperladderI, Bioline) were added on each gel. 1µ SERVA DNA stain SYBRGreen (Serva) was mixed in a 50ml gel for DNA visualization.

2.2.9.3 Ligation of PCR fragments into plasmid vectors

Ligation of PCR products into the pGEM®-T Easy vector (Promega, Mannheim, Germany) were facilitated by using the T-tail of the vector for sticky end ligation. In case of any other vector, restriction sites were introduced into the PCR products via appropriate primer design. Prior to ligation, the PCR product and the respective vector were digested with corresponding restriction enzymes (Fermentas). Afterwards the Enzymes were heat inactivated (85°C, 15-20min) and the DNA purified (DNA Gel Extraction Kit, Qiagen, Hilden, Germany).

For a standard ligation 1µl 10x reaction buffer, 7µl insert-DNA (100 ng/µl), 1µl vector-DNA (200 ng/µl) and 1µl T4 DNA-ligase (Biotherm, Genecraft) were incubated at 15°C over night.

2.2.9.4 Transformation of *E.coli* cells

Chemically competent DH5α or TOP10F cells were mixed with corresponding DNA constructs and incubated on ice for 30min. Next, the cells were heat shocked (45sec, 42°C). Afterwards the cells were again incubated on ice for 10 min. For phenotypic expression, 900µl LB-medium were added and the cells were incubated for 45min at 37°C under constant shaking. Finally, cells were plated on LB agar supplemented with respective selection markers and / or antibiotics.

2.2.9.5 Plasmid preparation - mini scale

Single colonies were picked from LB agar plates and transferred into 3-5ml LB medium supplemented with a respective antibiotic for selective growth. Cultures were put on 37°C over night. Subsequent plasmid purifications were performed using the peqGOLD Miniprep Kit (Peqlab, Erlangen, Germany) according to the manufacturer´s instructions.

2.2.9.6 Isolation of genomic DNA

20-25 flies of a respective genotype were homogenized in 200µl homogenization buffer (100 mM Tris-HCl, 100 mM EDTA, 100 mM NaCl, 0.5% SDS, pH=7.5). 5µl of proteinase K (10mg/ml) were added to the sample with incubation for 45min at 37°C. Next, 80µl of 3M potassium acetate were added to induce protein precipitation. Subsequent to incubation on ice for 5min the sample was centrifuged (10min, 17000 x g, 4°C) and the supernatant containing the DNA was transferred into a new reaction cup. 180µl of Phenol/Chloroform/Isoamyl alcohol (25:24:1) were added and mixed carefully. Phase separation was induced by centrifugation (20.000 x g, 5min) and the upper phase was transferred to a new reaction cup. For DNA precipitation, twice the volume of isopropanol was added with incubation for 30min at room temperature. DNA was then pelleted via centrifugation (20.000 x g, 20min). The pellet was washed two times with 70% ice cold ethanol and centrifuged again (20.000g, 20min). Finally, the pellet was resuspended in 200µl H_2O and stored at 4°C.

2.2.9.7 Isolation of total RNA from tissue samples

Total RNA was isolated using the peqGOLD total RNA Kit (Peqlab, Erlangen, Germany) according to the manufacturer´s instructions.

2.2.9.8 First strand cDNA synthesis from total RNA

Total RNA was used as a template for reverse transcription to synthesize cDNA. 3µg of RNA were reverse transcribed in each reaction. 10µl containing the RNA were supplemented with 1µl of oligo-dT Primers and incubated for 10min at 70°C. Subsequently, 4µl 5x reaction buffer, 2µ dNTP Mix (10mM each), and 1µl Reverse Transcriptase (Biotherm, GeneScript™) were added. Reaction parameters are depicted in Table 5.

Step	Temp	Time
cDNA synthesis	42°C	50min
Heat inactivation	90°C	5min
Cooling	8°C	∞

Table 6| cDNA synthesis protocol.

cDNA samples were stored at -20°C until further usage.

2.2.9.9 Quantitative-real-time-PCR

Quantitative-real-time-PCRs were done using the DyNAmo SYBR Green qPCR Kit (FINZYMES, town, country). CYBER-Green intercalates into double stranded-DNA. After each amplification cycle, the fluorescence intensity, being proportional to the amount of amplified DNA, was measured (Biocycler, Biorad, town, country). Primer pairs were designed using Quantprime (Arvidsson et al., 2008) in order to consider regions containing at least one intron and as many splice variants as possible. Cycle threshold (CT) was defined by determining the PCR cycle in which the fluorescence intensity reached a specific value. Normalized expression and mean normalized expression were calculated as described in (Simon, 2003). For each gene at least three biological replicates were conducted, each of them consisting of at least three technical replicates.

2.2.9.10 NMR metabolomics

NMR metabolomic approaches were done in collaboration with Prof. Dr. Anders Malmendal (University of Copenhagen) and performed as described in Hallier et al., 2016.

2.2.9.11 NMR data analysis

NMR data were analyzed in collaboration with Prof. Dr. Anders Malmendal (University of Copenhagen) as described in Hallier et al., 2016.

2.2.9.12 Cell culture, protein purification, and enzymatic cleavage assays

Utilizing the Bac-to-Bac baculoviral expression system (Life Technologies, Carlsbad, CA, U.S.A.) heterologous expression of Nep4B was realized in SF21 cells. The His-tagged (C-terminal) protein was cloned downstream of the polyhedrin promoter into an *E.coli/S.cerevisiae/*Baculovirus triple-shuttle derivative of the pFastBac Dual vector (Life Technologies) adapted for cloning by homologous recombination *in vivo*. The pJJH1460 vector (6.2.1) was used which was constructed according to (Paululat and Heinisch, 2012). As an infection control, an *egfp* reporter gene was cloned downstream of the p10 promotor into the same vector.

SF21 cells were infected in 75cm^2 flasks for 72h, harvested (300 x g, 5min) resuspended in binding buffer (50 mM NaH2PO4, pH 7.9; 300 mM NaCl) and lysed. Subsequently, the samples were centrifuged (10 min, 10.000 x g) and the resulting supernatant was used for gravity-flow-based His-tag purification of Nep4B following the manufacturer's instructions (Protino Ni-NTA agarose, Macherey-Nagel, Düren, Germany). For cleavage assays, 2.5 µl of purified Nep4B (10 ng/µl) and 2.5 µl of a negative control (Nep4B purification protocol with untransfected SF21 cells) were mixed with 3.5 µl of individual peptide solutions (43 ng/µl in H$_2$O). Each sample was incubated for 5h at 35°C and subsequently analyzed via ESI mass spectrometry (Hallier et al., 2016)

2.2.9.13 ESI mass spectrometry

Each sample was loaded onto a trap column (Acclaim Pepmap C18, 5 µm, 0,1x20mm, Thermo Scientific, Sunnyvale, CA, U.S.A.). Bound substrates were eluted via an acetonitrile gradient resulting from adequate intermixing of Buffer A (99% water, 1 % acetonitrile, 0.1% formic acid) and Buffer B (80% acetonitrile, 20 % water and 0.1% formic acid). The gradient started with 100% Buffer A and 0% Buffer B, and ended with 20% Buffer A and 80% Buffer B after 45 min. A constant flowrate of 0.3 µL/min was applied. Eluted components were analyzed by measuring the masses of both, whole molecules and their fragments. Fragments were generated by CID (collision induced dissociation) of the corresponding parent ion, using an ESI-iontrap (Amazon ETD Speed with a captive spray ionization unit, Bruker Corporation, Billerica, MA, U.S.A.)

The Mascot search algorithm (Matrix Science, Boston, MA, U.A.S.) was used for identification of peptide specific amino acid sequences. As enzyme, the option "none"

was chosen, which guaranteed that every subsequence of every protein was used for identification.

2.2.10 Protein biochemistry

2.2.10.1 Immunohistochemistry

2.2.10.1.1 Collection and fixation of embryos

For collecting 0-24h embryos, respective fly lines were put on agar plates covered with yeast for oviposit. After 24 hours, flies were removed and the agar plates stored in the fridge to stop embryonic development until fixation. Prior to fixation, the embryos were collected from the agar plates and transferred into collection nets. In these nets the embryos were rinsed with water. Chorions were removed in a 1:1 (v/v) water/bleach (Danklorix, Germany) mixture for 5 min. Subsequently, embryos were rinsed to wash of chorion remains. Embryos were then transferred into 1.5 ml reaction cups containing fixative solution (125 μl 16% methanol free formaldehyde, 375 μl 1x PBS, and 500 μl n-heptane) for fixation under constant shaking. After fixation the solution was replaced by 500 μl n-heptane and 500 μl methanol, followed by vigorous shaking to remove the vitelline membrane. After washing once in methanol and three times in ethanol, embryos were stored in ethanol at -20°C until further usage.

2.2.10.1.2 Immunostaining of embryos

For rehydration, embryos were washed several times in PBT before primary antibodies were applied. In case of anti-Nep4 antibody usage, tissues were incubated in 1x PBT containing 0.15% SDS for 30min to partially unfold the protein and ensure epitope accessibility. Prior to primary antibody application the tissue was blocked with Roti®-Block (Carl Roth, Karlsruhe, Germany). Next, primary antibodies were diluted in PBT and incubated for individual timeframes (**Table 3**). After removing the primary antibodies and washing the samples several times in PBT, the tissue was incubated with secondary antibodies (**Table 4**). Secondary antibodies were removed and the animals were washed again prior to embedding in Fluoromount-G mounting medium (SouthernBiotech, Birmingham, USA).

2.2.10.1.3 Dissection, fixation and staining of 2nd instar larval body wall musculature

After dissection of the larval tissue on sylgard plates (Sylgard 184 Elastomer Base and Curing Agent, Dow Corning, Michigan, USA) in 1x PBS, the tissue was fixed in 3,7% formaldehyde for 10 min under constant shaking. Afterwards, the samples were washed several times in BBT (1x PBT (1xPBS + 0.1% TWEEN-20) + 0.01% BSA) and permeabilized in 1% Triton X-100 in BBT for 10min. After washing again in BBT for several times, the larvae were used immediately for staining with Phalloidin-TRITC (Sigmar Aldrich) to label filamentous actin. Phalloidin incubation was done at a dilution of 1:100 in 1xPBS for 1h. After several washing steps in BBT, larvae were embedded in Fluoromount-G mounting medium (SouthernBiotech, Birmingham, USA) for microscopy.

2.2.10.1.4 Dissection and staining of 3rd instar larval brains

Wandering 3rd instar larvae were opened by pulling the lateral cuticula with two forceps. Afterwards, the CNS was separated from the other organs and transferred into ice cold PBS until further usage. Brains were then fixed in 3.7% formaldehyde for 1 hour. After several washing steps, the brains were permeabilized in 1% Triton X-100 in PBS for 1 hour. In case of Nep4 antibody usage, the tissue was incubated in 0.15% SDS in PBS for 30 min to allow for partial protein denaturation. After blocking (Roti®-Block, Carl Roth, Karlsruhe, Germany, 45 min) and washing (PBT, 4× 10 min each) the sample was incubated with primary antibodies in PBS overnight. To remove unbound antibodies, the tissue was washed in PBT (4x, 10min) and blocked again as previously described. All secondary antibodies were applied simultaneously in PBS for 90min. After washing off unbound secondary antibody (4x 10min, PBT) the samples were embedded in Fluoromount-G (SouthernBiotech, Birmingham, USA).

2.2.10.1.5 Dissection, fixation and staining of 3rd instar larvae

Wandering 3rd instar larvae were dissected in PBS and fixed in 3.7% formaldehyde in PBS for 1h on Sylgard plates. Subsequently, larvae were transferred into 1.5ml reaction cups and permeabilized in 1%Trition X-100 in PBS (1h). After blocking (Roti®-Block, Carl Roth, Karlsruhe, Germany, 45 min) and washing (PBT, 4× 10 min each) the

sample was incubated with primary antibodies in PBS overnight. To remove unbound antibodies the tissue was washed in PBT (4x, 10min) and blocked again as previously described. All secondary antibodies were put simultaneously in PBS for 90min. After washing off unbound secondary antibody (4x 10min, PBT) the samples were embedded in Fluoromount-G.

2.2.10.1.6 Sodium-Dodecyl-Sulfate polyacrylamide gel electrophoresis (SDS-PAGE)

Molecular weight based protein separation was done using 12% polyacrylamide gels (1.576 ml Acrylamide (40%), 262.5 µl Bisacrylamide (1%), 884 µl 2 M Tris-HCl pH 8.7, 25.5 µl SDS (20%), 2470 µl H_2O, 25.5 µl APS (10%), 7.5 µl TEMED) according to standard protocols (LAEMMLI, 1970). Protein samples were mixed with 5x SDS sample buffer (5x Laemmli,10% β-Mercaptoethanol) and boiled for 3min at 99°C. Subsequently, samples were applied to the gel together with 5 µl of a prestained molecular weight marker (Protein-Marker VI, AppliChem) and subjected to an electric field (20mA) until they reached the separation gel. After crossing the border between stacking and separation gel, the current was raised to 40 mA. The gel run was stopped based on the migration of the corresponding standard proteins.

2.2.10.2 Semidry Western blot, Ponceau-S staining and immunodetection

To transfer the separated proteins to nitrocellulose membranes (Nitrocellulose Optitran BA-383, Whatman[TM], GE Healthcare, Frankfurt am Main, Germany), semidry Western blots were performed. Firstly, four layers of Whatman-paper and one membrane (slightly larger than the gel) were equilibrated in Western blot transfer buffer (25 mM Tris, 20 mM Glycine, 20% v/v Methanol) and stacked onto the blotting device. Next the gel was put on top of the nitrocellulose membrane, followed by 4 equilibrated sheets of Whatman-paper. Protein transfer was done at 50mA for 90min per gel. To monitor transfer efficiency, the membranes were stained with Ponceau-S solution (AppliChem, Darmstadt, Germany). Prior to antibody application, membranes were blocked in TBS (50 mM Tris, 150 mM NaCl, pH=7.6) containing 5% powdered milk for one hour. Subsequently, the membranes were incubated with the respective primary antibodies (diluted in 2.5% powdered milk in TBS) overnight at 7°C under constant shaking. After

washing of excess primary antibodies (4x, TBS supplemented with 0.05% (v/v) TWEEN20, 15min) membranes were incubated with alkaline phosphatase conjugated secondary antibodies (2.5% powdered milk in TBS) for one hour (constant shaking). After washing as described above to remove unbound antibodies, detection was done in 10ml AP-buffer (0.1 M Tris, 0.1 M NaCl and 0.05 M $MgCl_2$ in milliQ-H_2O, pH: 9.5) containing 100µl NBT/BCIP solution (Roche, Mannheim, Germany). Once an optimal signal to noise ratio was reached, the reaction was stopped by washing the membranes several times in H_2O. Finally, membranes were dried and the respective results documented.

3 Results

This chapter is composed of two major topics investigated in this thesis. First, the characterization of the catalytic activity of Neprilysin 4 and its influence on the physiology of *Drosophila melanogaster* larvae was investigated. The second part of this section is about the characterization of Nep4 mutants. In this respect, two individual *nep4* mutant alleles were analyzed.

3.1 Altering expression of *neprilysin 4* severely affects *Drosophila* larval development

Previous experiments showed that *Drosophila* Neprilysin 4 (Nep4) is expressed in numerous glial cells of the central nervous system, as well as in body wall muscles (Meyer et al., 2009; Panz et al., 2012). Furthermore, it was shown that increasing expression of the membrane bound isoform Nep4A in a muscle specific manner (*mef2-*Gal4 driver) leads to a severe muscle degeneration phenotype, due to a complete loss of sarcomeric structure, a disorganization of the actin-myosin filaments, as well as additional morphological changes. On the other hand, *nep4* knockdown via RNAi in body wall muscles did not result in such severe phenotypes; the tissue appeared almost wild typically (Panz et al., 2012).

3.1.1 Altering expression of *neprilysin 4* in muscle tissue affects larval size, mass and lifespan

In this thesis, the effects of modulating *nep4* expression in the muscle tissue of *Drosophila melanogaster* were further analyzed. In addition to the phenotypes described above, overexpression also results in a significant decrease of body size and weight (**Figure 6**| A-C). Interestingly, this phenotype is caused by the enzymatic activity of the extracellular domain, as overexpression of a catalytically inactive Nep4A, in which an essential glutamate within the zinc-binding center had been replaced by a glutamine (E973Q), did not exert any significant effect on body size or weight. Knockdown of the enzyme in body wall muscles did also not significantly affect these parameters (**Figure 6**| A-C). Increasing the expression level of *nep4A* in glial cells, where the peptidase is also expressed (Meyer et al., 2009), does not show any effect.

However, decreased expression in the same tissue slightly affects body size and weight of 3rd instar larvae (**Figure 6**| C). To confirm RNAi specificity, a fly line was generated overexpressing *nep4A* in glial cells, in a glial cell specific *nep4* knockdown background. In this experiment, the reduced body size and weight observed upon *nep4* knockdown were completely rescued (**Figure 6**| C), thus confirming specificity of the RNAi construct.

Furthermore, overexpression of the peptidase within muscles generates a biphasic lethality of the respective animals, with an early phase occurring during embryonic and early larval development, and a late phase being evident in late larval stages (**Figure 6**| D). In contrast to overexpressing the active peptidase, increased expression of catalytically inactive Nep4A did not result in a significant change of viability. This again demonstrates that the increased enzymatic activity is critical to the described phenotypes (**Figure 6**| C, D). Knockdown of *neprilysin 4* in musculature led to similar effects, compared to overexpression of the active peptidase in the same tissue. In this case however, in addition to an early phase of increased mortality during embryogenesis, the late phase of lethality occurred during metamorphosis rather than during late larval development. None of the respective individuals reached adult stage (**Figure 6**| D). To confirm RNAi specificity, flies expressing the respective RNAi construct simultaneously with a *nep4* overexpressing construct were analyzed. In line with the effects on size and weight, simultaneous overexpression of Nep4 in muscles completely rescued the biphasic lethality at late embryogenesis and metamorphosis caused by muscle specific knockdown of *nep4*. However, corresponding animals exhibited a slightly but significantly increased lethality rate during the 3rd instar larval stage, indicating that the overexpression of Nep4 in a *nep4* knockdown background does not restore *nep4* expression exactly to wildtype level, but eventually results in a slightly increased *nep4* expression. In contrast to the muscle-specific effects, overexpression or knockdown of *neprilysin 4* in the CNS did not affect viability in a significant manner (**Figure 6**| D). Thus, especially muscle bound Nep4 activity appears to be critical to proper *Drosophila* physiology and development.
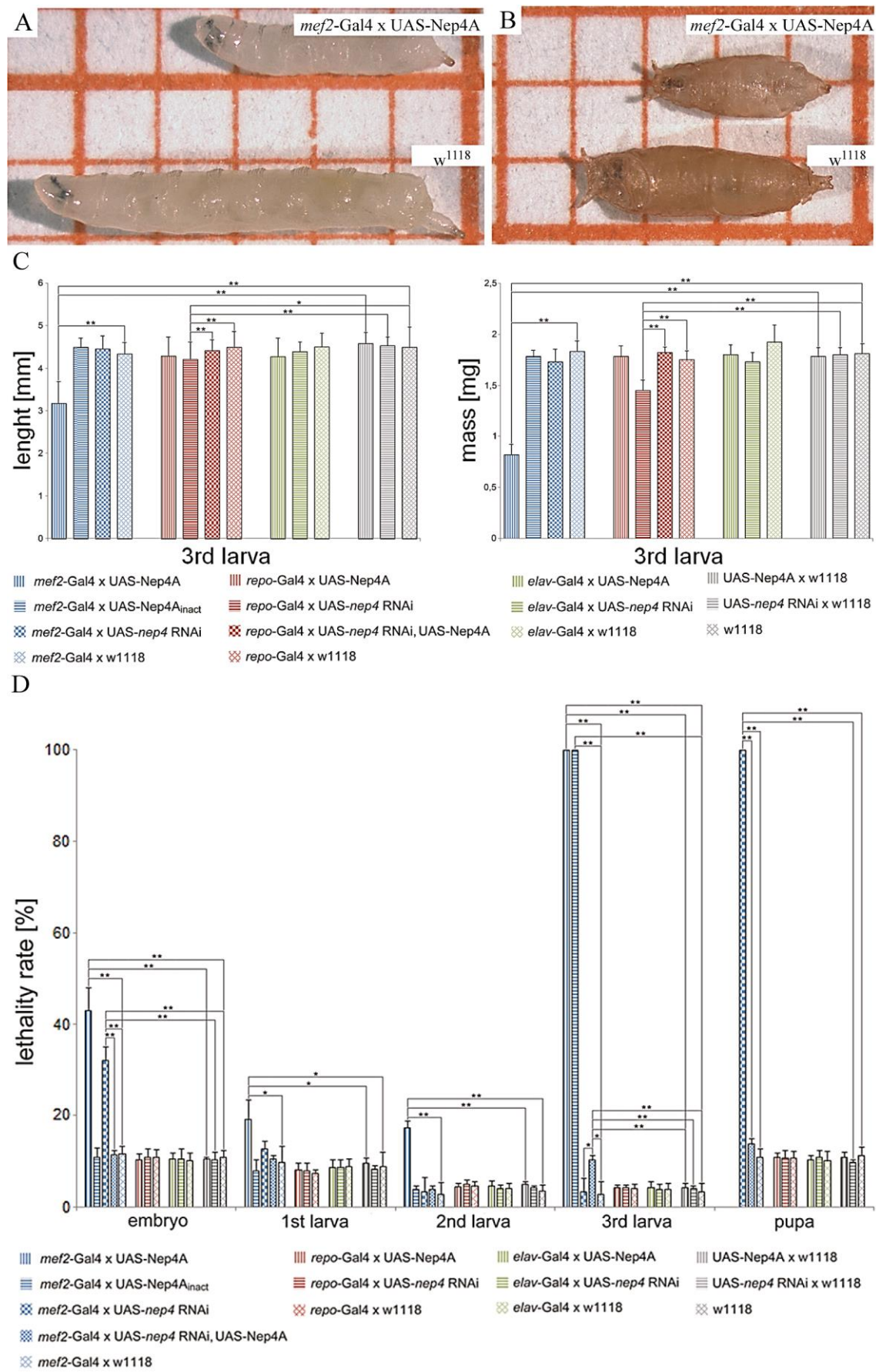
Figure 6| Altering *nep4* expression affects body size, weight and life span. A: Comparison of wildtype (w[1118]) and Nep4A overexpressing (*mef2*-Gal4 x UAS-Nep4A) 3rd instar larvae on

scale paper. Overexpression of Nep4A in the musculature leads to a severe decrease in size during development. **B:** Comparison of respective pupae (genotypes are the same as in A). Overexpression of Nep4A in musculature leads to a severe decrease in size during development. **C:** Size and weight measurements. Muscle specific overexpression of Nep4A (*mef2*-Gal4 x UAS-Nep4A) leads to a decrease in length and wet mass of 3rd instar larvae. Overexpression of a catalytically inactive Nep4A (*mef2*-Gal4 x UAS-Nep4A$_{inact)}$ as well as RNAi knockdown of *nep4A* (*mef2*-Gal4 x UAS-*nep4* RNAi) in muscle tissue shows no significant effect on body size or mass. Overexpression of Nep4A in glial cells or neurons (*repo*-Gal4 x UAS-Nep4A; *elav*-Gal4 x UAS-Nep4A) does not alter size or weight, which is also true for neuronal knockdown (*elav*-Gal4 x UAS-*nep4* RNAi). Downregulation of *nep4* in glial cells slightly reduces size and body weight. *mef2*-Gal4 x w1118, *repo*-Gal4 x w1118, *elav*-Gal4 x w1118, UAS-Nep4A x w1118, UAS-*nep4* RNAi x w1118, and w1118 were used as controls. (*P < 0.01, **P < 0.001, Student's t-test). **D:** Lethality assay. Shown are animals [%] of a specific developmental stage that did not reach the next respective stage. Muscle specific overexpression (*mef2*-Gal4 x UAS-Nep4A) leads to lethality during embryogenesis and late larval development. Overexpression of catalytically inactive Nep4A (*mef2*-Gal4 x UAS-Nep4A$_{inact}$) only leads to lethality in 3rd instar larval stage. Muscle specific knockdown of *nep4* showed an increased lethality rate during embryogenesis, but mostly during pupal stage. No effect on lifespan is visible in response to overexpression or knockdown of Nep4 in glial cells (*repo*-Gal4 x UAS-Nep4A; *repo*-Gal4 x UAS-nep4 RNAi) as well as neuronal overexpression or knockdown (*elav*-Gal4 x UAS-Nep4A; *elav*-Gal4 x UAS-*nep4* RNAi). As controls, the same lines as in **C:** were used. (*P < 0.01, **P < 0.001, Student's t-test). (modified after (Hallier et al., 2016))

3.1.2 Altering *neprilysin 4* expression in muscle tissue affects metabolite homeostasis

For a better understanding of Neprilysin 4 relevance to *Drosophila* physiology, the genotype-specific metabolite compositions in late larvae were analyzed via NMR – spectroscopy. Again, muscle specific *nep4* overexpression and knockdown were compared to control animals. As depicted in **Figure 7**, both, increase and downregulation of *nep4* expression results in a change in the overall composition of metabolites in respective transgenic 3rd instar larvae, compared to the wildtype metabolite composition (**Figure 7**| A).
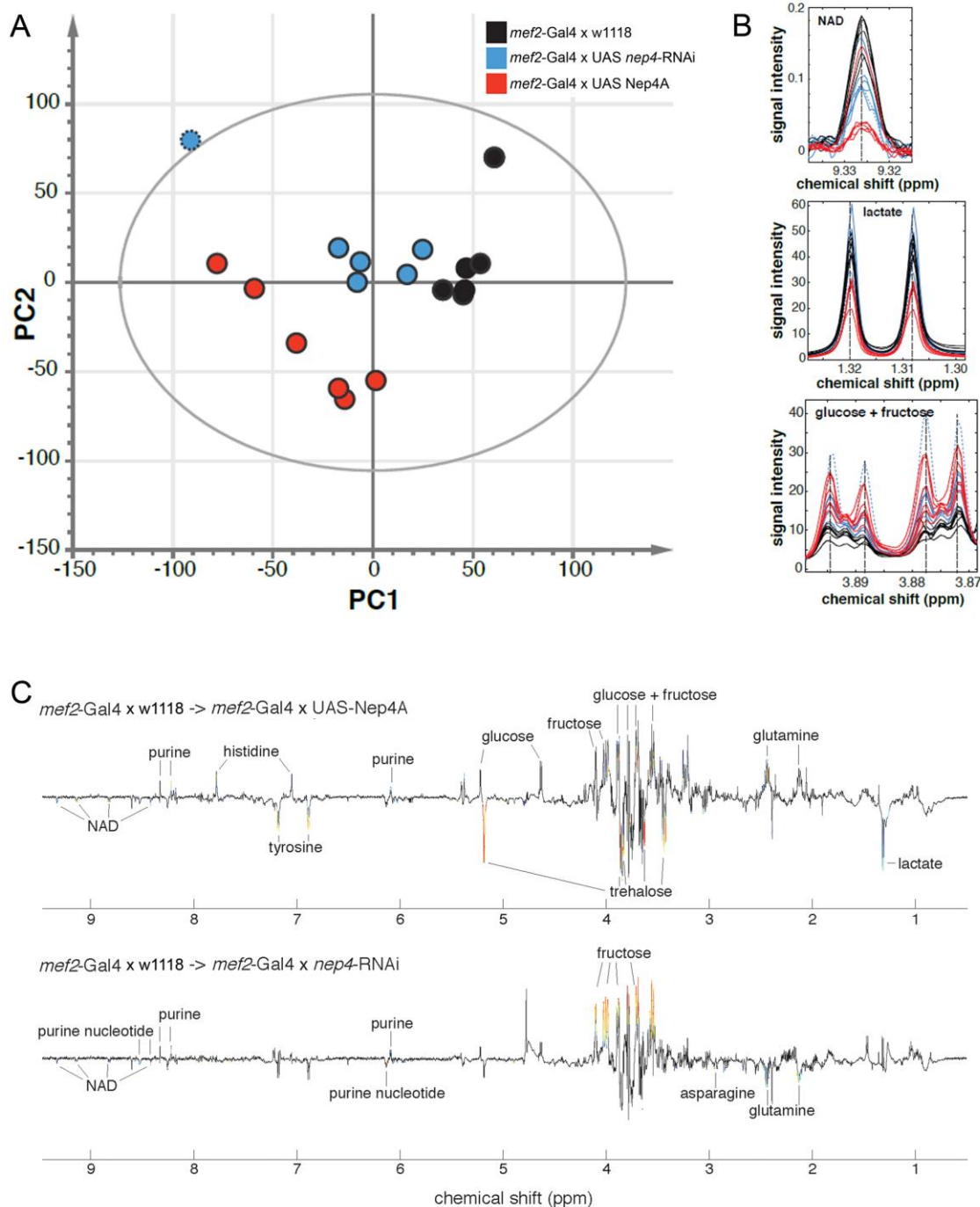
Figure 7| Modulation of muscle-specific expression of *neprilysin 4* disturbs metabolite homeostasis in 3rd instar larvae of *D. melanogaster*. A: NMR spectra based score plot. PCA (principal component analysis) score plot showing three genotypes (blue = *mef2*-Gal4 x UAS *nep4* RNAi, black = *mef2*-Gal4 x w^{1118}, and red = *mef2*-Gal4 x UAS-Nep4A), each representing the mean scores of 6 biological replicates. PCA was applied to identify metabolite changes in response to altering *nep4* expression in a muscle specific manner. The distribution of the scores on the blot shows a clustering of the biological replicates of each respective genotype. The only exception is one *nep4* knockdown score marked with a dotted border. This replicate was excluded from OPLS-DA identification of significantly affected metabolites. **B:** Examples of significantly affected metabolites (NAD, lactate and glucose / fructose). NAD and lactate concentrations are significantly reduced, whereas glucose and fructose concentrations are increased in Nep4A overexpression animals. *nep4* knockdown causes less severe changes in

metabolite composition, with NAD being reduced and fructose and glucose being slightly increased, compared to control animals. Color code is the same as in A. The knockdown outliner is marked with a dotted line. **C:** OPLS-DA loading plots summarizing the NMR spectral changes induced by *nep4* overexpression and knockdown. Shown are metabolic changes due to *nep4* overexpression or knockdown. Positive and negative signals represent elevated and reduced metabolite concentrations, respectively, with significant changes being colored from blue to red. Red indicates the highest variation between genotypes (Hallier et al., 2016).

Analysis of the dataset showed that many metabolites with altered concentrations in the transgenic samples are related to the energy metabolism. In Nep4A overexpressing animals, the individual signals of histidine, glutamine, and a purine, as well as the combined signals of fructose and glucose, are elevated. In *nep4* knockdown species the levels of fructose, NAD, a purine nucleotide, and glutamine are increased. On the other hand, lactate, NAD, trehalose and tyrosine are reduced in Nep4A-overexpressing mutants (**Figure 7**| B and C). Interestingly, decreased levels of NAD and lactate are a characteristic of impaired aerobic glycolysis. The aerobic glycolysis is a metabolic program starting about 12h before larval hatching. It enables larvae to generate biomass from dietary carbohydrates within a very short time frame. Utilizing this program, the larvae are able to sustain their considerable growth rate during larval development (Tennessen et al., 2014). Larval development without aerobic glycolysis would impair efficient metabolization of sufficient quantities of nutrients due to insufficient oxygen for common glycolysis. This leads to larval lethality (Tennessen et al., 2011). As depicted in **Figure 7**| B and C, Nep4A overexpressing flies exhibit substantially reduced lactate and NAD levels, indicating that altered expression of catalytic active Nep4A interferes with a proper aerobic glycolysis.

3.1.3 Neprilysin 4 activity regulates food intake and insulin-like peptide expression

Based on the fact that the results of the metabolomic assay are highly indicative of an impaired energy metabolism (**Figure 7**), energy uptake in form of dietary carbohydrates was analyzed. In this respect, particular attention was paid to a possible function of Nep4 in regulating food intake (**Figure 8**| A). Interestingly, overexpression of functional Neprilysin 4A in the musculature leads to a significantly reduced food intake in 3rd instar larvae. After 10min of feeding respective larvae exhibited 47% less food,

after 20min of feeding 59.5% less, and after 40min of feeding corresponding animals had accumulated 57% less food than control larvae (**Figure 8**| A). Muscle specific *nep4* knockdown did not affect food intake after 40min, but caused a delayed initiation of food intake. Corresponding larvae exhibited 52% less food intake after 10min and 28% less food intake after 20min, compared to control animals. Overexpressing catalytically inactive Nep4A did not affect feeding behavior, again indicating that enzymatic activity is crucial to the depicted overexpression phenotypes (**Figure 8**| A).

As shown previously, an increased level of glucose can be the result of impaired sugar uptake into body cells, which eventually leads to impaired metabolism. This might also be the case in Nep4A overexpression animals (**Figure 7**| B, C). Since insulin is critical to proper uptake of sugar into cells (Broughton et al., 2005; Rulifson et al., 2002) the expression levels of *Drosophila insulin-like peptides (dilps)* were measured in animals with altered *nep4* expression using quantitative real-time PCR (qRT-PCR) (**Figure 8**| B). The focus was laid on the peptides *dilp 1, 2, 3* and *5.* These encode the major insulin-like-peptides expressed in insulin producing cells (IPCs) within the CNS of *Drosophila* larvae (Brogiolo et al., 2001; Cao and Brown, 2001; Ikeya et al., 2002; Lee et al., 2008; Nässel et al., 2013; Rulifson et al., 2002). Ablation of the IPCs, which are located in the neurosecretory cell clusters of both brain hemispheres, leads to elevated levels of circulating glucose as well as to animals of decreased size and weight (Broughton et al., 2005; Rulifson et al., 2002). Interestingly, elevated glucose levels (**Figure 7**| B) concomitant with a reduction in size and weight (**Figure 6**| A-C) is also observed for Nep4A overexpressing larvae. In addition, transgenic larvae overexpressing Neprilysin 4A in muscles (*mef2*-Gal4 x UAS-Nep4A) exhibit a considerable reduction of the analyzed *insulin-like peptides*. *dilp1* expression is decreased by 59%, *dilp2* expression by 83%, *dilp3* expression by 88% and *dilp5* expression by 84%, compared to control expression levels (**Figure 8**| B). By contrast, muscle specific knockdown of *nep4* (*mef2*-Gal4 x UAS-*nep4* RNAi) reduced only expression of *dilp 2* by 82%, whereas *dilp1, 3 and 5* did not show any significant changes in their expression levels (**Figure 8**| B). Given these rather mild effects on *dilp* expression, it appears likely that yet unknown, redundant peptidases can compensate for the reduced Nep4 activity. In line with the results of the feeding assay and the size and weight measurements (**Figure 6**| A, B; **Figure 8**| A), ectopic expression of catalytically inactive Nep4A (*mef2*-Gal4 x UAS-Nep4Ainact) has no significant effect on *dilp*

expression in larvae. This result again confirms that altered enzymatic activity, and thus aberrant peptide hydrolysis, is crucial to all observed phenotypes.
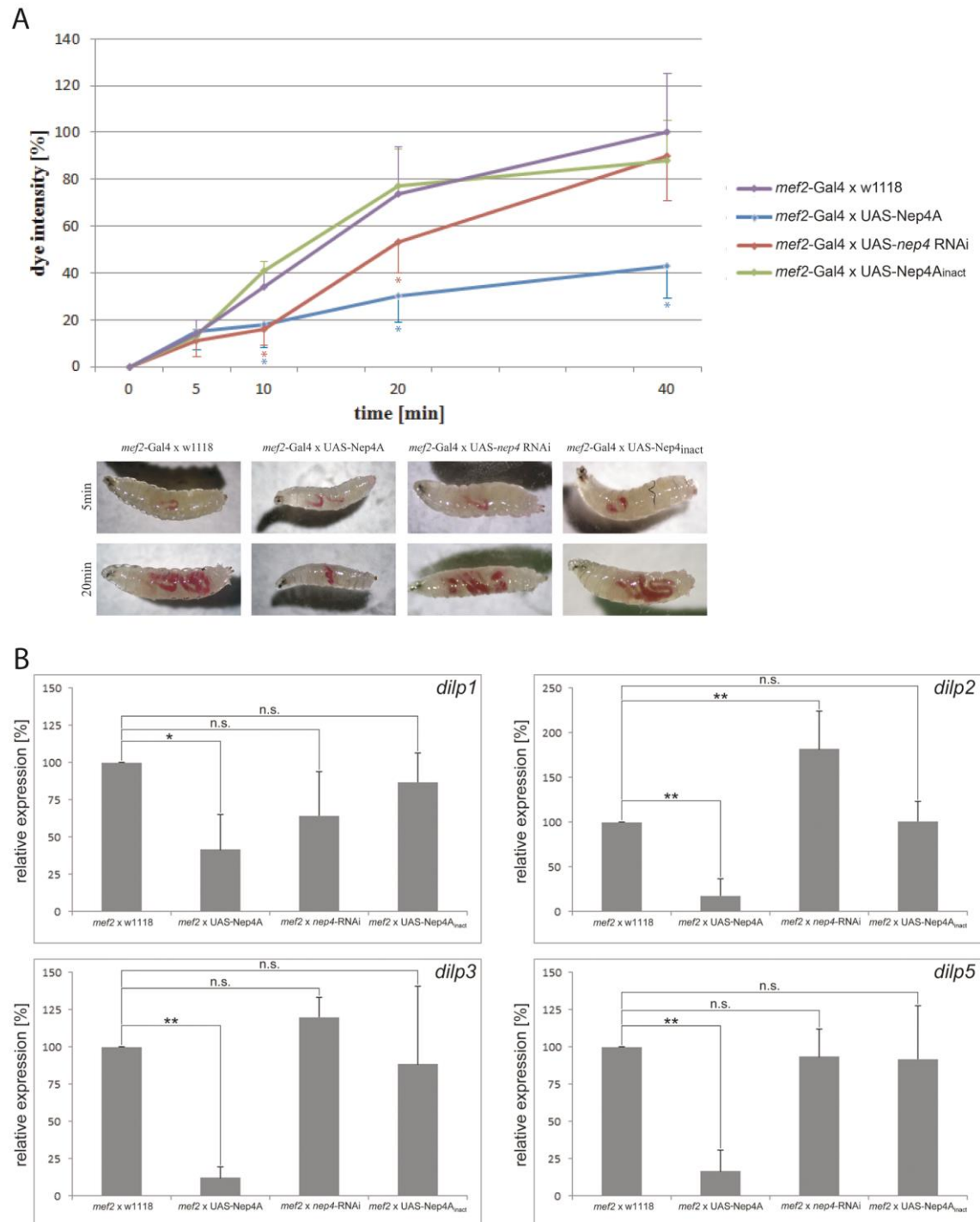
Figure 8| Modulation of muscle-specific expression of *neprilysin 4* reduces food intake and alters *dilp* expression in transgenic 3rd instar larvae of *D. melanogaster*. A: In the upper panel, the food intake of 3rd instar larvae with different genetic backgrounds is depicted in percentages (%), relative to the intake in control larvae (*mef2*-Gal4 x w[1118], purple). Nep4A overexpressing larvae (*mef2*-Gal4 x UAS-Nep4A, blue) show significantly reduced food intake at every time point measured. *nep4* knockdown animals (*mef2*-Gal4 x UAS-*nep4* RNAi, red)

exhibit significantly reduced feeding at 10min and 20 min. Animals with a muscle specific overexpression of catalytically inactive Nep4A (*mef2*-Gal4 x UAS-Nep4A$_{inact}$) exhibit no significant changes in food uptake. Values show the mean (+ / - s.d.) of at least 6 individual larvae of each genotype at each time point. Asterisks indicate significant differences in color intensity, compared to control animals. (*P > 0.05, Student's *t*-test). The lower panel shows representative examples of larvae from each genotype after 5 and 20 min of feeding. **B:** Expression levels of *dilp1, 2, 3* and *5* were measured via quantitative real-time PCR in 3rd instar larvae with different genetic backgrounds and compared to control larvae (*mef2*-Gal4 x w^{1118}). Nep4A overexpression in the musculature (*mef2*-Gal4 x UAS-Nep4A) causes a significantly decreased expression of every measured *dilp* in 3rd instar larvae. In contrast, *nep4* knockdown in the same tissue (*mef2*-Gal4 x UAS-*nep4* RNAi) causes an increased level of *dilp2*, whereas the other *dilp*s did not exhibit significant changes of expression levels in these transgenic larvae. Overexpression of catalytically inactive Nep4A (*mef2*-Gal4 x UAS-Nep4A$_{inact}$) results in no significant changes in the expression levels of the tested *dilp*s. Values represent the mean (+ / - s.d.) of at least six independent biological replicates. Asterisks indicate statistically significant deviations from controls (*P < 0.05, Student's t-test); n.s. indicates "not significant".(Hallier et al., 2016)

3.1.4 Neprilysin 4 localizes to the surface of larval body wall muscles and IPCs

Knowing that muscle-specific overexpression leads to severe phenotypes like decreased size and weight (**Figure 6**), impaired metabolism (**Figure 7**), impaired food intake and insulin expression (**Figure 8**), as well as lethality, the physiological explanation for these effects was addressed. To understand this issue, Nep4 localization studies were performed. As a result of these experiments, it was found that Neprilysin 4 localizes to body wall muscles in 3rd instar larvae. Within the musculature the peptidase localizes to the cell surface, as shown in **Figure 9** (arrows). Additionally, Nep4 accumulates at membranes surrounding the nuclei of the muscle cells; these membranes were already identified as being sarcoplasmic reticulum (SR) related (**Figure 9**| A (arrowheads) (Panz et al., 2012). Localizing Nep4 to the surface of body wall muscles indicates that the peptidase is required for regulating homeostasis of certain signaling peptides that circulate through the hemolymph.
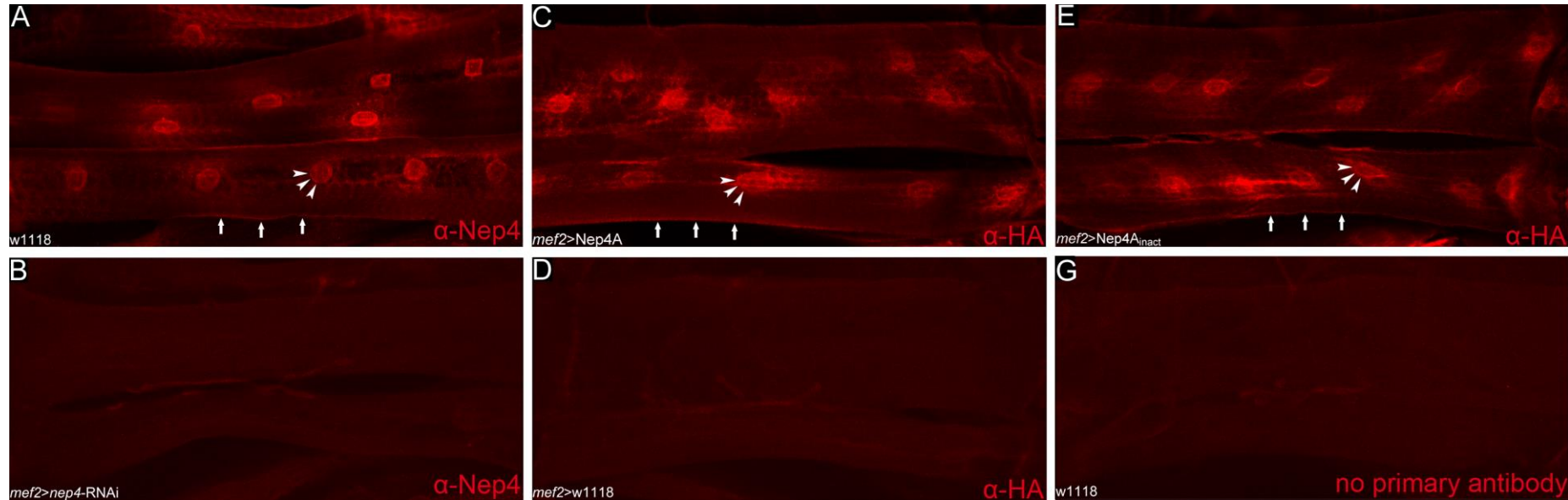
Figure 9| Neprilysin 4 localizes to the surface of muscle cells and to membranes of the sarcoplasmic reticulum. A: Nep4 protein was labeled using α-Nep4 antibodies (red). Nep4 accumulates at the surface of body wall muscles (arrows). Additionally, Nep4 accumulates at the sarcoplasmic reticulum surrounding the nuclei of muscle cells (arrowheads). **C, E:** Muscle-specific overexpression of HA tagged Nep4A (*mef2* > Nep4A) and HA tagged catalytically inactive Nep4A (*mef2* > Nep4A$_{inact}$). Labeling via an anti HA-tag antibody. The subcellular localization of both constructs is identical to the endogenous protein. **B:** Muscle-specific knockdown of *nep4* (*mef2* > *nep4*-RNAi) abolishes detection of endogenous Nep4. **D, G:** Control stainings do not exhibit any signal above background. Modified after (Hallier et al., 2016)

To assess whether overexpressed Nep4A behaves like the endogenous protein, HA tagged Nep4A constructs were expressed using the muscle specific driver *mef2*-Gal4 (*mef2*-Gal4>Nep4A-HA, *mef2*-Gal4>Nep4$_{inact}$-HA). Subsequently, anti-HA antibodies were used for labeling exclusively the ectopic protein but not endogenous Nep4. As depicted in **Figure 9**| C and E, Nep4A-HA and Nep4A$_{inact}$-HA clearly localize to the surface and the SR of body wall muscle cells, thus exhibiting the same localization pattern as endogenous Nep4. This result confirms that the observed phenotypes (**Figure 6**; **Figure 7**; **Figure 8**) are not caused by a false localization of the overexpressed proteins. *nep4* knockdown transgenes were also stained to assess the knockdown efficiency. In *mef2>nep4*-RNAi flies (**Figure 9**| B) no detection above background is visible using α-Nep4 antibodies. Furthermore, no signal is visible in a control line that does not express the UAS construct (*mef2*>w^{1118}) (**Figure 9**| D). In this experiment, detection was done using the HA antibody, thus confirming that no ectopic expression occurs without the UAS construct. In wildtype animals (w^{1118}) staining without primary antibodies did also not result in any distinct signal, which again confirms specificity of the applied antisera (**Figure 9**| G).

To characterize expression within the CNS, a reporter line was employed driving nuclear (n)GFP under the control of the endogenous enhancer of *nep4* (Meyer et al., 2009). Reporter gene expression is clearly detected within the two brain hemispheres and the ventral nerve cord (**Figure 10**| A, D, G). Within the hemispheres, expression is mainly obvious in the lamina, the central brain cells and in a few medulla cells (**Figure 10**| A, Brackets, dashed line and bar). Along the ventral nerve cord, the *nep4* reporter signal can be detected in numerous cells within every segment. Colocalization studies with anti-reversed polarity (Repo) antibodies, marking all glial cells (**Figure 10**| B, E, H), show that *nep4* is mainly expressed in glial cells (**Figure 10**| C, F, I). However, in the median region of the central brain only partial colocalization can be seen, indicating expression of *nep4* also in certain neurons.
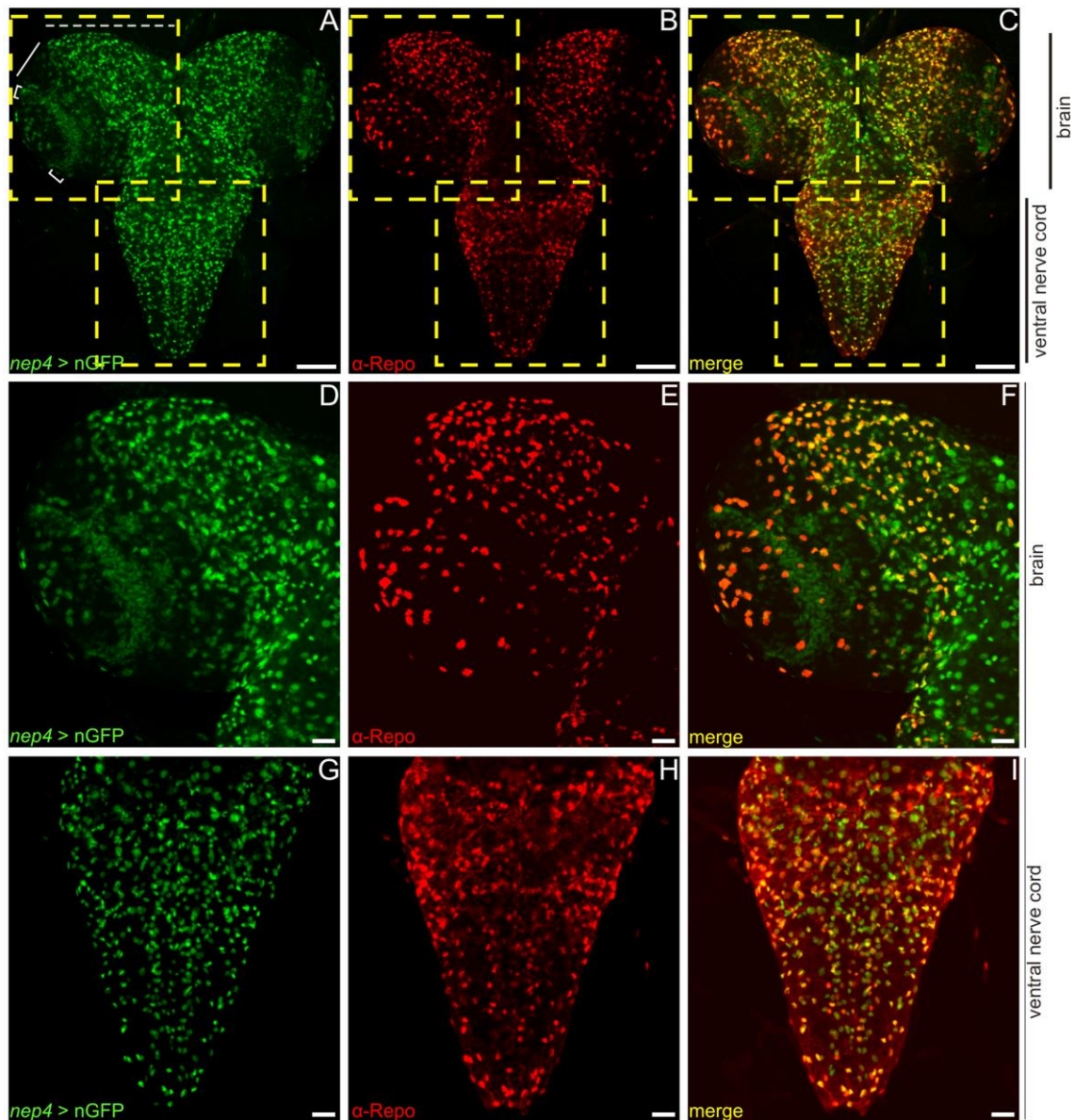
Figure 10| Expression of *neprilysin 4* in glial cells and neurons of the CNS. GFP is expressed using a reporter construct driving nuclear GFP (nGFP) under the control of the endogenous enhancer of *nep4* (*nep4* > GFP, green). Repo (Reversed polarity) was detected using monospecific antibodies (red) as a marker for glial cells. **A-C:** Optical projections of a 3rd instar larval brain, consisting of two brain hemispheres and a ventral nerve cord. View from dorsal, anterior up. Scale bar: 100µm. Yellow boxes represent areas of magnification, left hemisphere (depicted in **D-F**) and ventral nerve cord (depicted **G-I**). In the two brain hemispheres, strongest expression of *nep4* is obvious within the central brain (**A**, dashed line), and in lamina cells (**A**, brackets). Less *nep4* expressing cells are detected in the medulla (**A**, bar). Within the ventral nerve cord, *nep4* is expressed in numerous cells in all segments. **D-F:** Magnification of left brain hemisphere of a 3rd instar larva. Scale bar: 20µm. **G-I:** Magnification of ventral nerve cord. Scale bar: 20µm. **C**, **F** and **I**. *nep4* exhibits extensive co-localization with Repo (yellow). (Hallier et al., 2016)

To address the question, if *nep4* is expressed in insulin producing cells (IPCs), IPCs were marked using a *dilp2 (Drosophila insulin-like peptide 2)* reporter construct and compared on the one hand to *nep4* reporter gene expression (nGFP, **Figure 11**| A-C) and on the other hand to a Nep4 antibody staining (**Figure 11**| D-F). Colocalization of *dilp2* − specific reporter gene expression with *nep4-* specific reporter gene expression (**Figure 11**| C) confirms that *nep4* is expressed in IPCs, which reside within the median neurosecretory cell cluster of the brain hemispheres. Both reporter constructs express nuclear localized fluorophores, thus colocalization is obvious in the corresponding IPC nuclei. The Nep4 antibody staining reveals that the peptidase localizes to the surface of the insulin producing cells (**Figure 11**| F). Based on fluorescence intensity measurements (**Figure 11**| D-F and panels below) an increased intensity of the Nep4 signal (red) at the cell surface and a decreased Nep4 signal intensity within the cytoplasm of the IPCs becomes evident. On the other hand, intensity of the green signal (cytoplasmic GFP driven by the *dilp2* enhancer) is high within the cytoplasm of the IPCs, but very low at the surface of these respective neurons.
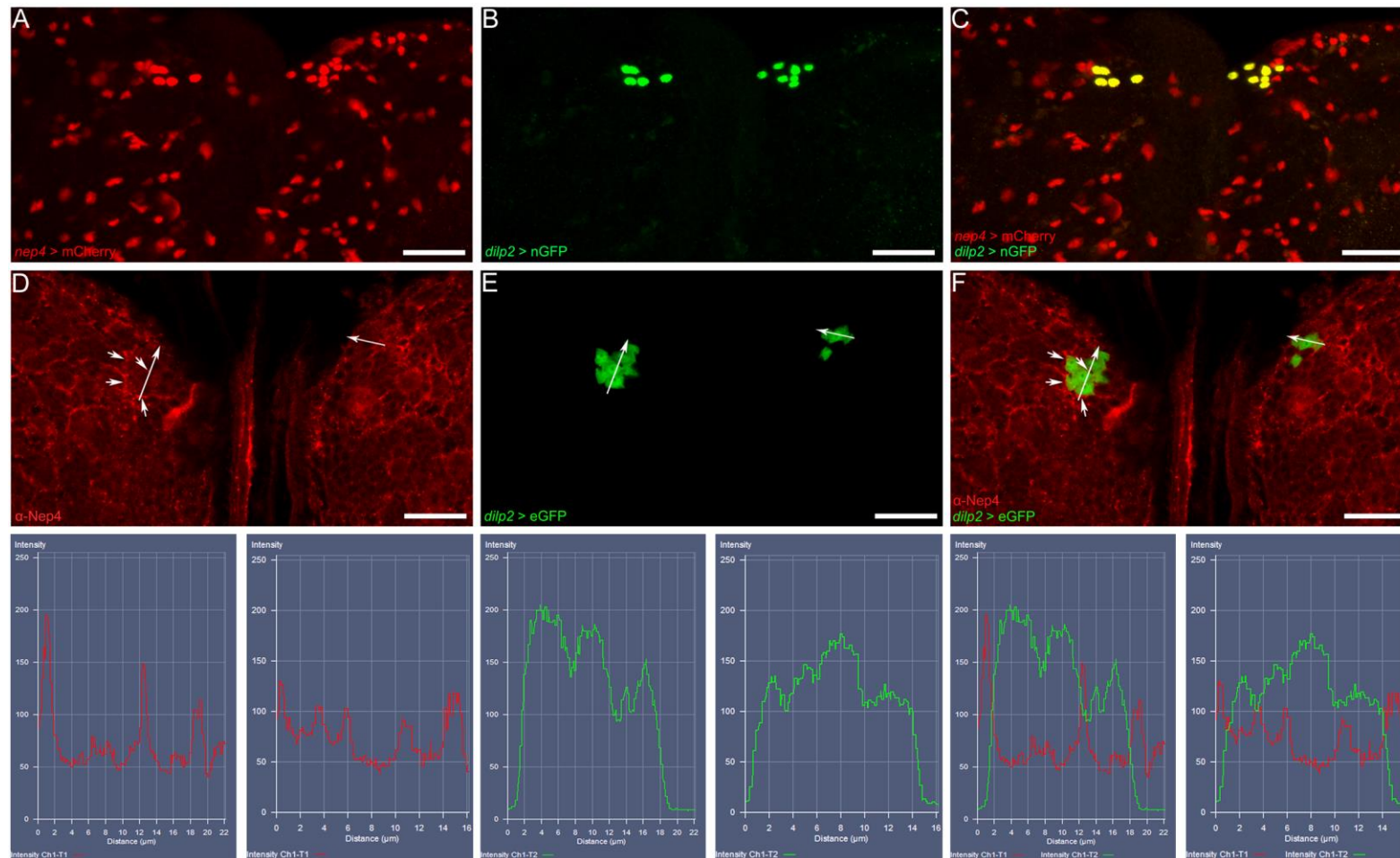
Figure 11| Nep4 localizes to the surface of insulin producing cells within the larval brain. **A, C**: Nuclear mCherry expression resembling the expression pattern of *nep4* (*nep4 > mCherry*, red). **B, C**: nGFP expression under the control of the *dilp 2* enhancer (*dilp2 > nGFP*, green). **A-C**: Optical sections (10μm) of a 3rd instar larval central brain. Scale bars: 20 μm; dorsal view, anterior up. *nep4* and *dilp2* expression colocalize in IPCs.

D-F: Nep4 protein was detected using monospecific antibodies (red). *dilp2* expression was visualized using an eGFP reporter line (*dilp2 > eGFP*, green). (**D–F**) Optical sections (10 μm) of a 3rd instar larval central brain. Scale bars: 20 μm; dorsal view, anterior up. Nep4 is detected at the surface of numerous cells, including IPC's (arrowheads). Nep4 subcellular localization was assessed using fluorescence intensity measurements (lower panel) along the arrows depicted in **D-F** (Hallier et al., 2016).

3.1.5 Nepilysin4 colocalizes with the short Neuropeptide F-receptor

Localization of Nep4 to the plasma membrane of insulin producing cells within the CNS is highly indicative for a function of Nep4 in regulating the IPC adjacent extracellular peptide composition. For a more detailed characterization of this activity, the regulatory influence of Nep4 on short neuropeptide F (sNPF) and its receptor (sNPFR) was investigated. As shown for Nep4 (**Figure 11**) the sNPFR is also expressed in IPCs and localizes to the cell surface (Lee et al., 2008). sNPF signaling has been shown to regulate the expression of *dilps* in an extracellular signal-regulated kinase (ERK) dependent manner. Lee et al., (2008) showed that increased sNPF levels result in an upregulation of *dilp* expression, while a reduced sNPF level causes decreased *dilp* expression. The fact that this characteristic phenotype of decreased sNPF is phenocopied by Nep4 overexpression (**Figure 8**) indicates a functional relation between peptide and peptidase.

The short neuropeptide F precursor (sNPFp) protein is mainly expressed in Kenyon cells of the lateral neurosecretory cells (LNCs) and in the lobes of the mushroom body. Furthermore, cells forming longitudinal tracts within the ventral nerve cord (VNC) as well as segmentally distributed neurons of the abdominal neuromers express sNPFp (Nässel et al., 2008). The expression pattern of the sNPF receptor (**Figure 12**| B, E, H) differs from the expression pattern of its peptide ligand. The receptor is expressed in lateral and median neurosecretory cells of larval brains. In addition, it is expressed in ventro-medially and ventro-laterally located large cell bodies within the first abdominal segments of the VNC (**Figure 12**| B, E, H; Carlsson et al., 2013). As depicted above, Nep4 is also expressed in both compartments of the CNS, the brain hemispheres and the VNC (**Figure 10**-

Figure 12). Interestingly, expression of *snpfr* and Nep4 colocalize in numerous cells of the CNS (**Figure 12**| C, F, I). Strongest colocalization is detected in the lateral and the median neurosecretory cells (LNC, MNC; **Figure 12**| D-F). Incidentally, Nep4 antibodies were used to detect the plasma membrane bound peptidase, while *snpfr* expression was visualized with a specific eGFP-reporter construct. This explains, why in cells exhibiting colocalization, the red signal (Nep4) is located around the cytoplasmic green signal (*snpfr* > eGFP).
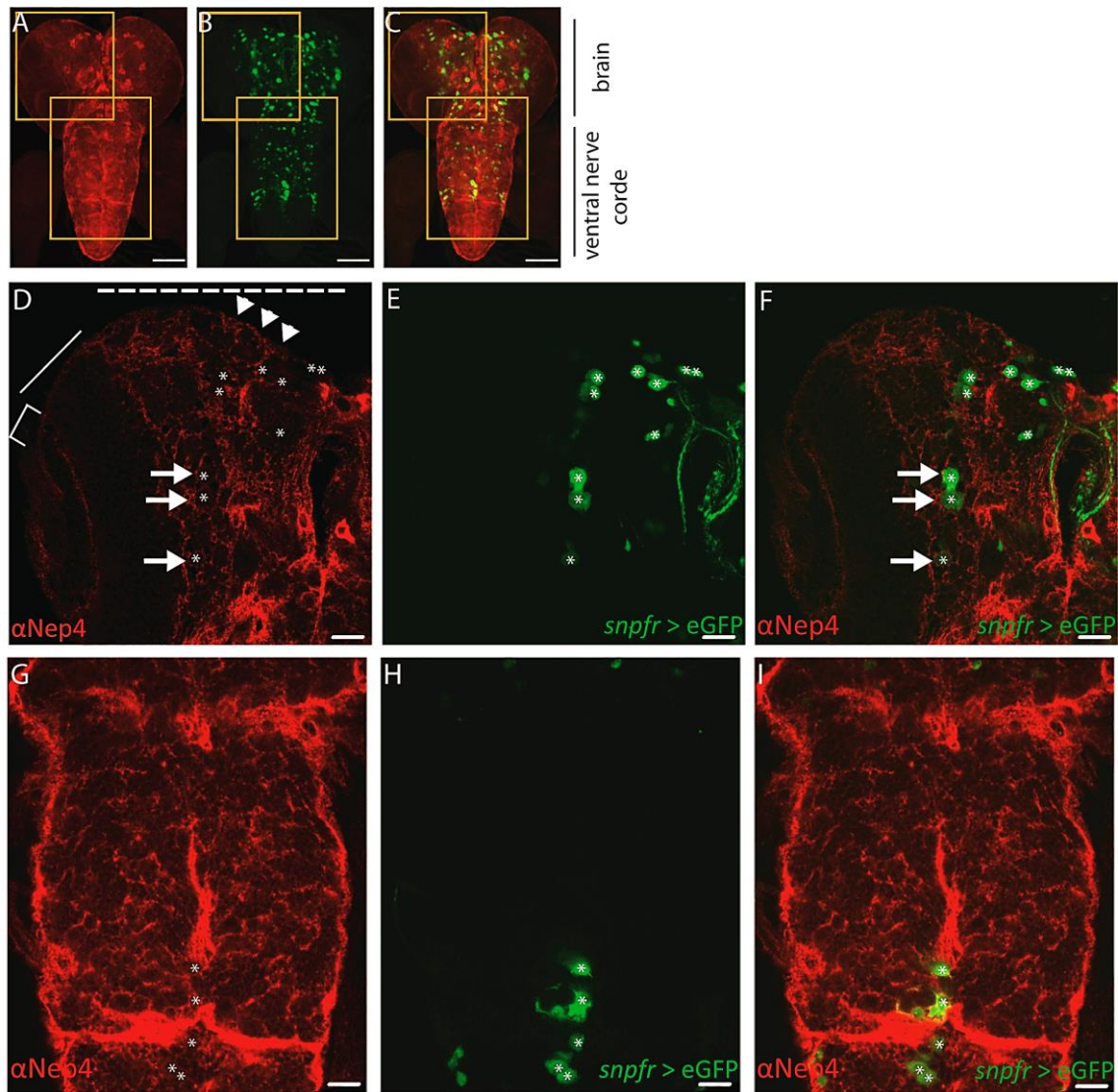
Figure 12| Nep4 colocalizes with *snpfr* expression. Nep4 protein was labeled using monospecific α-Nep4 antibodies (Panz et al., 2012) (red). *snpfr* expression was visualized by a reporter construct driving eGFP (green) in a *snpfr* specific manner. **A-C:** Optical projections of a 3rd instar larval whole brain hemispheres and ventral nerve cord complex. 100μm scale bars, dorsal view, anterior up. Boxes indicate areas of higher magnification as depicted in **D-F** and **G-I. D-F:** 2 μm optical sections of a 3rd instar larval brain hemisphere. 20 μm scale bars, dorsal surface of brain, anterior up, midline to right. **D:** Nep4 is mainly expressed at the surface (arrowheads) of the central brain (dashed line), while expression is considerably reduced in medulla (bar) and lamina cells (bracket). Increased expression is also visible in cells comprising the lamina furrow. **F:** Nep4 and *snpfr* colocalize in numerous cells of the central brain (asterisks), particularly in lateral neurosecretory cells (LNC) as well as median neurosecretory cells (MNC). Nep4 is detected in the plasma membrane (arrows) and *snpfr* expression in the cytoplasm (asterisks). **G-I:** 2 μm optical sections of a 3rd instar larval ventral nerve cord (VNC). 20 μm scale bars, dorsal surface of VNC, anterior up. **G** and **I**: Nep4 is expressed along the surface of the VNC, while only a few *snpfr* expressing cells (asterisks) are detected (**H, I**).

3.1.6 Neprilysin 4 catalyzes sNPF hydrolysis

To further investigate a possible physiological relation between short neuropeptide F and Nep4 it was analyzed whether the peptidase is able to hydrolyze the peptide. As a result of the proteolytic cleavage of a larger precursor protein, a number of different sNPF species are present in *Drosophila* and other insects (Baggerman et al., 2005; Dillen et al., 2013; Garczynski et al., 2006; Predel et al., 2004; Wegener et al., 2006,
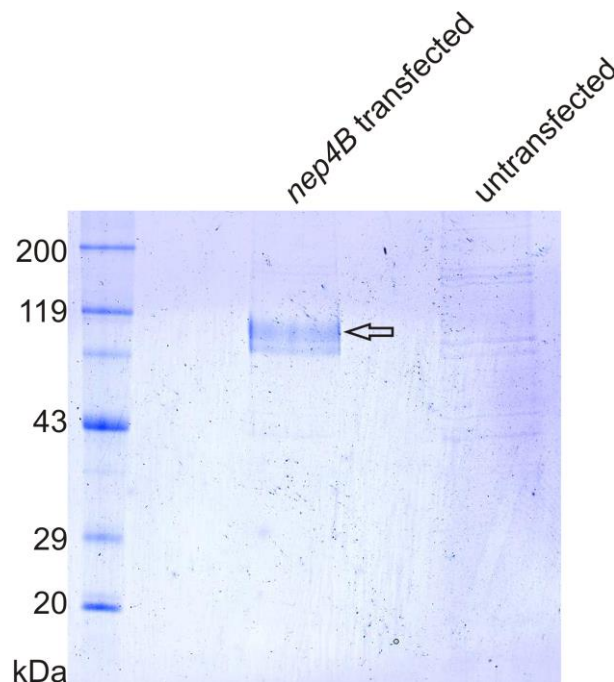
Figure 13| Purified Nep4B from transfected SF21 cells. SDS-PAGE stained with coomassie-blue. The left lane shows the molecular weight marker. The middle lane shows an elution fraction of the Ni^{+}-NTA purification of Nep4B (ca. 113kDa). The right lane shows an elution fraction after Ni^{+}-NTA purification of untransfected SF21 cells. (Hallier et al., 2016)

2008; Yew et al., 2009). sNPF1$_{1-11}$ corresponds to the sequence AQRSPSLRLRFa. The peptide SPSLRLRFa corresponds to sNPF1$_{4-11}$ and sNPF2$_{12-19}$. The sequences of sNPF3 and sNPF4, also arising from the sNPF precursor protein, are KPQRLRWa and KPMRLRWa (Nässel and Winther, 2010). All respective peptides were tested for cleavage by Nep4. The soluble isoform Nep4B, containing an identical catalytic center as Nep4A, was expressed in SF21 insect cells and purified via affinity chromatography (Ni^{+}-NTA-column). As a control, the same purification was performed using untransfected SF21 cells. After purification of Nep4B, an SDS-PAGE followed by coomassie-staining was done. The fraction from the transfected cells shows a strong band exhibiting the predicted mass of Nep4B (ca. 113kDa (Meyer et al., 2009)). The

fraction isolated from untransfected cells contains only faint background bands (**Figure 13**).
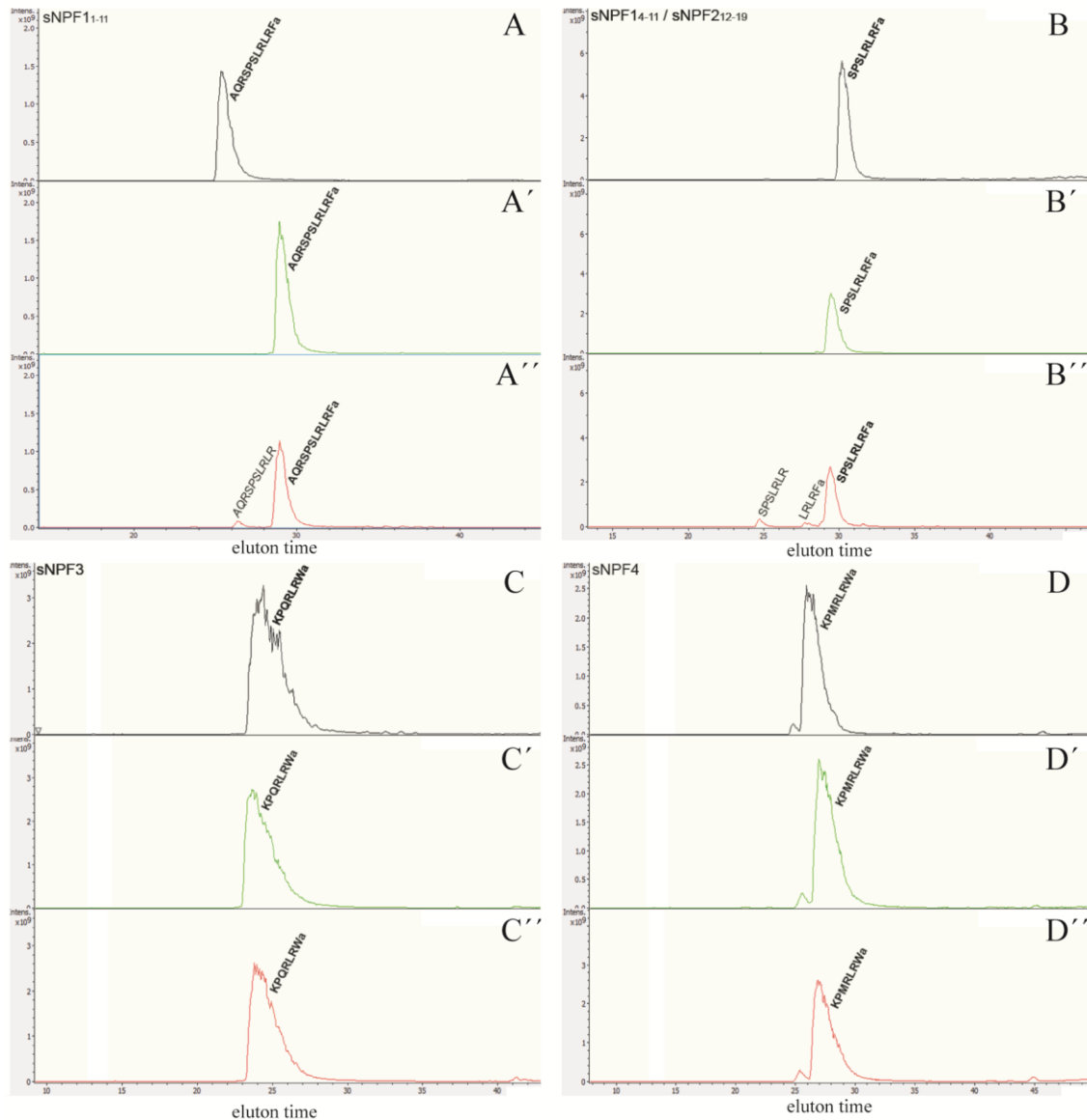
Figure 14| Nep4 catalyzes cleavage of sNPF. A: Base peak all MS chromatogram of short Neuropeptide F1$_{1-11}$. sNPF1$_{1-11}$ is detected with expected mass (1328.8 Da) and sequence (AQRSPSLRLRFa). **A´:** Base peak all MS chromatogram of sNPF1$_{1-11}$. sNPF1$_{1-11}$ incubated with a control preparation isolated from untransfected SF21 cells. sNPF$_{1-11}$ is detected with expected mass (1328.8 Da) and sequence (AQRSPSLRLRFa). **A´´:** Base peak all MS chromatogram of sNPF1$_{1-11}$ incubated with purified Nep4B. sNPF1$_{1-11}$ is detected in an uncleaved form (right peak (1328.8 Da; AQRSPSLRLRFa)) and a cleaved form (left peak (1026.6 Da AQRSPSLRL)). **B:** Base peak all MS chromatogram of sNPF1$_{4-11}$/sNPF2$_{12-19}$. sNPF1$_{4-11}$/sNPF2$_{12-19}$ is detected with expected mass (973.6 Da) and sequence (SPSLRLRFa). **B´:** Base peak all MS chromatogram of sNPF$_{4-11}$/sNPF$_{12-19}$ incubated with a control preparation isolated from untransfected SF21 cells. sNPF1$_{4-11}$/sNPF2$_{12-19}$ is detected with expected mass (973.6 Da) and sequence (SPSLRLRFa). **B´´:** Base peak all MS chromatogram of sNPF$_{4-11}$/sNPF$_{12-19}$ incubated with purified Nep4B. sNPF$_{4-11}$/sNPF$_{12-19}$ is detected in an uncleaved form (right peak (973.6 Da; SPSLRLRFa)) and two cleaved forms (left (SPSLRLR; 827, Da) and middle peak

(LRLRFa; 702,5 Da)). **C, D:** Base peak all MS chromatogram of sNPF3 and sNPF4 (KPQRLRWa 981.6 Da and KPMRLRWa 984.6 Da). **C´, D´:** Base peak all MS chromatogram of sNPF3 and sNPF4 (KPQRLRWa 981.6 Da and KPMRLRWa 984.6 Da) incubated with a control preparation isolated from untranfected SF21 cells. **C´´, D´´:** Base peak all MS chromatogram of sNPF3 and sNPF4 incubated with purified Nep4B. sNPF3 and sNPF4 are detected exclusively in an uncleaved form ((KPQRLRWa 981.6 Da and KPMRLRWa 984.6 Da). Modified after (Hallier et al., 2016)

sNPF peptides were incubated with control preparations or purified Nep4B. Subsequently, the rate of Nep4 mediated hydrolysis was measured via mass spectrometry (**Figure 14**). Incubation of sNPF1$_{1-11}$ with Nep4B reveals that the peptidase is able to hydrolyze the peptide in a highly efficient manner (**Figure 14**| A´´), whereas incubation with a control preparation lacking Nep4B had no effect (**Figure 14**| A´). sNPF1$_{1-11}$ (AQRSPSLRLRFa, 1328.8 Da) is cleaved at a specific position (between Arg^{10} and the terminal Phe^{11}). The remaining peptide AQRSPSLRLR has a mass of 1026.6 Da. The peptide sNPF1$_{4-11}$/ sNPF2$_{12-19}$ (SPSLRLRFa, 973.6 Da) is hydrolyzed by Nep4B at two specific positions, resulting in two individual cleavage products: SPSLRLR (ca. 827.5 Da) and LRLRFa (ca. 702.5 Da) (**Figure 14**| B´´). Again no background cleavage is measurable in the control preparation (**Figure 14**| B´). Cleavage occurs between Arg^7 and Phe^8 and between Ser^3 and Leu^4. Incubation of sNPF3 and sNPF4 with Nep4B did not result in specific cleavage products, thus these peptides are not hydrolyzed by the neprilysin (**Figure 14**| C, C´, C´´, D, D´, D´´).Noteworthy, up to now almost nothing is known on how sNPF activity is regulated. By confirming Nep4 mediated cleavage of distinct sNPF1 and sNPF2 species, this thesis demonstrates that enzymatic hydrolysis represents an important factor. In addition, the described cleavage may be the physiological explanation for the phenotypes depicted above (**Figure 6; Figure 7; Figure 8**).

3.2 Characterization of *neprilysin 4* mutant alleles and their effects on the development of *Drosophila melanogaster*

In this thesis two *neprilysin 4* mutant alleles were characterized. On the one hand, a line generated by the *Drosophila* Gene Disruption Project (Bellen et al., 2011) was characterized. On the other hand, a mutant allele created in the course of this thesis via the CRISPR/CAS9 method was investigated.

3.2.1 Line BL36979 harbors a truncated *neprilysin 4* allele

The Line BL36979 (y[1] w[*]; Mi{y[+mDint2]=MIC}Nep4[MI03765]) was created by Bellen et al. (2011) and originates from the *Drosophila* Gene Disruption Project (GDP), a collection of publicly accessible mutant strains containing single transposon insertions within individual genes. In the respective line a Dhyd\minos based Mi{MIC} transposon is inserted in the second exon of the *nep4* gene (*nep4*[MI03765]).

In order to localize the position of the Mi{MIC} transposon within the *nep4* gene exactly, genomic DNA of the respective line BL36979 was isolated from adult homozygous flies and sequenced. In this effort a forward primer was used, which binds about 300bp upstream of the Mi{MIC}element, and a reverse primer binding ca. 1 kbp downstream of the Mi{MIC} 5´-end.
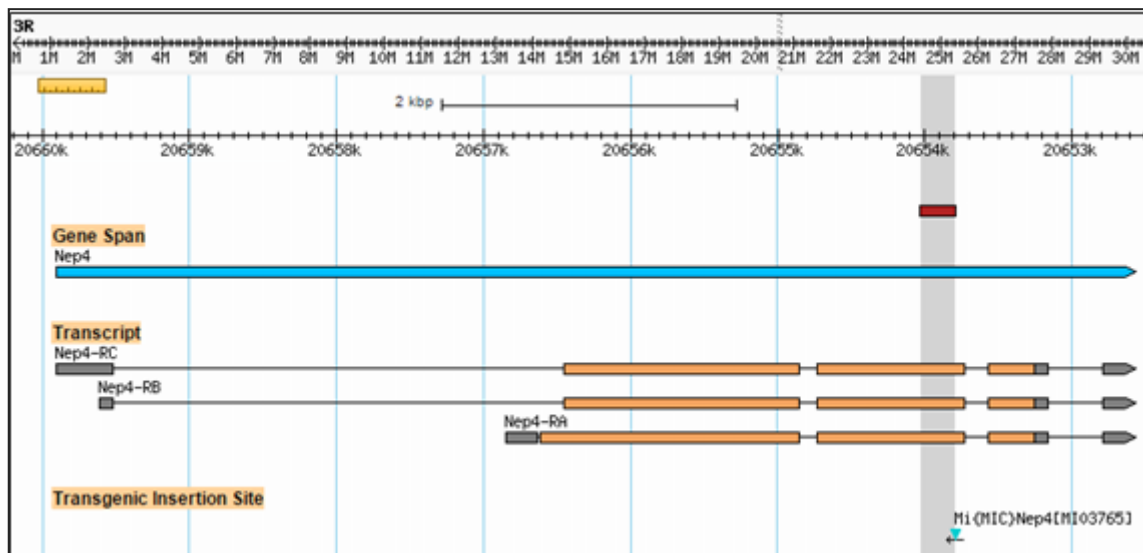
Figure 15| Scheme of the *nep4* locus including transcript variants in *Drosophila*. Three different transcripts are expressed from the *nep4* gene. Two of them, *nep4B* and *nep4C,* have identical coding sequences. The sequence flanking the inserted Mi{MIC} element is present in all transcripts and depicted in grey.

As a result, the insertion point of the Mi{MIC} element could be exactly defined: it is located 2730 bp downstream of the *nep4A* start codon (**Figure 15**). In silico translation of the resulting sequence showed that in line BL36979 all Nep4 isoforms are C-terminally truncated by 130 amino acids (aa). This truncation includes one of the two motifs that are critical to catalytic activity. At the C-terminus, 33 aa are added based on the Mi{MIC} sequence, until translation is terminated by a stop-codon (**Figure 16**). The Nep4A isoform in line BL36979 (Nep4[MI03765]A) has a calculated mass of 108.8 kDa.
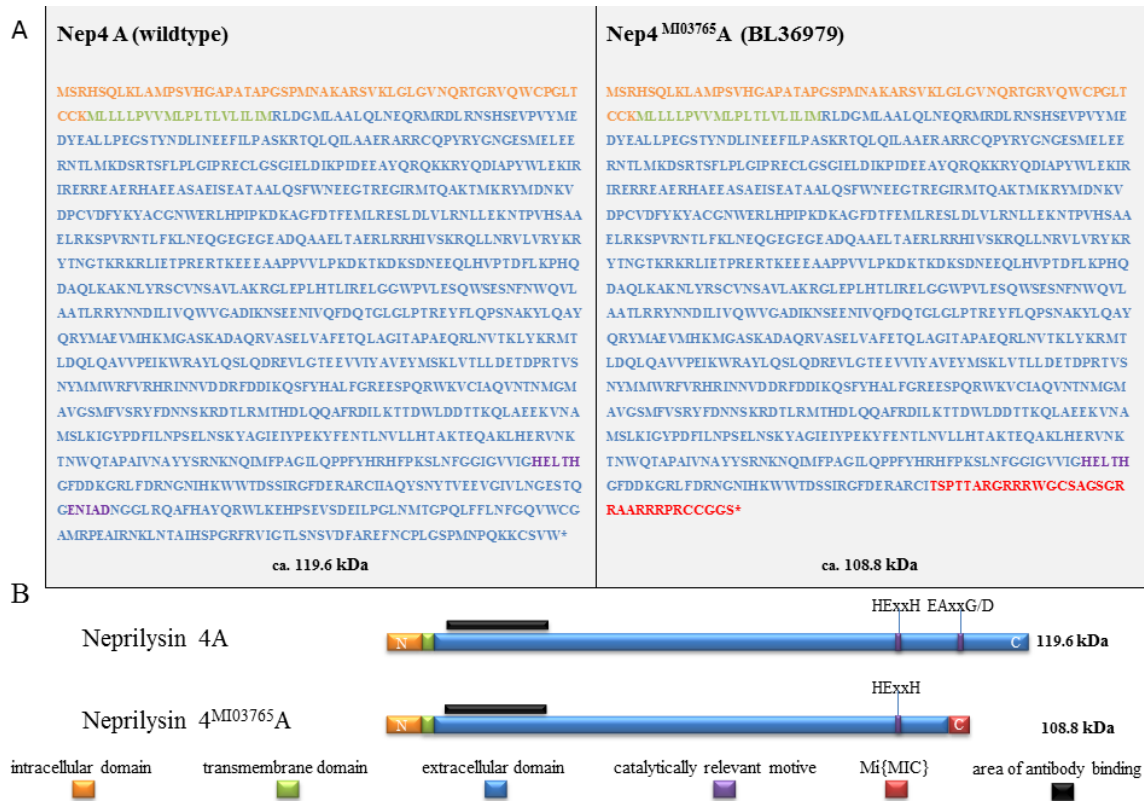
Figure 16| Amino acid sequences of wildtype Nep4A and Nep4^MI03765A. A: Comparison of the amino acid sequence of wildtype Nep4A (flybase.org) with the sequence of Nep4A in line BL36979. Wildtype Nep4A is 1040 amino acids long and has a calculated mass of 119.6 kDa. The amino acids marked in orange and green represent the extracellular and transmembrane domain of Nep4A, respectively. The sequence of the extracellular domain is marked in blue and the catalytically relevant motifs of the peptidase are marked in purple. Nep4A in line BL36979 (Nep4^MI03765A) is 943 amino acids long and C-terminally truncated. Its calculated mass is 108.8 kDa. The intracellular domain and transmembrane domain are marked in orange and green, respectively, the extracellular domain in blue and the catalytically relevant motifs in purple. After 910 amino acids the Mi{MIC}-Transposon sequence starts. 33 transposon derived amino acids are added to the Nep4 sequence (depicted in red) until a stop-codon terminates translation (red asterisk). **B:** Schematic representation of Nep4A and Nep4^MI03765A proteins. Intracellular domain (orange), transmembrane domain (green), extracellular domain (blue) containing the motifs that are critical to enzymatic activity (purple), and the Mi{MIC}-Transposon fragment (red) are indicated. Black bar indicates area of Nep4 antibody binding.

In order to confirm the sequence based data on the Nep4 protein composition in line BL36979 (**Figure 16**), as a next step western blots were performed to assess the size and maintenance of the truncated protein. In this effort, total protein extract was isolated from homozygous mutant adult BL36979 males and control males (w^{1118}). As depicted in **Figure 17**, compared to wildtype Nep4A, the protein from Line BL36979 is detected and slightly reduced in size. The shift corresponds to the sequence based anticipation (wildtype Nep4A: 119 kDa, truncated Nep4A: 109 kDa).
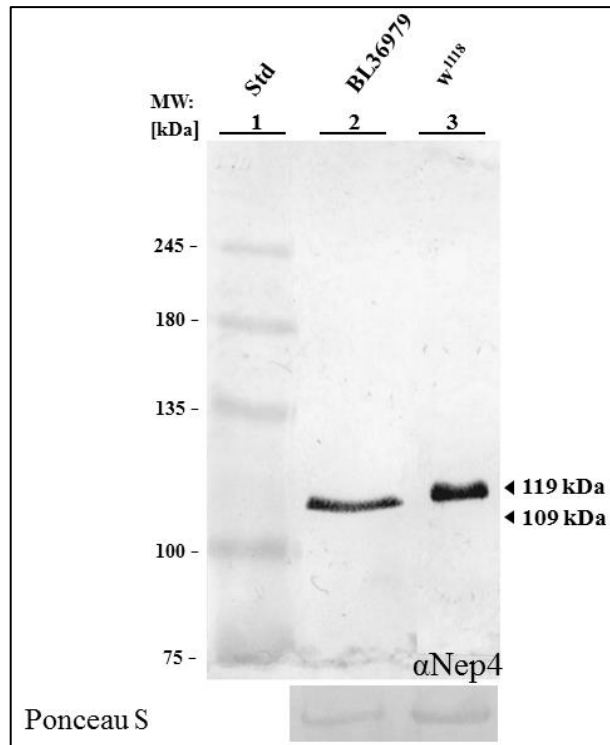
Figure 17| Western blot of adult male total protein extracts from lines w¹¹¹⁸ and BL36979 (homozygous mutant). The western blot shows the detection of Nep4 in total protein extracts isolated from adult male flies of two genotypes. The first lane depicts the molecular weight marker. Ponceau S staining is shown as a loading control. The detected Nep4 protein in lane 2 (BL36979) shows a lower molecular mass compared to the detected Nep4 in the wildtype sample (line 3, w^{1118}).

3.2.1.1 Effects of Nep4 truncation on embryogenesis

After showing that line BL36979 produces a truncated Nep4 protein, which lacks a conserved motif essential to its catalytic activity, it was further investigated if the lack of this activity affects embryonic development. Initially, line BL36979 was rebalanced over a TDLZ balancer on the third chromosome, carrying a wildtype *nep4* allele. Embryos were collected and stained for distinct tissue markers to investigate the development of animals homozygous for the *nep4*^{MI03765} allele in comparison to heterozygous animals carrying a *nep4*^{MI03765} allele and a wildtype *nep4* allele (due to the balancer chromosome). The TDLZ balancer chromosome harbors a *lacZ* reporter gene coding for a β-Galactosidase. Consequently, simultaneous staining of the β-Galactosidase allows for differentiation of *nep4*^{MI03765} homozygous and heterozygous animals.

Animals stained for Nep4 (**Figure 18|** A, A´) show an expression pattern as described earlier (Meyer et al., 2009). In both genotypes expression can be detected within the

even-skipped positive pericardial cells, within the dorsal vessel as well as in the ventral and lateral cells of the CNS. The expression pattern and the development of the marked organs seem comparable. Only small differences between the two genotypes can be seen, probably due to biological variability or due to slightly different developmental stages. Most importantly, Nep4 was detected also in animals homozygous for the truncated $nep4^{MI03765}$ allele, again indicating transcription and translation of the truncated $Nep4^{MI03765}$ protein. A tissue Nep4 is also expressed in is the somatic musculature. It was shown that elevated levels of Nep4 in body wall muscles result in a degeneration phenotype and that knockdown of $nep4$ in this tissue affects larval movement (Panz et al., 2012). Therefore, the development of the musculature was further investigated in the Nep4 Mi{MIC} insertion mutant. Using an anti β3Tubulin antibody the musculature in both genotypes was stained (**Figure 18|** B, B´). In all animals tested the staining shows the esophagus (es) and the contractile ventricle and aorta of the dorsal vessel. The somatic body wall muscle tissue can be seen segmentally around the whole embryo. Muscle development in both genotypes showed no abnormalities and the body wall muscles in the homozygous mutants are properly formed during embryogenesis. In addition to somatic muscles Nep4 is expressed within the CNS (Meyer et al., 2009). Thus, the development of neuronal cells was studied using Fascilin2 staining as a neuronal marker (**Figure 18|** C, C´). Comparing control animals and homozygous mutants revealed that formation of the neurons in the CNS and their axon distribution in the PNS (peripheral nervous system) is identical in both genotypes. Subsequently, the formation of glial cells was investigated analogously (**Figure 18|** D D´). Reverse polarity (Repo) is a widely used glial cell marker. Embryos stained against Repo confirmed that the glial cells along the ventral midline as well as the lateral glial of the PNS develop normal in homozygous mutant animals. During embryogenesis Nep4 is expressed in even-skipped positive pericardial cells (Meyer et al., 2009). To investigate if the formation of the heart is affected in animals expressing only truncated $Nep4^{MI03765}$, the respective animals were stained for Odd-skipped, a marker that labels, among other cells, Odd-skipped positive pericardial cells (**Figure 18|** E, E´). Corresponding stainings confirmed that formation of the dorsal vessel, including pericardial cells, is not affected in the $nep4$ mutant line.
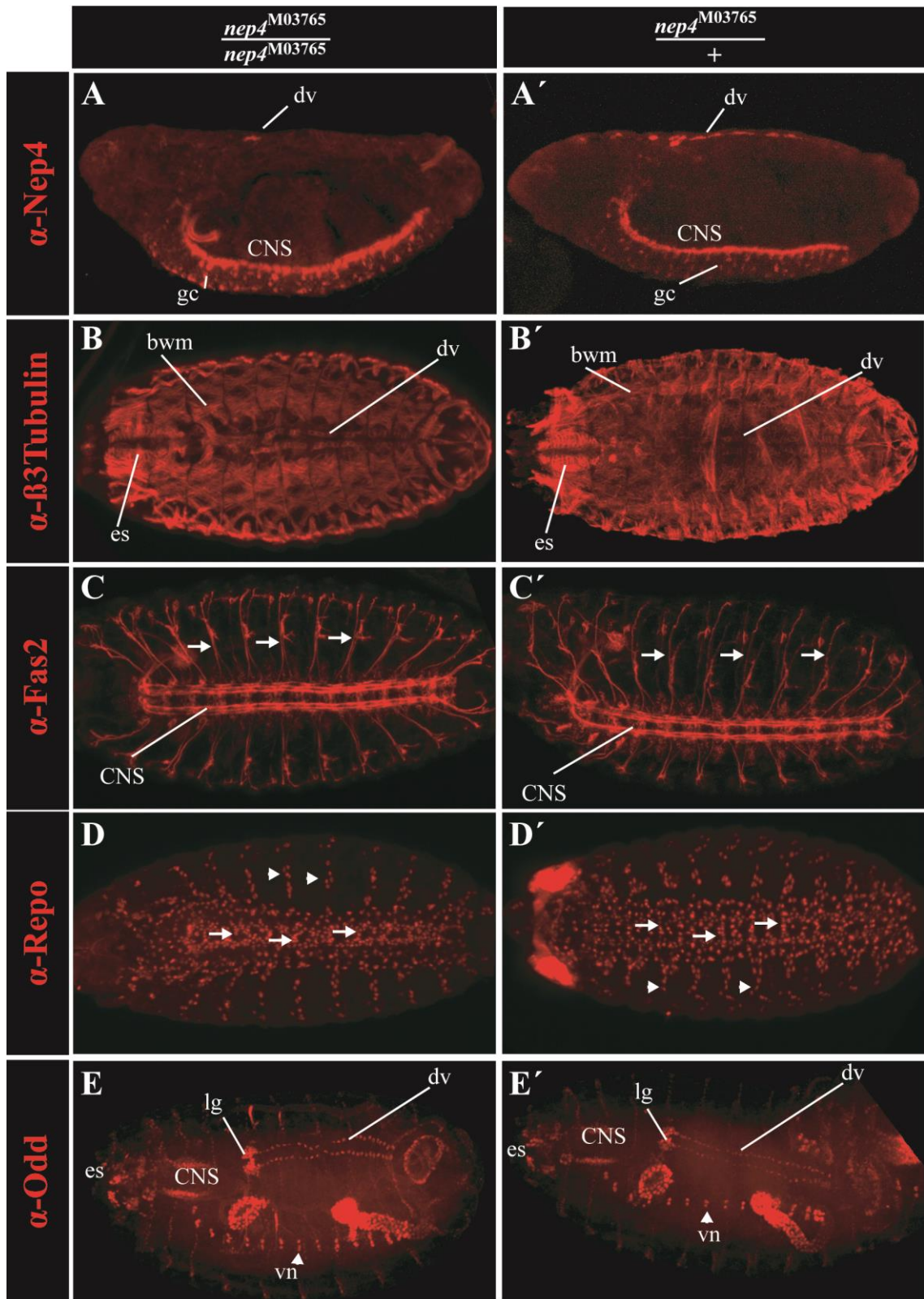
Figure 18| cLSM maximum projections of late *Drosophila* embryos stained with different antibodies. The left column (A, B, C, D, E) shows embryos homozygous for the *nep4*[MI03765] Mi{MIC} insertion. The right column (A´, B´, C´, D´, E´) depicts animals heterozygous for the respective insertion and was used as a control. **A and A´**: late stage embryos stained with anti Nep4 antibody, lateral view. The embryos of both genotypes show dorsal expression of Nep4 within cardiac tissue in the even-skipped positive pericardial cells (dv= dorsal vessel) and ventrally the expression of Nep4 within the CNS (central nervous system) in glial cells (gc). **B**

and B´: late stage embryos stained against β3Tubulin marking all muscle cells, dorsal view. Both pictures show anterior the muscle structure of the esophagus (es). At the dorsal midline the dorsal vessel (dv) is visible. Surrounding the animal, the somatic body wall musculature (bwm) is detected. **C and C´**: late stage embryos stained for Fascilin2 (Fas2). Fas2 is expressed in many neurons of the CNS including their lateral axons (arrows). Ventral view. **D and D´**: late stage embryos stained against Repo (reverse polarity), ventral view. Repo is expressed within glial cells along the ventral midline (arrows) and also in lateral glial cells (arrowheads). **E and E´:** late stage embryos stained with an anti-Odd-skipped antibody. In the dorsolateral view Odd-skipped is detected in the dorsal vessel (dv), the lymph gland (lg), in cells of the CNS as well as ventral nervs (vn), and in the esophagus (es).

3.2.1.2 Effects of Neprilysin 4 truncation on larval development

Since embryogenesis in the $nep4^{MI03765}$ mutant animals, which produces a truncated Nep4 protein lacking one of the catalytically relevant motifs and thus catalytic activity (**Figure 16**; **Figure 17**), appears to be unaffected, larval development was analyzed for any abnormalities. Panz et al. (2012) showed that during larval development altered *nep4* expression, especially in the somatic musculature, leads to severe phenotypes. RNAi mediated knockdown results in decreased locomotion speed and a reduced contraction rate of the larval body. In addition, corresponding animals die as pupae. Based on these data, the survival rate of animals of the line BL36979 was observed under homozygous conditions and compared to heterozygous conditions as a control. Out of 180 embryos, 101 (ca. 56%) 1st instar larvae hatched. 43 larva were homozygous and 58 heterozygous for the $nep4^{MI03765}$ allele. During larval development 4 heterozygous and 9 homozygous larvae died, thus 54 (30%) heterozygous and 34 (19%) homozygous animals reached metamorphosis. 45 (25%) heterozygous and 32 (17%) homozygous animals survived metamorphosis and hatched as imagos.
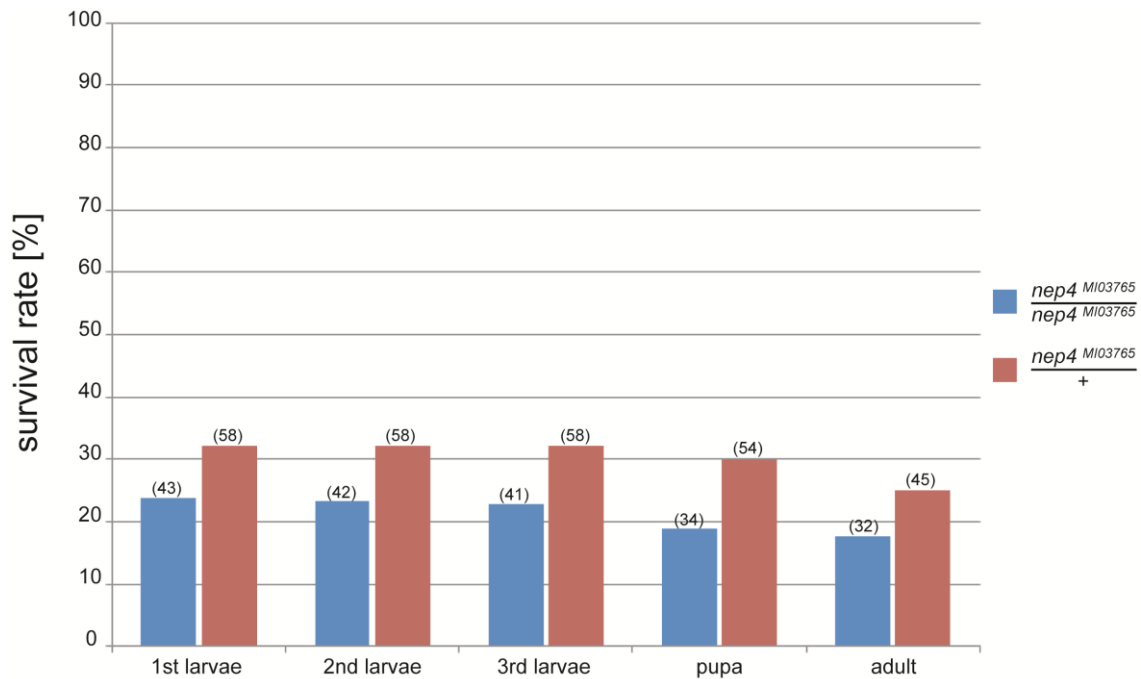
Figure 19| Truncation of Nep4 has no effect on larval development. 180 embryos were observed for their rate of survival. From these 180 embryos, 43 homozygous (blue, 23.9%) and 58 heterozygous (red, 32.2%) 1st instar larvae hatched. From the 58 hatched heterozygous mutant larvae all animals reached the 2nd and 3rd larval stage (32.2%) and 54 animals reached the pupal stage (30%). 45 (25%) heterozygous adult flies hatched after metamorphosis. Out of the 43 hatched homozygous mutant larva from line BL36979, 42 animals (23.3%) reached the 2nd and 41 animals (22.8%) reached the 3rd larval developmental stage. 34 individuals (18.9%) reached metamorphosis. 32 (17%) adult flies hatched after metamorphosis

3.2.1.3 Effects of Neprilysin 4 truncation on male fertility

In former work it has been shown that Nep4 is expressed in the gonads of adult male *Drosophila* (Meyer et al., 2009; Panz et al., 2012). In addition, it has been confirmed that *Drosophila* neprilysins, including Nep4, are critical to male fertility (Sitnik et al., 2014). The fact that homozygous animals reach adulthood (**Figure 19**), is in contrast to the observation that during stock keeping, line BL36979 was not segregating the balancer chromosome. In addition, it was not possible to maintain the homozygous line. Therefore, fertility of male and female (as control) flies being either homozygous or heterozygous for the truncated Nep4 ^{MI03765} protein was assessed by single pair crossings. As shown in **Figure 20** males homozygous for the truncated Nep4^{MI03765} protein generate no offspring, which indicates sterility. By contrast, heterozygous males are fertile and produce an average offspring of 57.5 individuals in single pair crossings. Females homozygous for the truncated protein generated an average offspring of 59.1 individuals and heterozygous mutant females generated a mean offspring of 58.2

individuals in all single pair crossings. Differences in the average offspring between the fertile genotypes were not significant.
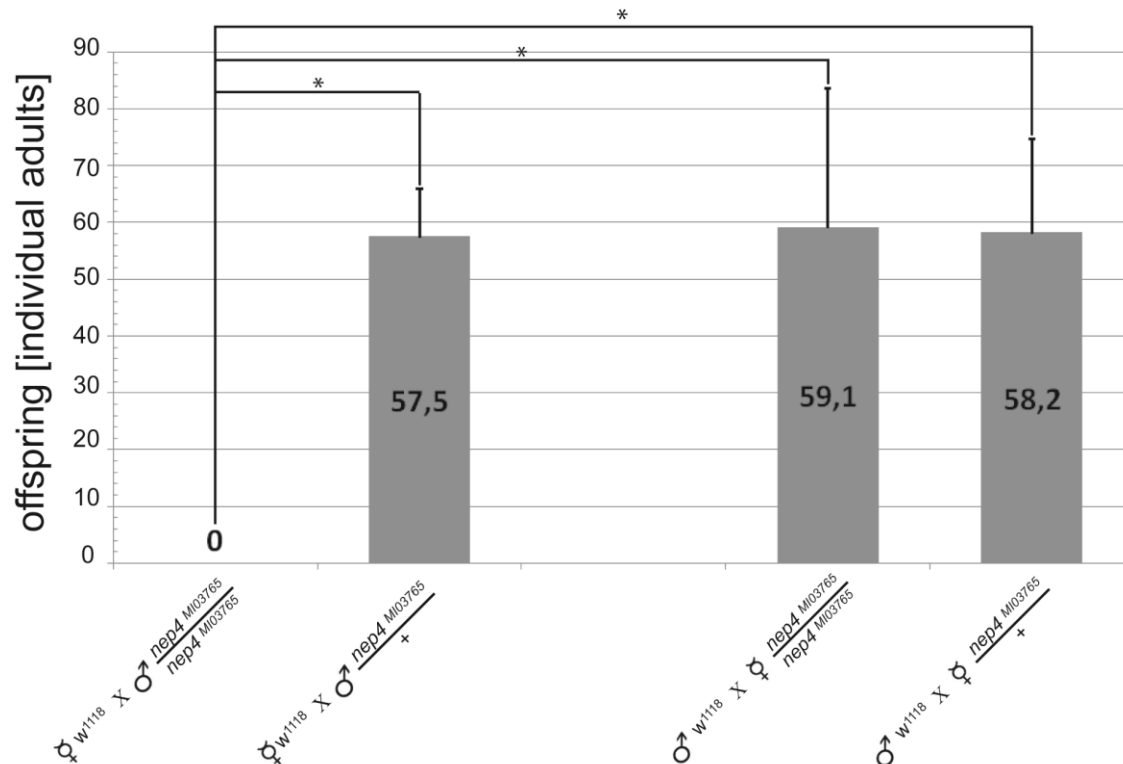
Figure 20| Fertility assay of adult flies from line BL36979. The diagram shows the quantity of the adult progeny from w[1118] virgin females crossed to either heterozygous or homozygous *nep4* [MI03765] males, and w[1118] males crossed to either heterozygous or homozygous *nep4* [MI03765] virgin females. The average offspring number of crossing heterozygous males to w[1118] females was 57.5 adults (n=6, single pair crossings). Crossing w[1118] females to homozygous mutant males of line BL36979 did not generate any offspring (n=6, single pair crossings). The average offspring number of crossing homozygous females to w[1118] males was 59.1 adults (n=7, single pair crossings). The average offspring number of crossing heterozygous females to w[1118] males was 58.2 adults (n=9, single pair crossings). Asterisks indicate statistically significant deviations (*P < 0.005, Student's t-test).

3.2.2 CRISPR/Cas9 mediated genome engineering as a tool to generate a novel Nep4 mutant line

As depicted above, line BL36979 holds a transposon insertion within the *nep4* gene that causes production of a C-terminally truncated Nep4 protein. While this protein can be considered to be catalytically inactive, it is still possible that the remaining protein domains fulfill certain physiological functions that are not depending on catalytic activity. Thus, in order to generate a novel *nep4* knockout mutant, the CRISPR/Cas9

technique was utilized (see section 2.2.8). As a basis, line BL36979 was used. Two guide RNAs were selected with the aim to delete a large part of the *nep4* gene along with the complete Mi{MIC} element. Cutting was considered to occur 843 base pairs downstream of the *nep4* start codon and 152 base pairs upstream of the *nep4* stop codon. In case of a positive deletion event, the sequence between the two cutting sites (ca. 2.5 kbp of the *nep4* coding sequence as well as the complete Mi{MIC} element) would be removed. Since line BL36979 has a y⁻ genetic background and since the Mi{MIC} element holds the *yellow* gene as a marker, lack of *yellow* expression and thus reduced cuticle pigmentation could be used as a readout for successful deletion.

As a result of injecting 200 Cas9 expressing embryos with the respective two gRNAs, one line was returned that exhibited the expected yellow phenotype. This line was investigated further. First, the exact extent of the CRISPR induced deletion was assessed. Therefore, the anticipated gene region was amplified using primers aligning on the one hand at the 5` end and on the other hand at the 3´end of the *nep4A* coding sequence. The respective pcr-product was sequenced and blasted against the cds of *neprilysin 4* (flybase.org). The sequence aligns from the 5`end of *nep4* exactly until reaching the first CRISPR cutting site. From the 3`end, the sequence aligns only until the beginning of the Mi{MIC} transposon. Thus, the sequence between these two positions is deleted (**Figure 21**). The resulting *nep4* allele, which is named *nep4*$^{\Delta 281-1040}$, is 2074kbp in size and composed of the 845bp downstream of the *nep4A start* codon and ca. 394bp upstream of the *nep4* stop codon. In addition, 835bp of Mi{MIC}-sequence remain.
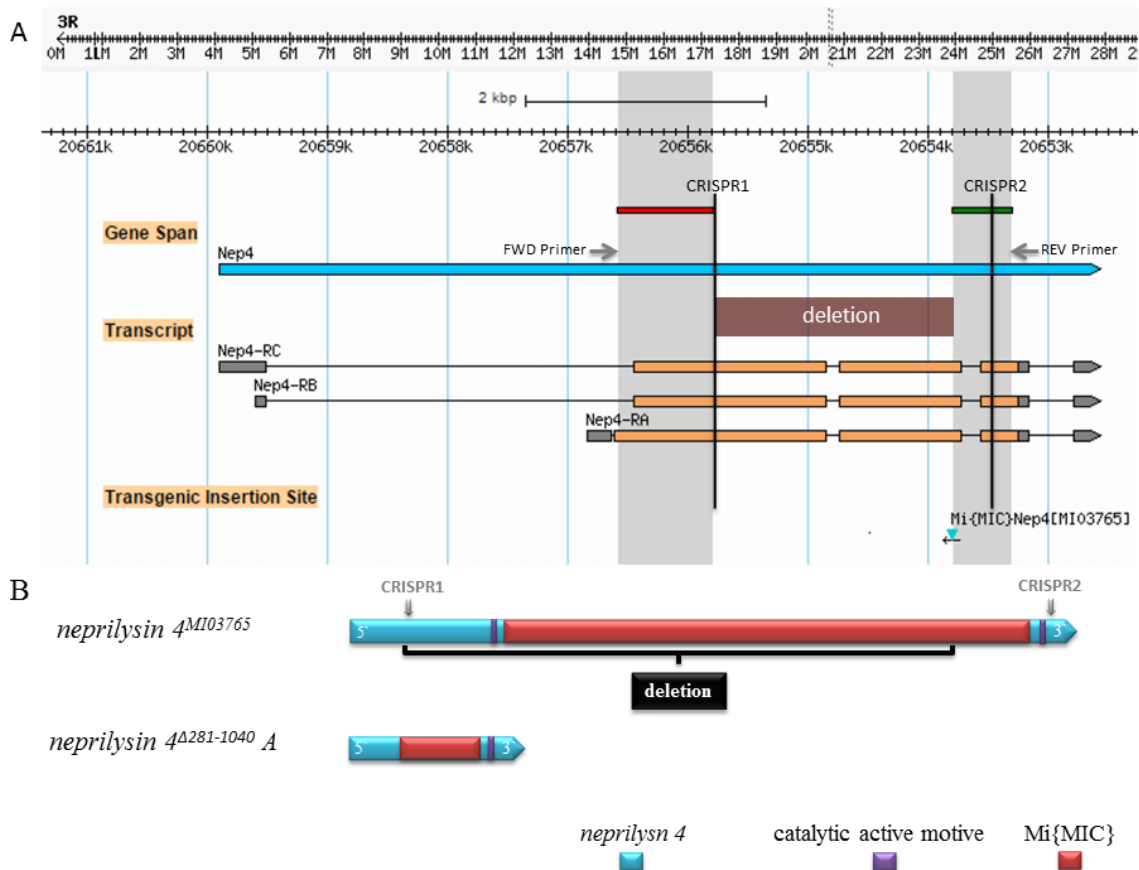
Figure 21| Scheme of the *neprilysin 4* gene locus including transcript variants in *Drosophila*. A: The sequence amplified by using the *nep4* forward primer (red block in grey bar) aligns from the start codon until the first CRISPR cutting site (indicated by left black bar). The sequence amplified by using the *nep4* reverse primer (green block in grey bar) aligns from the *nep4* stop codon until reaching the position of the Mi{MIC}-element (blue triangle). The sequencing results are based on the alignment of PCR products amplified with DNA from line Nep4$^{\Delta281\text{-}1040}$ in comparison to the DNA sequence of w^{1118} animals. **B:** Scheme of the *nep4*^{MI03765} coding sequence. The Mi{MIC} sequence (depicted in red) is inserted between the two catalytically relevant motifs. The intended CRISPR cutting sites are indicated by grey arrows. Subsequent to CRISPR mediated editing, the deletion spans 1884bp of the *nep4* coding sequence and ca. 6.3kbp of the Mi{MIC} sequence, resulting in the severely truncated *nep4*$^{\Delta281\text{-}1040}$ allele.

3.2.3 The Nep4$^{\Delta281\text{-}1040}$ protein is truncated but not degraded

Nep4A (wildtype)	Nep4$^{\Delta281\text{-}1040}$ A
MSRHSQLKLAMPSVHGAPATAPGSPMNAKARSVKLGLGVNQRTGRVQWCPGLTC CKMLLLLPVVMLPLTLVLILIMRLDGMLAALQLNEQRMRDLRNSHSEVPVYMEDY EALLPEGSTYNDLINEEFILPASKRTQLQILAAERARRCQPYRYGNGESMELEERNT LMKDSRTSFLPLGIPRECLGSGIELDIKPIDEEAYQRQKKRYQDIAPYWLEKIRIRER REAERHAEEASAEISEATAALQSFWNEEGTREGIRMTQAKTMKRYMDNKVDPCVD FYKYACGNWERLHPIPKDKAGFDTFEMLRESLDLVLRNLLEKNTPVHSAAELRKSP VRNTLFKLNEQGEGEGEADQAAELTAERLRRHIVSKRQLLNRVLVRYKRYTNGTK RKRLIETPRERTKEEEAAPPVVLPKDKTKDKSDNEEQLHVPTDFLKPHQDAQLKA KNLYRSCVNSAVLAKRGLEPLHTLIRELGGWPVLESQWSESNFNWQVLAATLRRY NNDILIVQWVGADIKNSEENIVQFDQTGLGLPTREYFLQPSNAKYLQAYQRYMAEV MHKMGASKADAQRVASELVAFETQLAGITAPAEQRLNVTKLYKRMTLDQLQAVV PEIKWRAYLQSLQDREVLGTEEVVIYAVEYMSKLVTLLDETDPRTVSNYMMWRFV RHRINNVDDRFDDIKQSFYHALFGREESPQRWKVCIAQVNTNMGMAVGSMFVSRY FDNNSKRDTLRMTHDLQQAFRDILKTTDWLDDTTKQLAEEKVNAMSLKIGYPDFI LNPSELNSKYAGIEIYPEKYFENTLNVLLHTAKTEQAKLHERVNKTNWQTAPAIVN AYYSRNKNQIMFPAGILQPPFYHRHFPKSLNFGGIGVVIGHELTHGFDDKGRLFDR NGNIHKWWTDSSIRGFDERARCIIAQYSNYTVEEVGIVLNGESTQGENIADNGGLRQ AFHAYQRWLKEHPSEVSDEILPGLNMTGPQLFFLNFGQVWCGAMRPEAIRNKLNT AIHSPGRFRVIGTLSNSVDFAREFNCPLGSPMNPQKKCSVW*	MSRHSQLKLAMPSVHGAPATAPGSPMNAKARSVKLGLGVNQRTGRVQWCPGLTC CKMLLLLPVVMLPLTLVLILIMRLDGMLAALQLNEQRMRDLRNSHSEVPVYMEDY EALLPEGSTYNDLINEEFILPASKRTQLQILAAERARRCQPYRYGNGESMELEERNT LMKDSRTSFLPLGIPRECLGSGIELDIKPIDEEAYQRQKKRYQDIAPYWLEKIRIRER REAERHAEEASAEISEATAALQSFWNEEGTREGIRMTQAKTMKRYMDNKVDPCVD FYNQWCAPGRSLRAWRT*
ca. 119.8 kDa	ca. 33.9 kDa

Figure 22| Amino acid sequences of wildtype Nep4A and Nep4$^{\Delta281\text{-}1040}$. A: Comparison of the amino acid sequence of Nep4A (flybase.org) with the sequence of Nep4$^{\Delta281\text{-}1040}$. Nep4A is 1040 amino acids long and has a calculated mass of 119.6kDa. The residues marked in orange and green constitute the intracellular and transmembrane domain. The sequence of the extracellular domain is marked in blue and the two catalytically relevant motives of the peptidase are marked in purple. The corresponding protein in line Nep4$^{\Delta281\text{-}1040}$ is 296 amino acids long and C-terminally truncated. Its calculated mass is 33.9kDa. The intracellular domain and transmembrane domain are marked in orange and green, respectively, while the extracellular domain is marked in blue. After 281 amino acids the Mi{MIC} sequence begins. 15 amino acids of the transposon are added to the Nep4 sequence until a stop-codon terminates translation (red). **B:** Schematic representation of Nep4A and Nep4$^{\Delta281\text{-}1040}$. Intracellular domain (orange), transmembrane domain (green), extracellular domain (blue) containing the sequence motifs that are critical to enzymatic activity (purple) and the Mi{MIC}-transposon fragment (red) are indicated. Black bar indicates area of antibody binding.

Based on in silico translation of the respective nucleotide sequences, it is evident that Nep4$^{\Delta281\text{-}1040}$ represents a C-terminally truncated protein, consisting only of 281 N-terminal amino acids (**Figure 22**). Following these 281 Nep4 residues, 15 amino acids are added based on the sequence of the Mi{MIC} transposon, until a stop-codon present within the Mi{MIC}-sequence terminates translation (**Figure 22**). Thus, Nep4$^{\Delta281\text{-}1040}$A has a calculated mass of 33.9 kDa. Thus, Nep4$^{\Delta281\text{-}1040}$A consists of the intracellular

domain, the transmembrane domain and a short fragment of the extracellular domain, which lacks both catalytically active motifs.

Based on these data, it was analyzed, if Nep4$^{\Delta281\text{-}1040}$ is produced and if the truncated protein is stable in the animals or if it is recognized as a defective protein and degraded. **Figure 23** shows a western blot based on total extracts of two different genotypes. Nep4 was detected with α-Nep4 antibodies. In the control (w^{1118}) and Nep4$^{\Delta281\text{-}1040}$ heterozygous flies a protein could be detected, matching the sizes of Nep4A (ca. 120 kDa) (**Figure 23|** arrowheads). In the heterozygous Nep4$^{\Delta281\text{-}1040}$ flies, which hold in addition to the wildtype *nep4* allele the truncated *nep4$^{\Delta281\text{-}1040}$* allele, an additional protein was detected by the Nep4 antibody. The apparent masse of this protein corresponds to the predicted masse of the truncated Nep4$^{\Delta281\text{-}1040}$ A (ca. 34 kDa) (**Figure 23|** arrows). In homozygous *nep4$^{\Delta281\text{-}1040}$* larvae only this second protein is present (**Figure 23|** arrow). The apparent mass of this smaller protein corresponds to the expected mass of truncated Nep4$^{\Delta281\text{-}1040}$A.
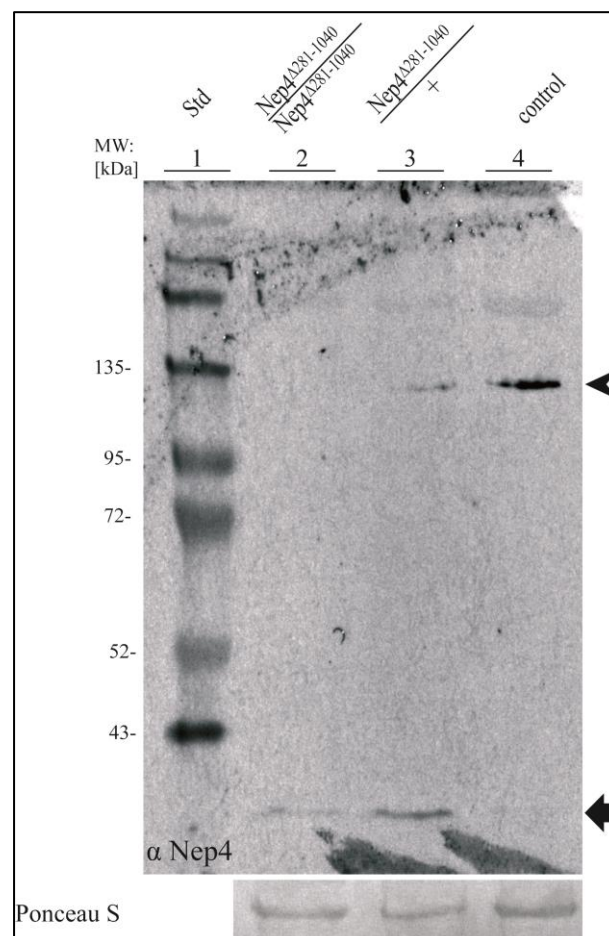

Figure 23| Western blots of total protein extracts from lines w^{1118} (control) and Nep4$^{\Delta281\text{-}1040}$. Detection with α-Nep4 antibodies. Total protein extracts of second instar larvae from control (w^{1118}), heterozygous, and homozygous Nep4$^{\Delta281\text{-}1040}$ animals were applied. In the

control lane one protein is detected with a size of ca. 120 kDa, representing Nep4A (arrowhead) (lane 4). In heterozygous Nep4$^{\Delta281\text{-}1040}$ preparations two proteins are detected: one protein with a mass of ca. 120 kDa, representing Nep4A (arrowhead), and a smaller protein with a mass of ca. 35 kDa, presumably representing Nep4$^{\Delta281\text{-}1040}$A (arrow) (lane 3). In homozygous Nep4$^{\Delta281\text{-}1040}$ larvae, only the latter protein is detected, presumably representing Nep4$^{\Delta281\text{-}1040}$A (lane 2). Ponceau S staining is shown as a loading control.

3.2.4 Analysis of development in line Nep4$^{\Delta281\text{-}1040}$

Further analysis of the Nep4$^{\Delta281\text{-}1040}$ protein confirmed that it represents a C-terminally truncated construct, lacking about 80% of the extracellular domain. The respective truncation encompasses both catalytically relevant domains (**Figure 22**). Western blot analysis of larval total protein extracts revealed that the truncated protein is synthesized and detectable using anti-Nep4 antibodies (**Figure 23**). In continuative experiments the effects of the Nep4 truncation on embryogenesis were investigated. Initially, the analyzed fly line was rebalanced over TDLZ, carrying a wildtype *nep4* allele. Embryos were collected and stained against tissue specific markers to investigate the development of animals homozygous for the *nep4*$^{\Delta281\text{-}1040}$ allele, compared to heterozygous animals carrying a *nep4*$^{\Delta281\text{-}1040}$ allele and a wildtype *nep4* allele due to the balancer chromosome as a control. The TDLZ balancer chromosome carries a *lacZ* reporter gene coding for a β-Galactosidase. Simultaneous staining against the β-Galactosidase allows for differentiation of *nep4*$^{\Delta281\text{-}1040}$ homozygous and heterozygous animals.

First, late embryos of the respective genotypes were stained against Nep4 (**Figure 24|** A, A´). The control embryos as well as the mutant embryos show an expression pattern as described in the literature (Meyer et al., 2009). Expression is detected in even-skipped positive pericardial cells, within the dorsal vessel and in the ventral and lateral cells of the CNS. Except for small differences between the expression patterns of both genotypes due to biological variability or due to slight differences in the developmental stage, no abnormal development is visible during embryogenesis. The fact that the detection of Nep4 in animals homozygous for the truncated *nep4*$^{\Delta281\text{-}1040}$ allele was successful supports the observation from the western blot analysis (**Figure 23**) that the Nep4$^{\Delta281\text{-}1040}$ protein is stable and localizes correctly. As already mentioned, Nep4, also expressed in the somatic musculature and elevated catalytic activity in the respective tissue, was shown to be causative to a muscle degeneration phenotype within the body wall musculature. RNAi mediated knockdown of *nep4* leads to a decreased movement

of larvae (Panz et al., 2012). Therefore, the development of the musculature was also investigated in the Nep4$^{\Delta281-1040}$ line. The musculature of both genotypes was stained using anti β3Tubulin antibodies (**Figure 24**| B, B´). In both genotypes the staining labels the esophagus (es) and the contractile ventricle and aorta of the dorsal vessel along the dorsal midline. The somatic body wall musculature can be seen segmentally surrounding the whole embryo. Muscle development in both genotypes shows no abnormalities. The body wall muscles in homozygous mutants are properly formed during embryogenesis. Since it is known that *nep4* is expressed in the CNS (Meyer et al., 2009) the embryonic development of the CNS was also investigated. Using an anti-Fascilin2 antibody as a neuronal marker, the development of motor neurons was analyzed along the ventral midline and the lateral distributing axons (**Figure 24**| C, C´). Comparing control animals and mutant animals, the formation of the neurons in the CNS and the axon distribution in the PNS (**Figure 24**| C, C´, arrows) is comparable. The formation of glial cells was investigated using an anti-Repo antibody as a glial cell marker (**Figure 24**| D, D´). Embryos stained against Repo revealed that the glial cells along the ventral midline (**Figure 24**| D, D´, arrows) as well as the lateral glial of the PNS (**Figure 24**| D, D´, arrowheads) develop equally in both genotypes. During embryogenesis Nep4 is also expressed in even-skipped positive pericardial cells (Meyer et al., 2009). To investigate if the formation of the heart is affected by the Nep4 truncation, respective animals were stained against Odd-skipped, another marker for heart cells (**Figure 24**| E, E´). In animals stained for Odd-skipped, formation of the dorsal vessel, including the pericardial cells, is normal in both, control animals heterozygous for the truncated *nep4$^{\Delta281-1040}$* allele, as well as in homozygous *nep4$^{\Delta281-1040}$* animals. In summary, as depicted in **Figure 24**, all tissues investigated develop normally in animals expressing only the truncated Nep4$^{\Delta281-1040}$ protein that lacks most of the enzyme´s extracellular domain, including the catalytically relevant motifs. Thus, Nep4 derived catalytic activity appears to be dispensable to embryonic development.
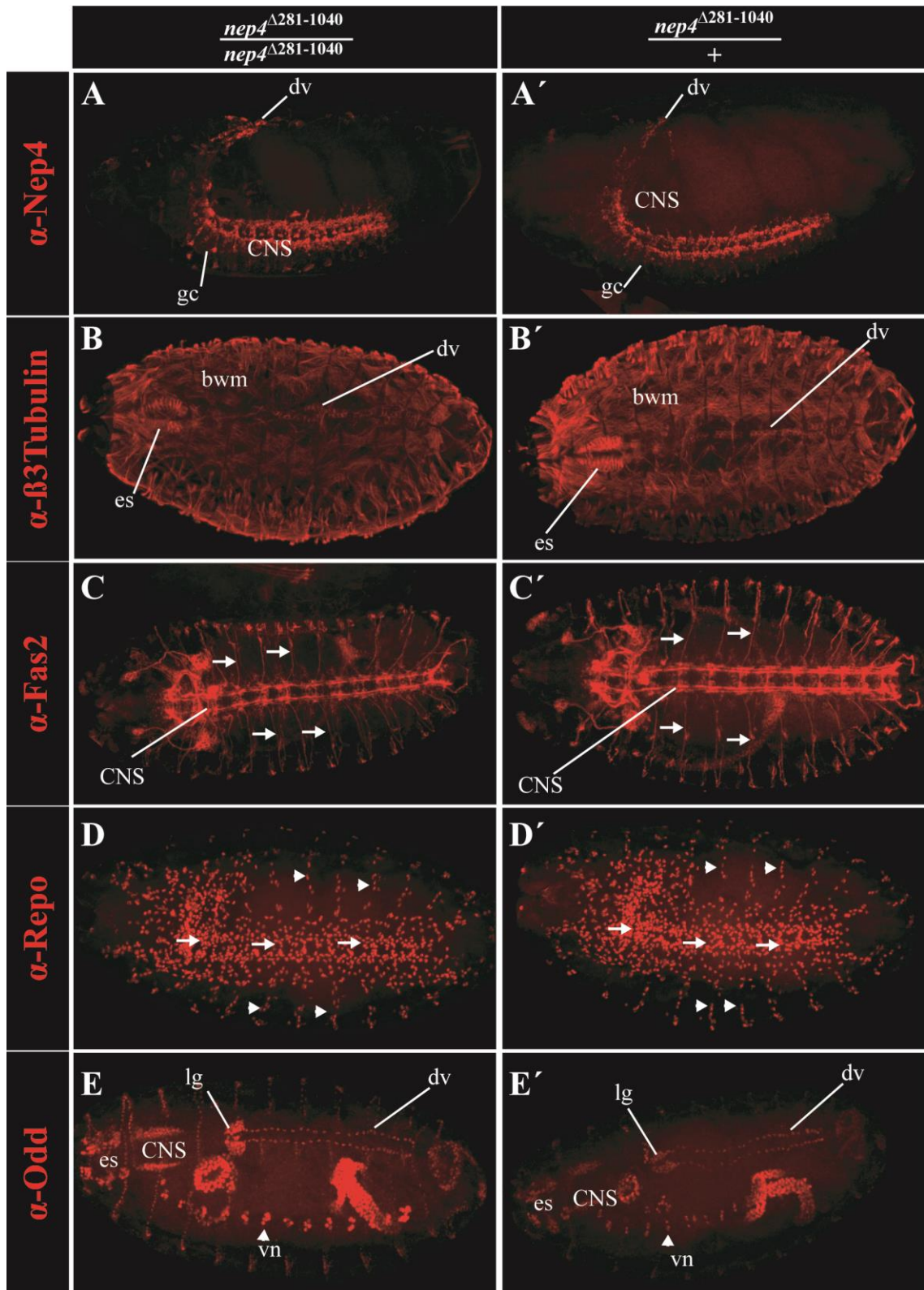
Figure 24| cLSM maximum projections of late stage embryos stained with tissue-specific antibodies. The left embryos (A, B, C, D, E) show maximum projections of embryos homozygous for the *nep4^Δ281-1040* allele. The right embryos (A´, B´, C´, D´, E´, F´) display animals heterozygous for the *nep4^Δ281-1040* allele as a control. **A and A´:** cLSM stacks of late stage embryos stained with anti Nep4 antibodies, lateral view. The embryos of both genotypes show dorsally the expression of Neprilysin 4 within cardiac tissue in the even-skipped positive pericardial cells (dv= dorsal vessel) and ventrally the expression of Nep4 within the CNS

(central nervous system) in glial cells (gc). **B and B´:** cLSM stacks of late stage embryos stained against β3Tubulin marking all muscle cells; dorsal view. Both pictures show anterior the muscle structure of the esophagus (es). At the dorsal midline the contractile dorsal vessel (dv) is visible. Surrounding the animals the somatic body wall muscle tissue is stained (bwm). **C and C´:** cLSM stacks of late stage embryos stained with anti Fascilin2 (Fas2) antibody. Fas2 is expressed in numerous neurons of the CNS including their lateral axons (arrows); ventral view. **D and D´:** cLSM stacks of late stage embryos stained for Repo (reverse polarity). Repo is expressed within glial cells along the ventral midline (arrows) and also in lateral glila cells (arrowheads); ventral view. **E and E´:** cLSM stacks of late stage embryos stained with an anti-Odd-skipped antibody. In the dorsolateral view Odd-skipped is detected in the dorsal vessel (dv), the lymph gland (lg), in cells of the CNS and ventral nerves (vn), as well as in the esophagus (es); dorsolateral view.

3.2.5 Analysis of larval development in line Nep4$^{\Delta281\text{-}1040}$

Analysis of embryogenesis in line Nep4$^{\Delta281\text{-}1040}$ revealed no distinct developmental phenotypes in embryos expressing only Nep4$^{\Delta281\text{-}1040}$, which lacks ca. 80% of the extracellular domain (**Figure 22**; **Figure 23**)

In further experiments the larval development and the metamorphosis of line Nep4$^{\Delta281\text{-}1040}$ was investigated (**Figure 25**). In this effort, the development of 150 embryos was observed over time. Out of these 150 animals, 66 heterozygous (44%) and 26 homozygous (17%) animals hatched as 1st instar larvae. From both genotypes all first instar larvae developed into 2nd instar larvae. The 3rd instar larval stage was reached by 43% (64) of the control animals and by 14% (21) of the mutant animals. Metamorphosis was initiated by 11% (18) of the mutant larvae and by 42% (63 animals) of the control animals. Adulthood was reached by none of the homozygous animals expressing only the truncated Nep4$^{\Delta281\text{-}1040}$, while 62 of the control animals (41%) survived metamorphosis (**Figure 25**).
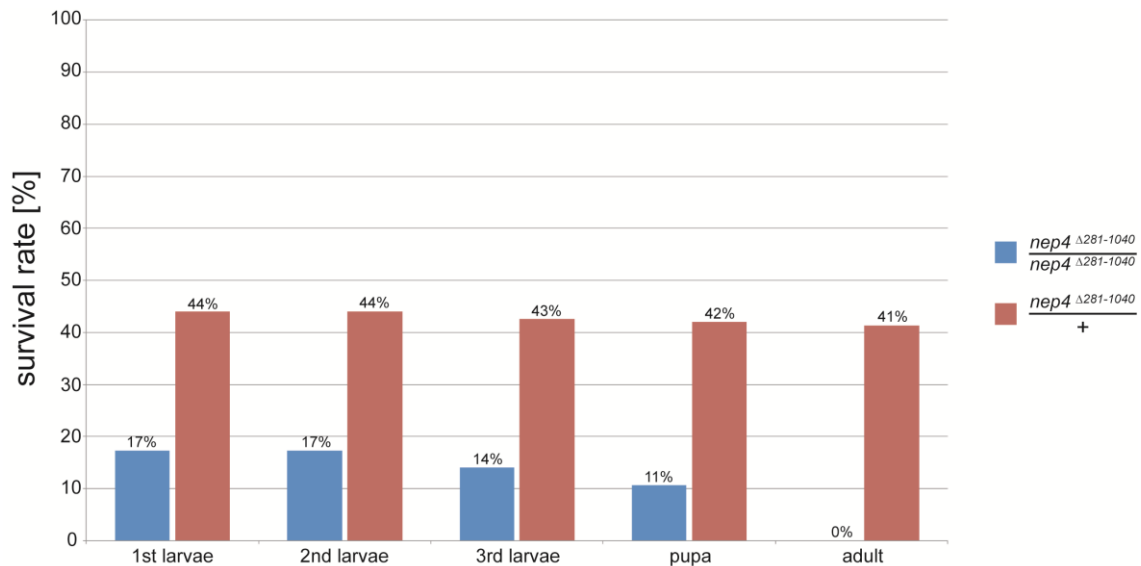
Figure 25| Animals homozygous for the *nep4^{Δ281-1040}* allele die during embryogenesis and metamorphosis. 150 embryos were analyzed for their survival rate during development. Of these 150 embryos, 66 animals (44%) heterozygous for the *nep4^{Δ281-1040}* allele (red) became 1st instar larvae, while only 26 homozygous animals (17.3%, blue) reached this stage. Of the hatched heterozygous larvae all animals reached the 2nd instar larval stage, and 64 animals (42.6%) reached the 3rd stage of larval developmental. 63 of these animals reached the pupal stage (42%). From these 62 animals hatched as imagos. Of the 26 1st instar larvae homozygous for the *nep4^{Δ281-1040}* allele, all animals reached the 2nd instar larval stage and 21 animals (14%) reached the 3rd larval developmental stage. 18 animals (11%) initiated metamorphosis, yet none of the respective animals survived this developmental process.

As a result of the viability assay depicted above, it became evident that a large portion of animals expressing only truncated Nep4$^{\Delta281\text{-}1040}$ die during metamorphosis. In line with these data, earlier work already demonstrated that animals exhibiting reduced *nep4* expression in muscles are characterized by pupal lethality as well as a reduced larval locomotion. Thus, Nep4$^{\Delta281\text{-}1040}$ animals phenocopy pupal lethality. The question whether these animals are also characterized by reduced larval locomotion was further examined. As a result it was found that larvae homozygous for the *nep4^{Δ281-1040}* allele exhibit a mean locomotion speed of ca. 1.1mm/s, which is significantly slower, compared to the locomotion speed of both controls (heterozygous *nep4^{Δ281-1040}*, w^{1118}) showing a mean value of 1.7mm/s (**Figure 26**).
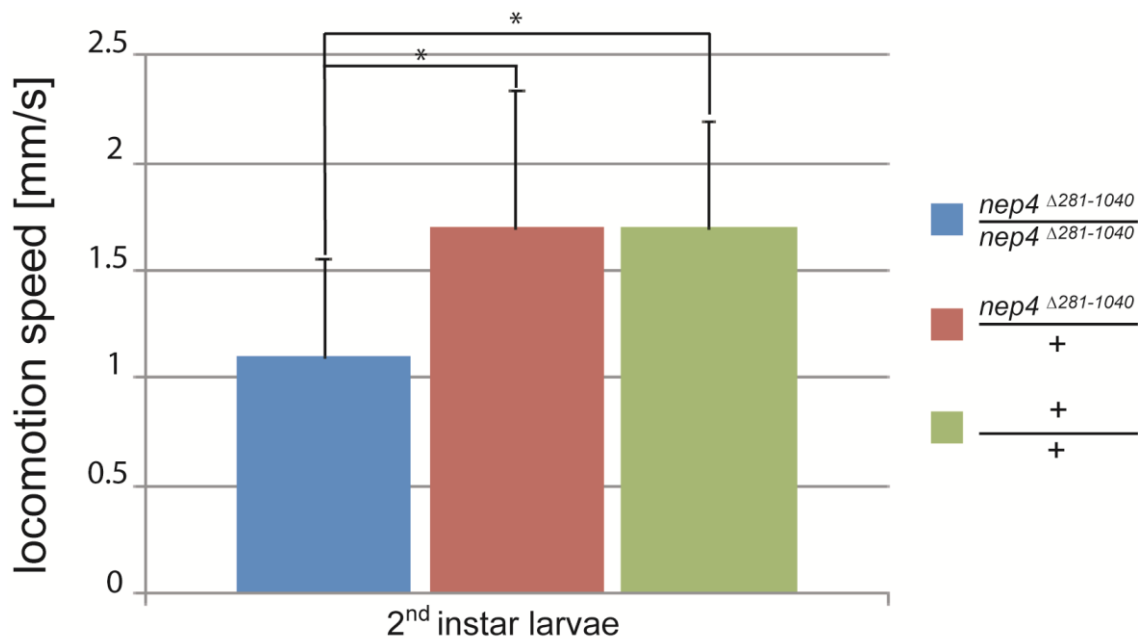
Figure 26| Impaired locomotion of homozygous Nep4$^{\Delta281\text{-}1040}$ animals. Depicted is the locomotion speed (mm/s) of 2nd instar larvae of 3 different genotypes (n $\geq$ 20). Animals homozygous for the *nep4$^{\Delta281\text{-}1040}$* allele show a mean locomotion speed of 1.1mm/s (blue), whereas the locomotion speed of larvae heterozygous for the *nep4$^{\Delta281\text{-}1040}$* allele (red) and of wildtype animals (green) is significantly faster (1.7mm/s). . (*P < 0.05, Student's t-test)

On the basis of the locomotion assay (**Figure 26**) it became necessary to analyze whether the impaired locomotion speed of larvae expressing only the truncated Nep4$^{\Delta281\text{-}1040}$ protein is due to impaired muscle integrity. Since the same genotypes did not exhibit any muscle phenotype during embryogenesis (**Figure 24| B, B´**), larvae where dissected and stained to investigate the structure of the body wall musculature. **Figure 27** shows a representative image of a body wall muscle of a larva homozygous for the *nep4$^{\Delta281\text{-}1040}$* allele (**Figure 27| A, A´**), compared to a control animal (**Figure 27| B, B´**). The musculature of the mutant animal shows a wildtype sarcomeric structure, diameter and form. Thus, no degeneration phenotype compared to the control was visible
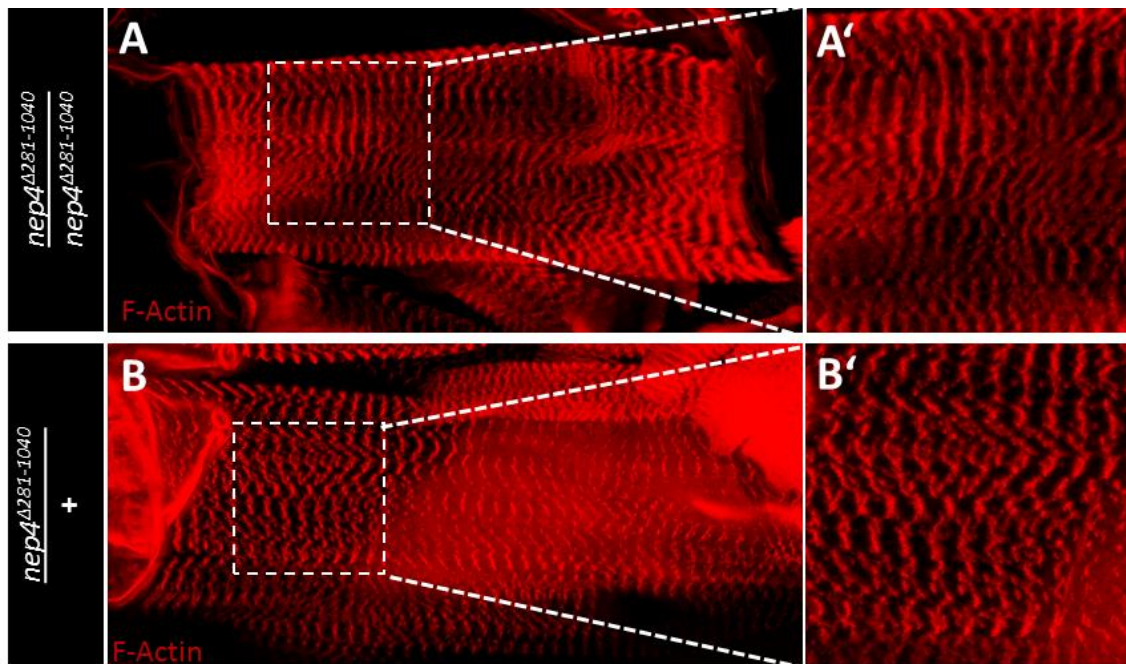
Figure 27| F-Actin staining shows no degeneration phenotype in Nep4$^{\Delta281\text{-}1040}$ larvae.
Phalloidin-TRITC stainings of body wall muscles of 2nd instar larvae homozygous and
heterozygous for the *nep4$^{\Delta281\text{-}1040}$* allele are depicted. Compared to control specimen (B, B´) the
sarcomeric structure in mutant animals (A, A´) is formed properly and exhibits no degeneration
phenotype. The muscles show wildtype size and shape.

As depicted above, this work showed that muscle-specific *nep4* knockdown animals
have an altered composition of metabolites, a reduced food intake rate and an increased
level of insulin expression (**Figure 7**; **Figure 8**). As a first experiment to test, if the
truncated Nep4$^{\Delta281\text{-}1040}$ line phenocopies these phenotypes, a feeding assay was
conducted (**Figure 28**). Interestingly, animals expressing only Nep4$^{\Delta281\text{-}1040}$ exhibit a
significantly reduced food intake at every measured time point of the observed 40min
time frame. By the end of the measurement (after 40min of feeding) the mutant animals
had ingested 94% less food than heterozygous *nep4$^{\Delta281\text{-}1040}$*animals, and 88.5% less food
than the wildtype control larvae (**Figure 28**).
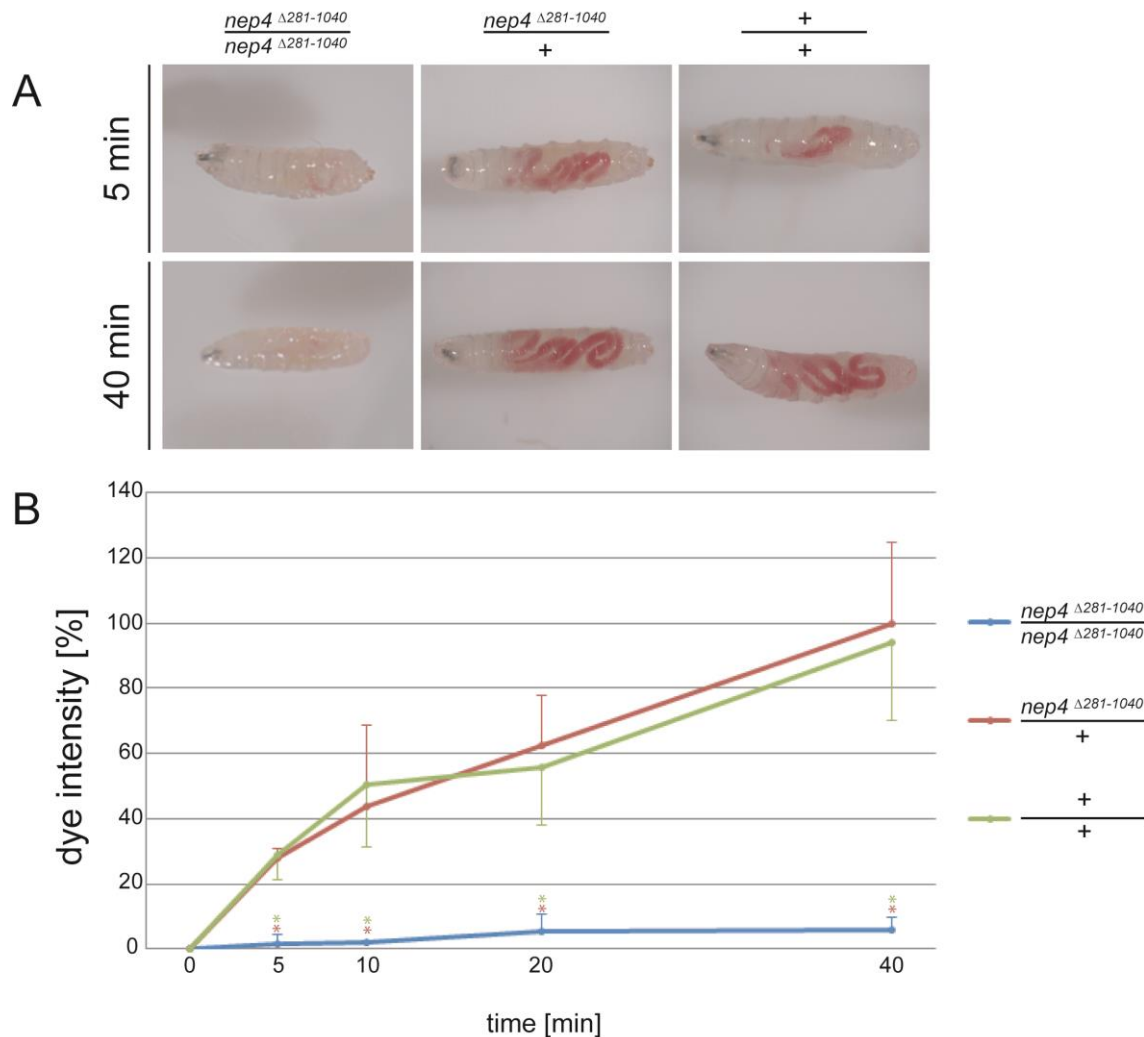
Figure 28| Animals homozygous for the *nep4^Δ281-1040* allele show a considerably reduced food intake. The upper panel shows examples of larvae from all genotypes tested after 5 and 40 min of feeding. In the lower panel the food intake of 3rd instar larvae with a homozygous mutant genomic background (*nep4^Δ281-1040^/ nep4^Δ281-1040^*, blue) is depicted in percentages (%) relative to the intake in control larvae (*nep4^Δ281-1040^/ +*, red; *+ / +*, green). Food intake in *nep4^Δ281-1040^/ +* larvae after 40 min of feeding was set to 100%. *nep4^Δ281-1040^/ nep4^Δ281-1040^* larvae show significantly reduced food intake at every time point measured compared to both control genotypes. Control animals of both genotypes exhibit no significantly reduced feeding at any time point measured. Values show the mean (+ / - s.d.) of at least 6 individual larvae of each genotype at each time point. Asterisks indicate significant differences in food intake compared to control animals. Asterisk colors indicate individual differences compared to the respective controls (*P > 0.05, Student's *t*-test).

The fact that homozygous *nep4^Δ281-1040^* animals exhibit a considerably reduced food intake, which is also true for *nep4* knockdown animals (Hallier et al., 2016), represents further evidence for an essential function of Nep4 in regulating energy metabolism in *Drosophila*.

4 Discussion

During the last decades the functional roles of insulins and IGF-signaling were studied intensively, but the mechanisms that regulate insulin production and release are not understood that well. This thesis shows that modulating expression of *Drosophila neprilysin 4* interferes with the production of insulin-like peptides (ILPs). By identifying short Neuropeptide F (sNPF) as a novel substrate of Nep4, a functional relation between neprilysin activity and the regulation of insulin signaling could be established for the first time. In addition to confirming cleavage of sNPF, which is known to regulate ILP expression (Lee et al., 2008), I could show that Nep4 localizes to the surface of Insulin Producing Cells (IPCs) within the CNS (**Figure 11**). Together with the localization at the surface of body wall muscles (**Figure 9**), these data strongly indicate that the Nep4 mediated regulation of the hemolymph circulating peptide composition is critical to proper insulin expression. This indication is corroborated by the result that only overexpression of the active enzyme leads to a decreased insulin expression in the respective animals, whereas overexpression of a catalytically inactive Nep4 has no significant effect on ILP production (**Figure 8**), confirming the catalytic activity of Nep4 as causative to the respective effects. Further evidence comes from the fact that the respective animals suffer from an inefficient sugar metabolization (**Figure 7**), which is manifested by the result that animals with increased *nep4* expression, and thus diminished *ilp* expression, exhibit increased levels of sugars in their hemolymph (**Figure 7**; **Figure 8**). Interestingly, the reduced *ilp* expression, which likely accounts for an inefficient sugar uptake, appears to overcompensate the reduced rate of food intake that is also characteristic to the respective animals (**Figure 8**). Thus, the sum of these two opposing effects eventually results in an accumulation of carbohydrates. The fact that all observed phenotypes manifest most severely in response to muscle specific Nep4 overexpression suggests that muscle-bound Nep4 activity is mainly responsible to maintain homeostasis of regulatory peptides within the hemolymph, whereas CNS-bound Nep4 appears less important (**Figure 6**). Since the midgut of *Drosophila* is the main source of circulating regulatory peptides within the hemolymph (Reiher et al., 2011; Veenstra et al., 2008), it is likely that Nep4 is required to regulate proper midgut-IPC communication.

In addition, this thesis demonstrates that C-terminal truncation of Nep4 affects male fertility and also causes reduced locomotion as well as impaired feeding and pupal lethality, with severity depending on the degree of truncation.

4.1 Short Neuropeptide F represents a novel substrate of Neprilysin 4

Peptides belonging to the sNPF family are known to play roles in many physiological processes, including locomotion (Kahsai et al., 2010), cardiac rhythm (Johard et al., 2009), and regulation of *Drosophila insulin like peptide* (*dilp*) expression (Lee et al., 2008, 2009). Knockdown of sNPF expression interferes with *dilp* expression, reduces body size and weight and increases the level of glucose within the hemolymph (Lee et al., 2008). Interestingly, these phenotypes are phenocopied by muscle-specific overexpression of Nep4 (**Figure 6**| C; **Figure 7**| B, C; **Figure 8**| B), which suggests an enzyme-substrate relation between Nep4 and sNPF. Indeed, incubation of purified Nep4 with synthesized sNPF proved that Nep4 cleaves the peptide. Furthermore, it became evident that Nep4 specifically cleaves sNPF1 and sNPF2, which are the major sNPF family members, while sNPF3 and sNPF4 are not cleaved, proving a high substrate specificity (**Figure 14**). The most severe phenotypes on size, weight, lifespan, locomotion, feeding behavior and *dilp* expression were observed in response to muscle-specific overexpression of Nep4, whereas overexpression of CNS bound Nep4 showed less dramatic effects (**Figure 6**; **Figure 8**). These facts indicate that mainly hydrolysis of hemolymph circulating sNPF via muscle bound Nep4 reaching into the hemolymph is responsible for the described effects. The finding that Nep4 colocalizes with the sNPF receptor (sNPFR) at the surface of distinct cells of the central brain, which also have access to the hemolymph, supports this indication. Notably, only little colocalization can be seen in cells located deeper within the tissue (**Figure 12**). Colocalization is mainly observed in the median neurosecretory cells of the central brain, where Nep4 and sNPFR colocalize at the surface of IPCs (**Figure 11**, **Figure 12**), which represent the major *dilp* expressing cells in *Drosophila* larvae (Brogiolo et al., 2001; Nässel et al., 2013). This result represents robust evidence for a physiological relation between Nep4 activity and the sNPF mediated regulation of *dilp* expression. The Nep4 activity in close proximity to the sNPFR at the IPC surface suggests tight control of *dilp* expression by

Nep4 via inactivation of sNPFR ligands. On the one hand, muscle bound Nep4 likely functions as a kind of filter for gut derived, hemolymph circulating sNPF. In this context, the muscle resident peptidase may be required to diminish the level of physiologically active sNPF within the hemolymph, in order to terminate the signaling. This interpretation is in line with the data on Nep4 substrate specificity, because all identified Nep4 substrates, $sNPF1_{1-11}$, $sNPF1_{4-11}$, and $sNPF2_{12-19}$ (**Figure 14**), are present in the hemolymph (Garczynski et al., 2006), and all of them exhibit high affinities towards the sNPFR (Dillen et al., 2013; Garczynski et al., 2006), emphasizing the need for effective ligand clearance. On the other hand, it was shown that DILP secretion by IPCs is regulated through humoral signals circulating through the hemolymph (Géminard et al., 2009). These data agree with the results presented in this thesis that the homeostasis of hemolymph circulating factors, such as neurosecretory sNPF species, is highly relevant to *dilp* expression in IPCs and that muscle bound Nep4 is needed to maintain this homeostasis. In addition, CNS bound Nep4 controls ligand concentrations in the direct vicinity of sNPFR at the surface of the IPCs. Elevated as well as decreased Nep4 catalytic activity presumably leads to a misbalance of sNPF levels and thus to an impaired regulation of insulin expression (**Figure 8**).

Significantly, the properties of sNPF are highly similar to those of its human homolog, Neuropeptide Y (NPY)(Lee et al., 2004). NPY also represents a substrate of human Neprilysin (Rose et al., 2009). This fact agrees with the assumption that Neprilysin mediated sNPF (NPY) cleavage represents an evolutionarily conserved mechanism to regulate activity of the respective peptides in flies as well as in humans.

4.2 Nepilysin 4 regulates food intake and insulin expression

After showing that Nep4 specifically cleaves distinct sNPF species, which are key regulators of insulins in *Drosophila,* a possible contribution of other hemolymph circulating regulatory peptides was assessed. Therefore, based on the findings of this thesis, a large peptide cleavage screen was performed (Hallier et al., 2016), in which 19 additional regulatory peptides were tested for Nep4 dependent hydrolysis (**Table 1**). The criteria for peptide selection were a known role in *dilp* expression, feeding behavior, or both (Nässel et al., 2013; Pool and Scott, 2014), as well as not being larger than 5kDa to possibly fit into the active center of Nep4 (Oefner et al., 2000). In the course of the screen 14 additional substrates of Neprilysin 4 were found (personal

communication, Ronja Schiemann, University of Osnabrück). In addition to $sNPF1_{1-11}$ and $sNPF1_{4-11}$ (also corresponding to $sNPF2_{12-19}$) (**Figure 14**), the adipokinetic hormone (AKH), allatosta- tin A1-4, corazonin, diuretic hormone 31 (DH_{31}), drosulfakinins 1 and 2, leucokinin, and tachykinins 1, 2, 4, and 5 were found to be specifically cleaved by Nep4 (Hallier et al., 2016) (**Table 7**).

Interestingly, corazonin is known to elevate food intake (Hergarden et al., 2012), whereas allatostatin A and drosulfakinin work antagonistically on food intake (Chen et al., 2016a; Hergarden et al., 2012; Söderberg et al., 2012). Thus, Nep4 mediated hydrolysis affects peptides enhancing as well as repressing food intake. The finding that Nep4 regulates factors of antagonistic physiological function indicates that multiple aspects of feeding behavior are affected by the peptidase. In line with this result is the finding of this thesis that both, *nep4* knockdown as well as overexpression larvae exhibit reduced food intake (**Figure 8**). This fact indicates a role of Nep4 in maintaining the general peptide homeostasis within the hemolymph in a manner that ensures optimal food intake. An altered *nep4* expression in either direction appears to misbalance the respective peptide composition, which eventually causes impaired feeding behavior (**Figure 8**). In case of *nep4* knockdown, the reduced feeding only occurs up to 20 min of feeding. This delay in food intake indicates a complex regulation of optimal food intake, in which redundant peptidases or an elevated expression of e.g. corazonin might compensate reduced cleavage of e.g. allatostatin A, and drosulfakinin that inhibit feeding behavior.

In addition to the hydrolysis of peptides regulating feeding behavior, Nep4 also cleaves numerous peptides involved in the regulation of insulin like peptide expression. Additionally to sNPF1 and sNPF2, Hallier, Schiemann et al., (2016) could show that Nep4 hydrolyses tachykinin1, 2, 4 and 5, allatostatin A, DH_{31} and AKH, all of which are known to regulate *dilp* expression (**Table 7**). These findings indicate that the Nep4 mediated regulation of *dilp* expression in *Drosophila* is not only depending on proper sNPF hydrolysis, but also on the cleavage of other regulatory peptides, with sNPF probably being a key player. However, Nep4 evidently cleaves a wide range of peptides that are regulative to feeding behavior and insulin expression, which identifies the peptidase as a major regulator of corresponding signaling cascades in *Drosophila*.

Name	Sequence	Mass (Da)	Δ(Da)	Sequence of cleavage products	Mass (Da)	Δ(Da)	Cleavage position
Allatostatin A1	VERYAFGLa[4]	953.5	−0.0676	VERYAFG	840.4	−0.0893	G/L
				VERYAF	783.4	−0.0898	F/G
Allatostatin A2	LPVYNFGLa[5]	920.5	−0.0205	LPVYNFG	808.4	−0.0492	G/L
				LPVYNF	751.4	−0.0148	F/G
				LPVYN	604.3	−0.0223	N/F
Allatostatin A3	SRPYSFGLa[1, 4]	924.5	−0.0523	YSFGLa	584.3	−0.0241	P/Y
Allatostatin A4	TTRPQPFNFGLa[1, 4, 5]	1275.7	−0.0629	TTRPQPFNFG	1163.6	−0.0850	G/L
				TTRPQPFN	959.5	−0.0790	N/F
				FNFGLa	595.3	−0.0301	P/F
AKH	QLTFSPDWa[1, 2, 3, 4]	992.5	0.0051	TFSPDWa	750.3	−0.0360	L/T
				FSPDWa	649.3	−0.0473	T/F
Corazonin	QTFQYSRGWTNa[1, 2, 3, 4, 5]	1385.6	−0.0582	FQYSRGWTNa	1156.5	−0.0319	T/F
				QTFQYSRG	985.5	−0.0743	G/W
DH[31]	TVDFGLARGYSGTQ-EAKHRMGLAAANFA-GGPa[n.d.]	3149.5	−0.0814	YSGTQEAKHRMG	1363.6	−0.1761	G/Y; G/L
				TVDFGLARG	934.5	−0.0198	G/Y
Drosulfakinin 1	FDDYGHMRFa[1, 4, 5]	1185.5	−0.0572	FDDYGHMR	1039.4	−0.1147	R/F
Drosulfakinin 2	GGDDQFDDYGHMRFa[1, 4, 5]	1657.7	−0.0298	GGDDQFDDYGHMR	1511.6	−0.1201	R/F
				FDDYGHMRFa	1185.5	−0.0711	Q/F
Leucokinin	NSVVLGKKQRFHSWGa[1, 3, 4, 5]	1741.0	−0.0905	NSVVLGKKQRFHS	1498.3	−0.1474	S/W
				NSVVLGKKQRFH	1411.8	−0.1094	H/S
				NSVVLGKKQR	1127.7	−0.1121	R/F
				FHSWGa	631.3	−0.0100	R/F
sNPF1[1-11]	AQRSPSLRLRFa[2, 3, 4]	1328.8	−0.0520	AQRSPSLRL	1026.6	−0.0962	L/R
sNPF1[4-11]/ sNPF2[12-19]	SPSLRLRFa[1, 2, 3, 4, 5]	973.6	−0.0859	SPSLRLR	827.5	−0.1543	R/F
				LRLRFa	702.5	−0.1451	S/L
Tachykinin 1	APTSSFIGMRa[1, 4]	1064.5	−0.0579	APTSSFIG	778.4	−0.0434	G/M
				FIGMRa	621.3	−0.0706	S/F
Tachykinin 2	APLAFVGLRa[1, 5]	941.6	−0.0396	LAFVGLRa	773.5	−0.0858	P/L
				APLAFVG	673.4	−0.0202	G/L
				FVGLRa	589.4	−0.0686	A/F
				APLAF	517.3	−0.0183	F/V
Tachykinin 4	APVNSFVGMRa[1, 4, 5]	1075.6	−0.0742	APVNSFVG	789.4	−0.0314	G/M
Tachykinin 5	APNGFLGMRa[1, 5]	960.5	0.0231	FLGMRa	621.3	−0.0666	G/F
Hugin	SVPFKPRLa[1, 2, 3, 4, 5]	941.6	−0.0776				
NPF	SNSRPPRKNDVNTMA-DAYKFLQDLDTYYGD-RARVRFa[n.d.]	4278.2	0.50				
Proctolin	RYLPT[n.d.]	648.4	−0.0841				
sNPF3	KPQRLRWa[5]	981.6	−0.05				
sNPF4	KPMRLRWa[5]	984.6	−0.05				
Tachykinin 3	APTGFTGMRa[1]	935.5	−0.0733				
Tachykinin 6	AALSDSYDLRGKQQR-FADFNSKFVAVRa[n.d.]	3087.6	−0.1694				

Table 7| List of substrates tested for Neprilysin 4 mediated cleavage. The molecular masses of full-length peptides and respective cleavage products are depicted as the monoisotopic value. The cleavage position and deviations from the respective theoretical masses (Δ) are shown separately. All cleaved peptides are marked in blue and all non-cleaved peptides are marked in red. Superscripts indicate the studies that biochemically characterized the respective peptides [1](Baggerman et al., 2005; [2]Predel et al., 2004; [3]Wegener et al., 2006, [4]2008; [5]Yew et al., 2009). n.d. indicated not detected, thus the respective sequence represents a genomic data based prediction. (Hallier et al., 2016)

4.3 Neprilysin 4 controls metabolic homeostasis

This thesis reveals that animals with altered *nep4* expression exhibit a misregulated expression of insulins due to an impaired homeostasis of signaling peptides, being regulative to either *ilp* expression, feeding behavior, or both (**Figure 8**; **Table 7**) (Hallier et al., 2016). Aiming to correlate these findings to the observed phenotypes of suffering from a decreased body size, body weight and, above all, pupal lethality, *nep4*

overexpression and knockdown larvae were analyzed for their metabolic composition and compared to wildtype animals. This analysis revealed substantial differences in the respective metabolite concentrations (**Figure 7**). Among other changes, Nep4A overexpressing animals exhibit significantly reduced NAD and lactate concentrations, whereas glucose and fructose levels are significantly elevated in the respective animals, compared to control specimen (**Figure 7**| B, C). Interestingly, reduced concentrations of lactate and NAD are indicative of impaired aerobic glycolysis. Aerobic glycolysis is a metabolic program, which is activated ca. 12h before the end of embryogenesis in *Drosophila melanogaster*. This program allows the hatched first instar larvae to efficiently metabolize the fed carbohydrates into biomass, which is necessary to sustain the dramatic increase in body mass that occurs during larval development. An impairment of aerobic glycolysis during the larval growth phase results in larval lethality due to the inability of the respective animals to metabolize sufficient amounts of sugar (Kannan and Fridell, 2013; Tennessen et al., 2011, 2014). The facts that Nep4A overexpression animals die during larval development (**Figure 6**| D), are significantly decreased in size and weight (**Figure 6**| C), and exhibit a reduced concentration of lactate and NAD as well as elevated levels of glucose and fructose (**Figure 7**| B, C), indicate impaired onset or progression of aerobic glycolysis. A physiological reason for this impairment could be the fact that corresponding animals also exhibit severely decreased levels of *dilp* expression (**Figure 8**| B), which likely reduces the extent of sugar resorption by muscle or fat body cells.

It therefore appears reasonable that elevated Nep4A activity at the surface of somatic muscles detrimentally increases cleavage of gut derived hemolymph circulating regulatory peptides (such as sNPF), which inhibits proper signal transduction and thus decreases expression of insulins by the IPCs. The decreased insulin levels likely result in impaired sugar resorption into body cells, which interrupts aerobic glycolysis and causes elevated levels of circulating glucose and fructose as well as a reduced accumulation of NAD and lactate (**Figure 29**).
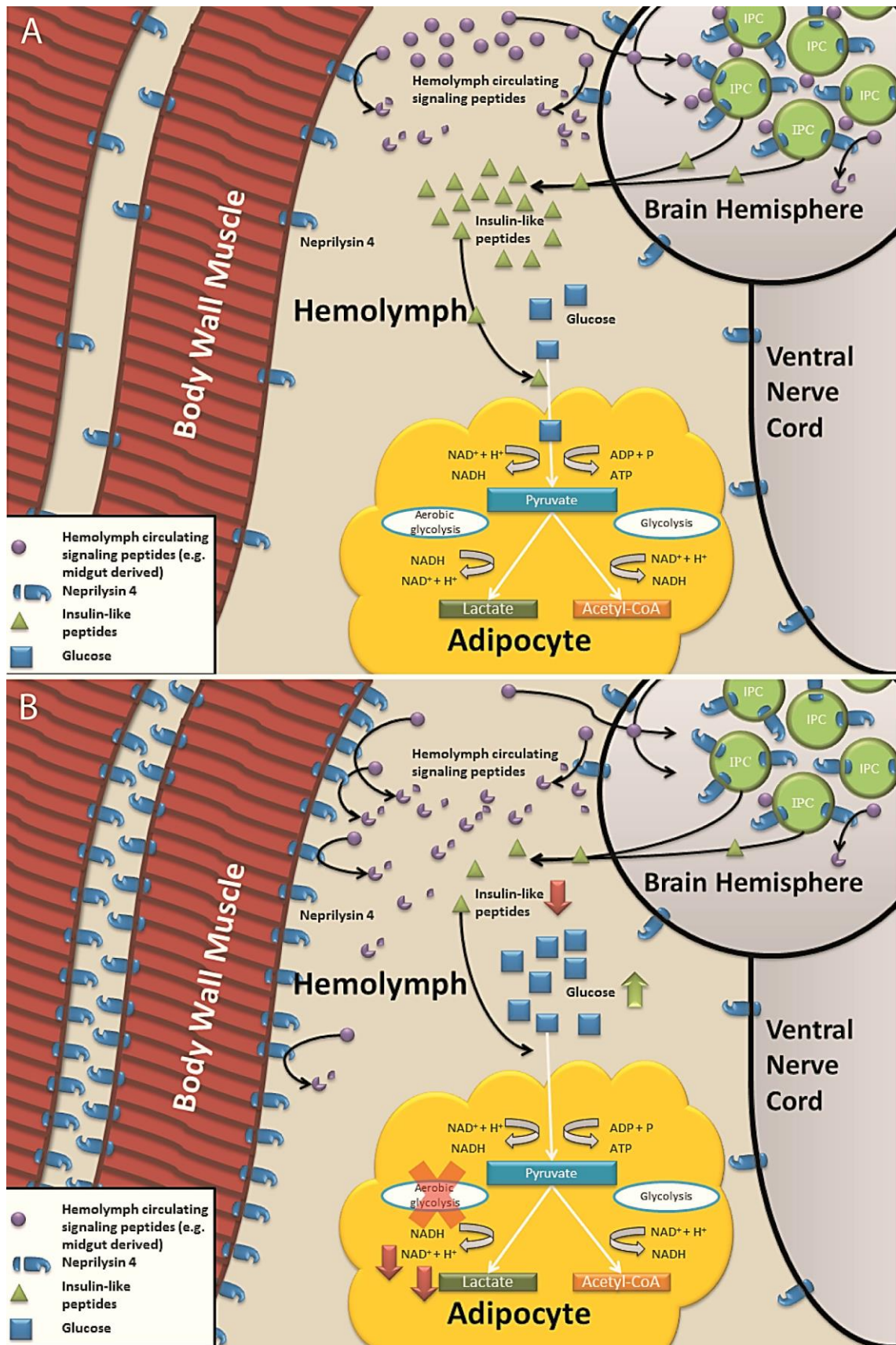
Figure 29| Working model. A: Neprilysin 4A localizes to the surface of body wall muscles as well as of the CNS consisting of the ventral nerve cord, two brain hemispheres, and the insulin producing cells (IPCs) embedded therein. Nep4A hydrolyzes hemolymph circulating signaling peptides (e.g. short Neuropeptide F), which are mainly midgut derived. The signaling peptides

bind to their respective receptor at the surface of the IPCs, thus stimulating *insulin-like peptide (ilp)* expression. ILP production and release lead to uptake of glucose by somatic cells (predominately muscle cells and adipocytes) which metabolize glucose to pyruvate. In the presence of oxygen, pyruvate is further metabolized to Acetyl-CoA. In contrast to this, under conditions of oxygen limitation lactate is formed under the consumption of NADH to $NAD^+ + H^+$ (aerobic glycolysis). **B:** Under Nep4A overexpressing (muscle specific) conditions, the elevated levels of Nep4A lead to an increased rate of Nep4A mediated cleavage of hemolymph circulating signaling peptides. This causes reduced activation of their corresponding receptors on the surface of the IPCs and thus a decreased production of ILPs. This course of events results in an impaired resorption of glucose into somatic cells that interrupts aerobic glycolysis and thus causes increased levels of glucose and decreased levels of lactate and NAD.

Neprilysins and many of its identified substrates (this thesis and Hallier et al., 2016) are evolutionary conserved factors. It is thus likely that the neprilysin mediated regulation of insulin signaling and feeding behavior characterized in *Drosophila* is also relevant to the corresponding processes in vertebrates, including humans. It has recently been shown that neprilysins in mice cleave the Glucagon-like peptide (homolog of *Drosophila* sNPF*)* and thereby affect insulin expression (Willard et al., 2016). This indicates that the physiological functionality of Neprilysin activity is evolutionarily conserved. Thus, the principles characterized in this study presumably apply to a multitude of species and may pave the way for numerous future studies addressing the corresponding processes in higher eukaryotes, including humans.

4.4 Truncation of one catalytically relevant motif of Neprilysin 4 affects male fertility, but not animal development

This thesis revealed that the *nep4^{MI03765}* allele of the fly line Bl36979 is truncated by 130 aa at the C-terminus and that this truncation includes one of the two major catalytically relevant motifs of Nep4 (EAxxG/D (Oefner et al., 2000)) (**Figure 16**). In addition, the CxxW motif is deleted, which is responsible for correct protein folding (Bland et al., 2008). Despite the deletion, it is evident that the truncation has no effect on either protein synthesis or maintenance, as the truncated form is still detectable by western blot using adult protein preparations (**Figure 17**). In addition, wildtypic subcellular localization of truncated Nep4 is confirmed by antibody stainings in embryos (**Figure 18**| A, A´). Interestingly, the truncation has no distinct effect on embryogenesis, which

is also true for larval and pupal development. Homozygous mutant animals still develop into adult flies (**Figure 18**; **Figure 19**). Notably, *nep4* knockdown animals as well as homozygous specimen of the *nep4$^{\Delta281\text{-}1040}$* allele, exhibiting a considerably larger C-terminal truncation (**Figure 22**), suffer from pupal lethality (**Figure 6**; **Figure 25**). Taking this into consideration, it appears possible that the protein Nep4^{MI03765} retains some of its catalytic activity, which is sufficient to survive metamorphosis. However, it is more likely that the extracellular domain of Nep4 has a yet unknown function independent of its catalytic activity, which is still present in Nep4^{MI03765}, but absent in Nep4$^{\Delta281\text{-}1040}$ or *nep4*-RNAi animals. This yet uncharacterized function may account for the difference between pupal lethality and survival.

Among other tissues, *nep4* is expressed in male gonads, apparently starting in early spermatocytes and persisting until late stage spermatids (Meyer et al., 2009; Zhao et al., 2010). This finding indicates a function of Nep4 during spermatogenesis, thus flies of line Bl36979 where tested for fertility. All male adults homozygous for the truncated *nep4^{MI03765}* allele failed to generate offspring in all analyzed single pair crossings, whereas homozygous female flies and heterozygous female and male flies were fertile (**Figure 20**). This result is in line with the fact that the fly stock Bl36979 cannot be maintained under homozygous conditions, thus only heterozygous animals, holding a balancer chromosome, are stable as a stock. Up to now the specific function(s) or substrates of Neprilysin 4 in testes remains unknown. Interestingly, *nep4* is not the only *neprilysin* expressed in male gonads. Nep2 and Nep5 are also known to be present in testes (Sitnik et al., 2014; Thomas et al., 2005). In addition, the mammalian Neprilysin family members SEP/NL1, as well as the angiotensin converting enzyme (ACE), were found to be present in male gonads of mice, participating in spermatogenesis. Furthermore, it was shown that mice mutant for SEP or ACE show reduced fertility (Carpentier et al., 2004; Ghaddar et al., 2000; Hurst et al., 2003; Krege J. H. et al., 1995). Based on the putatively conserved functionality of neprilysins in male gonads, further investigation of neprilysin function and the identification of tissue-specific substrates appear necessary to understand the relevance of the peptidases to male fertility in more detail.

4.5 Severe truncation of Neprilysin 4 affects larval development

One subordinate aim of this thesis was the generation of a *neprilysin 4* knockout line. In this effort, a CRISPR/Cas9 mediated approach was performed (2.2.8), which resulted in a fly line lacking ca. 1,9kbp of the *nep4* coding sequence (**Figure 21**). The resulting C-terminally truncated *nep4* allele was named *nep4*$^{\Delta281-1040}$ to indicate the truncation on the amino acid level. In this line, ca. 80% of the extracellular Nep4 domain is deleted, which includes both catalytically relevant motifs (HExxH and ExxA/GD) (**Figure 22**). Although 759 amino acids of the total 1040 amino acids are removed, the protein is synthesized, stable, and localizes correctly in the animals, as confirmed by western blot of larval proteome preparations and via antibody staining of developing embryos (**Figure 23**; **Figure 24**| A, A´). These results were rather unexpected. Since ca. 70% of the total protein is deleted, it was likely that the protein would be recognized as faulty and become degraded by proteasomes. However, apparently the intracellular and the transmembrane domain are stable, explaining the correct localization. Importantly, the epitope of the applied anti-Nep4 antibody is located in the remaining part of the protein (Meyer et al., 2009) (**Figure 22**). Considering that both catalytically relevant motifs (HExxH and ExxA/GD) as well as the CxxW motif, responsible for correct protein folding (Bland et al., 2008; Oefner et al., 2000), are deleted, it appears ensured that the Nep4$^{\Delta281-1040}$ protein is catalytically inactive. To further characterize the respective line, all tissues were stained in which *nep4* is expressed during embryogenesis to discover possible phenotypes. The fact that all tissues tested appeared wildtypic (**Figure 24**) represents good evidence that the catalytic activity of Nep4 is not essential to proper embryogenesis, which agrees with the results of line Bl36979, in which the respective animals also develop normally during embryogenesis (**Figure 18**). By contrast, characterization of the larval physiology of line Nep4$^{\Delta281-1040}$ identified clear phenotypes. Corresponding larvae exhibit a reduced locomotion speed (**Figure 26**) as well as an impaired feeding behavior (**Figure 28**). In addition, only a small amount of animals homozygous for the truncated n*ep4*$^{\Delta281-1040}$ allele reach metamorphosis and no respective animal survives the pupal stage (**Figure 25**). Interestingly, animals homozygous for the *nep4*^{MI03765} allele (line Bl36979) develop normally during larval stage and survive metamorphosis, although the Nep4^{MI03765} protein is likely also catalytically inactive. This discrepancy represents further support to the initial evidence

that the extracellular domain exhibits a yet unknown function critical to larval development and metamorphosis (see above). In future experiments cleavage assays using the two truncated proteins should be performed in order to assess, if both proteins, $Nep4^{MI03765}$ and $Nep4^{\Delta281-1040}$, are catalytically inactive. Therefore, the proteins could be expressed in insect cells and treated with known Nep4 substrates, which were identified in this thesis (e.g. sNPF) or in (Hallier et al., 2016).

The results that homozygous mutant larvae from line $Nep4^{\Delta281-1040}$ exhibit a reduced locomotion speed, which is not caused by muscle degeneration (**Figure 27**), and an impaired food intake, as well as pupal lethality, phenocopy *nep4* knockdown phenotypes. Corresponding animals also exhibit a reduced locomotion speed, pupal lethality and impaired feeding (**Figure 6**; **Figure 8**) (Panz et al., 2012). These facts support the hypothesis that the phenotypes observed in line $Nep4^{\Delta281-1040}$ are due to the truncated $Nep4^{\Delta281-1040}$ protein and not due to any CRISPR/Cas9 off target cutting event. However, this possibility cannot be excluded completely at the moment. Consequently, it is necessary to perform rescue experiments, in which wildtype Nep4 is expressed within the $Nep4^{\Delta281-1040}$ mutant animals, to potentially neutralize the observed phenotypes. Therefore, one could express ubiquitously, CNS- or muscle-specifically *nep4* via the UAS-GAL4 system in the *nep4* CRISPR mutant background. If the phenotypes can be (partially) rescued, this would prove that the observed effects are Nep4 dependent.

To further characterize the $Nep4^{\Delta281-1040}$ mutant, it would be interesting to check for the metabolic composition and the *dilp* expression levels. As shown in this thesis, altered *nep4* expression has an effect on the level of insulin expression in the fly and also on the metabolic composition (**Figure 7**; **Figure 8**), due to a misbalanced homeostasis of regulatory peptides cleaved by Nep4 (Hallier et al., 2016). If $Nep4^{\Delta281-1040}$ animals would also show corresponding phenotypes, these results would represent additional evidence that the phenotypes occurring in the mutant line are caused by the truncated $Nep4^{\Delta281-1040}$.

It is likely that larvae suffering from dysregulated insulin signaling, and thus from impaired aerobic glycolysis and insufficient food intake, are not able to store sufficient energy to reach or survive metamorphosis. Therefore, it is important to perform metabolomic analyses with the mutant fly lines, to check their metabolic composition, especially with respect to the levels of glucose, fructose, NAD and lactate. In order to

evaluate the expression levels of insulins within the mutant fly lines, an established method would be application of quantitative real time PCRs.

Taken together, the data raised in this thesis identify and characterize the peptidase Neprilysin 4 as a novel and essential factor controlling homeostasis of regulatory peptides within the hemolymph of *Drosophila melanogaster*. Increased Neprilysin activity as well as reduced or abolished activity results in an imbalance of the peptide homeostasis, which eventually leads to abnormal insulin signaling and reduced food intake. These impairments severely affect energy metabolism, which in the end leads to lethality of the respective animals during larval development or metamorphosis at the latest.

5 Literature

Arvidsson, S., Kwasniewski, M., Riaño-Pachón, D.M., and Mueller-Roeber, B. (2008). QuantPrime--a flexible tool for reliable high-throughput primer design for quantitative PCR. BMC Bioinformatics *9*, 465.

Ashburner, M., Golic, K.G., and Hawley, R.S. (2005). *Drosophila* : a laboratory handbook (Cold Spring Harbor Laboratory Press).

Baggerman, G., Boonen, K., Verleyen, P., De Loof, A., and Schoofs, L. (2005). Peptidomic analysis of the larval *Drosophila melanogaster* central nervous system by two-dimensional capillary liquid chromatography quadrupole time-of-flight mass spectrometry. J. Mass Spectrom. *40*, 250–260.

Barnes, K., Doherty, S., and Turner, A.J. (1995). Endopeptidase- 24.11 Is the Integral Membrane Peptidase Initiating Degradation of Somatostatin in the Hippocampus. J. Neurochem. *64*, 1826–1832.

Bayes-Genis, A., Barallat, J., and Richards, A.M. (2016). A Test in Context: Neprilysin. J. Am. Coll. Cardiol. *68*, 639–653.

Bellen, H.J., Levis, R.W., He, Y., Carlson, J.W., Evans-Holm, M., Bae, E., Kim, J., Metaxakis, A., Savakis, C., Schulze, K.L., et al. (2011). The *Drosophila* Gene Disruption Project: Progress Using Transposons With Distinctive Site Specificities. Genetics *188*, 731–743.

Belyaev, N.D., Nalivaeva, N.N., Makova, N.Z., and Turner, A.J. (2009). Neprilysin gene expression requires binding of the amyloid precursor protein intracellular domain to its promoter: implications for Alzheimer disease. EMBO Rep. *10*.

Bland, N.D., Thomas, J.E., Audsley, N., Shirras, A.D., Turner, A.J., and Isaac, R.E. (2007). Expression of NEP2, a soluble neprilysin-like endopeptidase, during embryogenesis in *Drosophila melanogaster*. Peptides *28*, 127–135.

Bland, N.D., Pinney, J.W., Thomas, J.E., Turner, A.J., and Isaac, R.E. (2008). Bioinformatic analysis of the neprilysin (M13) family of peptidases reveals complex evolutionary and functional relationships. BMC Evol. Biol. *8*, 16.

Bland, N.D., Robinson, P., Thomas, J.E., Shirras, A.D., Turner, A.J., and Isaac, R.E. (2009). Locomotor and geotactic behavior of *Drosophila melanogaster* over-expressing neprilysin 2. Peptides *30*, 571–574.

Bonvouloir, N., Lemieux, N., Crine, P., Boileau, G., and Desgroseillers, L. (2001). Molecular Cloning, Tissue Distribution, and Chromosomal Localization of MMEL2, a Gene Coding for a Novel Human Member of the Neutral Endopeptidase-24.11 Family. *20*, 493–498.

Brand, A.H., and Perrimon, N. (1993). Targeted gene expression as a means of altering cell fates and generating dominant phenotypes. Development *118,* 401–415.

Brogiolo, W., Stocker, H., Ikeya, T., Rintelen, F., Fernandez, R., and Hafen, E. (2001). An evolutionarily conserved function of the *Drosophila* insulin receptor and insulin-like peptides in growth control. Curr. Biol. *11*, 213–221.

Broughton, S.J., Piper, M.D.W., Ikeya, T., Bass, T.M., Jacobson, J., Driege, Y., Martinez, P., Hafen, E., Withers, D.J., Leevers, S.J., et al. (2005). Longer lifespan, altered metabolism, and stress resistance in *Drosophila* from ablation of cells making insulin-like ligands. Proc. Natl. Acad. Sci. *102*, 3105–3110.

Brown, G., Hogg, N., and Greaves, M. (1975). Candidate leukaemia-specific antigen in man. Nature *258*, 454–456.

Cao, C., and Brown, M.R. (2001). Localization of an insulin-like peptide in brains of two flies. Cell Tissue Res. *304*, 317–321.

Carlsson, M.A., Enell, L.E., and Nässel, D.R. (2013). Distribution of short neuropeptide F and its receptor in neuronal circuits related to feeding in larval *Drosophila*. Cell Tissue Res. *353*, 511–523.

Carpentier, M., Guillemette, C., Bailey, J.L., Boileau, G., Jeannotte, L., DesGroseillers, L., and Charron, J. (2004). Reduced fertility in male mice deficient in the zinc metallopeptidase NL1. Mol. Cell. Biol. *24*, 4428–4437.

Cerdà-Costa, N., and Xavier Gomis-Rüth, F. (2013). Architecture and function of metallopeptidase catalytic domains. Protein Sci. *23*, 123–144.

Chen, J., Reiher, W., Hermann-Luibl, C., Sellami, A., Cognigni, P., Kondo, S., Helfrich-Förster, C., Veenstra, J.A., Wegener, C., Boonen, K., et al. (2016a). Allatostatin A Signalling in *Drosophila* Regulates Feeding and Sleep and Is Modulated by PDF. PLOS Genet. *12*, e1006346.

Chen, P.-T., Chen, C.-L., Lin, L.T.-W., Lo, C.-H., Hu, C.-J., Chen, R.P.-Y., Wang, S.S.-S., Jakob-Roetne, R., Jacobsen, H., Mangialasche, F., et al. (2016b). Design of Peptide

Substrate for Sensitively and Specifically Detecting Two Aβ-Degrading Enzymes: Neprilysin and Angiotensin-Converting Enzyme. PLoS One *11*, e0153360.

Dillen, S., Zels, S., Verlinden, H., Spit, J., Van Wielendaele, P., Vanden Broeck, J., Nässel, D., Wegener, C., Broeck, J. Vanden, Ons, S., et al. (2013). Functional Characterization of the Short Neuropeptide F Receptor in the Desert Locust, Schistocerca gregaria. PLoS One *8*, e53604.

De Felipe, C., Herrero, J.F., O'Brien, J.A., Palmer, J.A., Doyle, C.A., Smith, A.J., Laird, J.M., Belmonte, C., Cervero, F., and Hunt, S.P. (1998). Altered nociception, analgesia and aggression in mice lacking the receptor for substance P. Nature *392*, 394–397.

Fischer, H.S., Zernig, G., Hauser, K.F., Gerard, C., Hersh, L.B., and Saria, A. (2002). Neutral Endopeptidase Knockout Induces Hyperalgesia in a Model of Visceral Pain, an Effect Related to Bradykinin and Nitric Oxide. J. Mol. Neurosci. *129*.

Garczynski, S.F., Brown, M.R., and Crim, J.W. (2006). Structural studies of *Drosophila* short neuropeptide F: Occurrence and receptor binding activity. Peptides *27*, 575–582.

Géminard, C., Rulifson, E.J., and Léopold, P. (2009). Remote Control of Insulin Secretion by Fat Cells in *Drosophila*. Cell Metab. *10*, 199–207.

Ghaddar, G., Ruchon, F., Carpentier, lanie, Marcinkiewicz, M., Seidah, N.G., Crine, P., Desgroseillers, L., and Boileau, G. (2000). Molecular cloning and biochemical characterization of a new mouse testis soluble-zinc-metallopeptidase of the neprilysin family. Biochem. J *347*, 419–429.

Gomis-Rüth, F.X. (2003). Structural Aspects of the Metzincin Clan of Metalloendopeptidases. Mol. Biotechnol. *24*.

Green, M.R., and Sambrook, J. (2012). Molecular Cloning, A LABORATORY MANUAL (New York).

Hallier, B., Schiemann, R., Cordes, E., Vitos-Faleato, J., Heinisch, J., Malmendal, A., Paululat, A., Walter, S., and Meyer, H. (2016). *Drosophila* neprilysins control insulin signaling and food intake via cleavage of regulatory peptides. Elife 1–22.

Hergarden, A.C., Tayler, T.D., and Anderson, D.J. (2012). Allatostatin-A neurons inhibit feeding behavior in adult *Drosophila*. Proc. Natl. Acad. Sci. U. S. A. *109*, 3967–3972.

Hershl, L.B., and Morihara, K. (1986). Comparison of the Subsite Specificity of the Mammalian Neutral Endopeptidase 24.11 (Enkephalinase) to the Bacterial Neutral Endopeptidase Thermolysin " J. Biol. Chem. *261*, 6433–6437.

Hupe-Sodmann, K., McGregor, G.P., Bridenbaugh, R., Göke, R., Göke, B., Thole, H., Zimmermann, B., and Voigt, K. (1995). Characterisation of the processing by human neutral endopeptidase 24.11 of GLP-1(7–36) amide and comparison of the substrate specificity of the enzyme for other glucagon-like peptides. Regul. Pept. *58*, 149–156.

Hurst, D., Rylett, C.M., Isaac, R.E., and Shirras, A.D. (2003). The *Drosophila* angiotensin-converting enzyme homologue Ance is required for spermiogenesis. Dev. Biol. *254*, 238–247.

Ikeya, T., Galic, M., Belawat, P., Nairz, K., and Hafen, E. (2002). Nutrient-Dependent Expression of Insulin-like Peptides from Neuroendocrine Cells in the CNS Contributes to Growth Regulation in *Drosophila*. Curr. Biol. *12*, 1293–1300.

Isaac, R.E., Johnson, E.C., Audsley, N., and Shirras, A.D. (2007). Metabolic inactivation of the circadian transmitter, pigment dispersing factor (PDF), by neprilysin-like peptidases in *Drosophila*. J. Exp. Biol. *210*, 4465–4470.

Iwata, N., Higuchi, M., and Saido, T.C. (2005). Metabolism of amyloid-β peptide and Alzheimer's disease. Pharmacol. Ther. *108*, 129–148.

Johard, H. a D., Yoishii, T., Dircksen, H., Cusumano, P., Rouyer, F., Helfrich-Förster, C., and Nässel, D.R. (2009). Peptidergic clock neurons in *Drosophila*: ion transport peptide and short neuropeptide F in subsets of dorsal and ventral lateral neurons. J. Comp. Neurol. *516*, 59–73.

Kahsai, L., Martin, J.-R., and Winther, Å.M.E. (2010). Neuropeptides in the *Drosophila* central complex in modulation of locomotor behavior. J. Exp. Biol. *213*.

Kannan, K., and Fridell, Y.-W.C. (2013). Functional implications of *Drosophila* insulin-like peptides in metabolism, aging, and dietary restriction. Front. Physiol. *4*, 288.

Kenny, A.J., and Stephenson, S.L. (1988). Role of endopeptidase- 24.11 in the inactivation of atrial natriuretic peptide. FEBS Lett. *232*, 1–8.

Kerr, M.A., and Kenny, A.J. (1974). The Purification and Specificity of a Neutral Endopeptidase from Rabbit Kidney Brush Border. Biochem. J *137*.

Khalid, W., Vargheese, S.S., Lakshmanan, R., Sankari, M., and Jayakumar, N.D. (2016). Role of endothelin-1 in periodontal diseases: A structured review. Indian J. Dent. Res. *27*, 323–333.

Krege J. H., John S. W., Langenbach L. L., Hodgin J. B., Hagaman J. R., Bachman E. S., Jennette J. C., O'Brien D. A., and Smithies O. (1995). Male-female differences in fertility and blood pressure in ACE-deficient mice Nature. Nature *375*, 146–148.

LAEMMLI, U.K. (1970). Cleavage of Structural Proteins during the Assembly of the Head of Bacteriophage T4. Nature *227*, 680–685.

Lee, K.-S., You, K.-H., Choo, J.-K., Han, Y.-M., and Yu, K. (2004). *Drosophila* short neuropeptide F regulates food intake and body size. J. Biol. Chem. *279*, 50781–50789.

Lee, K.-S., Kwon, O.-Y., Lee, J.H., Kwon, K., Min, K.-J., Jung, S.-A., Kim, A.-K., You, K.-H., Tatar, M., and Yu, K. (2008). *Drosophila* short neuropeptide F signalling regulates growth by ERK-mediated insulin signalling. Nat. Cell Biol. *10*, 468–475.

Lee, K.-S., Hong, S.-H., Kim, A.-K., Ju, S.-K., Kwon, O.-Y., and Yu, K. (2009). Processed short neuropeptide F peptides regulate growth through the ERK-insulin pathway in *Drosophila melanogaster*. FEBS Lett. *583*, 2573–2577.

Martinez, A.N., and Philipp, M.T. (2016). Substance P and Antagonists of the Neurokinin-1 Receptor in Neuroinflammation Associated with Infectious and Neurodegenerative Diseases of the Central Nervous System. J. Neurol. Neuromedicine *1*, 29–36.

Mashaghi, A., Marmalidou, A., Tehrani, M., Grace, P.M., Pothoulakis, C., and Dana, R. (2016). Neuropeptide substance P and the immune response. Cell. Mol. Life Sci. 1–16.

Matsas, R., Fulcher, I.S., Kenny, A.J., and Turner, A.J. (1983). Substance P and [Leul]enkephalin are hydrolyzed by an enzyme in pig caudate synaptic membranes that is identical with the endopeptidase of kidney microvilli (neuropeptide degradation/peptidase/phosphoramidon/high-performance liquid chromatography). Neurobiology *80*, 3111–3115.

Matsas, R., Kenny, A.J., Turner, A.J., and Membrane, M.R.C. (1984). The metabolism of neuropeptides. Biochem. J *223*, 433–440.

Matthews, B.W. (1988). Structural Basis of the Action of Thermolysin and Related Zinc Peptidases Inhibitor Binding. Acc. Chem. Res *21*, 333–340.

McMurray, J.J. V, Packer, M., Desai, A.S., Gong, J., Lefkowitz, M.P., Rizkala, A.R., Rouleau, J.L., Shi, V.C., Solomon, S.D., Swedberg, K., et al. (2014). Angiotensin–Neprilysin Inhibition versus Enalapril in Heart Failure. N Engl J Med Novartis Pharm. N Engl J Med *37111371*, 993–1004.

Meyer, H., Panz, M., Zmojdzian, M., Jagla, K., and Paululat, A. (2009). Neprilysin 4, a novel endopeptidase from *Drosophila melanogaster*, displays distinct substrate specificities and exceptional solubility states. J. Exp. Biol. *212*, 3673–3683.

Meyer, H., Panz, M., Albrecht, S., Drechsler, M., Wang, S., Hüsken, M., Lehmacher, C., and Paululat, A. (2011). *Drosophila* metalloproteases in development and differentiation: the role of ADAM proteins and their relatives. Eur. J. Cell Biol. *90*, 770–778.

Mistrova, E., Kruzliak, P., and Chottova Dvorakova, M. (2015). Role of substance P in the cardiovascular system. Neuropeptides.

Molinaro, G., Rouleau, J.-L., and Adam, A. (2002). Vasopeptidase inhibitors: a new class of dual zinc metallopeptidase inhibitors for cardiorenal therapeutics. Curr. Opin. Pharmacol. *2*, 131–141.

Nässel, D.R., and Winther, Å.M.E. (2010). *Drosophila* neuropeptides in regulation of physiology and behavior. Prog. Neurobiol. *92*, 42–104.

Nässel, D.R., Enell, L.E., Santos, J.G., Wegener, C., and Johard, H.A. (2008). A large population of diverse neurons in the *Drosophila* central nervous system expresses short neuropeptide F, suggesting multiple distributed peptide functions. BMC Neurosci. *9*, 90.

Nässel, D.R., Kubrak, O.I., Liu, Y., Luo, J., and Lushchak, O. V. (2013). Factors that regulate insulin producing cells and their output in *Drosophila*. Front. Physiol. *4*.

Oefner, C., D'Arcy, A., Hennig, M., Winkler, F.K., and Dale, G.E. (2000). Structure of Human Neutral Endopeptidase (Neprilysin) Complexed with Phosphoramidon. J. Mol. Biol *296*, 341±349.

Oefner, C., Roques, B.P., Fournie-Zaluski, M.C., and Dale, G.E. (2004). Structural analysis of neprilysin with various specific and potent inhibitors. Acta Crystallogr. Sect. D Biol. Crystallogr. *60*, 392–396.

Panz, M., Vitos-Faleato, J., Jendretzki, A., Heinisch, J.J., Paululat, A., and Meyer, H. (2012). A novel role for the non-catalytic intracellular domain of Neprilysins in muscle

physiology. Biol. Cell *104*, 553–568.

Paululat, A., and Heinisch, J.J. (2012). New yeast / E . coli / *Drosophila* triple shuttle vectors for ef fi cient generation of *Drosophila* P element transformation constructs. *511*, 300–305.

Pool, A.-H., and Scott, K. (2014). Feeding regulation in *Drosophila*. Curr. Opin. Neurobiol. *29*, 57–63.

Predel, R., Wegener, C., Russell, W.K., Tichy, S.E., Russell, D.H., and Nachman, R.J. (2004). Peptidomics of CNS-associated neurohemal systems of adult *Drosophila melanogaster*: A mass spectrometric survey of peptides from individual flies. J. Comp. Neurol. *474*, 379–392.

Reiher, W., Shirras, C., Kahnt, J., Baumeister, S., Isaac, R.E., and Wegener, C. (2011). Peptidomics and Peptide Hormone Processing in the *Drosophila* Midgut. J. Proteome Res. *10*, 1881–1892.

Roques, B.P., Noble, F., Daugé, V., Fournié-Zaluski, M.C., and Beaumont, A. (1993). Neutral endopeptidase 24.11: structure, inhibition, and experimental and clinical pharmacology. Pharmacol. Rev. *45*, 87–146.

Rose, J.B., Crews, L., Rockenstein, E., Adame, A., Mante, M., Hersh, L.B., Gage, F.H., Spencer, B., Potkar, R., Marr, R.A., et al. (2009). Neuropeptide Y Fragments Derived from Neprilysin Processing Are Neuroprotective in a Transgenic Model of Alzheimer's Disease. Neurobiol. Dis. *29*, 1115–1125.

Rulifson, E.J., Kim, S.K., Nusse, R., Chen, C., Jack, J., Garofalo, R.S., Wyatt, G.R., Noyes, B.E., Katz, F.N., Schaffer, M.H., et al. (2002). Ablation of insulin-producing neurons in flies: growth and diabetic phenotypes. Science *296*, 1118–1120.

Saido, T.C., Iwata, N., Tsubuki, S., Takaki, Y., Watanabe, K., Sekiguchi, M., Hosoki, E., Kawashima-Morishima, M., Lee, H.-J., Hama, E., et al. (2000). Identification of the major A|[beta]|1|[ndash]|42-degrading catabolic pathway in brain parenchyma: Suppression leads to biochemical and pathological deposition. Nat. Med. *6*, 143–150.

Shipp, M.A., Tarr, G.E., Chen, C.-Y., Switzer, S.N., Hersh, L.B., Steins, H., Sundays, M.E., and Reinherz, E.L. (1991). CD10/neutral endopeptidase 24.11 hydrolyzes bombesin-like peptides and regulates the growth of small cell carcinomas of the lung (metalloendopeptidase/autocrine growth factors/cell surface enzyme/common acute lymphoblastic leukemia antigen). Cell Biol. *88*, 10662–10666.

Simon, P. (2003). Q-Gene: processing quantitative real-time RT-PCR data. Bioinformatics *19*, 1439–1440.

Sitnik, J.L., Francis, C., Hens, K., Huybrechts, R., Wolfner, M.F., and Callaerts, P. (2014). Neprilysins: An Evolutionarily Conserved Family of Metalloproteases That Play Important Roles in Reproduction in *Drosophila*. Genetics *196*, 781–797.

Söderberg, J.A.E., Carlsson, M.A., and Nässel, D.R. (2012). Insulin-Producing Cells in the *Drosophila* Brain also Express Satiety-Inducing Cholecystokinin-Like Peptide, Drosulfakinin. Front. Endocrinol. (Lausanne). *3*, 109.

Tennessen, J.M., Baker, K.D., Lam, G., Evans, J., and Thummel, C.S. (2011). The *Drosophila* estrogen-related receptor directs a metabolic switch that supports developmental growth. Cell Metab. *13*, 139–148.

Tennessen, J.M., Bertagnolli, N.M., Evans, J., Sieber, M.H., Cox, J., and Thummel, C.S. (2014). Coordinated metabolic transitions during *Drosophila* embryogenesis and the onset of aerobic glycolysis. G3 (Bethesda). *4*, 839–850.

Thomas, J.E., Rylett, C.M., Carhan, A., Bland, N.D., Bingham, R.J., Shirras, A.D., Turner, A.J., and Isaac, R.E. (2005). *Drosophila melanogaster* NEP2 is a new soluble member of the neprilysin family of endopeptidases with implications for reproduction and renal function. Biochem. J *386*, 357–366.

Tiraboschi, G., Jullian, N., Thery, V., Antonczak, S., Fournie-Zaluski, M.-C., and Roques, B.P. (1999). A three-dimensional construction of the active site (region 507 749) of human neutral endopeptidase (EC.3.4.24.11). Protein Eng. Des. Sel. *12*, 141–149.

Turner, a J., Isaac, R.E., and Coates, D. (2001). The neprilysin (NEP) family of zinc metalloendopeptidases: genomics and function. Bioessays *23*, 261–269.

Turrel, O., Lampin-Saint-Amaux, A., Préat, T., and Goguel, X.V. (2016). *Drosophila* Neprilysins Are Involved in Middle-Term and Long-Term Memory. J. Neurosci. *36*, 9535–9546.

Veenstra, J.A., Agricola, H.-J., and Sellami, A. (2008). Regulatory peptides in fruit fly midgut. Cell Tissue Res. *334*, 499–516.

Wang, Y., Peng, C., and Liu, Y. (2007). Low dose of bradykinin selectively increases intracellular calcium in glioma cells. J. Neurol. Sci. *258*, 44–51.

Ward, E.J., and Skeath, J.B. (2000). Characterization of a novel subset of cardiac cells and their progenitors in the *Drosophila* embryo. Development *127*, 4959–4969.

Wegener, C., Reinl, T., Jänsch, L., and Predel, R. (2006). Direct mass spectrometric peptide profiling and fragmentation of larval peptide hormone release sites in *Drosophila melanogaster* reveals tagma-specific peptide expression and differential processing. J. Neurochem. *96*, 1362–1374.

Wegener, C., Gorbashov, A., Conlon, J., Larhammar, D., Niall, H., Danielson, P., Dores, R., Holmgren, S., Jensen, J., Hoyle, C., et al. (2008). Molecular evolution of neuropeptides in the genus *Drosophila*. Genome Biol. *9*, R131.

Whitworth, J. (2003). Emerging drugs in the management of hypertension. Expert Opin. Emerg. Drugs *8*, 377–388.

Willard, J.R., Barrow, B.M., and Zraika, S. (2016). Improved glycaemia in high-fat-fed neprilysin-deficient mice is associated with reduced DPP-4 activity and increased active GLP-1 levels. Diabetologia.

William Sullivan, Michael Ashburner, and R. Scott Hawley (2000). *Drosophila* Protocols (Paperback).

Yew, J.Y., Wang, Y., Barteneva, N., Dikler, S., Kutz-Naber, K.K., Li, L., and Kravitz, E.A. (2009). Analysis of Neuropeptide Expression and Localization in Adult *Drosophila melanogaster* Central Nervous System by Affinity Cell-Capture Mass Spectrometry. J. Proteome Res. *8*, 1271–1284.

Zhao, J., Klyne, G., Benson, E., Gudmannsdottir, E., White-Cooper, H., and Shotton, D. (2010). FlyTED: the *Drosophila* Testis Gene Expression Database. Nucleic Acids Res. *38*, D710-5.

6 Appendix

6.1 Primer list

name	sequence
Dilp1 FWD (qRT-PCR)	GGGGCAGGATACTCTTTTAG
Dilp1 REV (qRT-PCR)	TCGGTAGACAGTAGATGGCT
Dilp2 FWD (qRT-PCR)	GTATGGTGTGCGAGGAGTAT
Dilp2 REV (qRT-PCR)	TGAGTACACCCCCAAGATAG
Dilp3 FWD (qRT-PCR)	AAGCTCTGTGTGTATGGCTT
Dilp3 REV (qRT-PCR)	AGCACAATATCTCAGCACCT
Dilp5 FWD (qRT-PCR)	AGTTCTCCTGTTCCTGATCC
Dilp5 REV (qRT-PCR)	CAGTGAGTTCATGTGGTGAG
CRISPR1	CTTCGATTTCTACAAGTACGCCTGG TTTTAGAGCTAGAAATAGCAAGTTA
CRISPR2	CTTCGTGCGGAGCGATGCGACCGGG TTTTAGAGCTAGAAATAGCAAGTTA
BL36979 Sequencing FWD	CACGAGAGGGTCAACAAGACC
BL36979 Sequencing REV	TATGTGAATGCCCGCCAATCT
Nep4$^{\Delta281\text{-}1040}$ Sequencing FWD	ATGAGTCGCCACAGCCAACTG
Nep4$^{\Delta281\text{-}1040}$ Sequencing REV	CTACCAAACGCTGCACTTTTTCTG
Nep4B CDS pFastBac EcoRI FWD	TACTCAGAATTC ATG GTA ATG CTG CCA CTG ACC
Nep4B CDS pFastBac NotI REV	TACTCA GCGGCCGC CTAATGATGATGATGATGATGA TGCCAAACGCTGCACTTTTT

6.2 Vector maps

6.2.1 pFastBac Dual
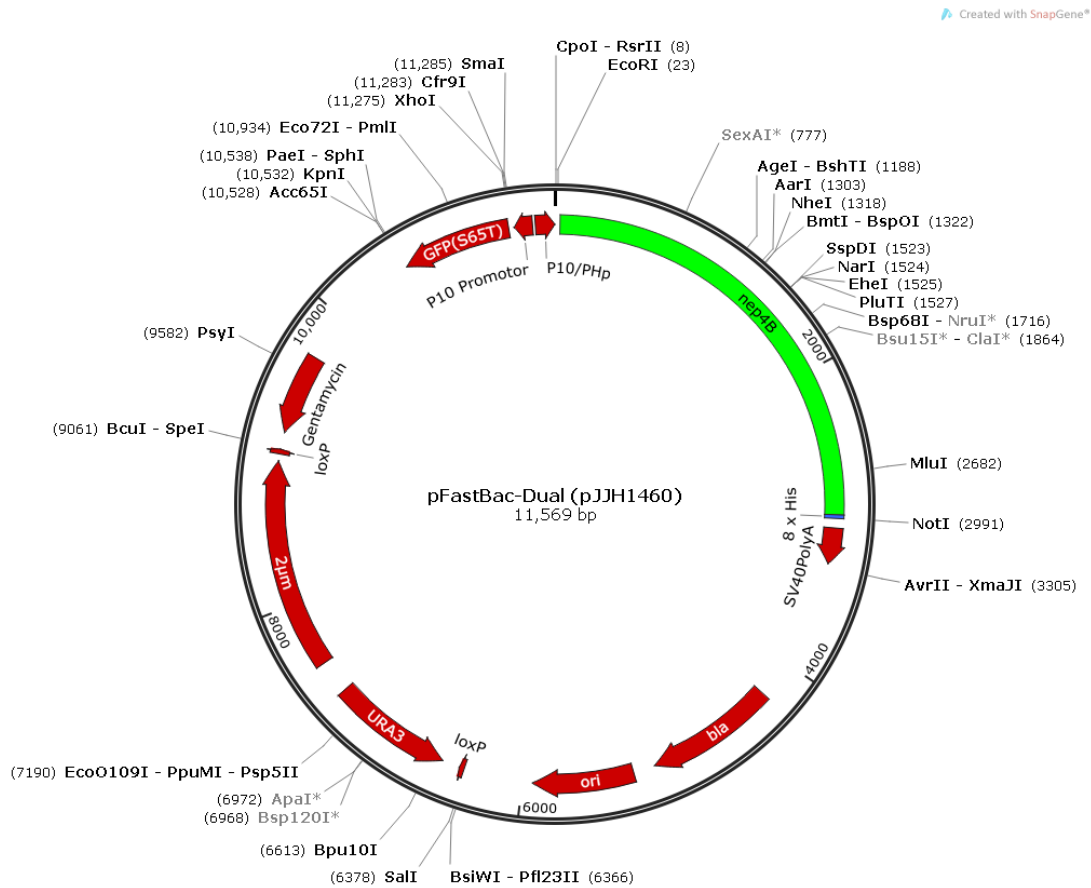
pFastBac-Dual-*nep4B*CDS-8xHis-EcoRI-NotI| The *nep4B* coding sequence fused to a C-terminal His-tag was cloned downstream of the polyhedrin promoter into an *E.coli*/*S.cerevisiae*/Baculovirus triple-shuttle derivative of the pFastBac Dual vector adapted for cloning by homologous recombination *in vivo* (Paululat and Heinisch, 2012). An *eGFP* reporter was inserted into the vector to track transfection efficiency.

6.2.2 pUAST
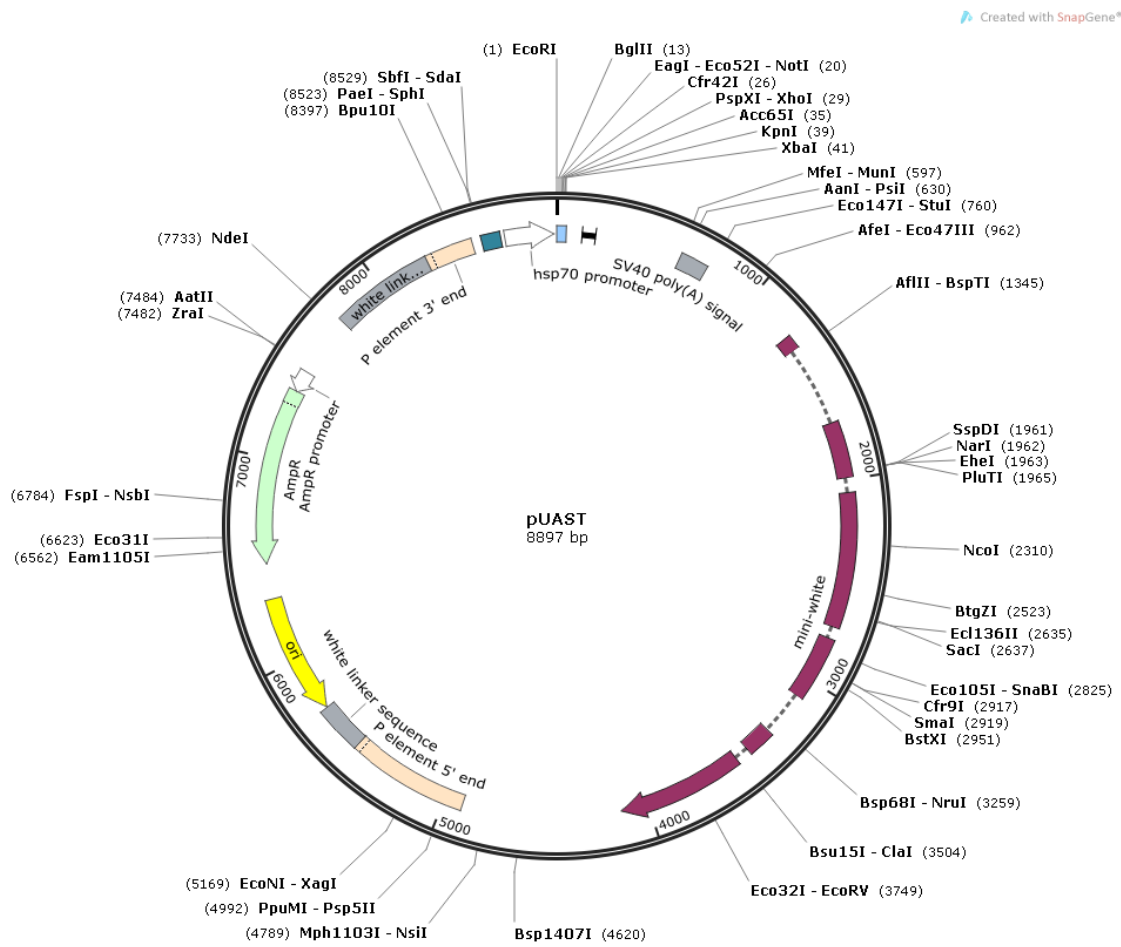
pUAST vector| UAS-Nep4 constructs were established by cloning the respective *nep4* coding sequence into the pUAST vector for subsequent injection into *Drosophila melanogaster* embryos (Panz et al., 2012).

6.2.3 pU6-BbsI-chiRNA

pU6-BbsI-chiRNA vector. Amplificates were ligated into the pU6-BbsI-chiRNA vector and sent to "The Best Gene" (Chino Hills. CA, U.S.A.) for injection into line Bl36979 crossed to BL51323 (y[1] M{vas-Cas9}ZH2A w[1118] to crate CRISPR/Cas9 mutant fly line.

6.3 Alignments

6.3.1 BL36979 CDS alignment

```
GCACATTGTCAGTAAGAGGCAGTTGCTTAACCGCGTTCTGGTGCGCTACAAGCGGTATACCAACGGAACGAAAAGGAAACGCCTCATCGAAACCCCACGGGAGAGAACCAAAGAGGAGGAAGC
++|++++|++++|++++|++++|++++|++++|++++|++++|++++|++++|++++|++++|++++|++++|++++|++++|++++|++++|++++|++++|++++|++++|++++|++++|++++|
CGTGTAACAGTCATTCTCCGTCAACGAATTGGCGCAAGACCACGCGATGTTCGCCATATGGTTGCCTTTTCCTTTGCGGAGTAGCTTTGGGGTGCCCTCTCTTGGTTTCTCCTCCTTCGA
```

```
                                   Nep4 1-2731Bp
```

```
 H  I  V  S  K  R  Q  L  L  N  R  V  L  V  R  Y  K  R  Y  T  N  G  T  K  R  K  R  L  I  E  T  P  R  E  R  T  K  E  E  E  A
        370          375          380          385          390          395          400          405
```

```
GCACATTGTCAGTAAGAGGCAGTTGCTTAACCGCGTTCTGGTGCGCTACAAGCGGTATACCAACGGAACGAAAAGGAAACGCCTCATCGAAACCCCACGGGAGAGAACCAAAGAGGAGGAAGC
```

```
TGCTCCACCAGTTGTCCTGCCAAAGGATAAAACCAAGGACAAGTCGGATAACGAAGAGCAACTACATGTGCCCACCGATTTCCTAAAGCCCCATCAAGATGCCCAGCTAAAAGCAAAGAATCT
++|++++|++++|++++|++++|++++|++++|++++|++++|++++|++++|++++|++++|++++|++++|++++|++++|++++|++++|++++|++++|++++|++++|++++|++++|++++|
ACGAGGTGGTCAACAGGACGGTTTCCTATTTTGGTTCCTGTTCAGCCTATTGCTTCTCGTTGATGTACACGGGTGGCTAAAGGATTTCGGGGTAGTTCTACGGGTCGATTTTCGTTTCTTAGA
```

```
                                   Nep4 1-2731Bp
```

```
 A  P  P  V  V  L  P  K  D  K  T  K  D  K  S  D  N  E  E  Q  L  H  V  P  T  D  F  L  K  P  H  Q  D  A  Q  L  K  A  K  N  L
        410          415          420          425          430          435          440          445
```

```
TGCTCCACCAGTTGTCCTGCCAAAGGATAAAACCAAGGACAAGTCGGATAACGAAGAGCAACTACATGTGCCCACCGATTTCCTAAAGCCCCATCAAGATGCCCAGCTAAAAGCAAAGAATCT
```

```
GTACCGGTCCTGCGTGAACAGCGCGGTGCTGGCCAAGCGGGGATTGGAACCGCTGCACACGCTCATTCGGGAACTAGGTGGCTGGCCAGTCCTGGAGTCCCAATGGAGTGAGTCCAACTTTAA
++|++++|++++|++++|++++|++++|++++|++++|++++|++++|++++|++++|++++|++++|++++|++++|++++|++++|++++|++++|++++|++++|++++|++++|++++|++++|
CATGGCCAGGACGCACTTGTCGCGCCACGACCGGTTCGCCCCTAACCTTGGCGACGTGTGCGAGTAAGCCCTTGATCCACCGACCGGTCAGGACCTCAGGGTTACCTCACTCAGGTTGAAATT
```

```
                                   Nep4 1-2731Bp
```

```
 Y  R  S  C  V  N  S  A  V  L  A  K  R  G  L  E  P  L  H  T  L  I  R  E  L  G  G  W  P  V  L  E  S  Q  W  S  E  S  N  F  N
        450          455          460          465          470          475          480          485
```

```
GTACCGGTCCTGCGTGAACAGCGCGGTGCTGGCCAAGCGGGGATTGGAACCGCTGCACACGCTCATTCGGGAACTAGGTGGCTGGCCAGTCCTGGAGTCCCAATGGAGTGAGTCCAACTTTAA
```

```
CTGGCAGGTGCTAGCCGCCACCCTTAGACGTTACAACAACGACATCCTCATCGTCCAGTGGGTGGGGGCGGACATCAAGAACTCCGAGGAGAACATTGTTCAGTTTGACCAGACGGGTCTGGGC
++|++++|++++|++++|++++|++++|++++|++++|++++|++++|++++|++++|++++|++++|++++|++++|++++|++++|++++|++++|++++|++++|++++|++++|++++|++++|
GACCGTCCACGATCGGCGGTGGGAATCTGCAATGTTGTTGCTGTAGGAGTAGCAGGTCACCCACCCCCGCCTGTAGTTCTTGAGGCTCCTCTTGTAACAAGTCAAACTGGTCTGCCCAGACCCG
```
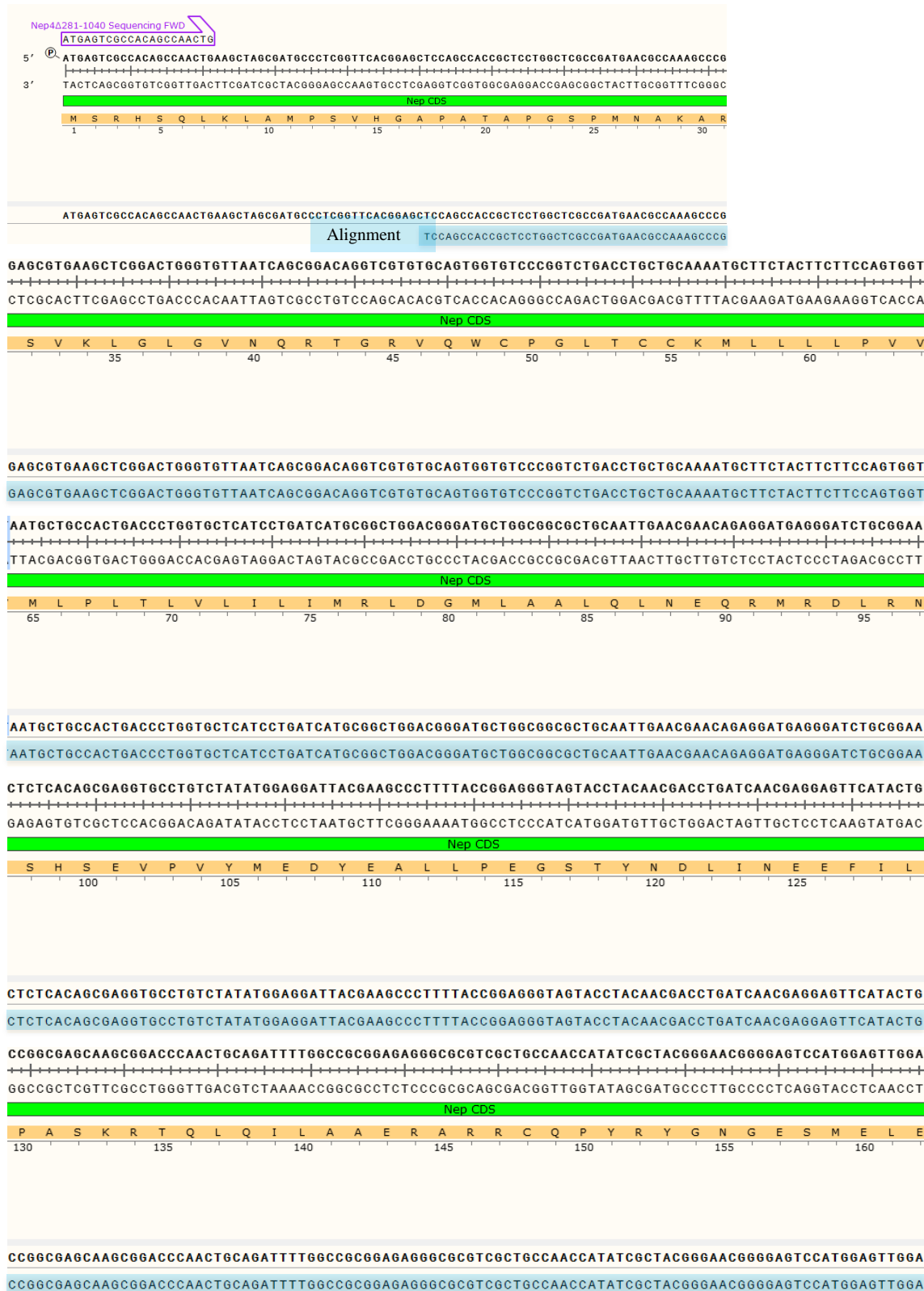
```
                                   Nep4 1-2731Bp
```

```
 W  Q  V  L  A  A  T  L  R  R  R  Y  N  N  D  I  L  I  V  Q  W  V  G  A  D  I  K  N  S  E  E  N  I  V  Q  F  D  Q  T  G  L  G
490          495          500          505          510          515          520          525          530
```

```
CTGGCAGGTGCTAGCCGCCACCCTTAGACGTTACAACAACGACATCCTCATCGTCCAGTGGGTGGGGGCGGACATCAAGAACTCCGAGGAGAACATTGTTCAGTTTGACCAGACGGGTCTGGGC
```

```
CTGCCCACCAGGGAGTACTTCCTCCAGCCGAGCAACGCCAAGTACCTACAGGCCTACCAGCGCTACATGGCCGAGGTGATGCACAAAATGGGCGCCTCCAAGGCGGATGCCCAGCGGGTGGC
++|++++|++++|++++|++++|++++|++++|++++|++++|++++|++++|++++|++++|++++|++++|++++|++++|++++|++++|++++|++++|++++|++++|++++|++++|++++|
GACGGGTGGTCCCTCATGAAGGAGGTCGGCTCGTTGCGGTTCATGGATGTCCGGATGGTCGCGATGTACCGGCTCCACTACGTGTTTTACCCGCGGAGGTTCCGCCTACGGGTCGCCCACCG
```

```
                                   Nep4 1-2731Bp
```

```
 L  P  T  R  E  Y  F  L  Q  P  S  N  A  K  Y  L  Q  A  Y  Q  R  Y  M  A  E  V  M  H  K  M  G  A  S  K  A  D  A  Q  R  V  A
        535          540          545          550          555          560          565          570
```

```
CTGCCCACCAGGGAGTACTTCCTCCAGCCGAGCAACGCCAAGTACCTACAGGCCTACCAGCGCTACATGGCCGAGGTGATGCACAAAATGGGCGCCTCCAAGGCGGATGCCCAGCGGGTGGC
```

```
CAGCGAGCTGGTGGCCGTTCGAAACGCAGCTGGCGGGGATTACAGCTCCAGCGGAGCAACGACTTAACGTCACCAAGCTCTACAAGCGCATGACGCTGGACCAACTGCAGGCGGTGGTTCCGGA
++|++++|++++|++++|++++|++++|++++|++++|++++|++++|++++|++++|++++|++++|++++|++++|++++|++++|++++|++++|++++|++++|++++|++++|++++|++++|
GTCGCTCGACCACCGCAAGCTTTGCGTCGACCGCCCCTAATGTCGAGGTCGCCTCGTTGCTGAATTGCAGTGGTTCGAGATGTTCGCGTACTGCGACCTGGTTGACGTCCGCCACCAAGGCCTT
```

```
                                   Nep4 1-2731Bp
```

```
 S  E  L  V  A  F  E  T  Q  L  A  G  I  T  A  P  A  E  Q  R  L  N  V  T  K  L  Y  K  R  M  T  L  D  Q  L  Q  A  V  V  P  E
        575          580          585          590          595          600          605          610
```

```
CAGCGAGCTGGTGGCCGTTCGAAACGCAGCTGGCGGGGATTACAGCTCCAGCGGAGCAACGACTTAACGTCACCAAGCTCTACAAGCGCATGACGCTGGACCAACTGCAGGCGGTGGTTCCGGA
```

```
AATCAAGTGGCGAGCTTACCTGCAGAGTCTGCAAGATCGCGAAGTTCTGGGCACCGAGGAAGTGGTCATCTACGCGGTGGAGTACATGAGCAAGCTGGTGACTCTTCTAGATGAAACGGATCC
++|++++|++++|++++|++++|++++|++++|++++|++++|++++|++++|++++|++++|++++|++++|++++|++++|++++|++++|++++|++++|++++|++++|++++|++++|++++|
TTAGTTCACCGCTCGAATGGACGTCTCAGACGTTCTAGCGCTTCAAGACCCGTGGCTCCTTCACCAGTAGATGCGCCACCTCATGTACTCGTTCGACCACTGAGAAGATCTACTTTGCCTAGG
```

```
                                   Nep4 1-2731Bp
```

```
 I  K  W  R  A  Y  L  Q  S  L  Q  D  R  E  V  L  G  T  E  E  V  V  I  Y  A  V  E  Y  M  S  K  L  V  T  L  L  D  E  T  D  P
        615          620          625          630          635          640          645          650
```

```
AATCAAGTGGCGAGCTTACCTGCAGAGTCTGCAAGATCGCGAAGTTCTGGGCACCGAGGAAGTGGTCATCTACGCGGTGGAGTACATGAGCAAGCTGGTGACTCTTCTAGATGAAACGGATCC
```

```
CCGAACGGTTTCCAATTACATGATGTGGCGCTTTGTGCGGCACAGGATCAACAACGTGGACGATCGATTCGATGACATCAAACAGAGTTTCTACCACGCCCTCTTTGGCCGCGAGGAGAGTCC
++|++++|++++|++++|++++|++++|++++|++++|++++|++++|++++|++++|++++|++++|++++|++++|++++|++++|++++|++++|++++|++++|++++|++++|++++|++++|
GGCTTGCCAAAGGTTAATGTACTACACCGCGAAACACGCCGTGTCCTAGTTGTTGCACCTGCTAGCTAAGCTACTGTAGTTTGTCTCAAAGATGGTGCGGGAGAAACCGGCGCTCCTCTCAGG
```

```
                                   Nep4 1-2731Bp
```

```
 R  T  V  S  N  Y  M  M  W  R  F  V  R  H  R  I  N  N  V  D  D  R  F  D  D  I  K  Q  S  F  Y  H  A  L  F  G  R  E  E  S  P
        655          660          665          670          675          680          685          690
```

```
CCGAACGGTTTCCAATTACATGATGTGGCGCTTTGTGCGGCACAGGATCAACAACGTGGACGATCGATTCGATGACATCAAACAGAGTTTCTACCACGCCCTCTTTGGCCGCGAGGAGAGTCC
```

```
GCAGAGATGGAAGGTATGCATCGCCCAGGTGAACACCAACATGGGCATGGCAGTGGGTTCCATGTTCGTGAGTCGCTATTTCGACAACAACAGCAAGCGGGACACCTTGCGGATGACTCACGAT
++|++++|++++|++++|++++|++++|++++|++++|++++|++++|++++|++++|++++|++++|++++|++++|++++|++++|++++|++++|++++|++++|++++|++++|++++|++++|
CGTCTCTACCTTCCATACGTAGCGGGTCCACTTGTGGTTGTACCCGTACCGTCACCCAAGGTACAAGCACTCAGCGATAAAGCTGTTGTTGTCGTTCGCCCTGTGGAACGCCTACTGAGTGCTA
```

```
                                   Nep4 1-2731Bp
```

```
 Q  R  W  K  V  C  I  A  Q  V  N  T  N  M  G  M  A  V  G  S  M  F  V  S  R  Y  F  D  N  N  S  K  R  D  T  L  R  M  T  H  D
695          700          705          710          715          720          725          730          735
```

```
GCAGAGATGGAAGGTATGCATCGCCCAGGTGAACACCAACATGGGCATGGCAGTGGGTTCCATGTTCGTGAGTCGCTATTTCGACAACAACAGCAAGCGGGACACCTTGCGGATGACTCACGAT
```

```
CTGCAGCAGGCCTTTCGGGATATCCTGAAAACCACTGATTGGCTGGACGACACCACAAAGCAGTTGGCCGAGGAAAAGGTTAACGCCATGTCCCTGAAGATCGGCTATCCAGACTTTATCCT
++|++++|++++|++++|++++|++++|++++|++++|++++|++++|++++|++++|++++|++++|++++|++++|++++|++++|++++|++++|++++|++++|++++|++++|++++|++++|
GACGTCGTCCGGAAAGCCCTATAGGACTTTTGGTGACTAACCGACCTGCTGTGGTGTTTCGTCAACCGGCTCCTTTTCCAATTGCGGTACAGGGACTTCTAGCCGATAGGTCTGAAATAGGA
```

```
                                   Nep4 1-2731Bp
```

```
 L  Q  Q  A  F  R  D  I  L  K  T  T  D  W  L  D  D  T  T  K  Q  L  A  E  E  K  V  N  A  M  S  L  K  I  G  Y  P  D  F  I  L
        740          745          750          755          760          765          770          775
```

```
CTGCAGCAGGCCTTTCGGGATATCCTGAAAACCACTGATTGGCTGGACGACACCACAAAGCAGTTGGCCGAGGAAAAGGTTAACGCCATGTCCCTGAAGATCGGCTATCCAGACTTTATCCT
```

```
TAATCCCAGTGAGTTAAATAGCAAGTACGCGGGCATAGAAATCTATCCGGAAAAGTATTTTGAGAACACTCTGAATGTTCTGCTTCACACGGCCAAAACGGAGCAGGC
+++++++++++++++++++++++++++++++++++++++++++++++++++++++++++++++++++++++++++++++++++++++++++++++++++++++++++++++
ATTAGGGTCACTCAATTTATCGTTCATGCGCCCGTATCTTTAGATAGGCCTTTTCATAAAACTCTTGTGAGACTTACAAGACGAAGTGTGCCGGTTTTGCCTCGTCCG
```
Nep4 1-2731Bp
```
N  P  S  E  L  N  S  K  Y  A  G  I  E  I  Y  P  E  K  Y  F  E  N  T  L  N  V  L  L  H  T  A  K  T  E  Q  A
        780           785           790           795           800           805           810
```
```
TAATCCCAGTGAGTTAAATAGCAAGTACGCGGGCATAGAAATCTATCCGGAAAAGTATTTTGAGAACACTCTGAATGTTCTGCTTCACACGGCCAAAACGGAGCAGGC
```

BL36979 Sequencing FWD
`CACGAGAGGGTCAACAAGACC`
```
CAAGCTCCACGAGAGGGTCAACAAGACCAACTGGCAGACAGCTCCTGCCATCGTCAATGCCTATTATAGCCGCAACAAGAACCAGATCATGTTTCCCGCCGGCATCCTGCAGCCGCCCTTCTA
+++++++++++++++++++++++++++++++++++++++++++++++++++++++++++++++++++++++++++++++++++++++++++++++++++++++++++++++++++++++++++++++
GTTCGAGGTGCTCTCCCAGTTGTTCTGGTTGACCGTCTGTCGAGGACGGTAGCAGTTACGGATAATATCGGCGTTGTTCTTGGTCTAGTACAAAGGGCGGCCGTAGGACGTCGGCGGGAAGAT
```
Nep4 1-2731Bp
```
K  L  H  E  R  V  N  K  T  N  W  Q  T  A  P  A  I  V  N  A  Y  Y  S  R  N  K  N  Q  I  M  F  P  A  G  I  L  Q  P  P  F  Y
     815           820           825           830           835           840           845           850
```
```
CAAGCTCCACGAGAGGGTCAACAAGACCAACTGGCAGACAGCTCCTGCCATCGTCAATGCCTATTATAGCCGCAACAAGAACCAGATCATGTTTCCCGCCGGCATCCTGCAGCCGCCCTTCTA
```

Alignment `CACGAGAGGGTCAACAAGACCAACTGGCAGACAGCTCCTGCCATCGTCAATGCCTATTATAGCCGCAACAAGAACCAGATCATGTTTCCCGCCGGCATCCTGCAGCCGCCCTTCTA`

```
CCACCGCCACTTTCCGAAGTCGCTGAACTTCGGCGGCATCGGTGTGGTCATTGGCCACGAACTGACCCACGGTTTCGATGACAAGGGTAGGCTCTTCGATCGCAACGGCAATATACATAAGTG
++++++++++++++++++++++++++++++++++++++++++++++++++++++++++++++++++++++++++++++++++++++++++++++++++++++++++++++++++++++++++++++++
GGTGGCGGTGAAAGGCTTCAGCGACTTGAAGCCGCCGTAGCCACACCAGTAACCGGTGCTTGACTGGGTGCCAAAGCTACTGTTCCCATCCGAGAAGCTAGCGTTGCCGTTATATGTATTCAC
```
Nep4 1-2731Bp
```
H  R  H  F  P  K  S  L  N  F  G  G  I  G  V  V  I  G  H  E  L  T  H  G  F  D  D  K  G  R  L  F  D  R  N  G  N  I  H  K  W
     855           860           865           870           875           880           885           890
```
```
CCACCGCCACTTTCCGAAGTCGCTGAACTTCGGCGGCATCGGTGTGGTCATTGGCCACGAACTGACCCACGGTTTCGATGACAAGGGTAGGCTCTTCGATCGCAACGGCAATATACATAAGTG
```
```
CCACCGCCACTTTCCGAAGTCGCTGAACTTCGGCGGCATCGGTGTGGTCATTGGCCACGAACTGACCCACGGTTTCGATGACAAGGGTAGGCTCTTCGATCGCAACGGCAATATACATAAGTG
```

```
GTGGACGGACTCCTCGATTCGCGGGTTCGACGAGCGCGCCCGCTGCATTAcGAGCCCCACCACagcacggggccgtcgccgatgggggtgttctgctggtagtggtcggcgagctgcacgccg
++++++++++++++++++++++++++++++++++++++++++++++++++++++++++++++++++++++++++++++++++++++++++++++++++++++++++++++++++++++++++++++++
CACCTGCCTGAGGAGCTAAGCGCCCAAGCTGCTCGCGCGGGCGACGTAATgCTCGGGGTGGTgtcgtgccccggcagcggctaccccacaagacgaccatcaccagccgctcgacgtgcggc
```
Nep4 1-2731Bp
MiMIC Element
```
W  T  D  S  S  I  R  G  F  D  E  R  A  R  C  I  T  S  P  T  T  A  R  G  R  R  R  W  G  C  S  A  G  S  G  R  R  A  A  R  R
  895           900           905           910           915           920           925           930           93
```
```
GTGGACGGACTCCTCGATTCGCGGGTTCGACGAGCGCGCCCGCTGCATTAcGAGCCCCACCACagcacggggccgtcgccgatgggggtgttctgctggtagtggtcggcgagctgcacgccg
```
```
GTGGACGGACTCCTCGATTCGCGGGTTCGACGAGCGCGCCCGCTGCATTACGAGCCCCACCACAGCACGGGGCCGTCGCCGATGGGGGTGTTCTGCTGGTAGTGGTCGGCGAGCTGCACGCCG
```

```
ccgtcctcgatgttgtggcggatcttga      3'
+++++++++++++++++++++++++++++      2832
ggcaggagctacaacaccgcctagaact   (P) 5'
```
```
R  P  R  C  C  G  G  S  +   →
5           940
```
```
ccgtcctcgatgttgtggcggatcttga
```
```
CCGTCCTCGATGTTGTGGCGGATCTTGA
```

6.3.2 Nep4 $^{\Delta281-1040}$ CDS alignment

Nep4Δ281-1040 Sequencing FWD
ATGAGTCGCCACAGCCAACTG

5′ Ⓟ ATGAGTCGCCACAGCCAACTGAAGCTAGCGATGCCCTCGGTTCACGGAGCTCCAGCCACCGCTCCTGGCTCGCCGATGAACGCCAAAGCCCG
3′ TACTCAGCGGTGTCGGTTGACTTCGATCGCTACGGGAGCCAAGTGCCTCGAGGTCGGTGGCGAGGACCGAGCGGCTACTTGCGGTTTCGGGC

Nep CDS

M S R H S Q L K L A M P S V H G A P A T A P G S P M N A K A R
1   5   10   15   20   25   30

ATGAGTCGCCACAGCCAACTGAAGCTAGCGATGCCCTCGGTTCACGGAGCTCCAGCCACCGCTCCTGGCTCGCCGATGAACGCCAAAGCCCG

Alignment   TCCAGCCACCGCTCCTGGCTCGCCGATGAACGCCAAAGCCCG

GAGCGTGAAGCTCGGACTGGGTGTTAATCAGCGGACAGGTCGTGTGCAGTGGTGTCCCGGTCTGACCTGCTGCAAAATGCTTCTACTTCTTCCAGTGGT
CTCGCACTTCGAGCCTGACCCACAATTAGTCGCCTGTCCAGCACACGTCACCACAGGGCCAGACTGGACGACGTTTTACGAAGATGAAGAAGGTCACCA

Nep CDS

S V K L G L G V N Q R T G R V Q W C P G L T C C K M L L L L P V V
     35   40   45   50   55   60

GAGCGTGAAGCTCGGACTGGGTGTTAATCAGCGGACAGGTCGTGTGCAGTGGTGTCCCGGTCTGACCTGCTGCAAAATGCTTCTACTTCTTCCAGTGGT
GAGCGTGAAGCTCGGACTGGGTGTTAATCAGCGGACAGGTCGTGTGCAGTGGTGTCCCGGTCTGACCTGCTGCAAAATGCTTCTACTTCTTCCAGTGGT

AATGCTGCCACTGACCCTGGTGCTCATCCTGATCATGCGGCTGGACGGGATGCTGGCGGCGCTGCAATTGAACGAACAGAGGATGAGGGATCTGCGGAA
TTACGACGGTGACTGGGACCACGAGTAGGACTAGTACGCCGACCTGCCCTACGACCGCCGCGACGTTAACTTGCTTGTCTCCTACTCCCTAGACGCCTT

Nep CDS

M L P L T L V L I L I M R L D G M L A A L Q L N E Q R M R D L R N
65   70   75   80   85   90   95

AATGCTGCCACTGACCCTGGTGCTCATCCTGATCATGCGGCTGGACGGGATGCTGGCGGCGCTGCAATTGAACGAACAGAGGATGAGGGATCTGCGGAA
AATGCTGCCACTGACCCTGGTGCTCATCCTGATCATGCGGCTGGACGGGATGCTGGCGGCGCTGCAATTGAACGAACAGAGGATGAGGGATCTGCGGAA

CTCTCACAGCGAGGTGCCTGTCTATATGGAGGATTACGAAGCCCTTTTACCGGAGGGTAGTACCTACAACGACCTGATCAACGAGGAGTTCATACTG
GAGAGTGTCGCTCCACGGACAGATATACCTCCTAATGCTTCGGGAAAATGGCCTCCCATCATGGATGTTGCTGGACTAGTTGCTCCTCAAGTATGAC

Nep CDS

S H S E V P V Y M E D Y E A L L P E G S T Y N D L I N E E F I L
     100   105   110   115   120   125

CTCTCACAGCGAGGTGCCTGTCTATATGGAGGATTACGAAGCCCTTTTACCGGAGGGTAGTACCTACAACGACCTGATCAACGAGGAGTTCATACTG
CTCTCACAGCGAGGTGCCTGTCTATATGGAGGATTACGAAGCCCTTTTACCGGAGGGTAGTACCTACAACGACCTGATCAACGAGGAGTTCATACTG

CCGGCGAGCAAGCGGACCCAACTGCAGATTTTGGCCGCGGAGAGGGCGCGTCGCTGCCAACCATATCGCTACGGGAACGGGGAGTCCATGGAGTTGGA
GGCCGCTCGTTCGCCTGGGTTGACGTCTAAAACCGGCGCCTCTCCCGCGCAGCGACGGTTGGTATAGCGATGCCCTTGCCCCTCAGGTACCTCAACCT

Nep CDS

P A S K R T Q L Q I L A A E R A R R C Q P Y R Y G N G E S M E L E
130   135   140   145   150   155   160

CCGGCGAGCAAGCGGACCCAACTGCAGATTTTGGCCGCGGAGAGGGCGCGTCGCTGCCAACCATATCGCTACGGGAACGGGGAGTCCATGGAGTTGGA
CCGGCGAGCAAGCGGACCCAACTGCAGATTTTGGCCGCGGAGAGGGCGCGTCGCTGCCAACCATATCGCTACGGGAACGGGGAGTCCATGGAGTTGGA

GGAGCGCAACACGCTGATGAAGGACTCCCGAACCTCCTTCCTGCCACTGGGCATTCCGCGAGAGTGCCTCGGCAGCGGCATTGAACTGGACATTAAAC
+++++|+++++++++|+++++++++|+++++++++|+++++++++|+++++++++|+++++++++|+++++++++|+++++++++|+++++++++|+++++++++|+++
CCTCGCGTTGTGCGACTACTTCCTGAGGGCTTGGAGGAAGGACGGTGACCCGTAAGGCGCTCTCACGGAGCCGTCGCCGTAACTTGACCTGTAATTTG

Nep CDS

E   R   N   T   L   M   K   D   S   R   T   S   F   L   P   L   G   I   P   R   E   C   L   G   S   G   I   E   L   D   I   K
        165   170   175   180   185   190

GGAGCGCAACACGCTGATGAAGGACTCCCGAACCTCCTTCCTGCCACTGGGCATTCCGCGAGAGTGCCTCGGCAGCGGCATTGAACTGGACATTAAAC
GGAGCGCAACACGCTGATGAAGGACTCCCGAACCTCCTTCCTGCCACTGGGCATTCCGCGAGAGTGCCTCGGCAGCGGCATTGAACTGGACATTAAAC

CCATAGATGAGGAGGCCTACCAGAGGCAGAAGAAGCGCTACCAGGACATAGCTCCGTATTGGCTGGAGAAGATCAGAATACGGGAGCGCCGCGAGGCCG
+++++|+++++++++|+++++++++|+++++++++|+++++++++|+++++++++|+++++++++|+++++++++|+++++++++|+++++++++|+++++++++|+++
GGTATCTACTCCTCCGGATGGTCTCCGTCTTCTTCGCGATGGTCCTGTATCGAGGCATAACCGACCTCTTCTAGTCTTATGCCCTCGCGGCGCTCCGGC

Nep CDS

P   I   D   E   E   A   Y   Q   R   Q   K   K   R   Y   Q   D   I   A   P   Y   W   L   E   K   I   R   I   R   E   R   R   E   A
195   200   205   210   215   220   225

CCATAGATGAGGAGGCCTACCAGAGGCAGAAGAAGCGCTACCAGGACATAGCTCCGTATTGGCTGGAGAAGATCAGAATACGGGAGCGCCGCGAGGCCG
CCATAGATGAGGAGGCCTACCAGAGGCAGAAGAAGCGCTACCAGGACATAGCTCCGTATTGGCTGGAGAAGATCAGAATACGGGAGCGCCGCGAGGCCG

AACGTCATGCAGAGGAGGCCAGTGCCGAGATCAGCGAGGCCACCGCCGCTCTGCAGAGTTTCTGGAACGAGGAAGGCACTCGGGAGGGCATTCGCATGA
+++++|+++++++++|+++++++++|+++++++++|+++++++++|+++++++++|+++++++++|+++++++++|+++++++++|+++++++++|+++++++++|+++
TTGCAGTACGTCTCCTCCGGTCACGGCTCTAGTCGCTCCGGTGGCGGCGAGACGTCTCAAAGACCTTGCTCCTTCCGTGAGCCCTCCCGTAAGCGTACT

Nep CDS

E   R   H   A   E   E   A   S   A   E   I   S   E   A   T   A   A   L   Q   S   F   W   N   E   E   G   T   R   E   G   I   R   M
        230   235   240   245   250   255   260

AACGTCATGCAGAGGAGGCCAGTGCCGAGATCAGCGAGGCCACCGCCGCTCTGCAGAGTTTCTGGAACGAGGAAGGCACTCGGGAGGGCATTCGCATGA
AACGTCATGCAGAGGAGGCCAGTGCCGAGATCAGCGAGGCCACCGCCGCTCTGCAGAGTTTCTGGAACGAGGAAGGCACTCGGGAGGGCATTCGCATGA

CCCAGGCCAAAACCATGAAGCGCTACATGGATAACAAAGTGGATCCCTGCGTGGATTTCTACAATCAatggtgcgctcctggacgtagccttcgggcat
+++++|+++++++++|+++++++++|+++++++++|+++++++++|+++++++++|+++++++++|+++++++++|+++++++++|+++++++++|+++++++++|+++
GGGTCCGGTTTTGGTACTTCGCGATGTACCTATTGTTTCACCTAGGGACGCACCTAAAGATGTTAGTtaccacgcgaggacctgcatcggaagcccgta

Nep CDS   MiMIC

T   Q   A   K   T   M   K   R   Y   M   D   N   K   V   D   P   C   V   D   F   Y   N   Q   W   C   A   P   G   R   S   L   R   A
        265   270   275   280   285   290

CCCAGGCCAAAACCATGAAGCGCTACATGGATAACAAAGTGGATCCCTGCGTGGATTTCTACAATCAatggtgcgctcctggacgtagccttcgggcat
CCCAGGCCAAAACCATGAAGCGCTACATGGATAACAAAGTGGATCCCTGCGTGGATTTCTACAATCAATGGTGCGCTCCTGGACGTAGCCTTCGGGCAT

ggcggacttga   3'
+++++++++| 891
ccgcctgaact ⓟ 5'

W   R   T ▪ →
        295

ggcggacttga

GGCGGACTTGA
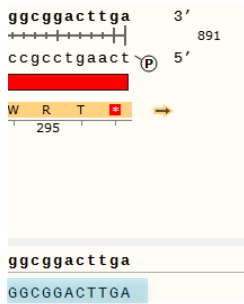
6.4 DVD

- Dissertation Benjamin Hallier 2017; PDF

- Survival rate BL36979; excel.

- Fertility assay, BL36979; excel

- Survival rate Nep4$^{\Delta281-1404}$; excel

- Locomotion assay Nep4$^{\Delta281-1404}$; excel

- Feeding assay Nep4$^{\Delta281-1404}$; excel

- Figures 1-29

- Working model.ppt

- Publications

  - Hallier et al., 2015

  - Hallier et al., 2016

6.5 Publications

6.5.1 The bHLH Transcription Factor Hand Regulates the Expression of Genes Critical to Heart and Muscle Function in *Drosophila melanogaster* (PLOS ONE, 2015)

Benjamin Hallier[1], Julia Hoffmann[2], Thomas Roeder[2], Markus Tögel[3], Heiko Meyer[1], Achim Paululat[1]*

1 Department of Zoology/Developmental Biology, University of Osnabrück, 49069 Osnabrück, Germany

2 Department of Animal Physiology, University of Kiel, 24098 Kiel, Germany

3 Weatherall Institute of Molecular Medicine, University of Oxford, OX3 9DS Oxford, United Kingdom

PLOS | ONE

RESEARCH ARTICLE

The bHLH Transcription Factor Hand Regulates the Expression of Genes Critical to Heart and Muscle Function in *Drosophila melanogaster*

Benjamin Hallier[1], Julia Hoffmann[2], Thomas Roeder[2], Markus Tögel[3], Heiko Meyer[1], Achim Paululat[1] *

1 Department of Zoology/Developmental Biology, University of Osnabrück, 49069 Osnabrück, Germany, 2 Department of Animal Physiology, University of Kiel, 24098 Kiel, Germany, 3 Weatherall Institute of Molecular Medicine, University of Oxford, OX3 9DS Oxford, United Kingdom

* Paululat@biologie.uni-osnabrueck.de

Abstract

Hand proteins belong to the highly conserved family of basic Helix-Loop-Helix transcription factors and are critical to distinct developmental processes, including cardiogenesis and neurogenesis in vertebrates. In *Drosophila melanogaster* a single orthologous *hand* gene is expressed with absence of the respective protein causing semilethality during early larval instars. Surviving adult animals suffer from shortened lifespan associated with a disorganized myofibrillar structure being apparent in the dorsal vessel, the wing hearts and in midgut tissue. Based on these data, the major biological significance of Hand seems to be related to muscle development, maintenance or function; however, up to now the physiological basis for Hand functionality remains elusive. Thus, the identification of genes whose expression is, directly or indirectly, regulated by Hand has considerable relevance with respect to understanding its biological functionality in flies and vertebrates. Beneficially, *hand* mutants are viable and exhibit affected tissues, which renders *Drosophila* an ideal model to investigate up- or downregulated target genes by a comparative microarray approach focusing on the respective tissues from mutant specimens. Our present work reveals for the first time that *Drosophila* Hand regulates the expression of numerous genes of diverse physiological relevancy, including distinct factors required for proper muscle development and function such as Zasp52 or Msp-300. These results relate Hand activity to muscle integrity and functionality and may thus be highly beneficial to the evaluation of corresponding *hand* phenotypes.

Introduction

Basic helix-loop-helix (bHLH) transcription factors are key regulators of numerous developmental processes including cardiovascular development, hematopoiesis, stem cell maintenance,

neurogenesis and myogenesis (reviewed by [1]). Among the class II bHLH family, Hand proteins constitute a prominent class regulating, e.g., trophoblast development, limb bud outgrowth, branchial arch development or cardiogenesis [2–14]. In higher vertebrates, e.g. mouse or human, two paralogous *hand* genes (*hand1*, *hand2*) are present in the genome, with both being expressed in the lateral plate mesoderm, distinct neural crest cells and the developing heart. With respect to the latter tissue, expression of both genes is initially overlapping. Upon formation of a linear heart tube however, *hand1* expression becomes restricted to the developing left ventricle, while *hand2* is still expressed throughout the complete heart primordium. As soon as cardiac looping initiates, *hand2* expression becomes restricted to the heart region the right ventricle arises from [5, 15, 16]. Thus, the two paralogous *hand* genes in higher vertebrates may have evolved different tissue specific functionalities during cardiogenesis. A critical function of Hand in cardiogenesis was demonstrated by analyzing the phenotypes of loss of function mutations in mice where severe malformations of the heart were observed in animals lacking Hand activity [5, 6, 17]. For instance, mice being mutant for both, *hand1* and *hand2* are embryonic lethal and, among other cardiac defects, characterized by severe ventricular hypoplasia [18]. In addition, Natarahan and colleagues reported that *hand1* expression is almost absent in hearts of patients suffering from ischemic or dilated cardiomyopathy, whereas *hand2* expression remains unchanged [19].

In *Drosophila*, only a single Hand orthologue was discovered by extensive genome-wide searches for bHLH sequences [20]. Notably, Hand represents the only transcription factor identified so far that is expressed in all three major embryonic cell types that comprise the *Drosophila* circulatory system (cardioblasts, pericardial cells, and hematopoietic progenitors in the lymph gland). In addition to these cells, *Drosophila hand* is expressed in the circular visceral musculature and in distinct cells belonging to the central nervous system [21–25]. Despite its expression in the embryonic tissues mentioned above, Hand knock-out phenotypes manifest primarily in the dorsal vessel and the gut of adult animals, indicating an essential role of Hand in the remodeling of these tissues during metamorphosis rather than being required for proper determination and differentiation of the respective tissues during embryogenesis. Apparently, the phenotypes are mainly characterized by an abnormal arrangement of muscle fibers in the corresponding tissues [24]. This observation together with recent data that also describe severe disarrangements in muscle cells of *hand* mutant wing hearts [26] indicates that lack of Hand activity predominantly affects muscle structure or integrity.

Here we took advantage of the fact that the *Drosophila* genome carries only a single *hand* orthologue and that homozygous *hand* mutant individuals survive into adulthood at significant rates. Cardiogenesis initially proceeds normally in such animals, however, the mature heart displays several structural malformations including sarcomere defects, which may account, together with other phenotypes manifesting in gut morphogenesis and wing heart development, for a shortened lifespan and reduced fitness. The facts depicted above render *Drosophila* an ideal model to identify genes regulated by Hand, which may also promote a detailed understanding of *hand* functionality in vertebrates. For instance, downregulation of human *hand1* in cardiomyopathies, as observed by [19], may result in misregulation of yet unknown target genes in the heart and thereby lead to an age-dependent aggravation of cardiac pathologies.

Herein we present a genome wide microarray based approach to identify genes that are, directly or indirectly, regulated by Hand. As a result we identified several genes that exhibit a considerably up- or downregulated expression in *hand* mutant animals, compared to wild type. Due to the Hand knock-out phenotypes depicted above, in subsequent experiments we focused primarily on genes that are involved in muscle cell development, muscle structure maintenance or muscle physiology. With respect to genes matching these criteria we did quantitative real-time PCRs as well as quantitative Northern blots in order to validate the

corresponding microarray data, thus minimizing the possibility of considering false positives. In sum, our data demonstrate for the first time that *Drosophila* Hand is regulating the expression of several muscle specific proteins and may thus be highly beneficial for understanding distinct *hand* null phenotypes described earlier. Furthermore, the catalogue of genes apparently regulated by Hand provides a solid basis for future investigations on the regulatory networks that are crucial to establishing heart and muscle architecture or functionality.

Materials and Methods

Fly strains

w1118 was used as wild type control. The *hand*[173] null mutant was kindly provided by Manfred Frasch [24].

Heart preparations

For optimal growth conditions, wild type (w1118) and homozygous mutant (*hand*[173]) flies were raised at low population density on standard medium at 22°C. Hearts were dissected from wandering 3rd instar larvae since the corresponding animals represent a clearly defined developmental stage. In addition, *hand*[173] 3rd instar larvae do neither exhibit increased lethality rates [23], nor any developmental delay (own observation), compared to wild type. By selecting such animals we minimize the possibility of analyzing dying animals, which may be characterized by a considerably altered transcript composition, compared to healthy specimen. Wandering 3rd instar larvae were collected, transferred into a tea basket and anesthetized by incubating the larvae at 60°C for 15 seconds in a water bath. Such treatment induces stretching of the larvae with a relaxed muscle contraction state, which facilitates the subsequent heart preparation. All further dissections were carried out in PBS. Firstly, individual larvae were pinned upside down to sylgard plates with preparation needles. The most anterior and posterior portion of each larvae was removed with microscissors. Next, larvae were opened from the ventral side and all viscera were carefully removed to allow direct access to the heart. About 100 heart tubes including associated tissue (pericardial cells, alary muscles) from both genotypes were carefully extracted and directly collected in Trizol (Invitrogen—Life Technologies, Frankfurt, Germany) for subsequent RNA preparations.

Microarray

Microarray analyses were essentially performed as described earlier [27, 28]. In brief, cDNA synthesis from RNA isolated from manually dissected larval hearts was performed with Prime Script RT (Takara, Saint-Germain-en-Laye, France) using the following primers: OdT T7 I (5'-GAG AGA GGA TCC AAG TAC TAA TAC GAC TCA CTA TAG GGA GAT TTT TTT TTT TTT TTT TTT TTT T G/A/C-3') and CapFinder Sp6rG (5'-CAG CGG CCG CAG ATT TAG GTG ACA CTA TAG A rGrGrG-3'). cDNA was amplified with OdT T7 II (5'-GAG AGA GGA TCC AAG TAC TAA TAC GAC TCA CTA TAG G-3'), Adaptor Sp6rG (5'-GAC GCC TGC AGG CGA TGA ATT TAG G-3') and LA Taq polymerase [29]. cDNA was transcribed with MEGAscript T7 including aminoallyl-UTP (Ambion—Life Technologies, Frankfurt, Germany) and subsequently labeled with Alexa Fluor 555 or 647 (Invitrogen—Life Technologies) for control or experimental sample, respectively. Samples were hybridized to *Drosophila* 14 k V2 DNA-microarrays (Canadian *Drosophila* Microarray Centre, Toronto, Canada) and scanned using a GenePix 4000B Microarray Scanner (Axon Instruments, Molecular Devices, Biberach, Germany). Data acquisition, normalization and analysis including hierarchical clustering were carried out with the programs GenePix 6.0 and Acuity 4.1 (Axon Instruments, Molecular Devices, Biberach, Germany). We performed two channel probe hybridizations with

three technical replicates. Genes with a more than 1.33 fold increased transcript level in *hand* deficient samples, compared to matching controls in at least two out of three technical replicates, were scored as upregulated; those with a less than 0.67 fold relative transcript level in at least two out of three technical replicates were scored as downregulated. In order to minimize the impact of possible variations between individual specimens, wild type and mutant RNA, respectively, was extracted from a high number of dissected heart tubes (>100). The corresponding individual preparations were pooled according to their genotype and further analyzed as depicted above. Due to the fact that 2–3 values per gene do not allow for a reliable statistical analysis we did not calculate p-values that would probably not reflect the real data situation. Instead of that we extracted the most relevant genes from these analyses and quantified their differential expression with alternative methods (see results).

The DNA-microarray experiments have been deposited in the GEO-database (accession number GSE64429).

qRT-PCR

Total-RNA isolated from complete wandering stage 3rd instar larvae (RNeasy Mini Kit, Qiagen, Hilden, Germany) was treated with DNase I (Invitrogen—Life Technologies) according to the manufacturer's instructions and used as a template for cDNA synthesis (SuperScript III Reverse Transcriptase, Invitrogen—Life Technologies). qRT-PCR was conducted according to standard protocols using DyNAmo ColorFlash SYBR Green qPCR Kit (Biozym, Hessisch Oldendorf, Germany) and an iCycler iQ Real-Time PCR System (Bio-Rad, Munich, Germany). Primer pairs were designed with QuantPrime [30] applying the presettings to consider only regions containing at least one intron and to accept splice variant hits. Data were evaluated as described in [31]. Genes with an at least 1.33 fold increased transcript level in *hand* deficient samples, compared to controls, were scored as upregulated, those with a less than 0.67 fold relative transcript level were scored as downregulated. Primers used are summarized in S2 Table. For each gene at least three biological replicates were performed.

Northern blot and riboprobe synthesis

Northern blots were conducted as described [32] using total RNA (15μg per lane) isolated from complete wandering stage 3rd instar larvae and a hybridization temperature of 66°C. Quantification of the relative band intensities in relation to the loading controls (ribosomal RNA) was done by densitometric analysis using a VersaDoc 4000 imaging system (Bio-Rad Laboratories, Hercules, CA, U.S.A.) and Quantity One software, version 4.6.9.

Templates for riboprobe synthesis were generated using the following primer pairs: *kugelei*: atgaagattaaaaaatatgta (forward, FW), gacattctcaaaaatgggatc (reverse, RV); *msp-300*: gcgcgataaggagcaacaggt (FW), cctgttgctcggctaatgcgc (RV); *zasp52*: atggcccaaccacagctgctg (FW), gctgttgctgctgctatagtt (RV); *cubitus interruptus*: atggacgcctacgcgttacc (FW), agccttcaaacgtgc atttgt (RV); *hedgehog*: atggataaccacagctcagtg (FW), tcaatcgtggcgccagctctg (RV); *mef2*: atggg ccgcaaaaaaattcaa (FW), ctatgtgcccaatccgcccga (RV)

Probes were synthesized by *in vitro* transcription using "DIG RNA labeling kit" (Roche, Mannheim, Germany). For each gene at least three biological replicates were performed.

Results
The expression of numerous genes is altered in hand mutant hearts

In previous studies it was shown that *Drosophila* Hand functions as a potent transcriptional activator [23] that is essential for proper morphogenesis of adult heart and midgut tissue [24]

but also for wing heart differentiation [26]. However, the target genes of the transcription factor remained elusive up to now. In order to identify genes whose expression is regulated by Hand, we did genome wide microarrays using total RNA isolated from dissected 3rd instar larval hearts of wild type as well as *hand* null animals (*hand^{173}*, [24]) and compared the expression levels of the complete set of genes in the respective genetic backgrounds. In order to minimize the impact of variations between individual specimens, we extracted and pooled RNA from a high number of individual heart preparations instead of doing biological replicates with less hearts. Noteworthy, the semilethal phase of *hand* mutant animals is during 1st and 2nd larval instars with apparently no 3rd larval instar lethality [24]. Thus, the possibility of analyzing dying animals that may exhibit an abnormal gene expression can be excluded. Isolated hearts were selected since they represent the major Hand expressing tissue in *Drosophila* [21]. As shown in Fig 1, analysis of the microarray data yielded 545 genes exhibiting an altered expression in *hand^{173}* hearts, with 385 genes being downregulated in the mutant and 160 genes displaying an increased expression in the same line, compared to wild type. The fact that the number of downregulated genes exceeds that of activated genes by a factor of more than two indicates that Hand acts predominantly as a transcriptional activator rather than being a repressor in larval hearts. Noteworthy, the in principle capability of *Drosophila* Hand to act as a potent transcriptional activator has been shown previously, however, the respective study did not yield any *in vivo* target of the protein [23]. A functional classification of the protein products corresponding to the genes identified by the microarray revealed highly diverse physiological functions of the respective factors, with proteins involved in transcriptional regulation being most abundant (80 genes). Consistent with a high demand for energy in heart tissue, genes participating in metabolism are also enriched (72). As a third prominent category, signaling factors are abound (53). Other noteworthy classes include genes with protein products being involved in proteolysis (29), solute transport (24), protein biosynthesis (21), and cytoskeletal interactions (19). The remaining functional categories comprise genes involved in the progression of the cell cycle (15), vesicle transport (15), and cell-to-cell interactions (5). A last category contains "assorted other" genes that are either of unknown function or do not fit into any of the former categories (212). Individual genes within each group are depicted in S1 Table.

Hand regulates the expression of genes critical to muscle and heart development or function

Despite the high number of misregulated genes in *hand^{173}* animals (Fig 1), only mild phenotypes were observed in this line with the majority of them being related to impaired muscle and heart structure or integrity [24, 26]. Thus, the major biological significance of Hand is apparently related to muscle and heart development, maintenance or function. However, up to now the physiological basis for this functionality remained elusive. In order to analyze this issue in more detail we screened the microarray data for proteins that are known to be essential for these processes. In addition, we concentrated on genes that were confirmed to be expressed in pupal [33] or adult hearts [34] and on genes that were shown to be critical to heart functionality [35]. By applying these parameters we narrowed down the number of potentially most relevant target genes to 42, with 2 of these genes being upregulated in *hand^{173}* and 40 displaying a reduced expression in the same line, compared to wild type (Table 1).

In order to validate the corresponding microarray data we re-analyzed the expression levels of the selected 42 genes by quantitative real time-PCR (qRT-PCR). To monitor the overall changes in gene expression, irrespective of a possible isoform specific regulation, primers detecting multiple splice variants were generated. The corresponding sequences are depicted in
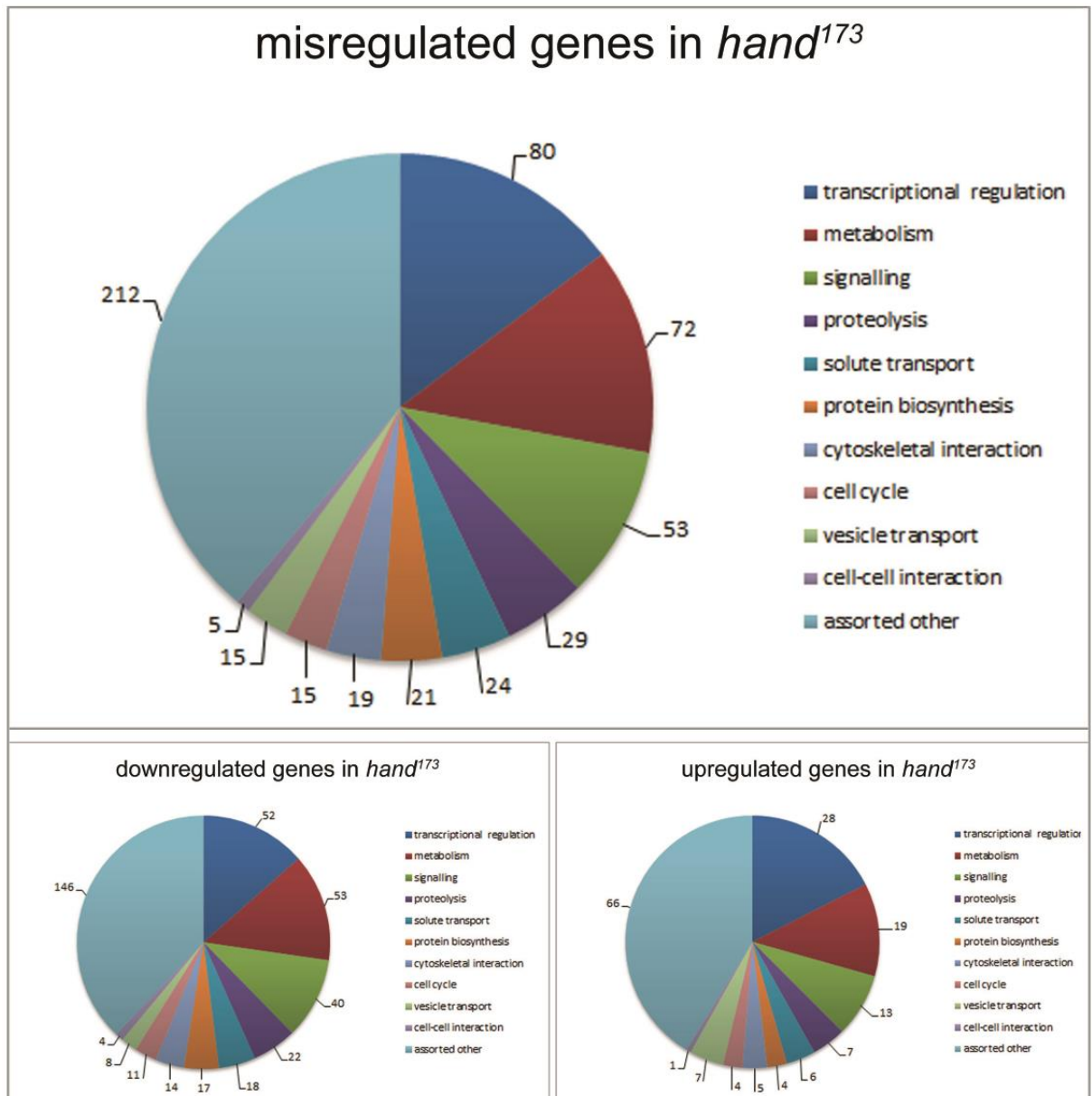
Fig 1. Functional classification of genes exhibiting deviant expression levels in hand[173] animals. *Drosophila* Hand is apparently involved in regulating the expression of 545 genes with 385 genes being downregulated in *hand* mutants (*hand[173]*) and 160 genes displaying an increased expression in the same line, compared to wild type. Functional classification of the corresponding protein products was done manually utilizing data from NCBI (http://www.ncbi.nlm.nih.gov/) and Flybase (http://flybase.org/). Factors with yet unknown physiological functions are allocated to the category "assorted other".

doi:10.1371/journal.pone.0134204.g001

Table 1. Preliminary selection of genes exhibiting deviant expression levels in *hand*[173] animals. By screening the microarray dataset for factors that are either significantly expressed in heart tissue or involved in muscle or heart development, maintenance or function, we identified 42 genes of potentially high physiological relevance. While 2 of these genes are upregulated in *hand*[173], 40 display a reduced expression in the same line, compared to wild type. Functional classification of the corresponding protein products was done manually utilizing data from NCBI (http://www.ncbi.nlm.nih.gov/) and Flybase (http://flybase.org/). Factors with yet unknown physiological functions are allocated to the category "assorted other".

#	gene	name	expression in *hand*[173]	functional category	#	gene	name	expression in *hand*[173]	functional category
1	CG1161	-	down	assorted other	22	CG10679	nedd8	down	proteolysis
2	CG1520	wasp	down	cytoskeletal interaction	23	CG10811	eukaryotic translation initiation factor 4G	down	cell cycle
3	CG1844	selenoprotein G	down	assorted other	24	CG11271	ribosomal protein S12	down	protein biosynthesis
4	CG2145	-	down	proteolysis	25	CG11525	cyclin G	down	cell cycle
5	CG2233	-	down	assorted other	26	CG11661	neural conserved at 73EF	down	metabolism
6	CG3186	eIF-5A	down	protein biosynthesis	27	CG12400	NADH dehydrogenase (ubiquinone) B14.5 B subunit	down	metabolism
7	CG3869	mitochondrial assembly regulatory factor	down	signaling	28	CG14035	msp-300	down	cytoskeletal interaction
8	CG4699	waharan	down	cell cycle	29	CG14616	lethal (1) G0196	up	metabolism
9	CG4716	methylenetetrahydrofolate dehydrogenase [NAD(P)+] activity	down	metabolism	30	CG15067	-	down	assorted other
10	CG5277	intronic protein 259	down	assorted other	31	CG16713	-	down	proteolysis
11	CG5320	glutamate dehydrogenase	up	metabolism	32	CG16747	ornithine decarboxylase antizyme	down	metabolism
12	CG5399	-	down	assorted other	33	CG17108	-	down	assorted other
13	CG6090	ribosomal protein L34a	down	protein biosynthesis	34				
14	CG6105	-	down	metabolism	35	CG17820	female-specific independent of transformer	down	assorted other
15	CG6746	-	down	signaling	36	CG18039	kaiRIA	down	signaling
16	CG7749	kugelei	down	cytoskeletal interaction	37	CG18107	-	down	assorted other
17	CG8226	translocase of outer membrane 7	down	solute transport	38	CG30084	zasp52	down	cytoskeletal interaction
18	CG8369	-	down	assorted other	39	CG30415	-	down	assorted other
19	CG8580	akirin	down	transcriptional regulation	40	CG31509	turandot A	down	assorted other
20	CG9470	metallothionein A	down	metabolism	41	CG33171	multiplexin	down	cytoskeletal interaction
21	CG10484	regulatory particle non-ATPase 3	down	proteolysis	42	CG33256	limpet	down	transcriptional regulation

doi:10.1371/journal.pone.0134204.t001

S2 Table. In individual cases, the qRT-PCR data were further validated by Northern blot analyses (see below). Due to the fact that especially the latter technique requires high amounts of RNA, we isolated total RNA from complete 3rd instar larvae instead of extracting it from dissected heart tissue. Since, in addition to the heart, only few other tissues are expressing Hand [21], we consider the comparability of these data with the microarray derived results as being acceptable. Furthermore, by isolating RNA from complete 3rd instar larvae, we minimize the

Table 2. Genes exhibiting deviant expression levels in *hand^173* animals, as confirmed by qRT-PCR. Genes listed are either expressed in heart tissue or involved in muscle and heart development, maintenance or function. Deviating expression of the particular genes in *hand^173* animals is depicted in percent (%) relative to the respective expression in wild type specimen, which was set to 100%. Statistically significant deviations are indicated (* $P<0.05$; ** $P<0.01$, Student´s *t*-test). Functional classification of the corresponding protein products was done manually utilizing data from NCBI (http://www.ncbi.nlm.nih.gov/) and Flybase (http://flybase.org/). Values represent means of at least three independent qRT-PCR experiments.

#	gene	name	expression in *hand^173* [%]	function / biological process
1	CG10484	regulatory particle non-ATPase 3	-38	protein degradation
2	CG11661	neural conserved at 73EF	-74,2	tricarboxylic acid cycle
3	CG12400	NADH dehydrogenase (ubiquinone) B14.5 B subunit	-51,9	mitochondrial electron transport
4	CG14035	muscle-specific protein 300 (msp-300)	-77	cellular component organization
5	CG15067	-	-73,5	neurogenesis
6	CG16747	ornithine decarboxy-lase antizyme	-42,6	cell differentiation
7	CG17108	-	-68	unknown
8	CG18107	-	-51	unknown
9	CG2145	-	-65,6	peptide degradation
10	CG2233	-	-69,2	unknown
11	CG30084	zasp52	-51	muscle structure development
12	CG30415	-	-53,9	unknown
13	CG33171	multiplexin	-33	cell adhesion
14	CG3869	mitochondrial assembly regulatory factor (marf)	-55,1	mitochondrion organization
15	CG7749	kugelei	-61	cellular component organization
16	CG8580	akirin	-33	muscle attachment / muscle development
17	CG9470	metallothionein A	-67	metal ion homeostasis

doi:10.1371/journal.pone.0134204.t002

possibility of systemic errors that may arise in the course of nucleotide amplification, which was a mandatory experimental step in order to obtain sufficient sample from heart tissue to conduct the microarrays (see materials and methods). By applying the corresponding non-amplified cDNA preparations in qRT-PCR analyses, we confirmed the microarray results with respect to 13 genes (Table 2), while 25 genes showed expression aberrations that were either below the minimal threshold for provisional acceptance or not congruent with the microarray data. The expression of four additional genes, *akirin*, *kugelei*, *multiplexin*, and *zasp52*, respectively, did not exhibit a statistically significant deviation in *hand^173* animals. However, due to the high functional relevance of the corresponding protein products to muscle functionality [36–39], as well as to address the discrepancy between microarray and qRT-PCR data, we decided to list the respective genes in Table 2 and re-analyze their expression in *hand^173* animals by applying Northern blot as a third method. This methodology is considered highly convenient for this issue since it provides a direct relative comparison of transcript abundance between the individual samples. As a positive control we also re-analyzed the expression of *msp-300* in wild type as well as *hand* mutant animals. As depicted in Fig 2, the comparative Northern blots proved a significant misregulation of all corresponding genes in *hand* mutant animals, thus confirming the microarray data and validating a Hand dependent expression of the respective factors: while *akirin* displays an expression that is reduced by 40.5% in the *hand* mutant, the expression of *kugelei* is lowered by 57.5%, that of *msp-300* by 65% and that of *multiplexin* by 28.5%, respectively. With regard to *zasp52*, two major transcripts are detected by the applied riboprobes with the larger one being downregulated by 44.8% in the *hand* mutant and the smaller one being upregulated by 34.9%. The latter result indicates a splice variant specific regulation of the corresponding gene, which has already been described [40] and which may account for the inconsistent qRT-PCR result that presumably reflects the simultaneous up- as well as downregulation of individual splice variants. Since the primers
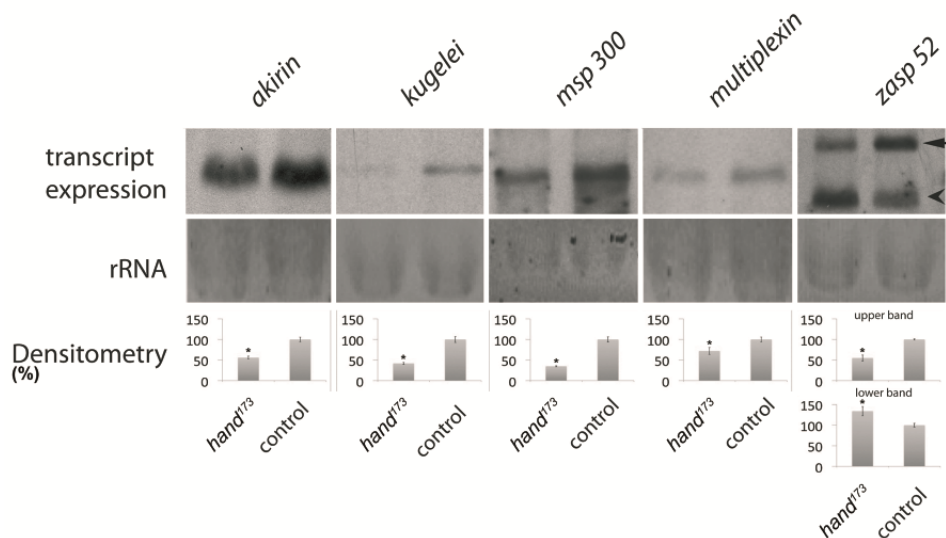
Fig 2. Relative expression of selected genes in hand mutant animals, compared to wild type. Expression levels were assessed by Northern blot. Statistically relevant deviations are evident with respect to all genes tested. While *akirin* displays an expression that is reduced by 40.5% in the *hand* mutant (*hand^{173}*), the expression of *kugelei* is lowered by 57.5%, that of *msp-300* by 65% and that of *multiplexin* by 28.5%, respectively. With regard to *zasp52*, two major transcripts are detected by the applied riboprobes with the larger one (arrow) being downregulated by 44.8% in the *hand* mutant and the smaller one (arrowhead) being upregulated by 34.9% in the same line. Bars represent mean values $\pm$ SD of at least three independent experiments. Asterisks indicate statistical significance (Student´s *t*-test *P*<0.05). Quantification of the relative band intensities in relation to the loading controls (ribosomal RNA, rRNA) was done by densitometric analysis.

applied in the respective qRT-PCR analyses are specific to 11 (C, F, I, K, L, M, R, S, T, U, W) of the 18 predicted *zasp52* splice variants (http://flybase.org), the individual changes in expression of these 11 transcripts may compensate for each other, thus resulting in an overall insignificant change in expression as determined by qRT-PCR (Table 2). By discriminating between individual splice variants the Northern blot data depicted in Fig 2 clearly confirm a Hand dependent expression of *zasp52*. Based on the apparent molecular masses of the detected transcripts, the larger one consists of about 4.7 kilobases, while the smaller one comprises about 3.1 kilobases (S1 Fig).

Hand activity is evolutionarily conserved

In order to evaluate a possible evolutionary conservation of Hand activity, in addition to the genes described above we also analyzed the Hand dependent expression of *Drosophila* genes whose vertebrate homologs had previously been identified as Hand targets. Genes tested were *hedgehog, cubitus interruptus* and *mef2*, with the former two factors being regulated by vertebrate Hand at the transcriptional level [41, 42] and the latter one being activated at the post-translational level [43]. The respective genes were selected independently of their microarray derived expression levels. As a result of comparative Northern blot analyses we found that all genes exhibit significantly deviant expression levels in the *hand* mutant: while *mef2* and *hedgehog* displayed an increased expression of 40.6% and 19.8%, respectively, the expression of *cubitus interruptus* was decreased by 19.8% in *hand^{173}* animals, thus confirming a Hand dependent expression of all selected genes (Fig 3).
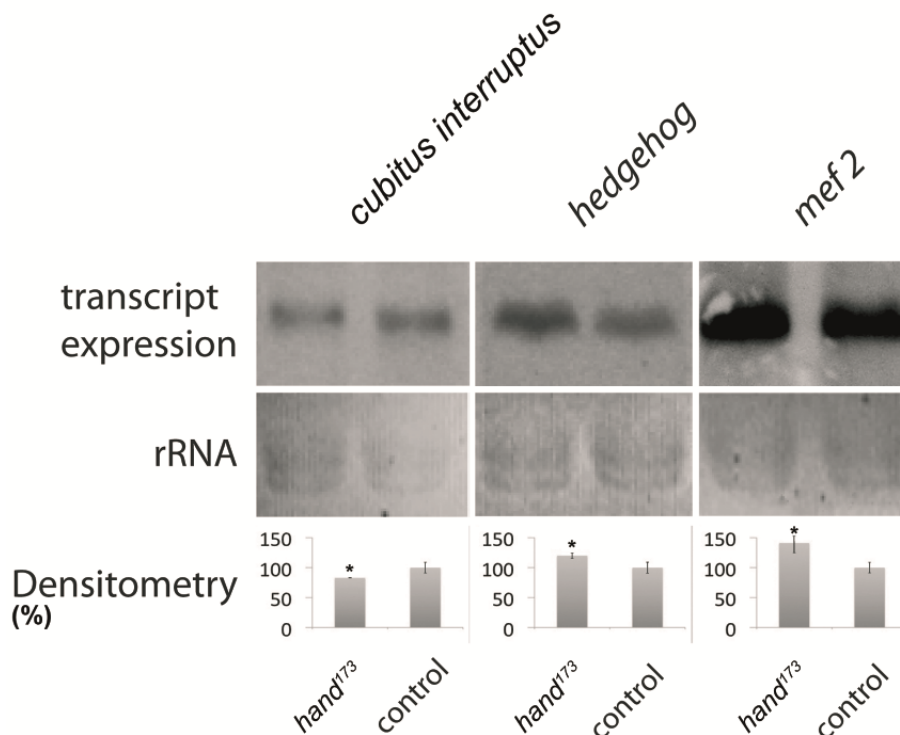
Fig 3. Relative expression of *Drosophila* homologs of selected vertebrate Hand target genes in *hand* mutant *Drosophila*, compared to wild type. Expression levels were assessed by Northern blot. Statistically relevant deviations are evident with respect to all genes tested. While *mef2* and *hedgehog* display an increased expression of 40.6% and 19.8% in *hand*[173] animals, respectively, the expression of *cubitus interruptus* is decreased by 19.8% in the same line. Bars represent mean values ± SD of at least three independent experiments. Asterisks indicate statistical significance (Student´s *t*-test *P*<0.05). Quantification of the relative band intensities in relation to the loading controls (ribosomal RNA, rRNA) was done by densitometric analysis.

doi:10.1371/journal.pone.0134204.g003

Discussion

Hand regulates the expression of numerous genes

Despite the fact that from embryogenesis to adulthood Hand is substantially expressed in all cells constituting the heart, animals lacking Hand expression do not exhibit any morphological abnormalities in the dorsal vessel at embryonic or larval stages. As previously shown, distinct phenotypes become apparent only later in development with adult *hand*[173] flies exhibiting severe malformations, such as disorganized myofibrils in heart and midgut tissue and a significantly reduced systolic and diastolic diameter of the heart lumen [24]. Nevertheless, the early expression of Hand in heart cells that is maintained during larval life indicates that Hand is of functional importance already in these stages of *Drosophila* development. In this context, a possible function could be the fine regulation of gene expression in the respective tissue rather than being a major transcriptional activator / repressor of factors that are essential for cardiac integrity and survival. To analyze this indication in more detail, we aimed to identify Hand target genes by making use of a microarray based approach that allowed us to examine alterations in gene expression in a genome-wide manner. As a result, we identified 545 genes that exhibited altered expression levels in a *hand* mutant background and that may thus represent target

genes of Hand. Based on these data we assume that Hand is part of a gene regulatory network that comprises numerous transcription factors, which, in addition to regulating the expression of different downstream genes, control their individual expression in a mutual manner. This assumption is supported by the result that a considerable share of the identified Hand targets is apparently involved in transcriptional regulation (80 of 545, Fig 1, S1 Fig).

One key feature of bHLH proteins represents their intrinsic ability to form homo- and heterodimers with other bHLH proteins, which eventually results in a highly heterogeneous mixture of activators or repressors in different cell types. As shown previously, Hand forms heterodimers with, e.g., class I bHLH proteins such as Daughterless (Da), class II bHLH proteins such as Twist or Nautilus [26, 44–46] or class-O transcription factors such as Hey [26]. Since *hand* null mutants display only mild phenotypes that do not result in embryonic lethality, we argue that Hand acts most likely as a tissue specific modulator of transcriptional activities rather than being a key regulator such as Twist or Da. This presumption is further supported by the fact that none of the putative Hand targets identified in this study exhibited a complete knock-out as a result of Hand deprivation. In any case a considerable residual expression remained, which is different compared to master transcription factors such as Twist, whose binding to a *cis*-regulatory module represents a prerequisite to activate expression of a large percentage of its target genes [47]. This disparity indicates that, unlike Twist, Hand modulates expression of its targets in a rather subtle manner.

Hand regulates the expression of genes that are critical to heart and muscle function

The most prominent phenotype in *hand* null mutants is a disorganized myofibrillar architecture being apparent in the dorsal vessel [24] and in wing heart muscles [26]. In the heart, the myofilaments are normally organized in a helical fashion, which allows the heart lumen to narrow upon contraction. This provides the driving force for hemolymph flow from the posterior heart chamber towards the anterior aorta portion of the heart. In *hand* null mutants the orientation of myofibers is disturbed, which likely accounts for the observed reduced systolic and diastolic diameter and abnormal heart beating [24]. Similarly, myofibrillar organization defects were found in muscle cells of the wing hearts of *hand* mutants [26]. Based on these observations, we expected Hand to be involved in regulating the expression of genes encoding proteins essential to sarcomere assembly or myofilament differentiation in general. Congruously, we found *akirin, kugelei, msp-300, multiplexin*, and *zasp52*, all of which known to be crucial to muscle architecture or function, being downregulated in *hand* mutant animals. While Akirin represents a critical cofactor of the key *Drosophila* mesoderm and muscle transcription factor Twist [36], Kugelei was reported to be essential for the spatial orientation of actin bundles [37]. Msp-300 is required for proper muscle function by forming a nuclear ring structure that recruits and associates with a network of polarized astral microtubules, enabling the dynamic movement and uniform spacing between the nuclei in each muscle fiber. Disruption of this mechanism considerably impairs muscle function and larval motility [48]. With respect to Multiplexin it was recently shown that the protein is required for heart morphogenesis by controlling the direction, timing, and presumably the extent of Slit/Robo activity and signaling at the luminal membrane of cardioblasts [38]. Finally, Zasp52 is a member of the PDZ-LIM domain protein family and required for muscle attachment as well as Z-disk assembly and maintenance [39]. Noteworthy, transcription of the respective genes is not completely blocked, a finding, which further substantiates the assumption that Hand participates in transcriptional fine regulation rather than being the sole regulator of these genes. Nevertheless, the

simultaneous knock-down of these factors could readily account for the disorganized myofibrillar architecture observed in *hand* mutant animals.

Moreover, the complex gene structure of *zasp52* and *msp-300* with several splice variants present (http://flybase.org/) raised the question whether Hand is also involved in regulating expression of these genes in a splice variant specific manner. At least with respect to *zasp52* our data indicate such a regulation. As depicted in Fig 2, Northern blot analysis revealed the expression of two major *zasp52* transcripts in 3rd instar larvae with the larger splice variant being downregulated by 44.8% in the *hand* mutant and the smaller one being upregulated by 34.9% in the same line. An estimation of the respective molecular masses yielded that the larger transcript consists of about 4700 nucleotides, while the smaller one comprises about 3100 nucleotides (S1 Fig). According to sequence predictions (http://flybase.org/), except for isoform Q the applied riboprobes should detect all 17 remaining *zasp52* splice variants ranging in length between 951 nucleotides (splice variant P) and 7418 nucleotides (splice variant F). Apparently, only two of them are expressed in considerable amounts in 3rd instar larvae (Fig 2, S1 Fig) with the corresponding size of the detected transcripts rendering it likely that the larger one represents either isoform I (4649 nucleotides), M (4790 nucleotides), or N (4637 nucleotides), while the smaller one presumably corresponds to either isoform E (3176 nucleotides), R (3002 nucleotides), S (3197 nucleotides), or U (2984 nucleotides), respectively. To unambiguously identify the respective transcript variants, clearly additional Northern blots with isoform-specific riboprobes are necessary; however, such an analysis was not the focus of the present study.

By providing evidence that the expression of distinct factors critical to muscle integrity and function is regulated by Hand, this work represents a promising starting point for future studies aiming to understand the physiology of distinct cardiac phenotypes that manifest in Hand mutant animals [24, 26]. Based on our data, further research will clarify whether or not impaired expression of the identified factors, either exclusively or in a concerted manner, is responsible for the respective phenotypes. Taking into account that Hand activity appears to be evolutionarily conserved, appreciation of Hand functionality in *Drosophila* may be highly beneficial with respect to understanding the physiological relevance of vertebrate Hand in a more complete manner.

Supporting Information

S1 Fig. Isoform specific expression of *zasp52* analyzed by Northern blot. In both, 3rd instar larvae of *hand* mutant animals (*hand*[173]) as well as wild type animals (control), two major transcripts are detected. The larger one (white arrow) migrates at about 4.7 kilobases while the smaller one has a length of about 3.1 kilobases (black arrow). MWM: molecular weight marker. (TIF)

S1 Table. Classification of genes exhibiting deviant expression levels in *hand*[173] animals. Analysis of the microarray data yielded 545 genes exhibiting an altered expression in *hand*[173] hearts, with 385 genes being downregulated in the mutant and 160 genes displaying an increased expression in the same line, compared to wild type. Classification of the corresponding protein products into functional groups was done manually utilizing data from NCBI (http://www.ncbi.nlm.nih.gov/) and Flybase (http://flybase.org/). Factors with yet unknown physiological functions are allocated to the category "assorted other". (XLSX)

S2 Table. qRT-PCR Primers. (DOCX)

Author Contributions

Conceived and designed the experiments: BH HM AP. Performed the experiments: BH JH MT. Analyzed the data: BH TR JH MT HM AP. Wrote the paper: BH HM AP.

References

1. Massari ME, Murre C. Helix-loop-helix proteins: regulators of transcription in eucaryotic organisms. Molecular and cellular biology. 2000; 20(2):429–40. PMID: 10611221; PubMed Central PMCID: PMC85097.

2. Cross JC, Flannery ML, Blanar MA, Steingrimsson E, Jenkins NA, Copeland NG, et al. Hxt encodes a basic helix-loop-helix transcription factor that regulates trophoblast cell development. Development. 1995; 121(8):2513–23. PMID: 7671815.

3. Cserjesi P, Brown D, Lyons GE, Olson EN. Expression of the novel basic helix-loop-helix gene eHAND in neural crest derivatives and extraembryonic membranes during mouse development. Developmental biology. 1995; 170(2):664–78. doi: 10.1006/dbio.1995.1245 PMID: 7649392.

4. Srivastava D, Cserjesi P, Olson EN. A subclass of bHLH proteins required for cardiac morphogenesis. Science. 1995; 270(5244):1995–9. PMID: 8533092.

5. Srivastava D, Thomas T, Lin Q, Kirby ML, Brown D, Olson EN. Regulation of cardiac mesodermal and neural crest development by the bHLH transcription factor, dHAND. Nature genetics. 1997; 16(2):154–60. doi: 10.1038/ng0697-154 PMID: 9171826.

6. Riley P, Anson-Cartwright L, Cross JC. The Hand1 bHLH transcription factor is essential for placentation and cardiac morphogenesis. Nature genetics. 1998; 18(3):271–5. doi: 10.1038/ng0398-271 PMID: 9500551.

7. Howard MJ, Stanke M, Schneider C, Wu X, Rohrer H. The transcription factor dHAND is a downstream effector of BMPs in sympathetic neuron specification. Development. 2000; 127(18):4073–81. PMID: 10952904.

8. D'Autreaux F, Morikawa Y, Cserjesi P, Gershon MD. Hand2 is necessary for terminal differentiation of enteric neurons from crest-derived precursors but not for their migration into the gut or for formation of glia. Development. 2007; 134(12):2237–49. doi: 10.1242/dev.003814 PMID: 17507395.

9. Doxakis E, Howard L, Rohrer H, Davies AM. HAND transcription factors are required for neonatal sympathetic neuron survival. EMBO reports. 2008; 9(10):1041–7. doi: 10.1038/embor.2008.161 PMID: 18724272; PubMed Central PMCID: PMC2572120.

10. Morikawa Y, Cserjesi P. Cardiac neural crest expression of Hand2 regulates outflow and second heart field development. Circulation research. 2008; 103(12):1422–9. doi: 10.1161/CIRCRESAHA.108.180083 PMID: 19008477.

11. Funato N, Chapman SL, McKee MD, Funato H, Morris JA, Shelton JM, et al. Hand2 controls osteoblast differentiation in the branchial arch by inhibiting DNA binding of Runx2. Development. 2009; 136(4):615–25. doi: 10.1242/dev.029355 PMID: 19144722.

12. Schmidt M, Lin S, Pape M, Ernsberger U, Stanke M, Kobayashi K, et al. The bHLH transcription factor Hand2 is essential for the maintenance of noradrenergic properties in differentiated sympathetic neurons. Developmental biology. 2009; 329(2):191–200. doi: 10.1016/j.ydbio.2009.02.020 PMID: 19254708; PubMed Central PMCID: PMC2746555.

13. Xiong W, He F, Morikawa Y, Yu X, Zhang Z, Lan Y, et al. Hand2 is required in the epithelium for palatogenesis in mice. Developmental biology. 2009; 330(1):131–41. doi: 10.1016/j.ydbio.2009.03.021 PMID: 19341725; PubMed Central PMCID: PMC2745957.

14. Osterwalder M, Speziale D, Shoukry M, Mohan R, Ivanek R, Kohler M, et al. HAND2 targets define a network of transcriptional regulators that compartmentalize the early limb bud mesenchyme. Developmental cell. 2014; 31(3):345–57. doi: 10.1016/j.devcel.2014.09.018 PMID: 25453830; PubMed Central PMCID: PMC4357275.

15. Biben C, Harvey RP. Homeodomain factor Nkx2-5 controls left/right asymmetric expression of bHLH gene eHand during murine heart development. Genes & development. 1997; 11(11):1357–69. PMID: 9192865.

16. Thomas T, Yamagishi H, Overbeek PA, Olson EN, Srivastava D. The bHLH factors, dHAND and eHAND, specify pulmonary and systemic cardiac ventricles independent of left-right sidedness. Developmental biology. 1998; 196(2):228–36. doi: 10.1006/dbio.1998.8849 PMID: 9576835.

17. Firulli AB, McFadden DG, Lin Q, Srivastava D, Olson EN. Heart and extra-embryonic mesodermal defects in mouse embryos lacking the bHLH transcription factor Hand1. Nature genetics. 1998; 18 (3):266–70. doi: 10.1038/ng0398-266 PMID: 9500550.

18. McFadden DG, Barbosa AC, Richardson JA, Schneider MD, Srivastava D, Olson EN. The Hand1 and Hand2 transcription factors regulate expansion of the embryonic cardiac ventricles in a gene dosage-dependent manner. Development. 2005; 132(1):189–201. doi: 10.1242/dev.01562 PMID: 15576406.

19. Natarajan A, Yamagishi H, Ahmad F, Li D, Roberts R, Matsuoka R, et al. Human eHAND, but not dHAND, is down-regulated in cardiomyopathies. Journal of molecular and cellular cardiology. 2001; 33 (9):1607–14. doi: 10.1006/jmcc.2001.1434 PMID: 11549340.

20. Moore AW, Barbel S, Jan LY, Jan YN. A genomewide survey of basic helix-loop-helix factors in Drosophila. Proceedings of the National Academy of Sciences of the United States of America. 2000; 97 (19):10436–41. doi: 10.1073/pnas.170301897 PMID: 10973473; PubMed Central PMCID: PMC27042.

21. Kolsch V, Paululat A. The highly conserved cardiogenic bHLH factor Hand is specifically expressed in circular visceral muscle progenitor cells and in all cell types of the dorsal vessel during Drosophila embryogenesis. Development genes and evolution. 2002; 212(10):473–85. doi: 10.1007/s00427-002-0268-6 PMID: 12424518.

22. Han Z, Olson EN. Hand is a direct target of Tinman and GATA factors during Drosophila cardiogenesis and hematopoiesis. Development. 2005; 132(15):3525–36. doi: 10.1242/dev.01899 PMID: 15975941.

23. Han Z, Yi P, Li X, Olson EN. Hand, an evolutionarily conserved bHLH transcription factor required for Drosophila cardiogenesis and hematopoiesis. Development. 2006; 133(6):1175–82. doi: 10.1242/dev.02285 PMID: 16467358.

24. Lo PC, Zaffran S, Senatore S, Frasch M. The Drosophila Hand gene is required for remodeling of the developing adult heart and midgut during metamorphosis. Developmental biology. 2007; 311(2):287–96. doi: 10.1016/j.ydbio.2007.08.024 PMID: 17904115; PubMed Central PMCID: PMC2128039.

25. Sellin J, Albrecht S, Kolsch V, Paululat A. Dynamics of heart differentiation, visualized utilizing heart enhancer elements of the Drosophila melanogaster bHLH transcription factor Hand. Gene expression patterns: GEP. 2006; 6(4):360–75. doi: 10.1016/j.modgep.2005.09.012 PMID: 16455308.

26. Togel M, Meyer H, Lehmacher C, Heinisch JJ, Pass G, Paululat A. The bHLH transcription factor hand is required for proper wing heart formation in Drosophila. Developmental biology. 2013; 381(2):446–59. doi: 10.1016/j.ydbio.2013.05.027 PMID: 23747982.

27. Wagner C, Isermann K, Fehrenbach H, Roeder T. Molecular architecture of the fruit fly's airway epithelial immune system. BMC genomics. 2008; 9:446. doi: 10.1186/1471-2164-9-446 PMID: 18823557; PubMed Central PMCID: PMC2566315.

28. Hoffmann J, Romey R, Fink C, Yong L, Roeder T. Overexpression of Sir2 in the adult fat body is sufficient to extend lifespan of male and female Drosophila. Aging. 2013; 5(4):315–27. PMID: 23765091; PubMed Central PMCID: PMC3651523.

29. Schramm G, Bruchhaus I, Roeder T. A simple and reliable 5'-RACE approach. Nucleic acids research. 2000; 28(22):E96. PMID: 11071950; PubMed Central PMCID: PMC113888.

30. Arvidsson S, Kwasniewski M, Riano-Pachon DM, Mueller-Roeber B. QuantPrime—a flexible tool for reliable high-throughput primer design for quantitative PCR. BMC bioinformatics. 2008; 9:465. doi: 10.1186/1471-2105-9-465 PMID: 18976492; PubMed Central PMCID: PMC2612009.

31. Simon P. Q-Gene: processing quantitative real-time RT-PCR data. Bioinformatics. 2003; 19(11):1439–40. PMID: 12874059.

32. Drechsler M, Schmidt AC, Meyer H, Paululat A. The conserved ADAMTS-like protein lonely heart mediates matrix formation and cardiac tissue integrity. PLoS genetics. 2013; 9(7):e1003616. doi: 10.1371/journal.pgen.1003616 PMID: 23874219; PubMed Central PMCID: PMC3708815.

33. Zeitouni B, Senatore S, Severac D, Aknin C, Semeriva M, Perrin L. Signalling pathways involved in adult heart formation revealed by gene expression profiling in Drosophila. PLoS genetics. 2007; 3 (10):1907–21. doi: 10.1371/journal.pgen.0030174 PMID: 17937502; PubMed Central PMCID: PMC2014791.

34. Cammarato A, Ahrens CH, Alayari NN, Qeli E, Rucker J, Reedy MC, et al. A mighty small heart: the cardiac proteome of adult Drosophila melanogaster. PLoS one. 2011; 6(4):e18497. doi: 10.1371/journal.pone.0018497 PMID: 21541028; PubMed Central PMCID: PMC3081823.

35.   Neely GG, Kuba K, Cammarato A, Isobe K, Amann S, Zhang L, et al. A global in vivo Drosophila RNAi screen identifies NOT3 as a conserved regulator of heart function. Cell. 2010; 141(1):142–53. doi: 10.1016/j.cell.2010.02.023 PMID: 20371351; PubMed Central PMCID: PMC2855221.

36.   Nowak SJ, Aihara H, Gonzalez K, Nibu Y, Baylies MK. Akirin links twist-regulated transcription with the Brahma chromatin remodeling complex during embryogenesis. PLoS genetics. 2012; 8(3):e1002547. doi: 10.1371/journal.pgen.1002547 PMID: 22396663; PubMed Central PMCID: PMC3291577.

37.   Gutzeit HO, Eberhardt W, Gratwohl E. Laminin and basement membrane-associated microfilaments in wild-type and mutant Drosophila ovarian follicles. Journal of cell science. 1991; 100 (Pt 4):781–8. PMID: 1814932.

38.   Harpaz N, Ordan E, Ocorr K, Bodmer R, Volk T. Multiplexin promotes heart but not aorta morphogenesis by polarized enhancement of slit/robo activity at the heart lumen. PLoS genetics. 2013; 9(6): e1003597. doi: 10.1371/journal.pgen.1003597 PMID: 23825967; PubMed Central PMCID: PMC3694841.

39.   Jani K, Schock F. Zasp is required for the assembly of functional integrin adhesion sites. The Journal of cell biology. 2007; 179(7):1583–97. doi: 10.1083/jcb.200707045 PMID: 18166658; PubMed Central PMCID: PMC2373490.

40.   Katzemich A, Long JY, Jani K, Lee BR, Schock F. Muscle type-specific expression of Zasp52 isoforms in Drosophila. Gene expression patterns: GEP. 2011; 11(8):484–90. doi: 10.1016/j.gep.2011.08.004 PMID: 21867777.

41.   McFadden DG, McAnally J, Richardson JA, Charite J, Olson EN. Misexpression of dHAND induces ectopic digits in the developing limb bud in the absence of direct DNA binding. Development. 2002; 129 (13):3077–88. PMID: 12070084.

42.   Holler KL, Hendershot TJ, Troy SE, Vincentz JW, Firulli AB, Howard MJ. Targeted deletion of Hand2 in cardiac neural crest-derived cells influences cardiac gene expression and outflow tract development. Developmental biology. 2010; 341(1):291–304. doi: 10.1016/j.ydbio.2010.02.001 PMID: 20144608; PubMed Central PMCID: PMC2854279.

43.   Morin S, Pozzulo G, Robitaille L, Cross J, Nemer M. MEF2-dependent recruitment of the HAND1 transcription factor results in synergistic activation of target promoters. The Journal of biological chemistry. 2005; 280(37):32272–8. doi: 10.1074/jbc.M507640200 PMID: 16043483.

44.   Dai YS, Cserjesi P. The basic helix-loop-helix factor, HAND2, functions as a transcriptional activator by binding to E-boxes as a heterodimer. The Journal of biological chemistry. 2002; 277(15):12604–12. doi: 10.1074/jbc.M200283200 PMID: 11812799.

45.   Firulli BA, Hadzic DB, McDaid JR, Firulli AB. The basic helix-loop-helix transcription factors dHAND and eHAND exhibit dimerization characteristics that suggest complex regulation of function. The Journal of biological chemistry. 2000; 275(43):33567–73. doi: 10.1074/jbc.M005888200 PMID: 10924525; PubMed Central PMCID: PMC2561327.

46.   Firulli BA, Krawchuk D, Centonze VE, Vargesson N, Virshup DM, Conway SJ, et al. Altered Twist1 and Hand2 dimerization is associated with Saethre-Chotzen syndrome and limb abnormalities. Nature genetics. 2005; 37(4):373–81. doi: 10.1038/ng1525 PMID: 15735646; PubMed Central PMCID: PMC2568820.

47.   Sandmann T, Girardot C, Brehme M, Tongprasit W, Stolc V, Furlong EE. A core transcriptional network for early mesoderm development in Drosophila melanogaster. Genes & development. 2007; 21 (4):436–49. doi: 10.1101/gad.1509007 PMID: 17322403; PubMed Central PMCID: PMC1804332.

48.   Elhanany-Tamir H, Yu YV, Shnayder M, Jain A, Welte M, Volk T. Organelle positioning in muscles requires cooperation between two KASH proteins and microtubules. The Journal of cell biology. 2012; 198(5):833–46. doi: 10.1083/jcb.201204102 PMID: 22927463; PubMed Central PMCID: PMC3432764.

6.5.2 *Drosophila* neprilysins control insulin signaling and food intake via cleavage of regulatory peptides (eLife, 2016)

Benjamin Hallier[1†], Ronja Schiemann[1†], Eva Cordes[1], Jessica Vitos-Faleato[2], Stefan Walter[3], Jürgen J Heinisch[4], Anders Malmendal[5], Achim Paululat[1], Heiko Meyer[1*]

1 Department of Developmental Biology, University of Osnabrück, Osnabrück, Germany

2 Department of Biomedical Research, Institute for Research in Biomedicine, Barcelona, Spain

3 Department of Microbiology, University of Osnabrück, Osnabrück, Germany

4 Department of Genetics, University of Osnabrück, Osnabrück, Germany

5 Department of Cellular and Molecular Medicine, University of Copenhagen, Copenhagen, Denmark

RESEARCH ARTICLE

Drosophila neprilysins control insulin signaling and food intake via cleavage of regulatory peptides

Benjamin Hallier[1†], Ronja Schiemann[1†], Eva Cordes[1], Jessica Vitos-Faleato[2], Stefan Walter[3], Jürgen J Heinisch[4], Anders Malmendal[5], Achim Paululat[1], Heiko Meyer[1*]

[1]Department of Developmental Biology, University of Osnabrück, Osnabrück, Germany; [2]Department of Biomedical Research, Institute for Research in Biomedicine, Barcelona, Spain; [3]Department of Microbiology, University of Osnabrück, Osnabrück, Germany; [4]Department of Genetics, University of Osnabrück, Osnabrück, Germany; [5]Department of Cellular and Molecular Medicine, University of Copenhagen, Copenhagen, Denmark

*For correspondence: Meyer@
biologie.uni-osnabrueck.de

†These authors contributed
equally to this work

Abstract Insulin and IGF signaling are critical to numerous developmental and physiological processes, with perturbations being pathognomonic of various diseases, including diabetes. Although the functional roles of the respective signaling pathways have been extensively studied, the control of insulin production and release is only partially understood. Herein, we show that in Drosophila expression of insulin-like peptides is regulated by neprilysin activity. Concomitant phenotypes of altered neprilysin expression included impaired food intake, reduced body size, and characteristic changes in the metabolite composition. Ectopic expression of a catalytically inactive mutant did not elicit any of the phenotypes, which confirms abnormal peptide hydrolysis as a causative factor. A screen for corresponding substrates of the neprilysin identified distinct peptides that regulate insulin-like peptide expression, feeding behavior, or both. The high functional conservation of neprilysins and their substrates renders the characterized principles applicable to numerous species, including higher eukaryotes and humans.
DOI: 10.7554/eLife.19430.001

Introduction

Neprilysins are highly conserved ectoenzymes that cleave and thereby inactivate many physiologically relevant peptides in the extracellular space, thus contributing considerably to the maintenance of peptide homeostasis in this compartment. Members of the neprilysin family generally consist of a short N-terminal cytoplasmic domain, a membrane spanning region, and a large extracellular domain with two highly conserved sequence motifs (HExxH; ExxA/GD) critical for zinc coordination, catalysis, and substrate or inhibitor binding (*Matthews, 1988*; *Oefner et al., 2000*). Because of these characteristics, neprilysins are classified as M13 zinc metallopeptidases. For human Neprilysin (NEP), the most well-characterized family member, identified substrates include endothelins, angiotensins I and II, enkephalins, bradykinin, atrial natriuretic peptide, substance P, and the amyloid-beta peptide (*Turner et al., 2001*). Because of this high substrate variability, NEP activity has been implicated in the pathogenesis of hypertension (*Molinaro et al., 2002*), analgesia (*Whitworth, 2003*), cancer (*Turner et al., 2001*), and Alzheimer's disease (*Iwata et al., 2000*; *Belyaev et al., 2009*). Recent clinical trials have demonstrated significant efficacy of Neprilysin inhibitors in the treatment of certain indications (*Jessup, 2014*; *McMurray et al., 2014*). However, despite the clinical relevance of the neprilysins, the physiological function and *in vivo* substrates of most family members are unknown.

eLife digest The hormone insulin and similar molecules called insulin-like peptides act as signals to control many processes in the body, including growth, stress responses and aging. Disrupting these signaling pathways can cause many diseases, with diabetes being the most common of these. Although the roles of the signaling pathways have been well studied, it is less clear how the body controls the production of insulin and insulin-like peptides.

Neprilysins are enzymes that can cut other proteins and peptides by a process known as hydrolysis. Their targets (known as "substrates") include peptides that regulate a range of cell processes, and neprilysins have therefore been linked with many diseases. Fruit flies have at least five different neprilysin enzymes, but their substrates have not yet been identified. One of these, known as Nep4A, is produced in muscle tissue and appears to be important for muscles to work properly.

Hallier, Schiemann et al. reveal that Nep4A regulates the production of insulin-like peptides. The experiments used fruit fly larvae that had been genetically engineered so that the level of Nep4A could be altered in muscle tissue. Larvae with very high or very low levels of Nep4A eat less food, have smaller bodies and produce different amounts of insulin-like peptides compared to normal larvae.

Further experiments show that Nep4A can hydrolyze a number of peptides that regulate the production and the release of insulin-like peptides. This suggests that the enzymatic activity of neprilysins plays a direct role in controlling the production of insulin. The next challenge is to find out whether these findings apply to humans and other animals that also have neprilysins.
DOI: 10.7554/eLife.19430.002

In *Drosophila melanogaster*, at least five neprilysin genes are expressed (*Meyer et al., 2011*; *Sitnik et al., 2014*), two of the corresponding protein products, Nep2 and Nep4, were reported to be enzymatically active (*Bland et al., 2007*; *Meyer et al., 2009*; *Thomas et al., 2005*). With respect to Nep4, a critical function of the enzyme's non-catalytic intracellular N-terminus has been demonstrated: when present in excess, the domain induces severe muscle degeneration concomitant with lethality during late larval development. Because the intracellular domain interacts with a carbohydrate kinase, impaired energy metabolism has been proposed as the underlying cause of the phenotype (*Panz et al., 2012*). In addition, Nep2 has been implicated in the regulation of locomotion and geotactic behavior (*Bland et al., 2009*), and neprilysin activity in general appears to be critical to the formation of middle- and long-term memory (*Turrel et al., 2016*), as well as to the regulation of pigment dispersing factor (PDF) signaling within circadian neural circuits (*Isaac et al., 2007*). However, despite these experiments and recent findings that suggest a critical role of neprilysins in reproduction (*Sitnik et al., 2014*), the physiological functionality of these enzymes is still far from being understood. In this respect, the lack of identified substrates with *in vivo* relevance is a major hindrance.

Herein, we describe the identification of numerous novel substrates of *Drosophila* Neprilysin 4 (Nep4) and provide evidence that Nep4-mediated peptide hydrolysis regulates insulin-like peptide (ILP) expression and food intake. These results establish a correlation between neprilysin activity and ILP expression and thus clarify our understanding of the complex mechanisms that control the production and release of these essential peptides.

Results

Modulating the expression of Neprilysin 4 affects lifespan and body size

In previous experiments, we showed that Nep4 is expressed in larval body wall muscles and that increased expression of the peptidase in this tissue interferes with muscle function and integrity and severely impairs movement of the larvae (*Panz et al., 2012*). In the present study, we found that an increase in Nep4A in muscle cells (*mef2*-Gal4 driver) also induced biphasic lethality. An early phase occurred throughout embryonic and early larval development, and a late phase was evident by the

end of larval development (*Figure 1A*). Significantly, early lethality was observed only upon overexpression of the active enzyme; expression of catalytically inactive Nep4A, carrying a glutamine instead of an essential glutamate (E873Q) within the zinc-binding motif, did not affect viability at this point of development. By contrast, overexpression of catalytically active or inactive Nep4A constructs induced late larval lethality. These distinct effects demonstrate that lethality during early development is caused exclusively by a detrimental increase in catalytic activity, whereas late larval lethality appears to be a consequence of multiple physiological impairments. Comparable overexpression levels of the wild-type enzyme and the mutated construct were demonstrated previously (*Panz et al., 2012*). Muscle-specific knockdown of *nep4* slightly increased embryonic mortality, but the majority of the respective animals died during metamorphosis (*Figure 1A*). To confirm RNAi specificity, we also analyzed flies expressing both the respective RNAi construct as well as the Nep4A overexpression construct. Simultaneous overexpression of Nep4A completely rescued the RNAi phenotypes (embryonic/pupal lethality), thus confirming specificity of the knockdown (*Figure 1A*). The result that respective animals exhibited a marginally, yet significantly increased lethality rate during third instar larval stage indicates that overexpression of Nep4A is somewhat more effective than knockdown, eventually resulting in slightly increased expression levels of the peptidase, which, as depicted above, result in elevated larval lethality.

As shown previously, in addition to muscle tissue *mef2* is expressed in distinct neurons, including clock neurons (*Blanchard, 2010*) and Kenyon cells (*Schulz et al., 1996*). To determine whether the effects described above (using *mef2*-Gal4 as a driver) are exclusively based on Nep4 activity in muscles, or if neuronal Nep4 is also involved, we used pan-neuronal *elav*-Gal4 as a driver to increase or reduce *nep4* expression. In this line of experiments, neither overexpression nor knockdown of *nep4* had any significant influence on viability (*Figure 1A*). This result indicates that the effects observed with *mef2*-Gal4 are muscle-specific.

In addition to muscle tissue, Nep4 is also expressed in glial cells of the central nervous system (CNS) (*Meyer et al., 2009*). However, in contrast to the effects observed in muscle cells, neither increased nor reduced *nep4* expression in glial cells, using glia-specific *repo*-Gal4 as a driver, significantly affected life span (*Figure 1A*).

Besides reduced viability, elevated Nep4A levels in muscle tissue affected body size. Interestingly, as with increased lethality during early development, the effects on body size depended on enzymatic activity. In third instar larvae, muscle-specific overexpression of the active enzyme decreased the size and weight of the animals relative to control animals, whereas overexpression of catalytically inactive Nep4A did not affect size or weight. Knockdown of the peptidase in the same tissue did also not significantly alter these parameters (*Figure 1B*). In contrast to the muscle-specific effects, increased *nep4A* expression in glial cells or neurons did not affect the size or weight of the larvae. Glial cell specific *nep4* knockdown slightly reduced both parameters, whereas neuronal knockdown had no effect (*Figure 1B*). In line with the lethality assay, the effects of *nep4* knockdown on size and weight were completely rescued by simultaneous overexpression of Nep4A, which again confirms specificity of the respective RNAi construct. The depicted results indicate essential functions of Nep4 in muscle tissue and glial cells. However, the effects of modifying *nep4* expression were more severe in muscles, suggesting the active enzyme has a critical function particularly in this tissue.

Modulating the expression of Neprilysin 4 interferes with basal metabolic processes

To understand the physiological basis of this function in more detail, we analyzed the metabolite composition in animals with increased or reduced *nep4* levels and compared the respective compositions to those in control specimens. As shown in *Figure 2A*, increasing or decreasing the expression of *nep4* in muscle tissue affected metabolite concentrations in transgenic third instar larvae. Of note, the depicted PCA scores plot is purely based on the amplitude of correlated between-sample variations, implicating that the strongest variations in metabolite composition are those separating the three genotypes. Further analysis of the respective data revealed that profound changes are related to the energy metabolism. Knockdown of *nep4* increased the levels of fructose and a purine and decreased the levels of NAD, a purine nucleotide, and glutamine (*Figure 2B,C*, *Figure 2— source data 1*). Nep4A overexpression increased the signals of histidine, glutamine, and the same purine. In addition, a significant increase was observed in the spectral regions specific to glucose and fructose, indicating elevated levels of the two monosaccharides. Of note, only the glucose and
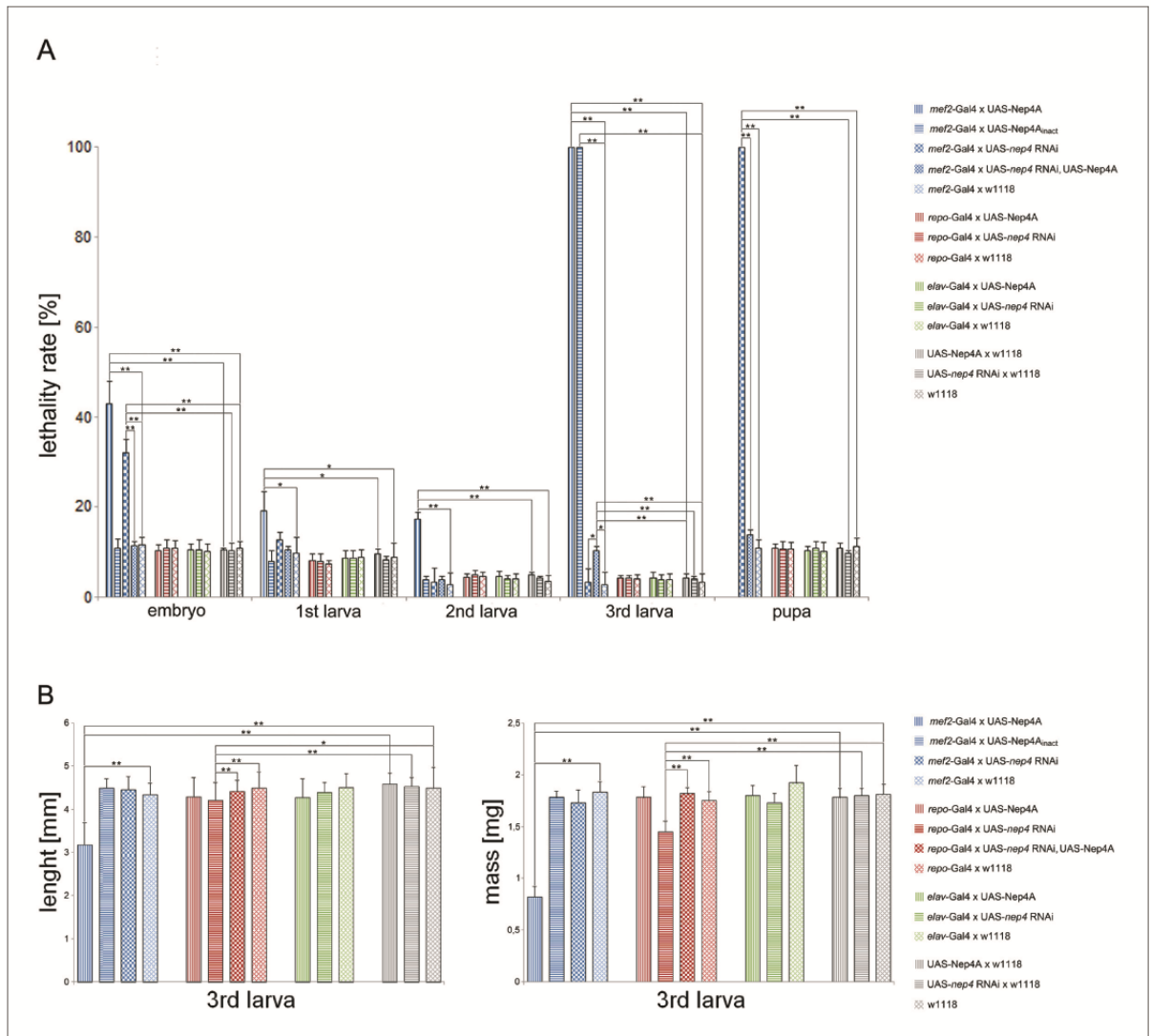
Figure 1. Modulating *nep4* expression affects life span and body size. (**A**) Lethality assay. The percentages (%) of animals of a specific stage that did not develop into the next stage are shown. While muscle-specific overexpression of Nep4A (*mef2*-Gal4 x UAS-Nep4A) led to biphasic lethality with critical phases during embryonic and late larval development, overexpression of catalytically inactive Nep4A in the same tissue (*mef2*-Gal4 x UAS-Nep4A$_{inact}$) led to lethality only in the third instar larval stage. Muscle-specific *nep4* knockdown (*mef2*-Gal4 x UAS-*nep4* RNAi) slightly increased embryonic lethality, but the majority of the animals died as pupae. Glial cell-specific overexpression (*repo*-Gal4 x UAS-Nep4A) or knockdown of the peptidase (*repo*-Gal4 x UAS-*nep4* RNAi) did not affect life span, which was also observed for neuronal overexpression or knockdown (*elav*-Gal4 x UAS-Nep4A; *elav*-Gal4 x UAS-*nep4* RNAi). *mef2*-Gal4 x w1118, *repo*-Gal4 x w1118, *elav*-Gal4 x w1118, UAS-Nep4A x w1118, UAS-*nep4* RNAi x w1118, and w1118 were used as controls. Asterisks indicate statistically significant deviations from the respective controls (*p<0.05, **p<0.01, one-way ANOVA with pairwise comparisons). (**B**) Size and weight measurements. While muscle-specific overexpression of Nep4A (*mef2*-Gal4 x UAS-Nep4A) reduced the size and wet mass of third instar larvae, neither overexpression of catalytically inactive Nep4A in the same tissue (*mef2*-Gal4 x UAS-Nep4A$_{inact}$) nor muscle-specific *nep4* knockdown (*mef2*-Gal4 x UAS-*nep4* RNAi) significantly affected these parameters. Glial cell-specific overexpression of the peptidase (*repo*-Gal4 x UAS-Nep4A) did not alter size or weight, while downregulation of the peptidase in the same tissue (*repo*-Gal4 x UAS-*nep4* RNAi) slightly, but significantly, reduced both parameters. Neuronal overexpression or knockdown of *nep4* (*elav*-Gal4 x UAS-Nep4A; *elav*-Gal4 x UAS-*nep4* RNAi) had

Figure 1 continued on next page

Figure 1 continued

no effect on size or weight. Control lines were the same as in A. Asterisks indicate statistically significant deviations from respective controls (*p<0.05, **p<0.01, one-way ANOVA with pairwise comparisons).

fructose signals with contributions from both sugars (depicted in *Figure 2B*) were significantly affected, implying that there is a more stable response in the sum of the two than in either of them. However, evaluation of the corresponding individual spectra clearly suggested that both sugars are increased (*Figure 2—figure supplement 1*). On the other hand, lactate, NAD, trehalose, and tyrosine concentrations were reduced in Nep4A-overexpressing animals (*Figure 2B,C*, *Figure 2—source data 1*). Of note, increased formation of lactate and NAD is a hallmark of aerobic glycolysis, a specific metabolic program that starts approximately 12 hr before the end of embryogenesis. Aerobic glycolysis enables hatched 1st instar larvae to efficiently convert dietary carbohydrates into biomass, thereby supporting the considerable increase in body mass that occurs during larval development (*Tennessen et al., 2014*). Inhibition of aerobic glycolysis in the course of this growth phase prevents the animals from metabolizing sufficient quantities of sugar, resulting in larval lethality (*Tennessen et al., 2011*). The fact that animals overexpressing Nep4A die primarily during the embryonic-larval transition and during larval development (*Figure 1A*) and exhibit considerably reduced lactate and NAD levels indicates that an excess of Nep4A may interfere with this distinct metabolic program. OPLS-DA loading plots summarizing the respective NMR spectral changes are depicted in *Figure 2C*.

Neprilysin 4 activity regulates food intake and insulin-like peptide expression

Given that the described metabolic abnormalities are indicative of an impaired energy metabolism, we analyzed whether modulating *nep4* expression affects feeding of corresponding animals. As depicted in *Figure 3A*, transgenes overexpressing the peptidase were characterized by considerably reduced food intake. After 10 min of feeding, the respective animals had ingested 47% less food than controls, after 20 min 59.5% less, and after 40 min 57% less, relative to controls. By contrast, *nep4* knockdown did not affect food intake after 40 min; however, corresponding animals were characterized by significantly reduced food intake after 10 min (47% of control intake) and 20 min (72% of control intake), indicating a delayed initiation of feeding. To investigate the possibility that the observed effects were caused by protein properties other than enzymatic activity, we also analyzed catalytically inactive Nep4A. Significantly, overexpression of this construct did not affect food intake, thus confirming abnormal catalytic activity as a causative factor (*Figure 3A*).

Since the increased glucose levels that are evident in Nep4A overexpression animals (*Figure 2B, C*) are symptomatic of impaired insulin signaling (*Broughton et al., 2005*; *Rulifson et al., 2002*), in a continuative set of experiments we analyzed whether altering *nep4* levels also affected the expression of *Drosophila* insulin-like peptides (*dilps*). We focused on *dilps 1, 2, 3*, and *5* because they encode the major insulin-like peptides expressed by larval insulin-producing cells (IPCs) (*Rulifson et al., 2002*; *Brogiolo et al., 2001*; *Cao and Brown, 2001*; *Ikeya et al., 2002*; *Lee et al., 2008*; *Nässel et al., 2013*). IPCs are located within the median neurosecretory cell cluster of the central brain and apparently function like pancreatic β-cells, since IPC ablation in *Drosophila* results in elevated levels of circulating glucose. In addition, animals with ablated IPCs are smaller than wild-type specimens, and they weigh less (*Broughton et al., 2005*; *Rulifson et al., 2002*). Significantly, these characteristic effects of IPC ablation were phenocopied by muscle-specific Nep4A overexpression (*Figures 1* and *2*). Furthermore, the respective transgenic animals exhibited considerably reduced expression of the selected *dilps*. In Nep4A-overexpressing animals, *dilp1* expression decreased by 59%, *dilp2* by 83%, *dilp3* expression by 88%, and *dilp5* expression by 84%, relative to expression in controls. On the other hand, muscle-specific *nep4* knockdown had no effect on the
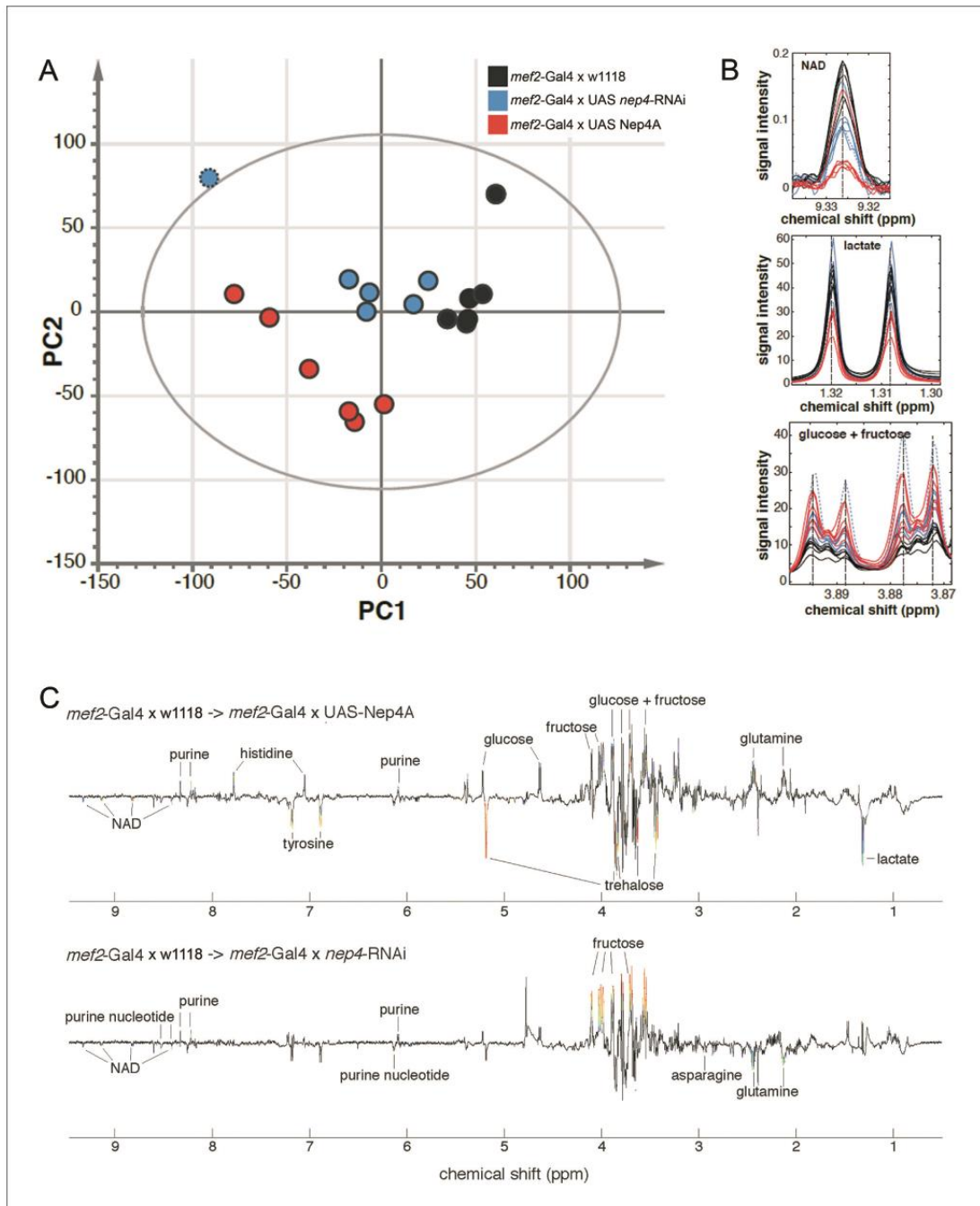
Figure 2. Muscle-specific modulation of *nep4* expression affects the metabolite composition in transgenic third instar larvae. (**A**) Score plot based on genotype-specific NMR spectra. PCA score plot showing the scores of six biological replicates for each genotype. Principal component analysis (PCA) was applied to identify metabolite changes in response to muscle-specific Nep4A overexpression (*mef2*-Gal4 x UAS-Nep4A; red) or knockdown (*mef2*-Gal4 x UAS *nep4*-RNAi; blue), relative to control animals (*mef2*-Gal4 x w1118; black). The score plot reveals genotype-specific clustering and thus
Figure 2 continued on next page

Figure 2 continued

distinct metabolite compositions in corresponding animals. One *nep4* knockdown sample was distinctly different from the other five. The outlier is marked by a dotted border and was excluded from OPLS-DA identification of significantly affected metabolites. (**B**) Examples of NMR signals from significantly affected metabolites. Evaluation of the dataset revealed that Nep4A overexpression significantly reduced NAD and lactate concentrations, while glucose and fructose levels were elevated in the same animals. The effects of *nep4* knockdown were less severe; NAD was reduced, and fructose was slightly elevated, compared to levels in control animals. The coloring is the same as in A. The knockdown outlier is marked by a dotted line. (**C**) OPLS-DA loading plots summarizing the NMR spectral changes induced by *nep4* overexpression and knockdown. Depicted is an overview of the metabolomic changes induced by modifying the expression of *nep4*. Positive and negative signals represent increases and decreases in metabolite concentrations, respectively. Significant alterations are color-coded from blue to red. Red represents the highest correlation between metabolite and genotype.

DOI: 10.7554/eLife.19430.006

The following source data and figure supplement are available for figure 2:

Source data 1. Chemical shifts and detected changes of significantly affected metabolites.
DOI: 10.7554/eLife.19430.007

Figure supplement 1. NMR-spectra of glucose and fructose.
DOI: 10.7554/eLife.19430.008

---

expression of *dilps 1, 3,* and *5*, although expression of *dilp2* increased by 82%, relative to expression in controls (*Figure 3B*). The rather mild effect of *nep4* knockdown on *dilp* expression, when compared to the effects of Nep4A overexpression, suggests that other, yet unknown peptidases can compensate for reduced Nep4 activity. In line with the results from the feeding assay (*Figure 3A*), *dilp* expression is only affected by the wild type enzyme, while overexpression of catalytically inactive Nep4A did not significantly alter expression of the selected *dilps* (*Figure 3B*).

To determine if expression of insulin-like peptides is regulated exclusively by muscle-derived Nep4 or if intrinsic CNS signaling is also involved, we altered *nep4* expression in a nervous-system-specific manner. As depicted in *Figure 3—figure supplement 1*, glial-cell-specific overexpression of Nep4A increased the expression of *dilp5*, while *nep4* knockdown in the same cells resulted in an upregulation of *dilp2* and downregulation of *dilp3*. Although these effects were minor compared to the effects of modulating the expression of muscle-bound Nep4 (*Figure 3B*), they demonstrate that proper regulation of *dilp* expression also requires adequate Nep4 levels within the CNS.

Neprilysin 4 localizes to the surface of larval body wall muscles and IPCs

In order to understand the physiological relation between *dilp* expression and Nep4 activity in more detail, we analyzed the expression pattern and the subcellular localization of the peptidase in larval body wall muscles and the larval CNS. As depicted in *Figure 4*, in body wall muscles Nep4 exhibits a dual localization: in addition to localizing to membranes continuous with the nuclear membrane (*Figure 4A*, arrowheads), which we previously identified as related to the sarco/endoplasmic reticulum (*Panz et al., 2012*), the peptidase accumulates at the surface of the muscles (*Figure 4A*, arrows). The latter localization is consistent with ectoenzymatic activity and indicative of a function in regulating the homeostasis of hemolymph circulating peptides. To confirm the specificity of the signal, we also stained the muscles of transgenic animals expressing *nep4*-specific RNAi (*mef2*-Gal4 driver). In these transgenic animals, no signal above background was observed (*Figure 4B*). In addition, staining wild-type muscles with secondary antibodies alone did not result in a distinct signal (*Figure 4C*). Of note, the proteins expressed from the two overexpression constructs (wild-type Nep4A and catalytically inactive Nep4A) exhibited subcellular localizations identical to that of the endogenous protein (*Figure 4A,D,F*), confirming that the observed overexpression phenotypes (*Figures 1–3*) were not impaired by mislocalization of the respective constructs. In order to distinguish the ectopic proteins from the endogenous protein, the ectopic constructs were fused to a C-terminal HA-tag and labeled with corresponding antibodies. Antibody specificity was confirmed by the lack of staining in animals expressing only the Gal4 transgene but not the UAS-construct (*Figure 4E,G*).

To characterize expression in the CNS, we employed a reporter line that expresses nuclear GFP (nGFP) in a manner that recapitulates endogenous *nep4* expression (*Meyer et al., 2009*). As shown in *Figure 5*, brain and ventral nerve cord tissue exhibited substantial reporter gene expression. With respect to the brain, expression was observed mainly in lamina (*Figure 5A*, brackets) and central

Figure 3. Muscle-specific modulation of *nep4* expression affects food intake and *dilp* expression in transgenic third instar larvae. (**A**) The genotype-specific rates of food intake are depicted as percentages (%) relative to the intake in control specimens (*mef2*-Gal4 x w1118) after 40 min of feeding, which was set to 100%. While *nep4* knockdown animals (*mef2*-Gal4 x UAS-*nep4* RNAi) exhibited reduced food intake after 10 and 20 min of feeding, Nep4A overexpression animals (*mef2*-Gal4 x UAS-Nep4A) were characterized by reduced intake throughout the whole measurement (up to 40 min). *Figure 3 continued on next page*

Figure 3 continued

Animals overexpressing catalytically inactive Nep4A (*mef2*-Gal4 x UAS-Nep4A$_{inact}$) did not exhibit any significant changes in food intake, when compared to controls. Values represent the mean (± s.d.) of at least six independent biological replicates. Asterisks indicate statistically significant deviations from controls (*p<0.05, one-way ANOVA with pairwise comparisons). The lower panel depicts representative images of the genotype-specific food intake at the indicated time points. (B) Changes in the expression of selected *dilp* genes are presented as percentages (%) relative to expression in control specimens (*mef2*-Gal4 x w1118), which was set to 100%. Muscle-specific overexpression of Nep4A (*mef2* x UAS-Nep4A) reduced the expression of every *dilp* gene analyzed, while *nep4* knockdown in the same tissue (*mef2* x *nep4*-RNAi) resulted in upregulation of *dilp2*. Animals overexpressing catalytically inactive Nep4A (*mef2* x UAS-Nep4A$_{inact}$) did not exhibit any significant changes in *dilp* expression, when compared to controls. Values represent the mean (+ s.d.) of at least three independent biological replicates, each consisting of at least three technical replicates. Asterisks indicate statistical significance (*p<0.1; **p<0.05, one-way ANOVA with pairwise comparisons); n.s. indicates 'not significant'.
DOI: 10.7554/eLife.19430.009

The following source data and figure supplement are available for figure 3:

Source data 1. Feeding assay.
DOI: 10.7554/eLife.19430.010
Figure supplement 1. Glial cell-specific modulation of *nep4* expression affects *dilp* expression in transgenic third instar larvae.
DOI: 10.7554/eLife.19430.011

brain cells (*Figure 5A*, dashed line), while only a few medulla cells exhibited a distinct signal (*Figure 5A*, bar). Within the ventral nerve cord, *nep4* was detected in numerous cells along all segments. As confirmed by extensive colocalization with the glial cell marker Reversed-polarity (Repo), *nep4* was expressed primarily in this cell type; however, especially in the median region of the central brain, only partial colocalization was evident. Thus, in addition to glial cells, *nep4* is expressed in certain neurons of the central brain (*Figure 5A-C*).

Interestingly, as confirmed by colocalization with *dilp2*-specific reporter gene expression, we found that these neurons included all IPCs, which reside within the median neurosecretory cell
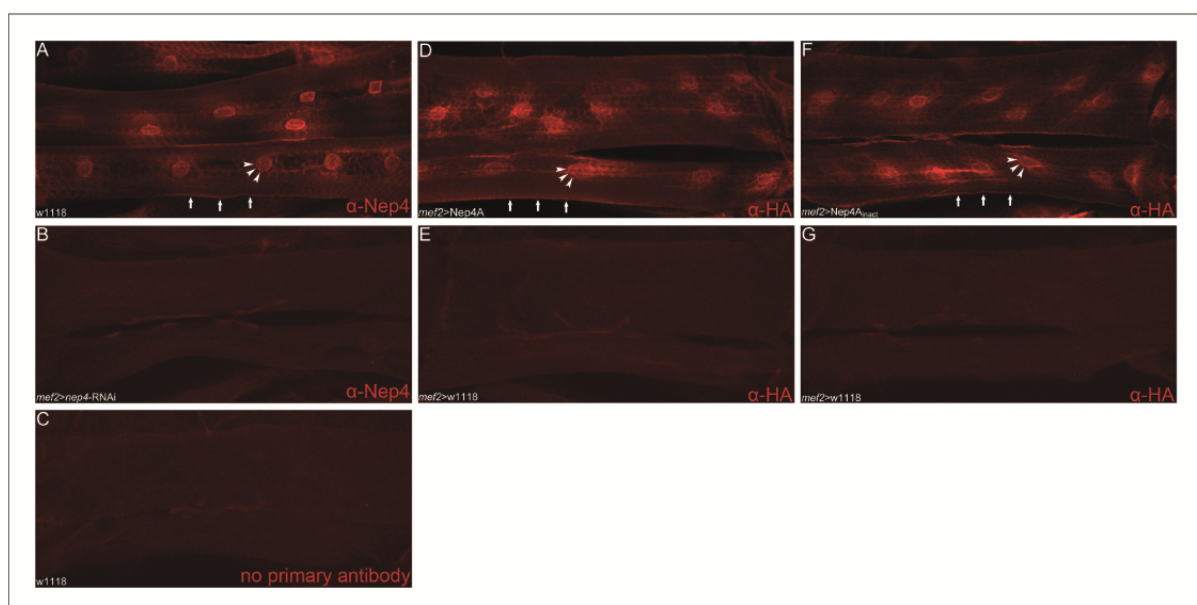
Figure 4. Nep4 localizes to the surface of muscle cells. (A) Nep4 protein was labeled with a monospecific antibody (red). In addition to membranes continuous with the nuclear membrane (arrowheads), Nep4 accumulated at the surface of body wall muscles (arrows). (D, F) Nep4 overexpression constructs (*mef2*>Nep4A, *mef2*>Nep4A$_{inact}$) exhibited subcellular localizations identical to that of the endogenous protein. The corresponding constructs were labeled with antibodies detecting the fused HA-tag. (B, C, E, G) Control stainings did not produce any signal above background.
DOI: 10.7554/eLife.19430.012
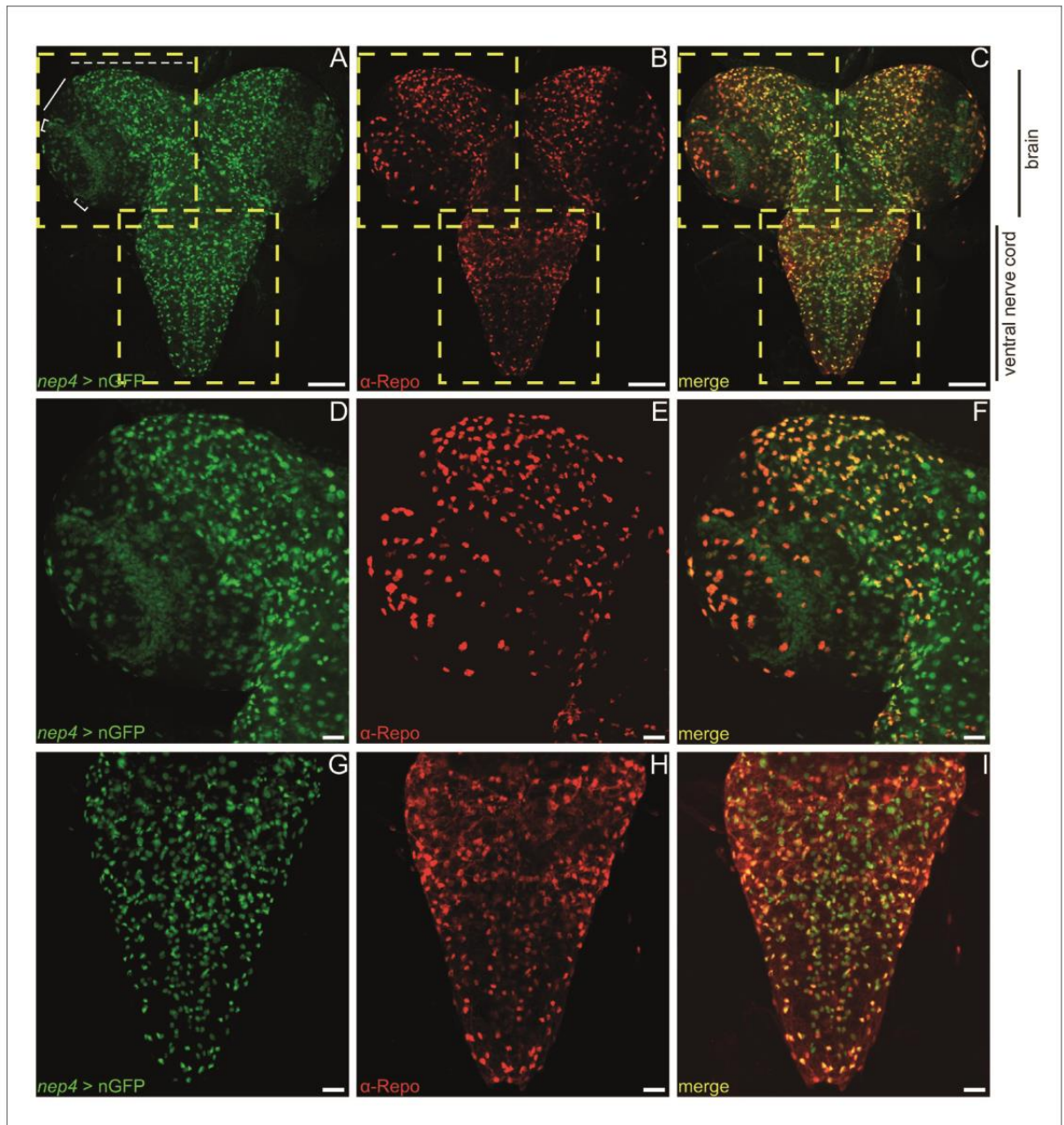
Figure 5. Nep4 is expressed in glial cells and neurons in the central nervous system. *nep4* expression was visualized using a reporter construct that drives nuclear GFP (nGFP) expression in a *nep4*-specific manner (*nep4* > nGFP, green). Reversed polarity protein was labeled with a monospecific antibody (α-Repo, red). (A–C) Optical projections of third instar larval whole brain-ventral nerve cord complexes. Scale bars: 100 μm; dorsal view, anterior up. Boxes indicate areas of higher magnification, as depicted in (D–F) and (G–I). Within the brain, *nep4* expression was strongest in the central brain (A, dashed line) and in lamina cells (A, brackets), while only few *nep4*-positive medulla cells were observed (A, bar). Within the ventral nerve cord,
Figure 5 continued on next page

Figure 5 continued

nep4 was expressed in numerous cells along all segments. (D–I) Optical projections of third instar larval brain hemisphere (D–F) and ventral nerve cord (G–I). Scale bars: 20 μm; dorsal view, anterior up, midline to right. *nep4* expression colocalized extensively with anti-Repo staining.

cluster of the brain hemispheres. The distinct localization of the respective signals is because both reporter constructs drive expression of a nuclear localized fluorophore (*Figure 6A–C*). To assess the subcellular localization of Nep4 in IPCs, we performed double labeling experiments using a reporter line expressing eGFP in a *dilp2*-specific manner, thus labeling the IPC cytoplasm, together with Nep4-specific antibodies. As depicted in *Figure 6D–F*, the peptidase accumulated at the surface of numerous cells of the central brain, including IPCs.

Neprilysin 4 efficiently hydrolyzes peptides that regulate *dilp* expression and feeding behavior

The fact that major phenotypes described in this study strictly depend on the catalytic activity of Nep4 (*Figures 1* and *3*) indicates that aberrant hydrolysis of peptides involved in regulating *dilp*
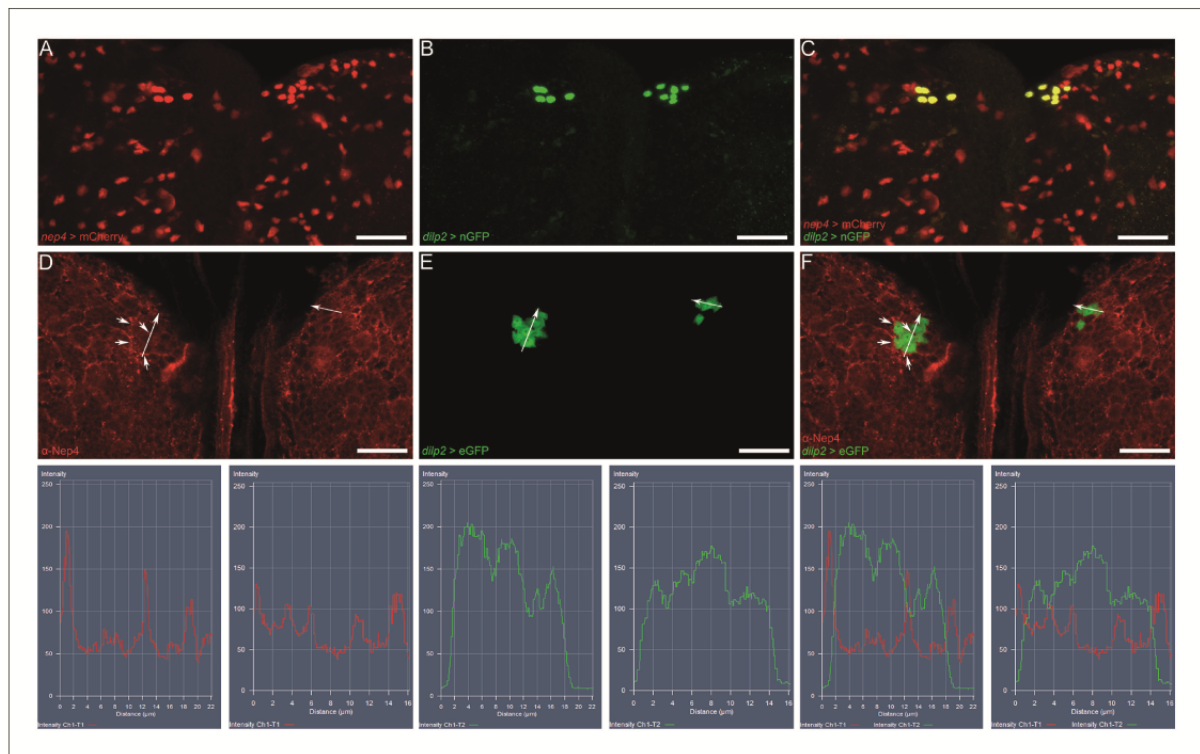
Figure 6. Nep4 localizes to the surface of insulin-producing cells. (A–C) *nep4* expression was assessed using a reporter line that drives nuclear mCherry expression in a *nep4*-specific manner (*nep4* > mCherry, red). *dilp2* expression was visualized using a reporter construct that drives nuclear GFP expression in a *dilp2*-specific manner (*dilp2* > nGFP, green). Depicted are optical sections (10 μm) of a third instar larval central brain. Scale bars: 20 μm; dorsal view, anterior up. *nep4* and *dilp2* expression colocalized in IPCs. (D–F) Nep4 protein was labeled with a monospecific antibody (red), and *dilp2* expression was visualized using an eGFP reporter line (*dilp2* > eGFP, green). Depicted are optical sections (10 μm) of a third instar larval central brain. Scale bars: 20 μm; dorsal view, anterior up. Nep4 accumulated at the surface of numerous cells, including IPCs (D, F, arrowheads). The subcellular localization was assessed with fluorescence intensity measurements (lower panel). The respective regions of evaluation are marked (arrows in D–F).

expression and / or feeding behavior is primarily responsible for the phenotypes. This indication is corroborated by the localization of Nep4 to the surface of body wall muscles and IPCs (*Figures 4 and 6*), with the latter constituting the major site of Dilp synthesis in *Drosophila* (*Rulifson et al., 2002*; *Brogiolo et al., 2001*; *Ikeya et al., 2002*). In order to identify the causative hydrolysis event (s), we analyzed every peptide known to be involved in regulating *dilp* expression, feeding behavior, or both (*Nässel et al., 2013*; *Pool and Scott, 2014*) for susceptibility to Nep4-mediated cleavage. The only additional prerequisite for consideration as a potential substrate was a size of less than 5 kDa, which for steric reasons represents the maximum mass of a neprilysin substrate (*Oefner et al., 2000*). As depicted in *Table 1*, we found 23 peptides matching these criteria. Among these candidates, 16 were hydrolyzed at distinct positions by purified Nep4, while the remaining seven peptides were not significantly cleaved. The identified substrates were adipokinetic hormone (AKH), allatostatin A1-4, corazonin, diuretic hormone 31 (DH_{31}), drosulfakinins 1 and 2, leucokinin, short neuropeptide $F1_{1–11}$, short neuropeptide $F1_{4–11}$ (also corresponding to $sNPF2_{12–19}$), and tachykinins 1, 2, 4, and 5. No Nep4-specific cleavage was observed for hugin, neuropeptide F, proctolin, short neuropeptide F3, short neuropeptide F4, and tachykinins 3 and 6. Analysis of the resulting hydrolysis products revealed that Nep4 preferentially cleaved next to hydrophobic residues, particularly with Phe or Leu at P1′ (*Table 1*). Identically treated control preparations lacking the peptidase did not exhibit any cleavage activity (*Figure 7*). Individual MS chromatograms are depicted in *Figure 7*. Nep4B purity was confirmed with SDS-PAGE (*Figure 7—figure supplement 1*).

Discussion

While the functional roles of insulin-like peptides (ILPs) and the corresponding insulin- and IGF-signaling have been intensively studied, the control of ILP production and release is not well understood. This study demonstrates that modulating the expression of a *Drosophila* neprilysin interferes with the expression of insulin-like peptides, thus establishing a correlation between neprilysin activity and the regulation of insulin signaling. A high physiological relevance is confirmed by the fact that altering *nep4* expression phenocopies characteristic effects of IPC ablation, including reduced size and weight of corresponding animals, as well as increased levels of carbohydrates such as glucose and fructose (*Figures 1* and *2*). The result that the levels of these sugars are increased, although food intake rates are reduced (*Figure 3A*) presumably reflects the physiological impact of the diminished *ilp* expression that is also obvious in corresponding animals (*Figure 3B*). In this respect, the impaired insulin signaling likely results in inefficient metabolization and thus accumulation of the sugars, which overcompensates the diametrical effects of reduced food intake. By identifying 16 novel peptide substrates of Nep4, the majority of which are involved in regulating *dilp* expression or feeding behavior (*Table 1*, *Figure 7*), and by localizing the peptidase to the surface of body wall muscles (*Figure 4*) and IPCs within the larval CNS (*Figure 6*), we provide initial evidence that neprilysin-mediated hydrolysis of hemolymph circulating as well as CNS intrinsic peptides is the physiological basis of the described phenotypes. The finding that only the catalytically active enzyme affected *dilp* expression whereas the inactive construct did not (*Figure 3B*), substantiates this evidence because it confirms aberrant enzymatic activity and thus abnormal peptide hydrolysis as a causative parameter. Interestingly, we observed the strongest effects on size and *dilp* expression with muscle-specific overexpression of Nep4; overexpression of the peptidase in the CNS was less detrimental (*Figure 1*, *Figure 3B*, *Figure 3—figure supplement 1*). These results indicate that hemolymph circulating peptides accessible to muscle-bound Nep4 are mainly responsible for the observed effects, while CNS intrinsic peptide signaling is less relevant. The fact that all peptides cleaved by Nep4 (*Table 1*) could be released into the hemolymph, either from enteroendocrine cells or from neurohormonal release sites (*Nässel and Winther, 2010*), substantiates this indication. Since the *Drosophila* midgut is the source of several neuropeptides (*Veenstra et al., 2008*; *Reiher et al., 2011*), it is conceivable that a main reason for the observed phenotypes is aberrant cleavage of certain gut-derived peptides that are required for proper midgut-IPC communication. Allatostatin A, neuropeptide F, diuretic hormone 31, and some tachykinins are produced by endocrine cells of the gut (*Veenstra et al., 2008*; *Reiher et al., 2011*; *Lenz et al., 2001*). Interestingly, all have been implicated in regulating *dilp* expression and/or feeding behavior (*Nässel et al., 2013*; *Pool and Scott, 2014*), and most of them, namely allatostatin A1-4, diuretic hormone 31, and tachykinin 1, 2, 4, and 5, were cleaved by Nep4 (*Table 1*), indicating enzyme-substrate relationships. Thus, these results suggest that Nep4 activity

eLIFE Research article

Table 1. Nep4 hydrolyzes peptides that regulate *dilp* expression or food intake.

Candidate peptides were analyzed for Nep4-specific cleavage. The individual molecular masses of full length peptides and cleavage products are depicted as the monoisotopic value. Cleavage positions and deviations from the respective theoretical masses (Δ) are shown separately. Cleaved peptides are highlighted in blue, and non-cleaved peptides are depicted in red. Superscripts indicate the studies that biochemically characterized the respective peptides ([1](*Baggerman et al., 2005*), [2](*Wegener et al., 2006*), [3](*Wegener and Gorbashov, 2008*), [4](*Predel et al., 2004*), [5](*Yew et al., 2009*)). n.d. indicates 'not detected', thus the respective sequences represent genomic data based predictions.

Name	Sequence	Mass (Da)	Δ(Da)	Sequence of cleavage products	Mass (Da)	Δ(Da)	Cleavage position
Allatostatin A1	VERYAFGLa[4]	953.5	−0.0676	VERYAFG	840.4	−0.0893	G/L
				VERYAF	783.4	−0.0898	F/G
Allatostatin A2	LPVYNFGLa[5]	920.5	−0.0205	LPVYNFG	808.4	−0.0492	G/L
				LPVYNF	751.4	−0.0148	F/G
				LPVYN	604.3	−0.0223	N/F
Allatostatin A3	SRPYSFGLa[1, 4]	924.5	−0.0523	YSFGLa	584.3	−0.0241	P/Y
Allatostatin A4	TTRPQPFNFGLa[1, 4, 5]	1275.7	−0.0629	TTRPQPFNFG	1163.6	−0.0850	G/L
				TTRPQPFN	959.5	−0.0790	N/F
				FNFGLa	595.3	−0.0301	P/F
AKH	QLTFSPDWa[1, 2, 3, 4]	992.5	0.0051	TFSPDWa	750.3	−0.0360	L/T
				FSPDWa	649.3	−0.0473	T/F
Corazonin	QTFQYSRGWTNa[1, 2, 3, 4, 5]	1385.6	−0.0582	FQYSRGWTNa	1156.5	−0.0319	T/F
				QTFQYSRG	985.5	−0.0743	G/W
DH$_{31}$	TVDFGLARGYSGTQ-EAKHRMGLAAANFA-GGPa[n.d.]	3149.5	−0.0814	YSGTQEAKHRMG	1363.6	−0.1761	G/Y; G/L
				TVDFGLARG	934.5	−0.0198	G/Y
Drosulfakinin 1	FDDYGHMRFa[1, 4, 5]	1185.5	−0.0572	FDDYGHMR	1039.4	−0.1147	R/F
Drosulfakinin 2	GGDDQFDDYGHMRFa[1, 4, 5]	1657.7	−0.0298	GGDDQFDDYGHMR	1511.6	−0.1201	R/F
				FDDYGHMRFa	1185.5	−0.0711	Q/F
Leucokinin	NSVVLGKKQRFHSWGa[1, 3, 4, 5]	1741.0	−0.0905	NSVVLGKKQRFHS	1498.3	−0.1474	S/W
				NSVVLGKKQRFH	1411.8	−0.1094	H/S
				NSVVLGKKQR	1127.7	−0.1121	R/F
				FHSWGa	631.3	−0.0100	R/F
sNPF1$_{1-11}$	AQRSPSLRLRFa[2, 3, 4]	1328.8	−0.0520	AQRSPSLRL	1026.6	−0.0962	L/R
sNPF1$_{4-11}$/ sNPF2$_{12-19}$	SPSLRLRFa[1, 2, 3, 4, 5]	973.6	−0.0859	SPSLRL	827.5	−0.1543	R/F
				LRLRFa	702.5	−0.1451	S/L
Tachykinin 1	APTSSFIGMRa[1, 4]	1064.5	−0.0579	APTSSFIG	778.4	−0.0434	G/M
				FIGMRa	621.3	−0.0706	S/F
Tachykinin 2	APLAFVGLRa[1, 5]	941.6	−0.0396	LAFVGLRa	773.5	−0.0858	P/L
				APLAFVG	673.4	−0.0202	G/L
				FVGLRa	589.4	−0.0686	A/F
				APLAF	517.3	−0.0183	F/V
Tachykinin 4	APVNSFVGMRa[1, 4, 5]	1075.6	−0.0742	APVNSFVG	789.4	−0.0314	G/M
Tachykinin 5	APNGFLGMRa[1, 5]	960.5	0.0231	FLGMRa	621.3	−0.0666	G/F
Hugin	SVPFKPRLa[1, 2, 3, 4, 5]	941.6	−0.0776				
NPF	SNSRPPRKNDVNTMA-DAYKFLQDLDTYYGD-RARVRFa[n.d.]	4278.2	0.50				
Proctolin	RYLPT[n.d.]	648.4	−0.0841				
sNPF3	KPQRLRWa[5]	981.6	−0.05				
sNPF4	KPMRLRWa[5]	984.6	−0.05				
Tachykinin 3	APTGFTGMRa[1]	935.5	−0.0733				
Tachykinin 6	AALSDSYDLRGKQQR-FADFNSKFVAVRa[n.d.]	3087.6	−0.1694				

DOI: 10.7554/eLife.19430.017
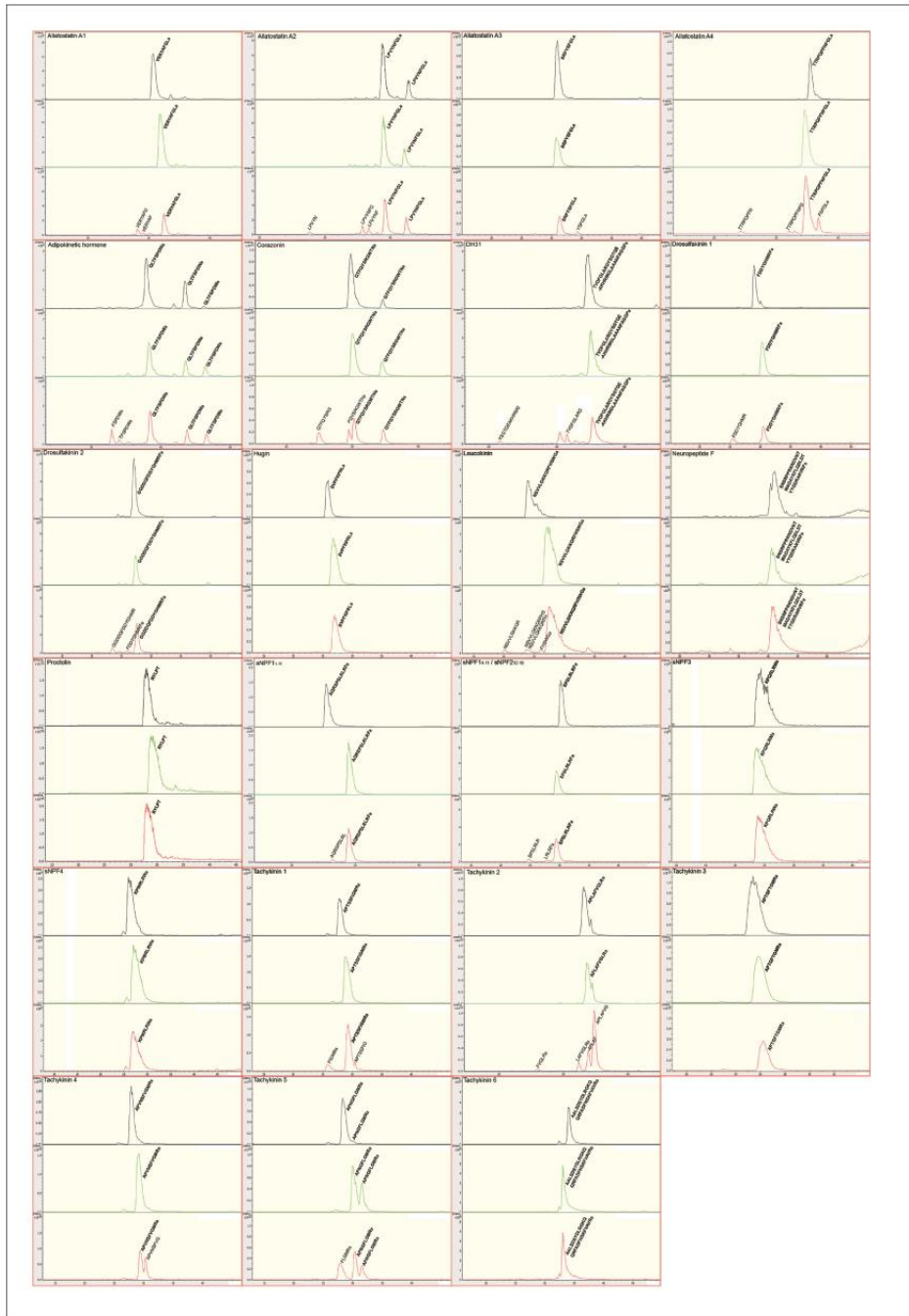
Figure 7. Nep4 catalyzes the hydrolysis of peptides that regulate *dilp* expression or feeding behavior. Base peak all MS chromatograms of analyzed peptides. The respective sequences of unprocessed full-length peptides (bold) and of identified Nep4-specific cleavage products are indicated. Unlabeled peaks were not identified. Spectra corresponding to untreated peptides are indicated in black, spectra corresponding to peptides incubated

Figure 7 continued on next page

Figure 7 continued

with control preparations lacking Nep4B are indicated in green, and spectra corresponding to peptides incubated with Nep4B-containing preparations are indicated in red. X-axes depict retention time (min).

The following figure supplement is available for figure 7:

Figure supplement 1. Heterologously expressed Nep4B can be purified to homogeneity.

at the surface of muscle cells is necessary to maintain homeostasis of distinct hemolymph circulating signaling peptides, probably gut-derived, thereby ensuring proper midgut-IPC communication. On the other hand, fat body-IPC feedback may be affected as well. However, the only factors known to mediate this process, Unpaired 2 (*Rajan and Perrimon, 2012*), DILP6 (*Bai et al., 2012*), and Stunted (*Delanoue et al., 2016*) have molecular masses of more than 5 kDa, and thus exceed the maximum mass of a putative neprilysin substrate (*Oefner et al., 2000*). Consequently, a direct regulatory influence of Nep4 on Unpaired 2, DILP6, or Stunted activity appears unlikely.

In addition to body wall muscles, *nep4* is expressed in numerous cells of the central nervous system, predominantly in glial cells (*Figure 5*). Interestingly, compared to the muscle-specific effects, modulating *nep4* expression in this tissue has distinct and less severe effects on *dilp* expression (*Figure 3B*, *Figure 3—figure supplement 1*). This result suggests that CNS intrinsic Nep4 activity affects different neuropeptide regulatory systems than the corresponding muscle-bound activity. Considering the rather broad expression in glial cells, it is furthermore likely that the CNS regulation affects more than one system. However, localization at the IPC surface (*Figure 6*) clearly supports a direct function in the regulation of *dilp* expression. In this context, spatial proximity of the peptidase may be necessary to ensure low ligand concentrations and thus tight regulation of specific neuropeptide receptors present at the surface of IPCs. Such receptors include an allatostatin A receptor (Dar-2) (*Hentze et al., 2015*), a tachykinin receptor (DTKR) (*Birse et al., 2011*), and the short neuropeptide F receptor (sNPFR) (*Lee et al., 2008*). All are essential to proper *dilp* expression (*Lee et al., 2008*; *Hentze et al., 2015*; *Birse et al., 2011*). Interestingly, with respect to sNPFR, corresponding ligands (sNPF1$_{1-11}$, sNPF1$_{4-11}$, and sNPF2$_{12-19}$) exhibit very high-binding affinities, with IC$_{50}$ values in the low nanomolar range (*Garczynski et al., 2006*), a finding that further emphasizes the need for effective ligand clearance mechanisms in order to prevent inadvertent receptor activation. Localization of Nep4 to the surface of IPCs (*Figure 6*) and confirmation of Dar-2, DTKR, and sNPFR ligands as substrates of the peptidase (*Table 1*, *Figure 7*) strongly indicate that Nep4 participates in such clearance mechanisms.

Of note, sNPF species were detected in both, CNS and hemolymph preparations, with neuroendocrine functions of the respective peptides being suggested (*Veenstra et al., 2008*; *Garczynski et al., 2006*; *Baggerman et al., 2005*; *Wegener and Gorbashov, 2008*; *Wegener et al., 2006*). The dual localization is interesting because both compartments are accessible to Nep4, either to the CNS resident or to the muscle-bound enzyme. Significantly, sNPF is a potent regulator of *dilp* expression. Increased sNPF levels result in upregulation of *dilp* expression, and decreased sNPF levels have the opposite effect (*Lee et al., 2008*). The fact that these results inversely correlate with the effects of modulating *nep4* expression (*Figure 3*) suggests a functional relationship between sNPF and the neprilysin. Nep4-mediated cleavage of distinct sNPF species (*Table 1*, *Figure 7*) represents further evidence for this relationship.

Besides sNPF, Nep4 also cleaves corazonin, drosulfakinins, and allatostatin A (*Table 1*, *Figure 7*). Interestingly, corazonin promotes food intake (*Hergarden et al., 2012*), while allatostatin A and drosulfakinins inhibit it (*Hergarden et al., 2012*; *Söderberg et al., 2012*; *Chen et al., 2016*). This regulatory activity on peptides with opposing physiological functions indicates that Nep4 affects multiple aspects of feeding control, rather than promoting or inhibiting food intake in a mutually exclusive manner. Our finding that both, *nep4* knockdown and overexpression larvae exhibit reduced food intake (*Figure 3A*) supports this indication since it suggests that regular Nep4 activity adjusts the general peptide homeostasis in a manner that promotes optimal food intake, with deviations in either direction being deteriorative. The result that *nep4* knockdown animals exhibit reduced food intake for only up to 20 min of feeding (*Figure 3A*) may reflect this complex regulation since it indicates that at the onset of feeding reduced cleavage of peptides inhibiting food intake (e.g.

allatostatin A, drosulfakinins) is a dominant factor. With ongoing feeding, accumulation of peptides promoting food intake (e.g. corazonin) may become decisive, thus restoring intake rates.

In addition, Nep4 hydrolyzes numerous peptides that regulate *dilp* expression, including tachykinins, allatostatin A, and sNPF. However, AKH, a functional homolog of vertebrate glucagon that acts antagonistically to insulin, is also a substrate of Nep4 (*Table 1*, *Figure 7*). This finding indicates that the Nep4-mediated regulation of *dilp* expression and sugar homeostasis can also not be attributed to a single substrate or cleavage event. Rather, it is a result of the concerted hydrolysis of several critical peptides, including both, hemolymph circulating and CNS intrinsic factors. Taking into account that overexpression and knockdown of *nep4* have discrete effects on *dilp* expression (*Figure 3B*), but comparable effects on feeding (*Figure 3A*), it furthermore appears likely that dysregulation of the Nep4-mediated peptide homeostasis affects both processes somewhat independently of each other. The fact that among the novel Nep4 substrates we identified peptides that presumably affect either *dilp* signaling (e.g. DH$_{31}$), or food intake (e.g. leucokinin, drosulfakinins) in a largely exclusive manner supports this indication.

Because neprilysins and many of the novel substrates identified in this study are evolutionarily conserved factors, neprilysin-mediated regulation of insulin-like peptide expression and feeding behavior may be relevant not only to the energy metabolism in *Drosophila*, but also to corresponding processes in vertebrates, including humans. Interestingly, a critical function of murine Neprilysin in determining body mass has already been reported. The regulation depended primarily on the catalytic activity of peripheral NEP, while the CNS-bound enzyme was less important (*Becker et al., 2010*). However, until now, the underlying physiology has been obscure, essentially because no causative hydrolysis event had been identified. Our finding that also in *Drosophila* mainly peripheral (muscle-bound) Nep4 activity affected body mass, while CNS-specific modulations had only minor effects on size or weight (*Figure 1*), indicates that the neprilysin-mediated regulation of food intake, body size and insulin expression involves similar physiological pathways in both species. Furthermore, the fact that altered catalytic activity and thus abnormal peptide hydrolysis is a critical factor in mice (*Becker et al., 2010*) and in *Drosophila* (*Figures 1* and *3*) emphasizes the need to generate comprehensive, enzyme-specific lists of neprilysin *in vivo* substrates. In this context, the results of our screen for novel Nep4 substrates (*Table 1*, *Figure 7*) may be a valuable resource in order to identify corresponding substrates in vertebrates and humans.

Materials and methods

Fly strains

The following *Drosophila* lines were used in this work. Strain w1118 (RRID:BDSC_5905) was considered wild type. The driver lines were *mef2*-Gal4 (RRID:BDSC_27390), *repo*-Gal4 (RRID:BDSC_7415), *elav*-Gal4 (RRID:BDSC_8760), and *dilp2*-Gal4 (RRID:BDSC_37516). UAS-lines were UAS-mCherry.NLS (RRID:BDSC_38424) and UAS-2xEGFP (RRID:BDSC_6874). The *nep4*-nGFP reporter line was described previously (*Meyer et al., 2009*). *nep4* knockdown was achieved using line 100189 (KK library, no off-targets, Vienna *Drosophila* Resource Center, VDRC). A high knockdown efficiency of the respective construct was shown previously (*Panz et al., 2012*). To confirm specificity of the knockdown, a line being homozygous for both, the UAS-*nep4* RNAi construct (chromosome II) and the UAS-Nep4A overexpression construct (chromosome III) was generated and crossed to either *mef2*-Gal4 or *repo*-Gal4. Tissue-specific rescue of the respective RNAi phenotypes by simultaneous overexpression of Nep4A was used as readout for knockdown specificity. A second *nep4* RNAi construct (line 16669, GD library, VDRC) did not significantly reduce *nep4* transcript levels (*Panz et al., 2012*). It was therefore excluded from further analysis.

Size and weight measurements

Staged (AEL 74–78 hr) male third instar larvae where grouped into genotype-specific cohorts of 10 individuals. The weights of at least five cohorts per genotype were averaged to calculate the mean weight of one respective larva. For size measurements, larvae where exposed to 60°C water for 10 s, resulting in maximum relaxation of the body. Subsequently, animals where photographed on scale paper using a stereomicroscope (Leica MZ16 FA), and individual lengths were calculated with the Adobe Photoshop CS5 measure tool using the scale paper as a reference.

Lethality assay

Animals of different genotypes were raised at 27 °C on apple agar plates supplemented with excess yeast paste. Stage-specific lethality rates were determined by calculating the percentage of animals of a specific stage that did not develop into the next stage. For each genotype and biological replicate, 550 embryos were analyzed. Three independent biological replicates were conducted.

Feeding assay

Staged (AEL 74–78 hr) male third instar larvae were starved for 1 hr. Subsequently, animals were fed with dyed yeast (0.3 mg Carmin, 4 mg dry yeast, dissolved in 10 ml H_2O) for 5, 10, 20, or 40 min, respectively, washed, and photographed (Stemi 2000-C, Zeiss, Jena, Germany). Dye intensities (no. of detected pixels) within the intestines were determined with Fiji software (http://fiji.sc/). At least six individuals per genotype and time point were analyzed.

NMR metabolomics

Staged (AEL 74–78 hr) male third instar larvae where grouped into genotype-specific cohorts, and six cohorts per genotype were independently analyzed to assess metabolite composition. Briefly, animals (50 mg/cohort) were homogenized (glass-Teflon homogenizer) in 500 µl ice-cold ACN/H_2O (50%) and centrifuged (10,000 × g, 10 min) to remove fly debris and precipitate. The resulting supernatant was lyophilized and frozen at −80°C for later use. Samples were rehydrated in 650 µl of 50 mM phosphate buffer in D_2O (pH 7.4) containing 50 mg/l 3-trimethylsilyl propionic acid D_4 (TSP) as a chemical shift reference and 50 mg/l sodium azide to prevent bacterial growth. The NMR measurements were carried out at 25 °C on a Bruker Avance-III 600 spectrometer (Bruker Biospin, Germany) equipped with a double tuned ^1H-^{13}C 5 mm cryoprobe and operated at a ^1H frequency of 600.13 MHz. The ^1H NMR spectra were acquired using a single 90° pulse experiment with a Carr Purcell Meiboom Gill (CPMG) delay added, in order to attenuate broad signals from high molecular weight components. The total CPMG delay was 40 ms, and the spin echo delay was 200 µs. The water signal was suppressed by pre-saturation of the water peak during the relaxation delay of 4 s. A total of 96k data points spanning a spectral width of 20 ppm were collected in 128 transients. For assignment purposes, two-dimensional ^1H-^1H TOCSY and ^1H-^{13}C HSQC spectra were acquired. The spectra were processed using iNMR (www.inmr.net). An exponential line broadening of 0.5 Hz was applied to the free induction decay, prior to Fourier transformation. All spectra were referenced to the TSP signal at −0.017 ppm, automatically phased and baseline corrected. The spectra were aligned using Icoshift (*Savorani et al., 2010*), and the region around the residual water signal (4.88–4.67 ppm) was removed. The integrals were normalized to total weight, and the data were scaled using pareto scaling (*Craig et al., 2006*) and centered.

NMR data analysis

Initially, the whole dataset was subjected to principal component analysis (PCA) (*Stoyanova and Brown, 2001*). Afterwards, orthogonal projection to latent structures discriminant analysis (OPLS-DA) models were created to separate either larvae overexpressing *nep4* from control larvae or *nep4* knockdowns from control larvae. OPLS-DA models are multivariate models that predict group membership based on a multivariate input, in this case the NMR spectra. The model separates variations due to group membership from other (orthogonal) variations (*Bylesjö et al., 2006*). The OPLS-DA models were validated by cross validation where models were made with randomly chosen groups of samples left out one at a time, and group membership was predicted for the left out samples. The predictability (Q^2) of the models, i.e. the correlation between predicted and actual classification, was 0.95 for the comparison between *mef2*-Gal4 x w1118 and *mef2*-Gal4 x UAS-Nep4A, and 0.74 for the comparison between *mef2*-Gal4 x w1118 and *mef2*-Gal4 x UAS *nep4*-RNAi, respectively, indicating high-quality models. The loadings and the correlation coefficient (R) between intensities at the individual frequencies and the predictive component were calculated. A cutoff value for R^2 corresponding to $p<0.05$ with Bonferroni correction for an assumed number of 100 metabolites was calculated from the distribution of R^2 values in 10,000 permutated data sets. Signal assignments were based on chemical shifts, using earlier assignments and spectral databases described elsewhere (*Cui et al., 2008*; *Malmendal et al., 2006*; *Pedersen et al., 2008*). All multivariate analysis was performed using the Simca-P software (Umetrics, Sweden).

Cell culture and enzymatic cleavage assay

Heterologous expression was performed in SF21 cells (RRID:CVCL_0518) using the Bac-to-Bac baculovirus expression system (Life Technologies, Carlsbad, CA, USA). The *nep4B* coding sequence was fused to a C-terminal His-tag using appropriate primer design and cloned downstream of the polyhedrin promoter into an *E.coli/S.cerevisiae*/Baculovirus triple-shuttle derivative of the pFastBac Dual vector adapted for cloning by homologous recombination *in vivo*. The respective vector (pJJH1460) was constructed similar to the vectors described in (*Paululat and Heinisch, 2012*). To track transfection efficiency, an *egfp* reporter gene was inserted into the same vector under the control of the p10 promoter. Transfected and non-transfected SF21 cells were cultured in 75-cm^2 flasks for 72 hr and harvested by centrifugation (300 $\times$ g, 5 min). Subsequently, cells were resuspended in 5 ml binding buffer (50 mM NaH$_2$PO$_4$, pH 7.9; 300 mM NaCl) and lysed with a glass-Teflon homogenizer. The resulting homogenates were centrifuged (10 min, 10,000 $\times$ g), and the supernatants were subjected to gravity-flow-based His-tag purification according to the manufacturer's instructions (Protino Ni-NTA agarose, Macherey-Nagel, Düren, Germany). To measure enzymatic activity, 2.5 µl of Nep4B-containing (10 ng/µl, purified from *nep4B* transfected cells) and non-containing (from untransfected control cells) preparations were supplemented with 3.5 µl (150 ng) of individual peptides. After 5 hr of incubation (35°C), 1 µl of each respective preparation was analyzed with ESI mass spectrometry. Peptides were synthesized at JPT Peptide Technologies (Berlin, Germany) with more than 90% purity. Individual cleavage assays were repeated at least three times.

Mass spectrometry

Samples were loaded onto a trap column (Acclaim PepMap C18, 5 µm, 0.1 $\times$ 20 mm, Thermo Scientific, Sunnyvale, CA, USA) and washed. The trap column was switched inline with a separation column (Acclaim PepMap C18 2 µm, 0.075 $\times$ 150 mm, Thermo Scientific). Subsequently, bound substances were eluted by changing the mixture of buffer A (99% water, 1% acetonitrile, 0.1% formic acid) and buffer B (80% acetonitrile, 20% water and 0.1% formic acid) from 100:0 to 20:80 within 45 min. The flow rate was kept constant at 0.3 µl/min. Successively eluted compounds were analyzed with an ESI-ion trap (Amazon ETD Speed with a captive spray ionization unit, Bruker Corporation, Billerica, MA, USA) by measuring the masses of the intact molecules as well as the masses of the fragments, which were generated by collision-induced dissociation (CID) of the corresponding parent ion.

All acquired data were used for determination of peptide-specific amino acid sequences with the Mascot search algorithm (Matrix Science, Boston, MA, USA) in combination with a custom-made database containing 37 different sequences of peptides. To avoid an increased false-positive identification rate the p-value was lowered to 0.005 (resulting in an individual ion score > 18). As enzyme, the option 'none' was chosen. Thus, every subsequence of every protein was used for identification.

Immunohistochemistry

Brains prepared from staged male third instar larvae (AEL 74–78 hr) were fixed (3.7% formaldehyde, 1 hr) and permeabilized (1% Triton X-100, 1 hr). Subsequently, tissues were incubated in PBS containing 0.15% SDS (30 min), blocked with Roti-Block (Carl Roth, Karlsruhe, Germany) for 45 min, washed in PBT (4×, 10 min each), and incubated in Roti-Block (45 min) and primary antibody (overnight). Samples were washed in PBT (4×, 10 min each) and blocked again as described above. Secondary antibodies were applied simultaneously for 90 min. Finally, samples were washed as described above and mounted in Fluoromount-G (SouthernBiotech, Birmingham, USA). For staining of body wall muscles, male third instar larvae were dissected on Sylgard plates (Sylgard 184 Elastomer Base and Curing Agent, Dow Corning, Michigan, USA), fixed in 3.7% formaldehyde in PBS for 1 hr, rinsed three times in PBS, and transferred into 1.5 ml reaction cups. Subsequently, tissues were permeabilized in 1% Triton X-100 for 1 hr, blocked in Roti-Block (45 min), and incubated with primary antibodies (overnight). Samples were washed in PBT (3×, 10 min each) and blocked again as described above. Secondary antibodies were applied for 90 min. Finally, samples were washed as described above and mounted in Fluoromount-G (SouthernBiotech, Birmingham, USA). The primary antibodies used were: anti-Nep4 (RRID:AB_2569115, 1:200, raised in rabbit, monospecificity was confirmed in [*Meyer et al., 2009*]), anti-GFP (RRID:AB_889471, 1:500, raised in mouse), anti-GFP (RRID:AB_305564, 1:2000, raised in rabbit), anti-HA (RRID:AB_262051, 1:100, raised in mouse), and

anti-Repo (RRID:AB_528448, 1:5, raised in mouse). The secondary antibodies were anti-mouse-Cy2 (RRID:AB_2307343, 1:100, raised in goat), anti-mouse-Cy3 (RRID:AB_2338680, 1:200, raised in goat), anti-rabbit-Cy2 (RRID:AB_2338021, 1:100, raised in goat), and anti-rabbit-Cy3 (RRID:AB_2338000, 1:200, raised in goat). Confocal images were captured with an LSM5 Pascal confocal microscope (Zeiss, Jena, Germany). To exclude a possible bleed-through of the signals, sequential channel acquisition was performed starting with Cy3 channel by using single excitation at 543 nm and a long pass emission filter LP560, followed by Cy2 channel acquisition with single excitation at 488 nm and a single bandpass filter BP 505–530 nm. There was no bleed-through of the Cy2 signal to the Cy3 channel because Cy2 is not excited by the 543 nm laser line. Using a narrow bandpass filter between 505 nm and 530 nm guaranteed that cross talk of Cy3 excitation by the 488 laser line is not detected during Cy2 channel acquisition. Z-stacks are displayed as maximum projections if not stated otherwise.

qRT-PCR

Total-RNA (RNeasy Mini Kit, Qiagen, Hilden, Germany) from staged male third instar larvae (AEL 74–78 hr) was treated with DNase I (Invitrogen, Carlsbad, CA, USA) according to the manufacturer's instructions and used as a template for cDNA synthesis (AMV First Strand cDNA Synthesis Kit for RT-PCR, Roche). qRT-PCR was conducted according to standard protocols using DyNAmo ColorFlash SYBR Green qPCR Kit (Biozym, Hessisch Oldendorf, Germany) and an iCycler iQ Real-Time PCR System (Bio-Rad, Munich, Germany). Data were evaluated as described in (*Simon, 2003*). All experiments were repeated at least three times (individual biological replicates, each consisting of at least three technical replicates). The sequences of primers used were as follows: *dilp1*, 5′-GGGGCAGGATACTCTTTTAG-3′ and 5′-TCGGTAGACAGTAGATGGCT-3′; *dilp2*, 5′-GTATGGTGTGCGAGGAGTAT-3′ and 5′-TGAGTACACCCCCAAGATAG-3′; *dilp3*, 5′-AAGCTCTGTGTGTATGGCTT-3′ and 5′-AGCACAATATCTCAGCACCT-3′; *dilp5*, 5′-AGTTCTCCTGTTCCTGATCC-3′ and 5′-CAGTGAGTTCATGTGGTGAG-3′; *rp49*, 5′-AGGGTATCGACAACAGAGTG-3′ and 5′-CACCAGGAACTTCTTGAATC-3′.

Statistics

Statistical analysis (one-way ANOVA with pairwise comparisons) was performed using OriginPro 8 software (OriginLab Corporation, Northampton, MA, USA).

Acknowledgements

Additional information

eLIFE Research article

Author contributions
BH, RS, SW, AM, Acquisition of data, Analysis and interpretation of data, Drafting or revising the article; EC, JV-F, Acquisition of data, Drafting or revising the article; JJH, AP, Analysis and interpretation of data, Drafting or revising the article; HM, Conception and design, Acquisition of data, Analysis and interpretation of data, Drafting or revising the article

Author ORCIDs
Heiko Meyer, http://orcid.org/0000-0002-3304-4523

References

Baggerman G, Boonen K, Verleyen P, De Loof A, Schoofs L. 2005. Peptidomic analysis of the larval *Drosophila melanogaster* central nervous system by two-dimensional capillary liquid chromatography quadrupole time-of-flight mass spectrometry. *Journal of Mass Spectrometry* **40**:250–260. doi: 10.1002/jms.744, PMID: 15706625

Bai H, Kang P, Tatar M. 2012. *Drosophila* insulin-like peptide-6 (dilp6) expression from fat body extends lifespan and represses secretion of *Drosophila* insulin-like peptide-2 from the brain. *Aging Cell* **11**:978–985. doi: 10.1111/acel.12000, PMID: 22935001

Becker M, Siems WE, Kluge R, Gembardt F, Schultheiss HP, Schirner M, Walther T. 2010. New function for an old enzyme: NEP deficient mice develop late-onset obesity. *PLoS One* **5**:e12793. doi: 10.1371/journal.pone.0012793, PMID: 20862277

Belyaev ND, Nalivaeva NN, Makova NZ, Turner AJ. 2009. Neprilysin gene expression requires binding of the amyloid precursor protein intracellular domain to its promoter: implications for Alzheimer disease. *EMBO Reports* **10**:94–100. doi: 10.1038/embor.2008.222, PMID: 19057576

Birse RT, Söderberg JA, Luo J, Winther AM, Nässel DR. 2011. Regulation of insulin-producing cells in the adult *Drosophila* brain via the tachykinin peptide receptor DTKR. *Journal of Experimental Biology* **214**:4201–4208. doi: 10.1242/jeb.062091, PMID: 22116763

Blanchard FJ, Collins B, Cyran SA, Hancock DH, Taylor MV, Blau J. 2010. The transcription factor Mef2 is required for normal circadian behavior in *Drosophila*. *Journal of Neuroscience* **30**:5855–5865. doi: 10.1523/JNEUROSCI.2688-09.2010, PMID: 20427646

Bland ND, Robinson P, Thomas JE, Shirras AD, Turner AJ, Isaac RE. 2009. Locomotor and geotactic behavior of *Drosophila melanogaster* over-expressing neprilysin 2. *Peptides* **30**:571–574. doi: 10.1016/j.peptides.2008.10.020, PMID: 19038301

Bland ND, Thomas JE, Audsley N, Shirras AD, Turner AJ, Isaac RE. 2007. Expression of NEP2, a soluble neprilysin-like endopeptidase, during embryogenesis in *Drosophila melanogaster*. *Peptides* **28**:127–135. doi: 10.1016/j.peptides.2006.08.032, PMID: 17157960

Brogiolo W, Stocker H, Ikeya T, Rintelen F, Fernandez R, Hafen E. 2001. An evolutionarily conserved function of the *Drosophila* insulin receptor and insulin-like peptides in growth control. *Current Biology* **11**:213–221. doi: 10.1016/S0960-9822(01)00068-9, PMID: 11250149

Broughton SJ, Piper MDW, Ikeya T, Bass TM, Jacobson J, Driege Y, Martinez P, Hafen E, Withers DJ, Leevers SJ, Partridge L. 2005. Longer lifespan, altered metabolism, and stress resistance in *Drosophila* from ablation of cells making insulin-like ligands. *PNAS* **102**:3105–3110. doi: 10.1073/pnas.0405775102, PMID: 15708981

Bylesjö M, Rantalainen M, Cloarec O, Nicholson JK, Holmes E, Trygg J. 2006. OPLS discriminant analysis: combining the strengths of PLS-DA and SIMCA classification. *Journal of Chemometrics* **20**:341–351. doi: 10.1002/cem.1006

Cao C, Brown MR. 2001. Localization of an insulin-like peptide in brains of two flies. *Cell and Tissue Research* **304**:317–321. doi: 10.1007/s004410100367, PMID: 11396725

Chen J, Reiher W, Hermann-Luibl C, Sellami A, Cognigni P, Kondo S, Helfrich-Förster C, Veenstra JA, Wegener C. 2016. Allatostatin a signalling in *Drosophila* regulates feeding and sleep and is modulated by PDF. *PLOS Genetics* **12**:e1006346. doi: 10.1371/journal.pgen.1006346, PMID: 27689358

Craig A, Cloarec O, Holmes E, Nicholson JK, Lindon JC. 2006. Scaling and normalization effects in NMR spectroscopic metabonomic data sets. *Analytical Chemistry* **78**:2262–2267. doi: 10.1021/ac0519312, PMID: 16579606

Cui Q, Lewis IA, Hegeman AD, Anderson ME, Li J, Schulte CF, Westler WM, Eghbalnia HR, Sussman MR, Markley JL. 2008. Metabolite identification via the madison metabolomics consortium database. *Nature Biotechnology* **26**:162–164. doi: 10.1038/nbt0208-162, PMID: 18259166

Delanoue R, Meschi E, Agrawal N, Mauri A, Tsatskis Y, McNeill H, Léopold P. 2016. *Drosophila* insulin release is triggered by adipose Stunted ligand to brain Methuselah receptor. *Science* **353**:1553–1556. doi: 10.1126/science.aaf8430, PMID: 27708106

Garczynski SF, Brown MR, Crim JW. 2006. Structural studies of *Drosophila* short neuropeptide F: Occurrence and receptor binding activity. *Peptides* **27**:575–582. doi: 10.1016/j.peptides.2005.06.029, PMID: 16330127

Hentze JL, Carlsson MA, Kondo S, Nässel DR, Rewitz KF. 2015. The neuropeptide allatostatin a regulates metabolism and feeding decisions in *Drosophila*. *Scientific Reports* **5**:11680. doi: 10.1038/srep11680, PMID: 26123697

Hergarden AC, Tayler TD, Anderson DJ. 2012. Allatostatin-A neurons inhibit feeding behavior in adult *Drosophila*. *PNAS* **109**:3967–3972. doi: 10.1073/pnas.1200778109, PMID: 22345563

Ikeya T, Galic M, Belawat P, Nairz K, Hafen E. 2002. Nutrient-dependent expression of insulin-like peptides from neuroendocrine cells in the CNS contributes to growth regulation in *Drosophila*. *Current Biology* **12**:1293–1230. doi: 10.1016/S0960-9822(02)01043-6, PMID: 12176357

Isaac RE, Johnson EC, Audsley N, Shirras AD. 2007. Metabolic inactivation of the circadian transmitter, pigment dispersing factor (PDF), by neprilysin-like peptidases in *Drosophila*. *Journal of Experimental Biology* **210**:4465–4470. doi: 10.1242/jeb.012088, PMID: 18055635

Iwata N, Tsubuki S, Takaki Y, Watanabe K, Sekiguchi M, Hosoki E, Kawashima-Morishima M, Lee HJ, Hama E, Sekine-Aizawa Y, Saido TC. 2000. Identification of the major Abeta1-42-degrading catabolic pathway in brain parenchyma: suppression leads to biochemical and pathological deposition. *Nature Medicine* **6**:143–150. doi: 10.1038/72237, PMID: 10655101

Jessup M. 2014. Neprilysin inhibition–a novel therapy for heart failure. *The New England Journal of Medicine* **371**:1062–1064. doi: 10.1056/NEJMe1409898, PMID: 25176014

Lee KS, Kwon OY, Lee JH, Kwon K, Min KJ, Jung SA, Kim AK, You KH, Tatar M, Yu K. 2008. *Drosophila* short neuropeptide F signalling regulates growth by ERK-mediated insulin signalling. *Nature Cell Biology* **10**:468–475. doi: 10.1038/ncb1710, PMID: 18344986

Lenz C, Williamson M, Hansen GN, Grimmelikhuijzen CJ. 2001. Identification of four *Drosophila* allatostatins as the cognate ligands for the Drosophila orphan receptor DAR-2. *Biochemical and Biophysical Research Communications* **286**:1117–1122. doi: 10.1006/bbrc.2001.5475, PMID: 11527415

Malmendal A, Overgaard J, Bundy JG, Sørensen JG, Nielsen NC, Loeschcke V, Holmstrup M. 2006. Metabolomic profiling of heat stress: hardening and recovery of homeostasis in *Drosophila*. *American Journal of Physiology Regulatory, Integrative and Comparative Physiology* **291**:R205. doi: 10.1152/ajpregu.00867.2005, PMID: 16469831

Matthews BW. 1988. Structural basis of the action of thermolysin and related zinc peptidases. *Accounts of Chemical Research* **21**:333–340. doi: 10.1021/ar00153a003

McMurray JJ, Packer M, Desai AS, Gong J, Lefkowitz MP, Rizkala AR, Rouleau JL, Shi VC, Solomon SD, Swedberg K, Zile MR, PARADIGM-HF Investigators and Committees. 2014. Angiotensin-neprilysin inhibition versus enalapril in heart failure. *New England Journal of Medicine* **371**:993–1004. doi: 10.1056/NEJMoa1409077, PMID: 25176015

Meyer H, Panz M, Albrecht S, Drechsler M, Wang S, Hüsken M, Lehmacher C, Paululat A. 2011. *Drosophila* metalloproteases in development and differentiation: the role of ADAM proteins and their relatives. *European Journal of Cell Biology* **90**:770–778. doi: 10.1016/j.ejcb.2011.04.015, PMID: 21684629

Meyer H, Panz M, Zmojdzian M, Jagla K, Paululat A. 2009. Neprilysin 4, a novel endopeptidase from *Drosophila melanogaster*, displays distinct substrate specificities and exceptional solubility states. *Journal of Experimental Biology* **212**:3673–3678. doi: 10.1242/jeb.034272, PMID: 19880729

Molinaro G, Rouleau JL, Adam A. 2002. Vasopeptidase inhibitors: a new class of dual zinc metallopeptidase inhibitors for cardiorenal therapeutics. *Current Opinion in Pharmacology* **2**:131–141. doi: 10.1016/S1471-4892(02)00138-8, PMID: 11950623

Nässel DR, Kubrak OI, Liu Y, Luo J, Lushchak OV. 2013. Factors that regulate insulin producing cells and their output in *Drosophila*. *Frontiers in Physiology* **4**:252. doi: 10.3389/fphys.2013.00252, PMID: 24062693

Nässel DR, Winther AM. 2010. *Drosophila* neuropeptides in regulation of physiology and behavior. *Progress in Neurobiology* **92**:42–104. doi: 10.1016/j.pneurobio.2010.04.010, PMID: 20447440

Oefner C, D'Arcy A, Hennig M, Winkler FK, Dale GE. 2000. Structure of human neutral endopeptidase (Neprilysin) complexed with phosphoramidon. *Journal of Molecular Biology* **296**:341–349. doi: 10.1006/jmbi.1999.3492, PMID: 10669592

Panz M, Vitos-Faleato J, Jendretzki A, Heinisch JJ, Paululat A, Meyer H. 2012. A novel role for the non-catalytic intracellular domain of Neprilysins in muscle physiology. *Biology of the Cell* **104**:553–568. doi: 10.1111/boc.201100069, PMID: 22583317

Paululat A, Heinisch JJ. 2012. New yeast/*E. coli*/*Drosophila* triple shuttle vectors for efficient generation of Drosophila P element transformation constructs. *Gene* **511**:300–305. doi: 10.1016/j.gene.2012.09.058, PMID: 23026211

Pedersen KS, Kristensen TN, Loeschcke V, Petersen BO, Duus JØ, Nielsen NC, Malmendal A. 2008. Metabolomic signatures of inbreeding at benign and stressful temperatures in *Drosophila melanogaster*. *Genetics* **180**:1233–1243. doi: 10.1534/genetics.108.089144, PMID: 18791253

Pool AH, Scott K. 2014. Feeding regulation in *Drosophila*. *Current Opinion in Neurobiology* **29**:57–63. doi: 10.1016/j.conb.2014.05.008, PMID: 24937262

Predel R, Wegener C, Russell WK, Tichy SE, Russell DH, Nachman RJ. 2004. Peptidomics of CNS-associated neurohemal systems of adult *Drosophila melanogaster*: a mass spectrometric survey of peptides from individual flies. *The Journal of Comparative Neurology* **474**:379–392. doi: 10.1002/cne.20145, PMID: 15174081

Rajan A, Perrimon N. 2012. *Drosophila* cytokine unpaired 2 regulates physiological homeostasis by remotely controlling insulin secretion. *Cell* **151**:123–137. doi: 10.1016/j.cell.2012.08.019, PMID: 23021220

eLIFE Research article

Reiher W, Shirras C, Kahnt J, Baumeister S, Isaac RE, Wegener C. 2011. Peptidomics and peptide hormone processing in the *Drosophila* midgut. *Journal of Proteome Research* **10**:1881–1892. doi: 10.1021/pr101116g, PMID: 21214272

Rulifson EJ, Kim SK, Nusse R. 2002. Ablation of insulin-producing neurons in flies: growth and diabetic phenotypes. *Science* **296**:1118–1120. doi: 10.1126/science.1070058, PMID: 12004130

Savorani F, Tomasi G, Engelsen SB. 2010. icoshift: A versatile tool for the rapid alignment of 1D NMR spectra. *Journal of Magnetic Resonance* **202**:190–202. doi: 10.1016/j.jmr.2009.11.012, PMID: 20004603

Schulz RA, Chromey C, Lu MF, Zhao B, Olson EN. 1996. Expression of the D-MEF2 transcription in the *Drosophila* brain suggests a role in neuronal cell differentiation. *Oncogene* **12**:1827–1831. PMID: 8622904

Simon P. 2003. Q-Gene: processing quantitative real-time RT-PCR data. *Bioinformatics* **19**:1439–1440. doi: 10.1093/bioinformatics/btg157, PMID: 12874059

Sitnik JL, Francis C, Hens K, Huybrechts R, Wolfner MF, Callaerts P. 2014. Neprilysins: an evolutionarily conserved family of metalloproteases that play important roles in reproduction in *Drosophila*. *Genetics* **196**: 781–797. doi: 10.1534/genetics.113.160945, PMID: 24395329

Stoyanova R, Brown TR. 2001. NMR spectral quantitation by principal component analysis. *NMR in Biomedicine* **14**:271–277. doi: 10.1002/nbm.700, PMID: 11410945

Söderberg JA, Carlsson MA, Nässel DR. 2012. Insulin-producing cells in the *Drosophila* brain also express satiety-inducing cholecystokinin-like peptide, drosulfakinin. *Frontiers in Endocrinology* **3**:109. doi: 10.3389/fendo.2012.00109, PMID: 22969751

Tennessen JM, Baker KD, Lam G, Evans J, Thummel CS. 2011. The *Drosophila* estrogen-related receptor directs a metabolic switch that supports developmental growth. *Cell Metabolism* **13**:139–148. doi: 10.1016/j.cmet.2011.01.005, PMID: 21284981

Tennessen JM, Bertagnolli NM, Evans J, Sieber MH, Cox J, Thummel CS. 2014. Coordinated metabolic transitions during *Drosophila* embryogenesis and the onset of aerobic glycolysis. *G3* **4**:839–850. doi: 10.1534/g3.114.010652, PMID: 24622332

Thomas JE, Rylett CM, Carhan A, Bland ND, Bingham RJ, Shirras AD, Turner AJ, Isaac RE. 2005. *Drosophila melanogaster* NEP2 is a new soluble member of the neprilysin family of endopeptidases with implications for reproduction and renal function. *Biochemical Journal* **386**:357–366. doi: 10.1042/BJ20041753, PMID: 15554877

Turner AJ, Isaac RE, Coates D. 2001. The neprilysin (NEP) family of zinc metalloendopeptidases: genomics and function. *BioEssays* **23**:261–269. doi: 10.1002/1521-1878(200103)23:3<261::AID-BIES1036>3.0.CO;2-K, PMID: 11223883

Turrel O, Lampin-Saint-Amaux A, Préat T, Goguel V. 2016. *Drosophila* neprilysins are involved in middle-term and long-term memory. *Journal of Neuroscience* **36**:9535–9546. doi: 10.1523/JNEUROSCI.3730-15.2016, PMID: 27629706

Veenstra JA, Agricola HJ, Sellami A. 2008. Regulatory peptides in fruit fly midgut. *Cell and Tissue Research* **334**: 499–516. doi: 10.1007/s00441-008-0708-3, PMID: 18972134

Wegener C, Gorbashov A. 2008. Molecular evolution of neuropeptides in the genus *Drosophila*. *Genome Biology* **9**:R131. doi: 10.1186/gb-2008-9-8-r131, PMID: 18717992

Wegener C, Reinl T, Jänsch L, Predel R. 2006. Direct mass spectrometric peptide profiling and fragmentation of larval peptide hormone release sites in *Drosophila melanogaster* reveals tagma-specific peptide expression and differential processing. *Journal of Neurochemistry* **96**:1362–1374. doi: 10.1111/j.1471-4159.2005.03634.x, PMID: 16441518

Whitworth JA. 2003. Emerging drugs in the management of hypertension. *Expert Opinion on Emerging Drugs* **8**:377–388. doi: 10.1517/14728214.8.2.377, PMID: 14661996

Yew JY, Wang Y, Barteneva N, Dikler S, Kutz-Naber KK, Li L, Kravitz EA. 2009. Analysis of neuropeptide expression and localization in adult *Drosophila melanogaster* central nervous system by affinity cell-capture mass spectrometry. *Journal of Proteome Research* **8**:1271–1284. doi: 10.1021/pr800601x, PMID: 19199706

Fellowships

01.11.2012-31.12.2012:   Fellow of the „integrated research training group" of the
                            SFB 944 of the University of Osnabrück

01.10.2013-31.03.2016:   Fellow of the "FAZIT-Stiftung" (Frankfurt am Main)

Talks and Posters (selection)

Panz M., Hallier B., Vitos J., Jendretzki A., Heinisch J., Paululat A., Harten H.

"A novel role for the non-catalytic intracellular domain of Neprilysins in muscle physiology"

23rd European *Drosophila* Research Conference; Barcelona, Spain; 2013, Poster

Hallier B., Panz M., Paululat A., Harten H.
"A novel role for the non-catalytic intracellular domain of Neprilysins in muscle physiology"
Regional *Drosophila* Meeting, Heidelberg, Germnay, 2014, Poster

Hallier B., Schiemann R., Paululat A., Harten H.
"Neprilysins provide insulin homeostasis via cleavage of regulatory peptides in *Drosophila melanogaster*"
Joint Meeting of the German and French Societies of Developmental Biologists, Nuremberg, Germany, 2015, Poster

Hallier B., Schiemann R., Dehnen L., Cordes E., Vitos-Faleato J., Walter S., Malmendal A., Paululat A., Harten H.,
"Neprilysins control insulin signaling via cleavage of regulatory peptides"
24th European *Drosophila* Research Conference, Heidelberg, Germany, 2015, Poster

Hallier B., Schiemann R., Walter S., Malmendal A., Paululat A., Harten H.,
"Neprilysins control insulin signaling via cleavage of regulatory peptides"
SFB 944 Retreat, Düsseldorf, Germany, 2015, Talk

Hallier B.

"Functional analysis of a novel Neprilysin 4 mutant"

Minisymposium 2016, Sylt, Germany, 2016, Talk

Hallier B., Schiemann R., Malmendal A., Paululat A., Harten H.,

"Neprilysins control insulin expression via cleavage of regulatory peptides"

IRTG-retreat, Osnabrück, Germany 2016, Poster

Curriculum vitae

Name: **Benjamin Christoph Hallier**

Day of Birth: June 8th, 1987

Place of Birth: Hannover

Academic education:

April 2013- March 2017:   PhD student at the department of Zoology and Developmental biology of the University of Osnabrück

SS 2010-SS 2012:   University of Osnabrück, Master of Science, cellular biology, final examination 5.09.2012.

WS 2006/2007-WS 2009/2010: University of Osnabrück, Bachelor of Science, cellular biology, final examination 12.03.2010.

School education:

30.06.2006   Allgemeine Hochschulreife (Abitur), KGS Salzhemmendorf

1997–2006   Orientierungsstufe, Gymnasium (Sekundarstufe I und II), KGS Salzhemmendorf

1993–1997   Grundschule im Saaletal, Oldendorf

Erklärung über die Eigenständigkeit der erbrachten wissenschaftlichen Leistung

Ich erkläre hiermit, dass ich die vorliegende Arbeit ohne unzulässige Hilfe Dritter und ohne Benutzung anderer als der angegebenen Hilfsmittel angefertigt habe. Die aus anderen Quellen direkt oder indirekt übernommenen Daten und Konzepte sind unter Angabe der Quelle gekennzeichnet.

Bei der Auswahl und Auswertung folgenden Materials haben mir die nachstehend aufgeführten Personen in der jeweils beschriebenen Weise unentgeltlich geholfen.

- Dr. Heiko Harten und Ronja Schiemann bei der Generierung und Analyse der massenspektrometrischen Daten.
- Prof. Dr. Anders Malmendal bei der Generierung und Analyse der NMR-spektroskopischen Daten.
- Lena Dehnen bei der Generierung der mutanten Fliegenlinie Nep4$^{\Delta281\text{-}1040}$.
- Joshua Strickmann und Marc Hellmann im Rahmen ihrer Master- und Bachelorarbeit bei der Erhebung von Daten zum Bewegungsassay, Nahrungsaufnahmeassay, Fertilitätsassay, Entwicklungsassay und Antikörperfärbungen an Embryonen.

Weitere Personen waren an der inhaltlichen und materiellen Erstellung der vorliegenden Arbeit nicht beteiligt. Insbesondere habe ich hierfür nicht die entgeltliche Hilfe von Vermittlungs- bzw. Beratungsdiensten (Promotionsberater oder andere Personen) in Anspruch genommen. Niemand hat von mir unmittelbar oder mittelbar geldwerte Leistungen für Arbeiten erhalten, die im Zusammenhang mit dem Inhalt der vorgelegten Dissertation stehen.

Die Arbeit wurde bisher weder im In- noch im Ausland in gleicher oder ähnlicher Form einer
anderen Prüfungsbehörde vorgelegt.

_____   _____

Ort, Datum   Unterschrift

Erklärung über etwaige frühere Promotionsversuche

gem. § 8 Abs. 2 Buchstabe g der Promotionsordnung der Fachbereiche Physik, Biologie/Chemie und Mathematik/Informatik der Universität Osnabrück

Hiermit bestätige ich, dass die vorzulegende Dissertation bisher weder im In- noch im Ausland in gleicher oder ähnlicher Form einer anderen Prüfungsbehörde vorgelegt wurde.

_____

   _____

   Ort, Datum   Unterschrift

Danksagung